ADVANCES IN POLYMER SCIENCE 224

Volume Editors W. P. Meier · W. Knoll

Polymer Membranes/ Biomembranes

Springer

224

Advances in Polymer Science

Advances in Polymer Science

Recently Published and Forthcoming Volumes

Polymer Membranes/Biomembranes
Volume Editors: Meier, W.P., Knoll, W.
Vol. 224, 2010

Organic Electronics
Volume Editors: Meller, G., Grasser, T.
Vol. 223, 2010

Inclusion Polymers
Volume Editor: Wenz, G.
Vol. 222, 2009

Advanced Computer Simulation Approaches for Soft Matter Sciences III
Volume Editors: Holm, C., Kremer, K.
Vol. 221, 2009

Self-Assembled Nanomaterials II
Nanotubes
Volume Editor: Shimizu, T.
Vol. 220, 2008

Self-Assembled Nanomaterials I
Nanofibers
Volume Editor: Shimizu, T.
Vol. 219, 2008

Interfacial Processes and Molecular Aggregation of Surfactants
Volume Editor: Narayanan, R.
Vol. 218, 2008

New Frontiers in Polymer Synthesis
Volume Editor: Kobayashi, S.
Vol. 217, 2008

Polymers for Fuel Cells II
Volume Editor: Scherer, G. G.
Vol. 216, 2008

Polymers for Fuel Cells I
Volume Editor: Scherer, G. G.
Vol. 215, 2008

Photoresponsive Polymers II
Volume Editors: Marder, S. R., Lee, K.-S.
Vol. 214, 2008

Photoresponsive Polymers I
Volume Editors: Marder, S. R., Lee, K.-S.
Vol. 213, 2008

Polyfluorenes
Volume Editors: Scherf, U., Neher, D.
Vol. 212, 2008

Chromatography for Sustainable Polymeric Materials
Renewable, Degradable and Recyclable
Volume Editors: Albertsson, A.-C., Hakkarainen, M.
Vol. 211, 2008

Wax Crystal Control · Nanocomposites Stimuli-Responsive Polymers
Vol. 210, 2008

Functional Materials and Biomaterials
Vol. 209, 2007

Phase-Separated Interpenetrating Polymer Networks
Authors: Lipatov, Y. S., Alekseeva, T.
Vol. 208, 2007

Hydrogen Bonded Polymers
Volume Editor: Binder, W.
Vol. 207, 2007

Oligomers · Polymer Composites Molecular Imprinting
Vol. 206, 2007

Polysaccharides II
Volume Editor: Klemm, D.
Vol. 205, 2006

Neodymium Based Ziegler Catalysts – Fundamental Chemistry
Volume Editor: Nuyken, O.
Vol. 204, 2006

Polymer Membranes/ Biomembranes

Volume Editors: Wolfgang Peter Meier
Wolfgang Knoll

With contributions by

S. Belegrinou · K. Bender · A. Bertin · D. de Bruyn Ouboter
K. Ch. Daoulas · R. Förch · C. Frank · H. Götz · C. Heibel
F. Hermes · T. Jenkins · U. Jonas · J.R. Joubert · A. Kibrom
W. Knoll · R. Kügler · V. Malinova · W.P. Meier · M. Müller
C. Naumann · C.A. Naumann · R. Naumann · A. Reisinger
J. Rühe · S.S. Saavedra · S. Schiller · H. Schlaad · A.P. Siegel
E.-K. Sinner · H. Zhang

Springer

Editors
Wolfgang Peter Meier
Universität Basel
Dept. Chemie
Klingelbergstr. 80
4056 Basel
Switzerland
wolfgang.meier@unibas.ch

Wolfgang Knoll
AIT Austrian Institute of Technology GmbH
Donau-City-Strasse 1
1220 Vienna
Austria
wolfgang.knoll@ait.ac.at

ISSN 0065-3195 e-ISSN 1436-5030
ISBN 978-3-642-10478-7 e-ISBN 978-3-642-10479-4
DOI 10.1007/978-3-642-10479-4
Springer Heidelberg Dordrecht London New York

Library of Congress Control Number: 2009936785

Cover design: WMXDesign GmbH, Heidelberg

Printed on acid-free paper

Springer is part of Springer Science+Business Media (www.springer.com)

Volume Editors

Wolfgang Peter Meier

Universität Basel
Dept. Chemie
Klingelbergstr. 80
4056 Basel, Switzerland
wolfgang.meier@unibas.ch

Wolfgang Knoll

AIT Austrian Institute of Technology GmbH
Donau-City-Strasse 1
1220 Vienna
Austria
wolfgang.knoll@ait.ac.at

Editorial Board

Advances in Polymer Sciences
Also Available Electronically

Advances in Polymer Sciences is included in Springer's eBook package *Chemistry and Materials Science*. If a library does not opt for the whole package the book series may be bought on a subscription basis. Also, all back volumes are available electronically.

For all customers who have a standing order to the print version of *Advances in Polymer Sciences*, we offer the electronic version via SpringerLink free of charge.

If you do not have access, you can still view the table of contents of each volume and the abstract of each article by going to the SpringerLink homepage, clicking on "Chemistry and Materials Science," under Subject Collection, then "Book Series," under Content Type and finally by selecting *Advances in Polymer Sciences*.

You will find information about the

- Editorial Board
- Aims and Scope
- Instructions for Authors
- Sample Contribution

at springer.com using the search function by typing in *Advances in Polymer Sciences*.

Color figures are published in full color in the electronic version on SpringerLink.

Aims and Scope

Advances in Polymer Sciences reviews actual trends in modern biotechnology.

Its aim is to cover all aspects of this interdisciplinary technology where knowledge, methods and expertise are required for chemistry, biochemistry, microbiology, genetics, chemical engineering and computer science.

Special volumes are dedicated to selected topics which focus on new biotechnological products and new processes for their synthesis and purification. They give the state-of-the-art of a topic in a comprehensive way thus being a valuable source for the next 3–5 years. It also discusses new discoveries and applications.

In general, special volumes are edited by well known guest editors. The series editor and publisher will however always be pleased to receive suggestions and supplementary information. Manuscripts are accepted in English.

In references *Advances in Polymer Sciences* is abbreviated as *Adv. Polym. Sci.* and is cited as a journal.

Special volumes are edited by well known guest editors who invite reputed authors for the review articles in their volumes.

Impact Factor in 2008: 6.802; Section “Polymer Science”: Rank 2 of 73

Preface

The multicomponent nature of biological membranes and their intra- and extracellular interactions make direct investigations on the membrane structure and processes nearly impossible. Clearly, a better understanding of the membrane properties and the mechanisms determining membrane protein functions is crucial to the implementation of biosensors, bioreactors and novel platforms for medical therapy. For this reason, the interest in model systems suitable for the construction and study of complex lipid/protein membrane architectures has increased steadily over the years. The classical portfolio of model membranes used for biophysical and interfacial studies of lipid (bi)layers and lipid/protein composites includes Langmuir monolayers assembled at the water/air interface, (uni- and multi-lamellar) vesicles in bulk (liposomal) dispersion, bimolecular lipid membranes (BLMs), and various types of solid-supported membranes. All these have specific advantages but also suffer from serious drawbacks that limit their technical applications. Polymer membranes comprised of entirely synthetic or hybrid (synthetic polymer/biopolymer) block copolymers appeared to be an attractive alternative to the lipid-based models. Generally, the synthetic block copolymer membranes are thicker and more stable and the versatility of polymer chemistry allows the adoption of relevant properties for a wide range of applications.

This volume provides a vast overview of the physico-chemical and synthetic aspects of artificial membranes. Numerous membrane models are described, including their properties (i.e. swelling, drying, lateral mobility, stability, electrical conductivity, etc.), advantages, and drawbacks. The potential applications of these models are discussed and supported by real examples.

Chapter 1 summarizes methods for the stabilization of artificial lipid membranes. They include synthesis of new types of polymerizable lipids and polymerization of membranes. Creation and characterization of novel poly(lipid) membrane systems, as well as their functionalization for biotechnological applications, are also described. Chapter 2 addresses experimental studies on the design and characterization of lipopolymer-based monolayers at the air-water interface. Thermodynamic and structural data collected with X-ray and neutron reflectrometry, infrared reflection absorption spectroscopy, and sum frequency generation spectroscopy provide

information on how the lipopolymers organize at the air-water interface. Important insight into the viscoelastic and lateral diffusion properties of these systems is also given. The assembly and the structural and functional characterization of various types of polymer-supported lipid bilayer membranes are discussed in Chapter 3. It has been shown that the chemical nature of the polymer cushion can be diverse, ranging from polyelectrolytes to glycopolymers and cross-linked hydrogels, which makes it possible to tailor the features of the polymer supports. Additionally, important properties of the tethered membranes such as swelling in water of the polymer tethers and lateral mobility of the lipid molecules are presented. Synthetic block copolymer membranes represented mainly by vesicles are introduced in Chapter 4. Here the discussion is focused on principles of vesicle formation, membrane properties, and methods for vesicle preparation and characterization. Numerous membrane-forming copolymer systems are presented, including copolymer membranes with responsiveness to external stimuli. In addition, recent examples demonstrating the use of vesicles as therapeutic formulations, for cellular targeting and as nanoreactors, revealed their high potential for bio-applications. Chapter 5 is dedicated to biohybrid vesicles consisting of a synthetic polymer and biologically relevant polymer, e.g. peptides and sugars. The self-assembly mechanism of biohybrid amphiphilic polymers is described as a function of polymer composition (geometrical packing of chains), hydrogen bonding, secondary structure interactions and supramolecular complexation. The potential use of biohybrid membranes as drug and gene carriers, bioreactors, and composite materials, as well as for cell recognition, is accented. Finally, Chapter 6 reviews molecular models and computer simulation techniques for amphiphilic vesicles formed either by lipid or block copolymer molecules. System-specific, atomistic and coarse-grained representations of amphiphilic vesicles are considered. The discussion of the coarse-grained models is particularly focused on how their parameterization can be related to the material properties of specific systems. As these models are particle-based, their equilibrium properties are obtained from a straightforward Monte-Carlo scheme. The mechanical properties of the vesicles are established and compared with the properties of a planar bilayer. Selected results demonstrated the effect of loading on the vesicle stability and the mechanical properties of its bilayer shell.

In summary, we attempted to collect contributions from several expert groups to summarize the current state of the art of artificial membranes. There still exist many challenges and opportunities for improvement before at least some of these developments are commercialized. Certainly, this process will call for a fruitful interdisciplinary research and we hope that the current volume could be a useful source of fundamental information.

The editors express their thanks to the authors and to the Springer group for their help in publishing this book, and special thanks to Dr. Violeta Malinova for her very valuable help in preparing this preface.

Basel and Vienna, Oct. 2009 *Wolfgang Peter Meier*
Wolfgang Knoll

Contents

Adv Polym Sci (2010) 224: 1–42
DOI:10.1007/12_2009_3

Published online: 16 June 2009

Membranes from Polymerizable Lipids

Han Zhang, James R. Joubert, and S. Scott Saavedra

Abstract Potential technological applications for artificial lipid and proteo-lipid membranes, such as capsules for controlled delivery of drugs and coatings for biosensors and biomaterials, are in many cases limited by the inherent instability of lipid lamellar phases. Development of methods to stabilize artificial lipid membranes has therefore been a focus of research efforts since the 1970s. Linear and cross-linking polymerization of synthetic lipid monomers is a well-studied strategy. Several comprehensive reviews on polymerizable lipids and supramolecular structures derived from them appeared between 1985 and 2002. Consequently, this review focuses on significant developments in this field during 2000–2008. These include synthesis of new types of polymerizable lipids, creation and characterization of novel poly(lipid) membrane systems, and applications of polymerized vesicles and membranes in chemical sensing, separations science, drug delivery, materials biocompatibility, and energy storage. Polymerization of membranes to achieve stability and their functionalization for technological applications are emphasized.

Keywords Lipid bilayer · Liposome · Lipo-polymer · Planar lipid membrane · Poly(lipid) · Polymerizable lipid · Stabilized membrane

Contents

S.S. Saavedra (✉)
Department of Chemistry and BIO5 Institute, University of Arizona, Tucson, AZ 85721-0041, USA
e-mail: saavedra@email.arizona.edu

Abbreviations

μCP	Microcontact printing
AAPD	2,2′-Azobis(2-methylpropionamidine) dihydrochloride
AcrylatePC	1-Palmitoyl-2-[12-(acryloyloxy)dodecanoyl]-*sn*-glycero-3-phosphocholine
AFM	Atomic force microscopy
bis-DenPC	1,2-Bis(octadeca-2,4-dienoyl)-*sn*-glycero-3-phosphocholine
bis-SorbPC	1,2-Bis[10-(2′,4′-hexadienoloxy)decanoyl]-*sn*-glycero-3-phosphocholine
BLM	Black lipid membrane
BMA	Butylmethacrylate
BSA	Bovine serum albumin
CE	Capillary electrophoresis
DDDB	Dicetyldimethylammonium 3,5-divinyl benzoate
DDVB	Dicetyldimethylammonium 4-vinyl benzoate
DEAP	Diethoxyacetophenone
DenSorbPC	1-Oleoyl-2-[14-sorbyl-2,4-tetradecadienoic]-*sn*-glycero-3-phosphocholine
DiPhyPC	1,2-Diphytanoyl-*sn*-glycero-3-phosphocholine
DiynePC	1,2-Bis(10,12-tricosadiynoyl)-*sn*-glycero-3-phosphocholine
DOPC	1,2-Dioleoyl-*sn*-glycero-3-phosphocholine
DPPC	1,2-Dipalmitoyl-*sn*-glycero-3-phosphocholine
EGDMA	Ethylene glycol dimethacrylate
GPCR	G-protein-coupled receptor
HBM	Hybrid bilayer membrane
LBS	Langmuir–Blodgett–Schaefer
MI	Metarhodopsin I
MII	Metarhodopsin II
OTS	Octadecyltrichlorosilane
PC	Phosphocholine
PE	Phosphoethanolamine
PEG	Poly(ethylene glycol)

PEM	Polyelectrolyte multilayer
POPC	1-Palmitoyl-2-oleoylphosphatidylcholine
PSLB	Planar supported lipid bilayer
PTPE	1-Palmitoyl-2,10,12-tricosadiynoyl-*sn*-glycero-3-phosphoethanolamine
PWR	Plasmon waveguide resonance
Rho	Bovine rhodopsin
SAM	Self-assembled monolayer
SUV	Small unilamellar vesicle
TEM	Transmission electron microscopy
TIRF	Total internal reflection fluorescence
TM	Thrombomodulin
TMP	Transmembrane protein
XPS	X-ray photoelectron spectroscopy

1 Introduction

Amphipathic lipids are composed of a hydrophilic headgroup and one or more hydrophobic tails [1]. When hydrated, the hydrophobic tails aggregate to minimize their energetically unfavorable interactions with water molecules, which drives the spontaneous organization of lipids into a variety of supramolecular assemblies [2]. The molecular organization and morphology of these assemblies depend on the lipid concentration, temperature, pressure, and the presence of nonamphiphilic additives (e.g., metal ions). The most familiar and widely studied lipid assemblies are the lamellar (bilayer) phases, principally the solid-analogous (L_β) phase and the more disordered liquid crystalline (L_α) phase. This is due to the fact that amphipathic lipids are the major architectural component of membranes in biological cells [1]. They function as barriers between subcellular compartments as well as between the cell and its surrounding environment. More importantly, cellular membranes mediate all communication between subcellular compartments, the cytoplasm, and the extracellular environment. In addition to regulating the transport of ions and molecules, membranes transmit information in the form of localized structural changes. For example, ligand binding to a TMP may cause a conformational change in the receptor, along with local membrane deformation, which triggers an enzymatic signaling cascade on the opposite side of the membrane.

The highly complex and variable composition of natural cell membranes makes them a difficult subject for experimental studies. Artificial lipid membranes have consequently been prepared and studied for many years as models of cell membranes [1, 3–7]. A diverse array of geometries has been developed, including small and large unilamellar vesicles, giant lipid vesicles, lipid membranes supported on solid and polymer-coated substrates, and BLMs. These have been used to study the physical and chemical properties of lipids and lipid mixtures as well as membrane-associated proteins, including reconstituted transmembrane receptors.

Potential technological applications for artificial lipid and proteo-lipid membranes, such as capsules for controlled delivery of drugs and biocompatible coatings for synthetic materials, were recognized early in their development [3, 8, 9]. For these and other applications, the inherent instability of lipid lamellar phases may pose a limitation. Specifically, the molecules in a bilayer composed of monomeric lipids are self-organized by relatively weak intermolecular interactions that are insufficient to maintain the lamellar structure under many types of chemical, mechanical, and/or thermal stresses. Consequently, partial or complete loss of the bilayer structure occurs upon exposure to conditions that may be encountered during use of a lipid-based molecular device, such as extended storage, removal from water, or exposure to chaotropic agents (e.g., surfactants)[10–14]. Development of methods to stabilize artificial lipid membranes has therefore been a focus of research efforts since the 1970s [8, 15–20]. These methods include: (1) linear and cross-linking polymerization of synthetic lipid monomers (e.g., [13]); (2) polymerization of nonlipid monomer units incorporated into the bilayer (e.g., [21]); (3) adsorption or surface grafting of hydrophilic polymers (e.g., [22]); (4) biospecific adsorption of protective protein coatings (e.g., [23]); and (5) incorporation of lipids that span both leaflets of the bilayer, such as bolaamphiphiles (e.g., [24]). This review focuses primarily on (1), with some coverage of (2) and (3).

Polymerizable groups are introduced into amphipathic lipids by chemical synthesis and can be located anywhere along the lipid tails or linked to the headgroup [25]. The self-organization of reactive lipids into a supramolecular assembly yields a regular array of the polymerizable groups. A large variety of these groups and methods to polymerize them have been described in the literature (see reviews [3, 25–29]). Mono-substituted lipids form linear polymers whereas bis-substituted lipids can be cross-linked. It is well established that the structural properties of poly(lipid) bilayers, such as the degree of polymerization (X_n), the extent of conversion, and the degree of cross-linking, are highly dependent upon a number of factors, including the type of polymerizable moiety and the method of polymerization. All of these parameters should in turn affect the fluidity, permeability, elastic moduli, and stability of the bilayer.

Several comprehensive reviews on polymerizable lipids and supramolecular structures derived from them appeared between 1985 and 2002 [3, 25–31]. Consequently, this review focuses on developments in this field during 2000–2008. These include synthesis of new types of polymerizable lipids, creation and characterization of novel poly(lipid) membrane systems, and applications of polymerized vesicles and membranes in chemical sensing, separations science, drug delivery, materials biocompatibility, and other fields.

This article is organized primarily on the geometry of the supramolecular structure (e.g., vesicle, planar supported film, etc.). Functionalization of poly(lipid) structures and their technological applications are presented in a separate section as these have expanded greatly as the field has matured. The analytical techniques available for characterization of substrate-supported, thin organic films have advanced considerably since polymerized lipid films were first reported in the early 1980s, and examples of the use of these techniques to study poly(lipid) membranes are presented throughout this review.

2 Supported Poly(Lipid) Membranes

Planar supported lipid membranes were first prepared and studied as simplified structural models of cell membranes [4, 6, 32], and more recently as biocompatible coatings for sensor transducers and other synthetic materials [33–37]. A major advantage of the planar geometry relative to vesicles, and a major contributor to the expansion of this field, is the availability of powerful surface-sensitive analytical/physical techniques. Confining a lipid membrane to the near-surface region of a solid substrate makes it possible to study its structural and functional properties in detail using a variety of techniques such as surface plasmon resonance, AFM, TIRF, attenuated total reflection, and sum frequency vibrational spectroscopy [38–42].

In this chapter, supported membrane structures are divided into two major classes as follows.

First, a PSLB is formed either directly on a hydrophilic solid substrate (e.g., glass or mica) or on a substrate that has been coated with a thin, hydrophilic layer, such as a PEG cushion [4]. The cushion serves as a spacer to decouple the inner lipid monolayer from the substrate surface, allowing for incorporation of membrane proteins having water-soluble domains that protrude beyond the lipid headgroups. PSLBs are typically deposited using either LBS techniques [43], self assembly via vesicle fusion [44], or a combination of these methods. The major advantage of LBS deposition is that the packing density and lipid composition of the film can be precisely controlled. With the appropriate choice of composition and deposition conditions, lateral organization and membrane asymmetry can be specified. Vesicle fusion is usually restricted to deposition of fluid-phase lipids and cannot be used to create asymmetric PSLBs; however, technically it is much simpler than LBS deposition and is therefore more widely used.

Second, several types of asymmetric supported bilayer structures, in which the composition of the two monolayers is different, have been created as alternatives to symmetric PSLBs. One example is the HBM [45, 46]. The inner monolayer in an HBM is an alkyl SAM, typically an alkanethiol on gold, upon which an outer lipid monolayer is deposited by either LBS or vesicle fusion methods. A more sophisticated type of asymmetric supported bilayer is the tethered bilayer lipid membrane (tBLM) in which the SAM is replaced with an inner lipid monolayer. Some or all of the molecules in the inner monolayer are covalently tethered to the underlying support, usually through a hydrophilic linker that creates a water-swollen spacer layer between the tBLM and the substrate surface [47–51].

In addition to planar substrates, both PSLBs and HBMs can be deposited on spherical particles such as silica or polymer beads [52–55]. Typically beads with diameters in the range of 0.1–5 μm are used. From the perspective of a single lipid molecule that occupies an area of ca. 60 $Å^2$ in the plane of a lipid bilayer, the surface of a bead in this size range can be approximated as planar.

PSLBs and HBMs composed of fluid-phase lipids, such as DOPC, can be stable under water for up to several days. However, the bilayer structure is degraded upon exposure to a variety of conditions such as surfactant solutions, surface-active

proteins, and removal from water [10, 11, 14]. In an asymmetric supported bilayer, covalent tethering of the inner monolayer enhances its structural stability. However, when the outer monolayer is composed of fluid lipids that are associated solely via noncovalent interactions, it is inherently unstable, similar to a fluid-phase PSLB [36, 56].

2.1 Hybrid Bilayer Membranes

Asymmetric bilayers have been fabricated using polymerizable lipids in an attempt to achieve stabilization through monolayer polymerization [36, 56–64]. In a series of publications, Chaikof and coworkers described HBMs formed by depositing monoacrylate-functionalized lipids on several types of substrate surfaces [36, 56, 62–64]. In an effort to develop more effective lipid polymerization methods, Orban et al. [56] compared photoinitiated free radical polymerization, using eosin Y/triethanolamine (Fig. 1), to thermal initiation using AAPD as in their earlier work [36]. A monolayer of acrylatePC was fused on a SAM formed from OTS on glass or an oxidized Si wafer. The advancing and receding water contact angles of the photopolymerized film were 57° and 39°, respectively, as opposed to 65° and 46° for the thermally polymerized film, suggesting fewer defects in the former type.

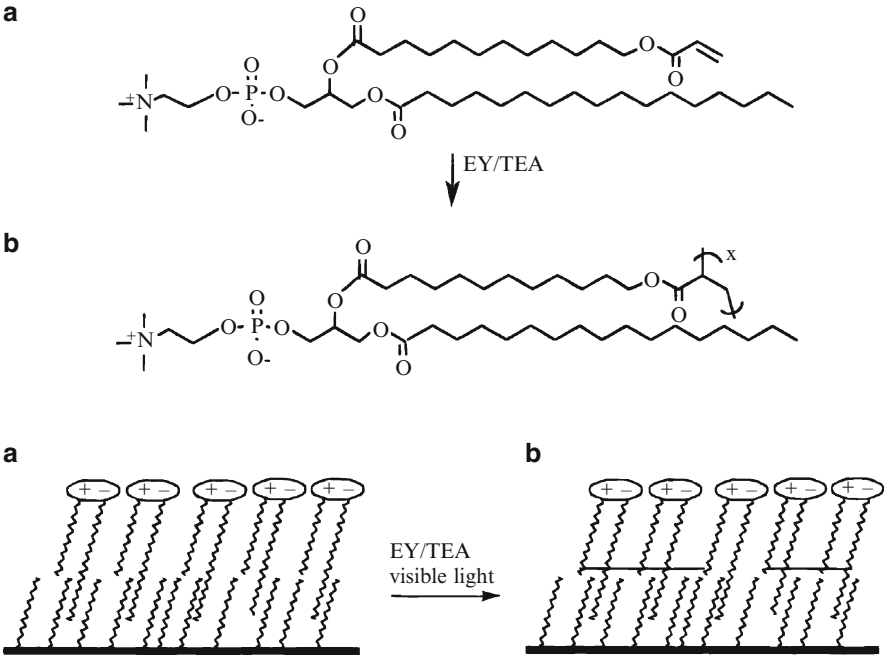

Fig. 1 Photopolymerization to generate a poly(acrylatePC) monolayer on an alkylated support. Reprinted with permission from [56]. Copyright 2000, American Chemical Society

The source of these defects may be monomer loss, which likely occurs during thermal polymerization because the reaction proceeds over a relatively long period at a temperature that exceeds the acrylatePC melting point.

Photoinitiation was found to enhance HBM stability relative to thermal initiation. Photopolymerized films showed little change in contact angle during a 1-week incubation period in water whereas for thermally polymerized films, increases $>10^{\circ}$ were observed. The authors hypothesized that thermal polymerization generates a higher proportion of oligomers and/or low molecular weight polymer chains that more readily desorb due to a lower average adsorption energy. However, the contact angle for both types of films increased significantly when they were incubated in surfactant solution. These results are consistent with studies showing that linearly polymerized lipids are significantly less stable to dissolution in surfactants than cross-linked lipids [11, 13, 65].

In another study, Liu et al. [66] used a PEM in place of an OTS SAM to create a new type of membrane for encapsulation of cultured cells. The PEM was composed of several alternating layers of poly(lysine) and alginate, capped with an amphiphilic terpolymer synthesized from *N*,*N*-dioctadecylcarbamoyl propionic acid, hydroxyethylacrylate, and styrene sulfonate. The octadecyl chains provided a hydrophobic surface on which the acrylatePC was fused, then photopolymerized (Fig. 2). Coating alginate beads with the PEM/HBM multilayer significantly reduced the release

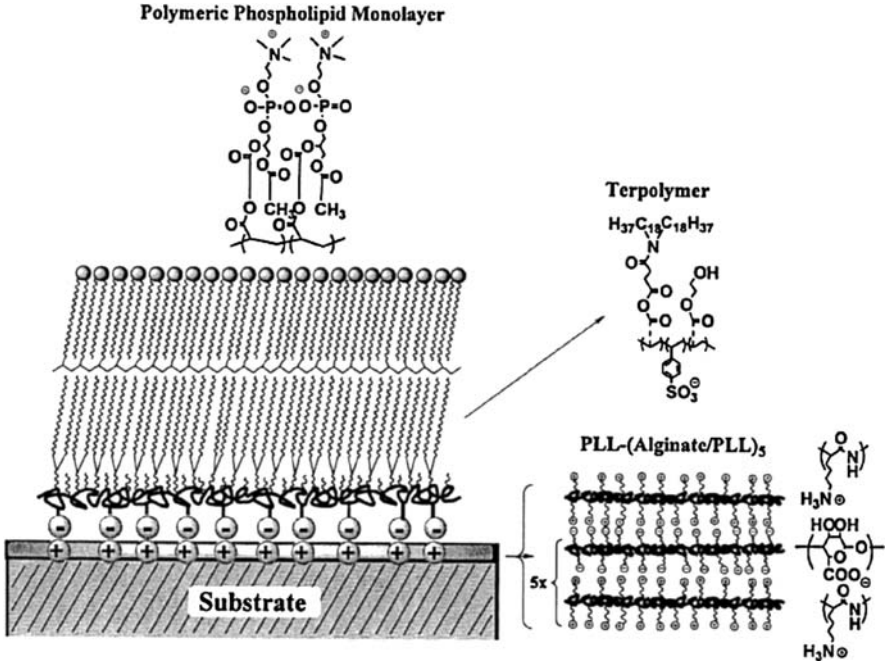

Fig. 2 Schematic representation of poly(acrylatePC) monolayer on an amphiphilic terpolymer supported on a PEM. Reprinted with permission from [66]. Copyright 2002, American Chemical Society

of fluorescently-tagged dextrans that were encapsulated in the beads. Using optimized coating conditions, the viability of encapsulated CHO cells was >90%. A subsequent study showed that the same strategy could be used to encapsulate rat pancreatic islets [67]. This work demonstrated the potential for using a poly(lipid) membrane to modulate and possibly control molecular transport to/from cells encapsulated in a hydrophilic polymer matrix. Additional studies addressed the ex vivo and in vivo biocompatibility of PEM/HBM multilayers, showing that they reduced platelet adhesion from flowing blood [68] and resisted cellular and fibrotic overgrowth when implanted in mice [69].

The outer surface of these HBMs can be functionalized by incorporating an acrylate-phosphoethanolamine (acrylatePE) into the lipid monolayer. Sun et al. [70, 71] described synthesis of acrylatePEs that were conjugated with biotin, a maleimidocaproyl group, or a fluorophore at the amino terminus of the headgroup. Fluorescent acrylatePEs mixed with acrylatePC were used to coat alginate beads, and enhanced stability characteristic of a poly(lipid) film was observed. The availability of these lipids indicates the potential for creating poly(HBM)-based materials for fluorescent tagging and biospecific labeling of cells and tissues.

In the HBMs described above, enhanced stability derives from multivalent intermolecular interactions among linear lipo-polymers in the outer monolayer, relative to the fewer number of interactions expected per monomer in an unpolymerized HBM. An alternative strategy is to link covalently the lipid tail(s) to the inner monolayer, as described by Krishna et al. [60]. They used a four-step approach to create poly(acrylatePC) coatings on silicone catheters (Fig. 3): (1) plasma polymerization of allyl alcohol on the catheter surface; (2) reaction with acryloyl chloride; (3) vesicle fusion of monoacryloyl-terminated lipids on the acryloyl functionalized

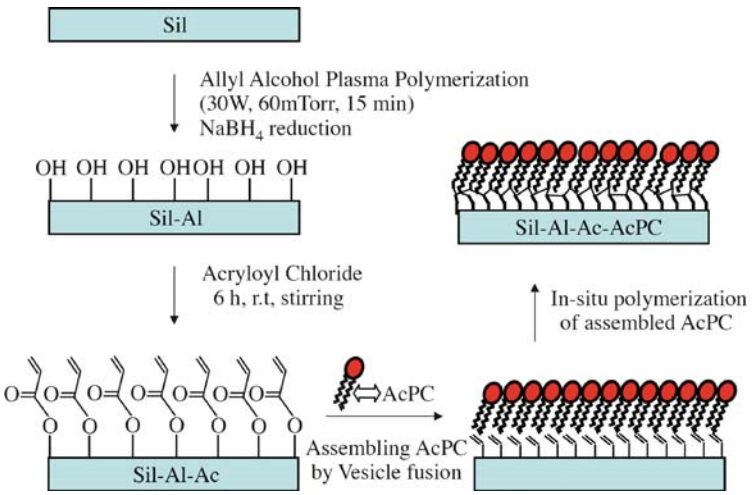

Fig. 3 Schematic illustration of the procedure for chemically grafting a polymerized lipid monolayer onto a silicon catheter surface. Reprinted with permission from [60]. Copyright 2005, Elsevier

catheter surface; (4) thermal initiation using AAPD, which should produce both intra- and intermonolayer linkages. The water contact angle of these films was 58°, significantly less than that measured for acryloyl-functionalized surfaces. These data along with XPS, scanning electron microscopy, and AFM data indicated that a lipid film was grafted onto the silicone surface. Furthermore, there was no significant change in contact angle after immersion in distilled water for 72 h, whereas physisorbed lipids were desorbed under the same conditions within a day [72]. The in vitro biocompatibility of catheter surfaces was assessed by measuring the surface coverage of adhered platelets and their morphology. Poly(lipid)-coated catheters were effective in reducing platelet adhesion relative to unmodified surfaces, suggesting that this approach may be useful for improving the blood compatibility of silicone medical devices. Similar results were achieved with an acrylated copolymer that was spin-coated onto silicon wafers prior to fusion and photopolymerization of acryloyl-lipids [72]. In a subsequent paper, HBMs modified with 10 mol% of a PEG-capped, acryloyl-terminated single chain amphiphile were described [57]. This design should further reduce protein adsorption and platelet adhesion although no evaluations of biocompatibility were reported.

2.2 Supported Lipid Bilayers

Fabricating a supported lipid bilayer in which both monolayers are composed of polymerizable lipids results in formation of a polymeric network in each monolayer. Furthermore, if the reactive groups are located at the termini of the acyl chains, the monolayers can be covalently linked, which is inherently more stable than a HBM in which lipid polymerization occurs in only one monolayer.

Some of the earliest research in poly(lipid) films and vesicles was based on bis-diacetylene-modified lipids [15, 19, 73]. Polymerization of these lipids can be readily initiated using UV light, and the polymer product can be easily detected by its visible absorbance or fluorescence. However, the efficiency of diacetylene polymerization is highly dependent on the molecular packing of the monomers. The topotactic nature of the reaction dictates that the bilayer must be in the solid-analogous (L_β) phase; thus film deposition is usually performed using the LBS technique. Incomplete conversion of monomer to polymer is a frequent problem. A consequence of incomplete polymerization is shown in Fig. 4. The AFM image and linescan were acquired on a PSLB composed of DiynePC that was deposited by the LBS technique, polymerized with UV light, removed from water, rinsed and dried [11]. The film morphology is rough with numerous defects having apparent depths of 2–6 nm. These defects were likely caused by desorption of oligomers or unreacted monomers when the PSLB was removed from water, as depicted schematically in Fig. 5.

It is important to note that the poly(DiynePC) bilayer shown in Fig. 4 was uniform in appearance when it was viewed by optical microscopy at a magnification of 400×. This comparison illustrates that assessment of defect density in a supported

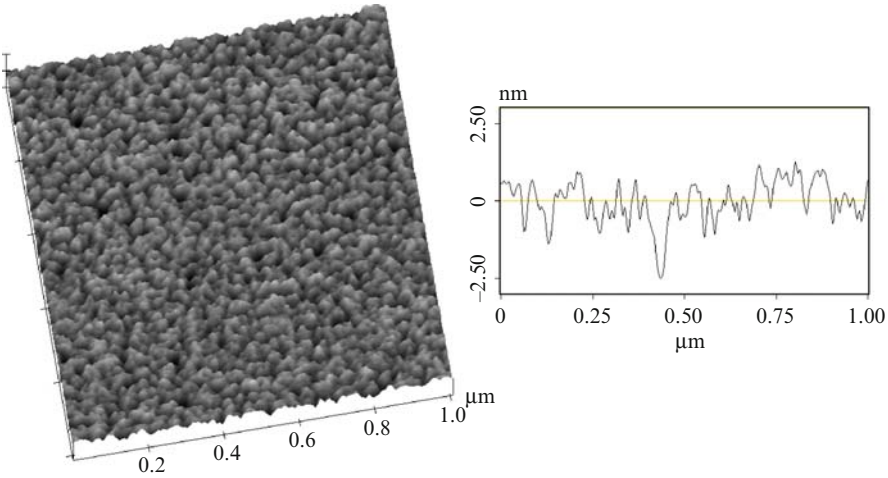

Fig. 4 AFM image and line scan of a dried poly(Diyne) PSLB deposited by the LBS technique and polymerized by direct UV irradiation for 1 h. The image area is $1 \times 1\ \mu m^2$ with a height scale of 5 nm

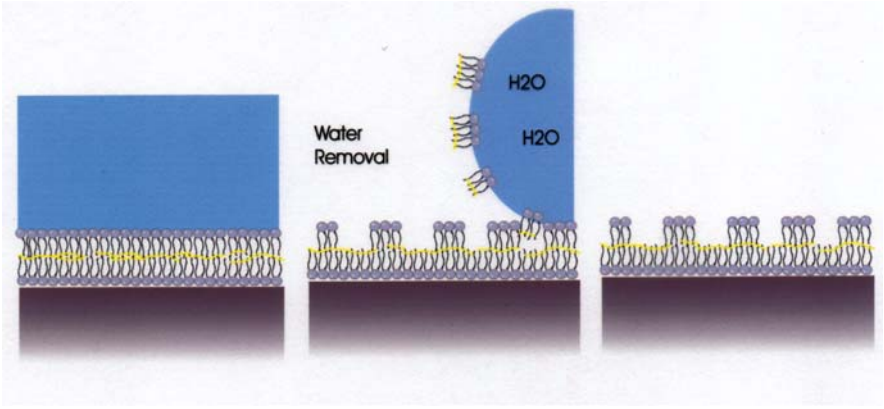

Fig. 5 Schematic of desorption of unreacted monomers and/or oligomers when a polymerized PSLB is rinsed and dried. This process creates defects that expose the hydrophobic core of the bilayer

poly(lipid) film depends on the measurement technique used and demonstrates the power of AFM for characterizing poly(PSLB) structure and defect density on submicron length scales.

In contrast to diacetylenes, lipids with alkene-functionalized chains (e.g., acryloyl, dienoyl) can be polymerized in the L_α phase to a high degree of conversion [74]. O'Brien and coworkers systematically studied polymerization of acryloyl and dienoyl lipids in bilayer vesicles (see [25, 26] for reviews). Subsequently, the Saavedra and O'Brien groups prepared and characterized solid supported bilayers composed of dienoyl lipids (Fig. 6) [11, 75–77]. Several parameters relating

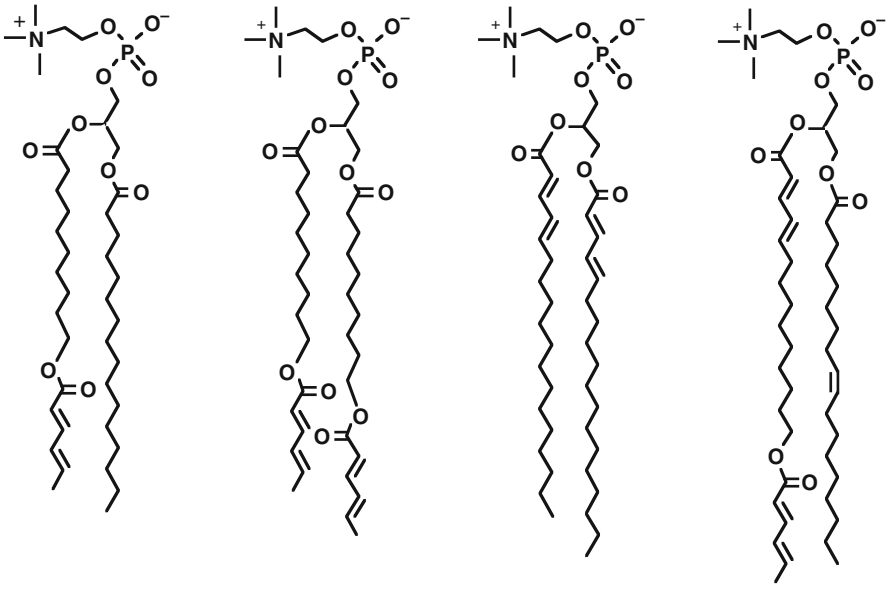

Fig. 6 Structures of some polymerizable dienoyl lipids. Reprinted with permission from [11]. Copyright 2003, American Chemical Society

poly(PSLB) structure and stability to observations made in studies of polymerized bilayer vesicles were examined, including comparisons of UV- and redox-initiated radical polymerization, the number and location of the polymerizable moieties in the lipid monomer, and deposition using either the LBS technique or vesicle fusion.

Some conditions were found to be particularly effective in producing highly uniform, extremely stable PSLBs [11]. For example, SUVs composed of bis-SorbPC (Fig. 6) were fused to silica or glass substrates and then redox polymerized. After rinsing and drying, these films have an ellipsometric thickness of 46 Å, consistent with that expected for a bis-SorbPC bilayer. AFM revealed a very low density of defects, as illustrated by a comparison of images of poly(bis-SorbPC) (Fig. 7) to poly(DiynePC) (Fig. 4). The sessile, advancing, and receding water contact angles of poly(bis-SorbPC) PSLBs are 32°, 37°, and 8°, respectively [11]. These values are very close to those reported for a PC-based SAM on Au [78] and, along with the data obtained on less-uniform PSLBs (see below), indicate that a well-ordered film of PC groups has a sessile water contact angle of less than 40°. It is notable that contact angles reported for poly(lipid) HBMs are significantly higher than 40° [36, 56, 60, 63]. A higher contact angle is indicative of a greater density of defects that expose the hydrophobic interior of the lipid film to the ambient environment, and the defect density reflects the relative stability of the film [11]. Thus the higher contact angles reported for linearly polymerized HBMs are consistent with the expectation that linear lipo-polymers should be less stable than cross-linked lipo-polymers.

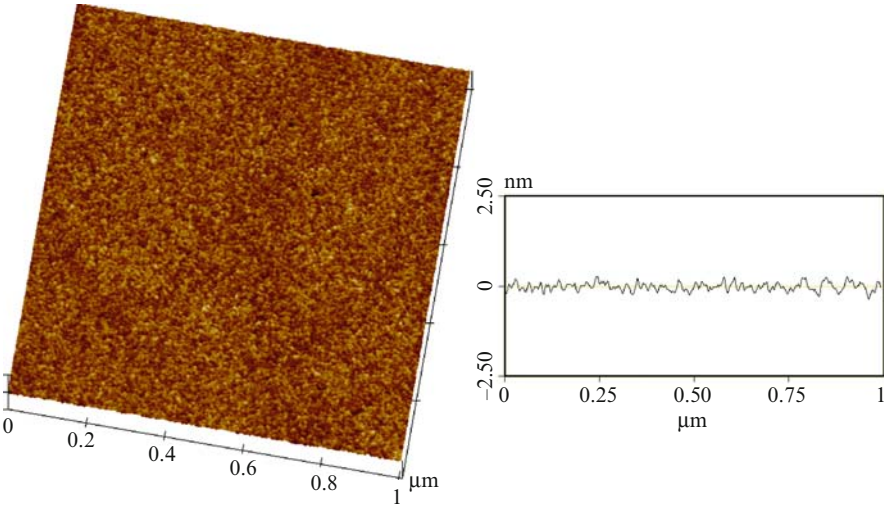

Fig. 7 AFM image and line scan of a dried poly(bis-SorbPC) PSLB deposited by the vesicle fusion and polymerized using redox initiation. The image area is $1 \times 1\ \mu m^2$ with a height scale of 5 nm

Despite the absence of a covalent tether between the membrane and the underlying substrate, redox polymerized poly(bis-SorbPC) PSLBs are remarkably inert to conditions that disrupt unpolymerized lipid bilayers [11]. No change in ellipsometric thickness was observed after repeated drying/rehydration or immersion in surfactants and organic solvents. Insolubility is attributed to a high degree of cross-linking coupled with multivalent interactions between polymer segments and the substrate surface.

It is well established that the PC lipid films are highly resistant to nonspecific protein adsorption [76, 79]. Ross et al. [76] examined the effects of polymerization of dienoyl PC lipids on their protein resistance using AFM and TIRF microscopy to measure the surface coverage of adsorbed BSA. Even after drying and rehydration or exposure to organic solvents or surfactants, redox polymerized bis-SorbPC PSLBs exhibited resistance to BSA adsorption equivalent to a fluid PSLB composed of POPC. Since cross-linking polymerization effectively eliminates lateral lipid diffusion, these results establish that fluidity is not required for a PC lipid bilayer to be protein resistant [79]. This work also demonstrated that measuring nonspecific protein adsorption is a useful method to assess defect density in PC lipid films.

Redox polymerization of fused bilayers composed of DenSorbPC (Fig. 6) also produced highly uniform and stable PSLBs [11]. Most of the other sets of conditions investigated (lipid structure, deposition method, and polymerization method) yielded PSLBs that contained a moderate density of defects after drying [11, 75]. These films were typically thinner and had higher contact angles than redox polymerized poly(bis-SorbPC). For example, UV-initiated polymerization of bis-SorbPC films deposited by vesicle fusion generated dried PSLBs with a

thickness of 28 Å and sessile, advancing, and receding water contact angles of 59°, 70°, and 16°, respectively [11]. Subsequent XPS and ToF-SIMS studies confirmed that these films were less structurally intact than the corresponding redox polymerized films [80]. The defects appear to be formed when unreacted monomers and/or oligomers are desorbed from the film as it is passed through the air/water interface, which generates a thinner film with a more hydrophobic surface (depicted in Fig. 5). In vesicles, UV-initiated polymerization predominately generates oligomers that are less stable to surfactant solubilization [13, 81], and it is assumed that this trend extends to PSLBs. A significant increase in nonspecific protein adsorption on UV polymerized PSLBs that had been dried and rehydrated confirmed that the defects appeared only after removal from water [76].

PSLBs were also prepared using bis-DenPC (Fig. 6) [11]. However, redox polymerization produced films that were less stable and more defective than poly(bis-SorbPC) films [11]. A possible explanation for this finding is that the two reactive groups in bis-DenPC are adjacent to the glycerol backbone. In contrast, DenSorbPC and bis-SorbPC have one and two polymerizable moieties located near the acyl termini, respectively; thus, it is possible that cross-linking occurs between the two monolayers in poly(PSLBs) composed of these lipids. Such cross-linking is unlikely to occur in poly(bis-DenPC) PSLBs. Ratnayaka et al. [82] addressed this topic by preparing HBMs composed of a monolayer of poly(bis-SorbPC) on OTS. Although cross-linking the outer lipid layer stabilized the HBM to drying, these films invariably contained a higher density of defects than poly(bis-SorbPC) PSLBs prepared under similar conditions by Ross et al. [11]. This difference is attributed to intermonolayer cross-linking, which can take place in a symmetric bis-SorbPC bilayer but cannot in an HBM.

Although intermonolayer cross-linking appears to impart a high degree of stability to a PSLB, it also severely attenuates the lateral diffusion of membrane constituents. In an effort to create lipid bilayers with intermonolayer linkages that accommodate lateral lipid mobility, Halter et al. [83] synthesized lipids with reactive groups at their acyl chain termini (see structures in Fig. 8). Complementary pairs of these molecules, when assembled into adjacent monolayers, react to form covalently bonded dimers that span the bilayer. This strategy is inspired by the structure of membrane-spanning bolaamphiphiles found in the membranes of archaebacteria that live in extreme environments [84].

Asymmetric PSLBs composed of 1,2-dimyristoyl-*sn*-glycero-3-phosphocholine (DMPC) and varying mole fractions of these lipids were deposited using the LBS technique (e.g., bilayers were composed of inner and outer monolayers of DMPC/acrylatePC and DMPC/SH-DPPC (Fig. 8), respectively). Two-dimensional electrophoresis monitored by fluorescence microscopy was used to measure lateral diffusion coefficients in PSLBs as a function of the mole fraction of reactive lipids in each monolayer. Bilayers containing 15 mol% of reactive lipids were fluid, but at 25 mol% or greater, they were immobile, suggesting that these synthetic bolaamphiphiles aggregate and present obstacles to lateral diffusion. Stability assessments were not reported.

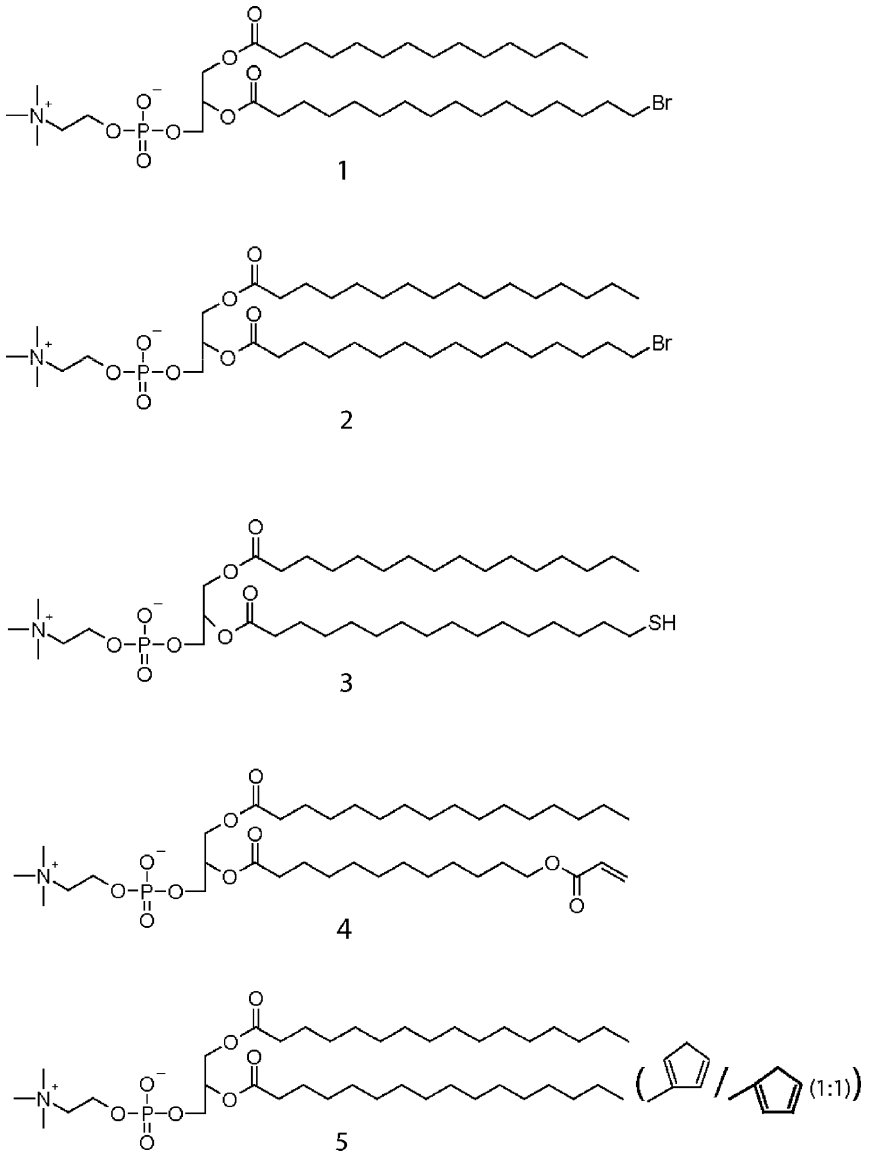

Fig. 8 Lipids designed to form intermonolayer covalent dimers: (1) Br-MPPC, (2) Br-DPPC, (3) SH-DPPC, (4) acrylatePC, and (5) CPD-PC. Reactive pairs are 1 + 3, 2 + 3, 3 + 4, 4 + 5. Reprinted with permission from [83]. Copyright 2004, American Chemical Society

2.3 Patterned Poly(Lipid) Films

High density, spatially addressable arrays of planar supported membranes have significant potential in high throughput bioanalytical applications, including screening

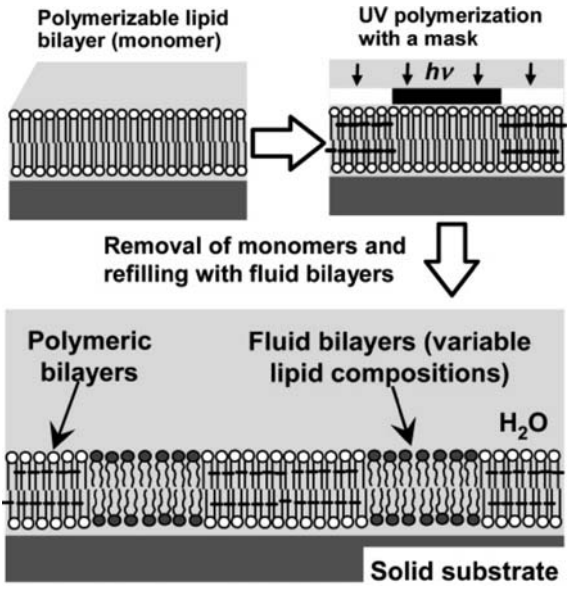

Fig. 9 Schematic of the procedure used by Morigaki and coworkers to create an array of fluid PSLB patches bounded by polymerized DiynePC. Reprinted with permission from [92]. Copyright 2007, American Chemical Society

for pharmaceuticals that target membrane-associated proteins [85–87]. Photolithography can be used to create micropatterns in supported bilayers of photopolymerizable lipids. In a series of papers [88–93], Morigaki and coworkers described preparation and characterization of composite PSLBs in which fluid lipid corrals are bounded by polymerized DiynePC. The PSLB is deposited using the LBS technique followed by UV-initiated polymerization through a mask to create a pattern of unpolymerized lipids and cross-linked poly(lipid) (Fig. 9). After rinsing away the monomers with organic solvent or surfactant, SUVs of a fluid lipid are then fused to form fluid bilayers on the bare regions of the substrate. Fluorescence micrographs in Fig. 10 illustrate the lateral organization of the composite membrane. Detailed studies of the fusion process by TIRF microscopy and quartz crystal microgravimetry indicate that the energetically unfavorable open edges of the poly(lipid) corrals catalyze the formation of the array by destabilizing adsorbed SUVs [91]. This finding suggests that the fluid lipid patches are stabilized by their interactions with the poly(lipid) corrals.

The temperature at which the Langmuir monolayers of DiynePC are formed and transferred to the substrate was found to affect significantly the homogeneity and defect density of the polymerized PSLB [92]. This result may explain the heterogeneous morphology of poly(DiynePC) PSLBs reported in previous papers [11, 89] and illustrated by the AFM data in Fig. 4. Varying the period of UV irradiation can be used to control the extent of polymerization in these composite membranes [90]. Vesicle fusion is used to incorporate monomeric lipids into partially polymerized regions which consist of poly(DiynePC) domains that likely act as barriers to restrict diffusion. This process can be used to create novel patterns such as a semipermeable

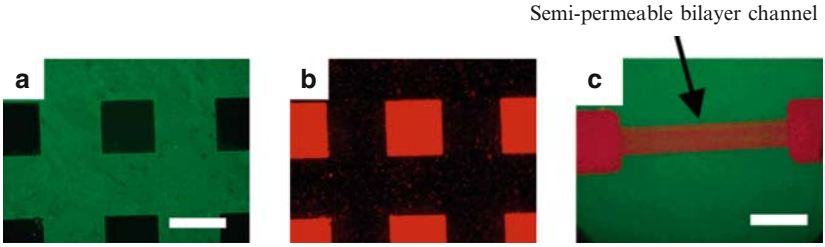

Fig. 10 Fluorescence microscopy images. **a** A photolithographically patterned poly(DiynePC) PSLB. The *darker squares* were blocked from UV illumination by the mask. The polymerized grid is fluorescent and thus appears brighter due to the highly conjugated polymer backbone. **b** A patterned PSLB composed of poly(DiynePC) (*darker grid*) and egg PC doped with Texas Red 1,2-dihexadecanoyl-*sn*-glycero-phosphoethanolamine (TR-PE) that was fused into square areas after removal of unpolymerized DiynePC. **c** A semipermeable bilayer channel (*lighter red*) that connects two fluid lipid bilayer corrals (*darker red*). The channel was created by polymerizing DiynePC with 40% of the UV light dose compared with the surrounding poly(DiynePC) area (*green*), then backfilling the unpolymerized regions with egg PC doped with TR-PE, The *scale bars* are 50 µm. Reprinted with permission from [90]. Copyright 2004, American Chemical Society

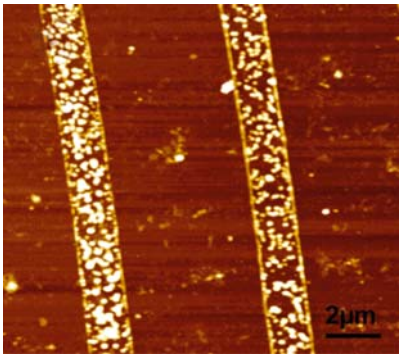

Fig. 11 Tapping mode AFM image of polymerized vesicle stripes deposited on glass substrates with µCP. Reprinted with permission from [94]. Copyright 2005, American Chemical Society

(i.e., less fluid) channel connecting two fluid corrals (Fig. 10). These results suggest the possibility of creating partially polymerized PSLBs that function as size- and shape-dependent separation media.

Microcontact printing (µCP) is a technically simple method to create supramolecular patterns on planar substrates. Fang and coworkers used µCP to deposit poly(DiynePC) vesicles in patterns onto glass slides (Fig. 11) [94]. The vesicles remained firmly adsorbed even after immersion in buffer for 2 days. One-dimensional lines and three-dimensional patterns were also adsorbed on glass using microfluidic delivery. These soft lithographic techniques could potentially be used to create substrate-supported microarrays of functionalized vesicles (e.g., vesicles that encapsulate molecular cargo and/or display membrane-bound ligands – see below) for numerous applications, such as biosensing and charge storage.

Aspinwall and coworkers have developed methods to create three-dimensional patterns of composite fluid and poly(lipid) bilayers in fused silica separation

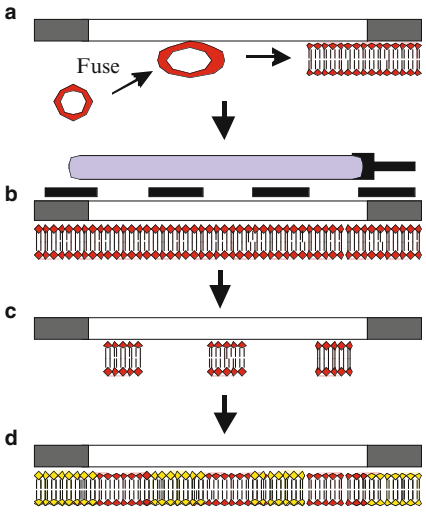

Fig. 12 Schematic representation of polymerized lipid patterning in a capillary. **a** SUVs prepared using bis-SorbPC are fused to the inner capillary surface to create a uniform supported bilayer. **b** The bilayer is polymerized via UV irradiation through a photomask placed over the capillary. **c** Unpolymerized lipid is removed from the capillary to yield a poly(lipid) pattern. **d** SUVs composed of other lipids are then fused into the bare silica regions between poly(bis-SorbPC) structures, generating chemically functionalized patterns. Reprinted with permission from [96]. Copyright 2007, American Chemical Society

Fig. 13 Fluorescence images of 50 and 10 μm inner diameter capillaries patterned with alternating segments of poly(bis-SorbPC) and 1:50 (mol/mol) Rhodamine-capped DPPE:DOPC. Reprinted with permission from [96]. Copyright 2007, American Chemical Society

capillaries [95, 96]. The process is depicted schematically in Fig. 12. Bis-SorbPC SUVs are fused on the inner wall of the capillary and polymerized using UV irradiation through a mask, generating a bar code-like pattern of fluid and polymerized segments. The unpolymerized lipid monomers can be removed and replaced by fusion of SUVs of a different composition, allowing the patterns to be visualized by fluorescence microscopy (Fig. 13). Patterns were produced in capillaries with an inner diameter down to 10 μm, which provides a very high ratio of bilayer surface area to volume of the contacting solution. Nonspecific protein adsorption to poly(bis-SorbPC)-coated capillaries was greatly attenuated compared to bare capillaries, consistent with prior evaluations [76]. The patterns are extraordinarily stable; no change was observed after exposure to chloroform, Triton X-100, or dry storage in excess of a year. Bioanalytical applications of these arrays can be realized by introducing functionalized lipids into the fluid bilayer segments, as described below in Sect. 4.

3 Polymerized Black Lipid Membranes

A free standing planar bilayer suspended across an aperture between two aqueous compartments, known as a BLM, is another geometry that has been widely used as a model for cell membranes [50, 97]. In contrast to substrate supported bilayers and vesicles, the BLM has the advantage of allowing direct access to both sides of the membrane. Thus BLMs have been widely used to perform electrochemical measurements of transmembrane ion and molecular transport, particularly transport mediated by reconstituted ion channel proteins. A significant disadvantage of BLMs is that they are very unstable, with rupture usually occurring within a few hours after formation [50, 97]. Development of methods to stabilize BLMs could open the way for their use in biosensing platforms for drug screening applications.

Lipid polymerization as an approach to stabilization of BLMs was pioneered by Benz et al. [98]. In two more recent papers, the UV-initiated polymerization of diacetylenic lipids was examined as a strategy for creating BLMs with enhanced stability as well as compatibility with incorporated membrane proteins. Both Shenoy et al. [99] and Daly et al. [100] reported that high impedance BLMs could be formed using a monofunctional lipid, PTPE (Fig. 14a), either pure or mixed with DiPhyPC. BLMs could not be formed reliably using bis-diacetylenic lipids (e.g., DiynePC), which may be attributable to phase segregation (the main phase transition temperature of DiynePC is near 40°C [92]). The high impedance of PTPE-based BLMs was maintained after polymerization, and the average lifetime before rupture of equimolar PTPE/DiPhyPC bilayers increased from 12.6 to 30.7 min [100].

The function of channel-forming proteins in these BLMs was also examined. α-Hemolysin could be reconstituted into pure PTPE BLMs and its ionic conductance was maintained after UV polymerization, although it was unclear whether a high conversion of monomer to polymer was achieved [99]. Gramicidin was inserted into equimolar PTPE/DiPhyPC BLMs that were subsequently UV irradiated [100]. Channel activity was observed in the polymerized membrane (Fig. 14c) showing that it was still fluid, which is a requirement for gramicidin to dimerize. Retention of fluidity is not surprising given the high DiPhyPC content of the membrane and that PTPE forms linear polymers; in fact, polymerization-induced phase segregation [26] with gramicidin concentrated in DiPhyPC domains may explain the observed increase in channel frequency after polymerization. Overall, these studies show that lipid polymerization is a promising approach to improve the stability of BLMs while maintaining their high impedance and compatibility with incorporated ion channels. However, polymerization of diacetylenes produces rather stiff polymers, which may not be the best choice for this application. In contrast, poly(dienes) are rubber-like materials [26] that may be better suited to the requirements of a poly(BLM) stated above.

Meier et al. [101] employed a different approach in which a BLM is formed from a mixture of nonpolymerizable lipids and water-insoluble, nonlipid monomers (styrene and divinylbenzene). After UV-initiated polymerization to produce a two-dimensional, cross-linked network in the membrane, its stability was enhanced as

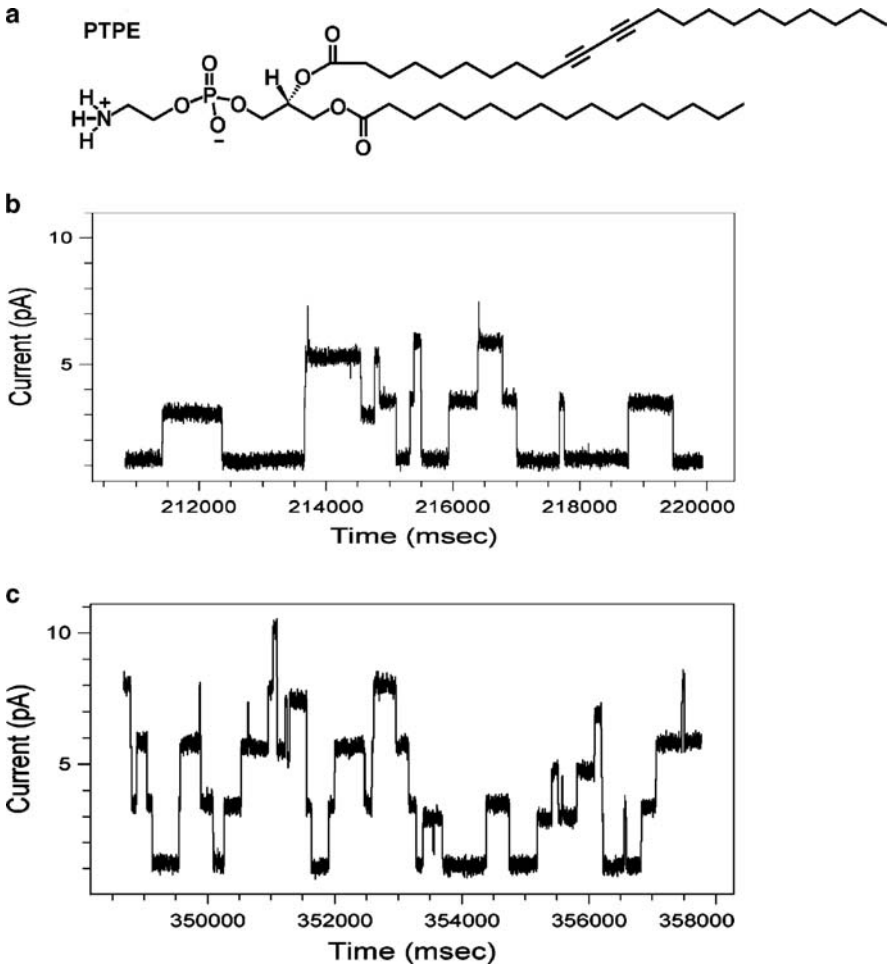

Fig. 14 **a** Structure of PTPE. **b,c** Ion transport through gramicidin channels inserted into an equimolar DiPhyPC/PTPE BLM **b** before irradiation and **c** after irradiation. Reprinted with permission from [99] (copyright 2005, American Chemical Society) and [100] (copyright 2006, American Chemical Society)

assessed by a significant increase in the voltage required to cause membrane rupture. However, after rupture the defect(s) resealed, showing the membrane fluidity was maintained.

4 Poly(Lipid) Vesicles

Lipid bilayer vesicles (liposomes) are generally grouped into three size regimes: giant (1 μm or larger), large (100 nm–1 μm), and small (less than 100 nm) [1, 7]. Giant vesicles are large enough to be studied individually via optical microscopy.

Large and small vesicles are more frequently studied as dispersed ensembles due to their ease of preparation and compatibility with solution phase analytical/physical methods. Lipid polymerization yields vesicles with enhanced stability to surfactants, organic solvents, dehydration, and heat [26]. Polymerization also alters membrane permeability to ions and molecules. These unique properties have spawned development of stable nanocapsules, bioreactors, and sensors. Many if not most of the liposomal architectures, methods to stabilize them, and technological applications discussed below have evolved from earlier pioneering work by many research groups. The reader is referred to previous key reviews [3, 26, 28].

4.1 New Types of Reactive Lipids and Polymerized Vesicles for Molecular Storage and Delivery

Most UV-polymerizable lipids are also sensitive to visible light, a problem that makes their synthesis and handling more difficult. Stanish and Singh [102] synthesized 1,2-bis(trideca-12-ynoyl)-*sn*-glycero-3-phosphocholine ($DC_{10}PC$; Fig. 15), a lipid having acyl chains terminated with acetylenic groups. $DC_{10}PC$ vesicles are in a fluid phase at room temperature and do not readily undergo polymerization in white light. Vesicles could be polymerized by γ-irradiation and retained their size, shape, and dispersity for several months, indicating their potential for long term storage of encapsulated molecules.

Liu and O'Brien [12] prepared extremely stable unilamellar vesicles from two different cross-linkable lipids, 1-palmitoyl-2-[14-acryloxy-2,4-tetradecadienoic]-*sn*-glycerol-3-phosphocholine (Fig. 16) and DenSorbPC (Fig. 6). Light scattering measurements showed that after redox-initiated radical polymerization, both types of vesicles were stable to the addition of 12 molar equivalents of Triton X-100

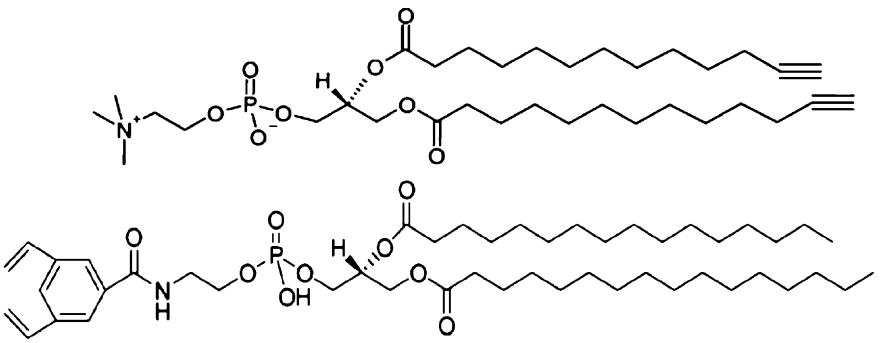

Fig. 15 *Upper*: $DC_{10}PC$ (1,2-bis(trideca-12-ynoyl)-sn-glycero-3-phosphocholine). Reprinted with permission from [102]. Copyright 2001, Elsevier. *Lower:* DPPE-DVBA (1,2-dipalmitoyl-*sn*-glycero-3-phospho-*N*-(2-hydroxyethyl)-3,5-divinylbenzamide). Reprinted with permission from [103]. Copyright 2003, American Chemical Society

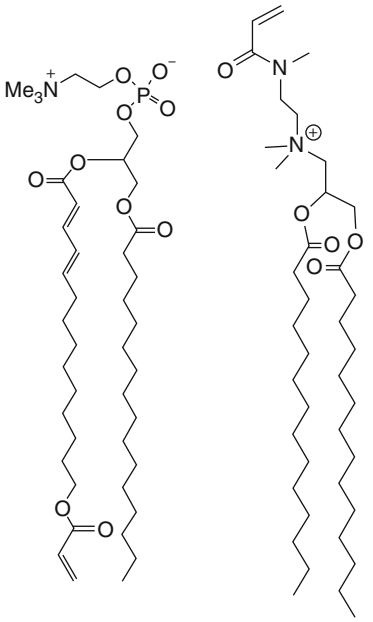

Fig. 16 *Left*: Acryl/DenPC$_{16,18}$ (1-palmitoyl-2-[14-acryloxy-2,4-tetradecadienoic]-*sn*-glycerol-3-phosphocholine). Reprinted with permission from [12]. Copyright 2002, American Chemical Society. *Right*: Polymerizable acrylamide cationic lipid. Reprinted with permission from [104]. Copyright 2001, American Chemical Society

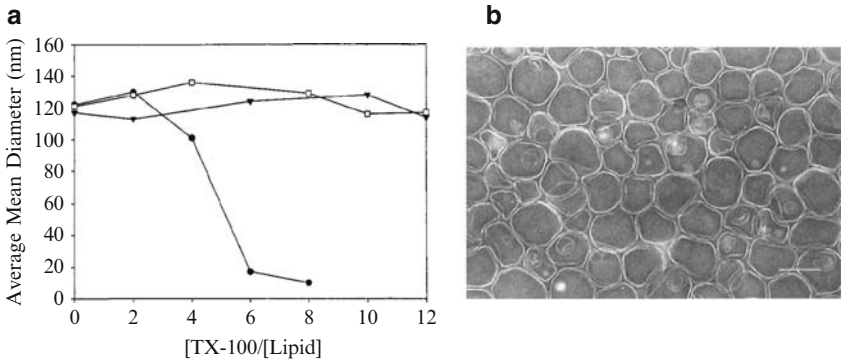

Fig. 17 **a** Mean diameters of lyophilized and redispersed vesicles of poly(DenSorbPC) (*triangles*) as a function of added equivalents of Triton X-100 at 25°C. Both monomeric (*circles*) and polymerized (*squares*) vesicles of the same lipid before lyophilization and redispersion are shown for comparison. **b** TEM images of poly(Acryl/DenPC$_{16,18}$) vesicles. Reprinted with permission from [12]. Copyright 2001, American Chemical Society

(Fig. 17a). After freeze-drying, vesicles could be rehydrated and redispersed, a process aided by incorporation of either a negatively charged lipid (e.g., 1,2-diacyl-*sn*-glycero-3-phosphatidic acid) or a hydrophilic polymer such as PEG. TEM images of lyophilized vesicles showed conformal contact between neighboring partially collapsed vesicles (Fig. 17b), demonstrating their permeability to water and

their elastomeric character (i.e., they are not hard spherical objects). The capability to lyophilize vesicles for storage and then quantitatively recover them increases their shelf life and hence their utility as carriers.

Lawson et al. [103] synthesized 1,2-dipalmitoyl-*sn*-glycero-3-phosphoethanolamine (DPPE) and 1,2-dilauryl-*sn*-glycero-3-phosphoethanolamine containing the 3,5-divinylbenzoyl moiety linked to the PE headgroup. Divinylbenzene polymerizes quickly and efficiently at room temperature, which is an important consideration when encapsulating labile species such as enzymes in vesicles. DPPE–DVBA (Fig. 15) vesicles were polymerized in only 5 min using 254 nm irradiation in the presence of the radical initiator AAPD. Cross-linked vesicles could be redispersed in water following freeze-drying and exposure to 95% ethanol. Phosphotriesterase was entrapped in DPPE–DVBA vesicles and maintained 52% of its original activity (hydrolysis of methyl parathion) after polymerization. In a subsequent study, organophosphorous hydrolase (OPH) stabilized in trehalose was encapsulated in poly(DPPE–DVBA) vesicles that were freeze-dried and then redispersed in buffer [105]. The OPH specific activity was about 80% of that measured before freeze-drying; however, the relative activity dropped to 18% after storage for 3 weeks at room temperature.

Cationic vesicles typically used for DNA delivery often self-aggregate or bind to plasma proteins in vivo. Wu et al. [104] attempted to improve vesicle stability using a cationic lipid with a cross-linkable acrylamide attached to the headgroup (Fig. 16). Vesicles were polymerized using thermal initiation with AAPD. Compared to monomeric vesicles, polymerized vesicles were less cytotoxic, more resistant to aggregation in serum, and comparable in transfection activity using a vector encoding firefly luciferase.

Nakano's group has explored the potential of poly(lipid) vesicles with encapsulated hemoglobin (Hb) as artificial substitutes for red blood cells [106]. For this application, the need for stability during preparation and storage must be balanced against the requirement for in vivo biodegradation to prevent accumulation in the liver and spleen, possibly leading to toxic side effects. Mixed vesicles composed of cholesterol, stearic acid, either bis-DenPC (Fig. 6) or 1-acyl-2-[(2E,4E)-octadecadienoyl]-*sn*-glycero-3-phosphocholine (mono-DenPC), and in some cases DPPC, were polymerized using γ-irradiation, which rendered them stable in size, with negligible Hb leakage, through repetitive freeze–thaw cycles. However, intravenously injected vesicles containing poly(bis-DenPC) persisted in rat spleens after 30 days. Vesicles composed of poly(mono-DenPC)/DPPC/cholesterol/stearic acid had poorer Hb retention but degraded much more rapidly in vivo, indicating that this lipid composition is a better choice as a blood substitute.

Liposomes can be sterically stabilized by coating them with PEG groups, a strategy that significantly increases their retention in vivo by masking them from the liver and the immune system [107]. However, PEG surface coatings can also interfere with the targeted release of encapsulated cargo. A potentially powerful strategy is to target a masked liposome to a specific site in vivo (e.g., at a tumor), then trigger an increase in membrane permeability, causing localized release of the cargo.

Spratt et al. [108] investigated polymerization-induced phase segregation as a mechanism for triggered release from vesicles composed of polymerizable and nonpolymerizable lipids. A typical vesicle composition was bis-SorbPC, 1,2-distearoyl-*sn*-phosphatidylcholine (DSPC), and a small mole fraction of a PE-Gylated lipid (PEG2000–1,2-distearoyl-*sn*-phosphatidylethanolamine) to prevent liposome fusion. A short period of UV irradiation caused large increases in the leakage rate of an entrapped dye, by factors ranging from a few hundred up to 28,000, which likely occurred due to contraction of bis-SorbPC domains upon cross-linking, opening defects in the membrane (Fig. 18). However, since it is not feasible to use UV irradiation to trigger release in vivo, other more biocompatible methods of polymerization must be implemented to make this approach clinically useful.

The storage and reactivity of electroactive molecules in polymerized diacetylene vesicles was the subject of studies reported by Stanish, Singh, and coworkers [109, 110]. They entrapped ferricyanide in large unilamellar vesicles of photopolymerized $PC_{8,9}PC$ (1-palmitoyl-2-(tricosa-10,12-diynoyl)-*sn*-glycero-3-phosphocholine). Cyclic voltammetry was used to demonstrate that the ferricyanide was electrochemically isolated by the poly(lipid) bilayer [110]. At pH 7 and 25°C, an anomalously long half-life of 2.4 weeks was calculated for $Fe(CN)_6^{3-}$ retention in polymerized vesicles. In a subsequent study [109], vesicles with entrapped ferricyanide were prepared from 2-bis(10,12-tricosadiynoyl)-*sn*-glycero-3-phosphatidylcholine ($DC_{8,9}PC$) doped with a disulfide-capped lipid (*N*-3-(pyridyl-2-dithio)propionyl-2-

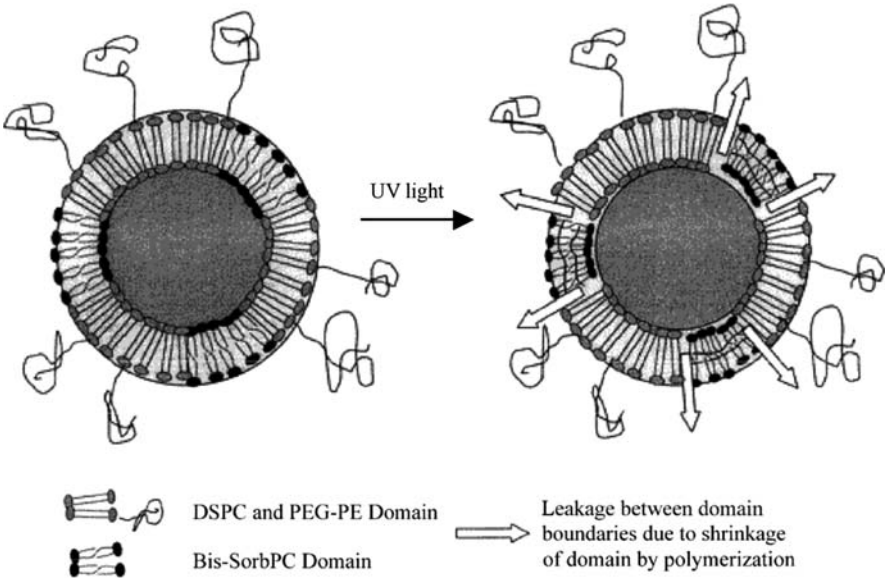

Fig. 18 Schematic cross-section of PEG-liposomes composed of domains of bis-SorbPC and stearoyl lipids. The photopolymerization-induced reduction in the surface area of the bis-SorbPC domains (*black areas*) during UV irradiation is shown on the right. Reprinted with permission from [108]. Copyright 2003, Elsevier

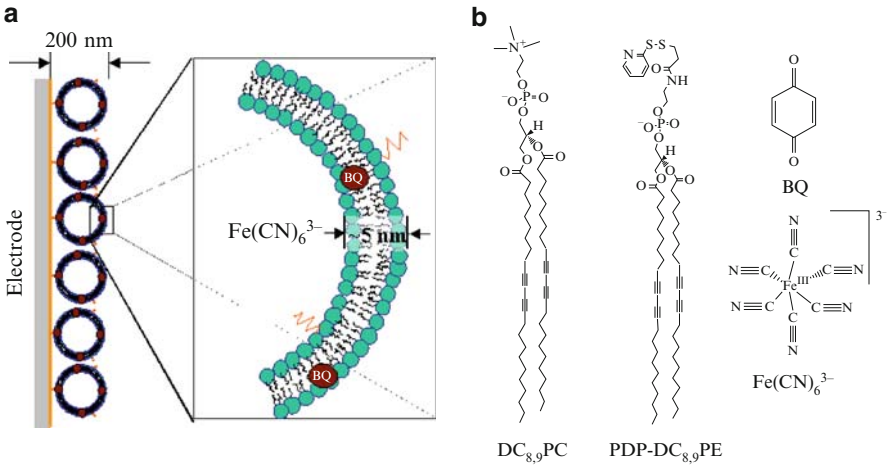

Fig. 19 **a** Schematic (not drawn to scale) of polymerized electroactive vesicles tethered to a gold electrode via mercaptoethyl tethers. Electrons flow reversibly from the electrode to the entrapped electron acceptor ($Fe(CN)_6^{3-}$) shuttled by an electron mediator (BQ) which also transports protons to maintain electrical neutrality. **b** Chemical structures of polymerizable $DC_{8,9}PC$ (major component) and PDP–$DC_{8,9}PE$ (minor component) lipids and electroactive components incorporated within the vesicle core ($Fe(CN)_6^{3-}$) and membrane (BQ). Reprinted with permission from [109]. Copyright 2004, American Chemical Society

bis(10,12-tricosadiynoyl)-*sn*-glycero-3-phosphatidyethanolamine, PDP-$DC_{8,9}PE$; Fig. 19b). The disulfide moiety was used to immobilize vesicles on a gold electrode (Fig. 19a). The electrochemical activity of ferricyanide was minimal until a lipophilic electron shuttle molecule, 1,4 benzoquinone (BQ), was added to the system. The voltammetry data were interpreted as evidence that BQ partitioned into the bilayers of immobilized vesicles and mediated the electrochemical reduction of entrapped ferricyanide. In a subsequent paper, this group created a simple battery that was capable of being discharged and recharged multiple times [111]. Collectively these studies illustrate the potential of poly(diacetylenic lipid) nanocapsules as an electrochemically active charge storage medium.

4.2 Vesicles Stabilized by Formation of Nonlipid Polymer Networks

One of the strategies described in Sect. 3 for BLM stabilization, mixing water-insoluble, nonlipid monomers with nonpolymerizable lipids, has also been applied to liposomes. Meier and coworkers [21] created stabilized, nanoscale bioreactors (Fig. 20) by incorporating OmpF, a channel-forming protein, into POPC vesicles to provide for passive transmembrane transport of low molecular weight compounds. β-Lactamase was entrapped during liposome formation, followed by addition of

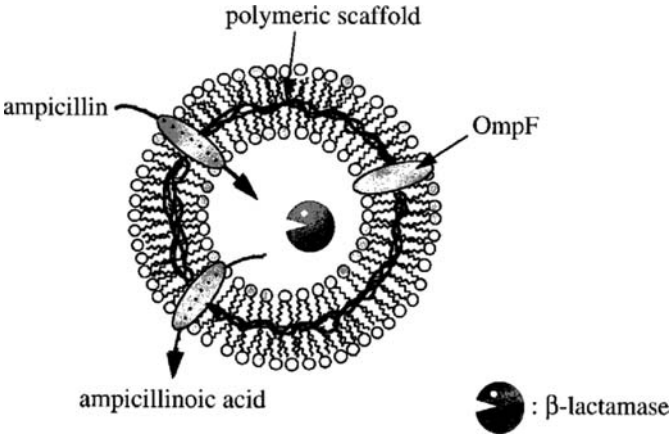

Fig. 20 Diagram of polymer-stabilized nanoreactor with encapsulated enzyme. Reprinted with permission from [21]. Copyright 2001, American Chemical Society

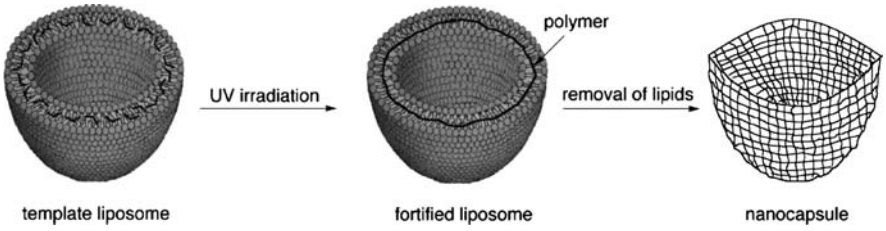

Fig. 21 Scheme of nanocapsule formation. The template liposome with homogeneously distributed monomers is irradiated with UV light, resulting in the formation of a fortified liposome. After lipid removal, the 2D polymer network constitutes an intact hollow nanocapsule. Reprinted with permission from [112]. Copyright 2006, American Chemical Society

BMA and EGDMA monomers and UV-initiated polymerization to generate a cross-linked poly(methacrylate) network in the POPC bilayer. The substrate, ampicillin, diffused into liposomes through the OmpF channels and was converted to ampicillinoic acid. Thus a polymer-stabilized, vesicle-sized bioreactor with selective permeability was created, allowing for retention of the enzyme and ingress/egress of substrate and product.

Gomes et al. [112] used a similar strategy to create spherical polymer shells (Fig. 21). Egg PC vesicles were used as templates for polymerization of membrane-incorporated, hydrophobic monomers (either BMA or hydroxyethyl methacrylate), EGDMA as a cross-linker, and a photoinitiator. The type of monomer, the ratio of lipid/monomer/cross-linker/photoinitiator, and the preparation procedures were varied to identify conditions that produced spheres that retained their monodisperse size and shape even after the template lipid was extracted with Triton X-100.

Cheng et al. [113] used nonlipid monomers to increase the stability of poly(bis-SorbPC) vesicles. EGDMA and DEAP, a photoinitiator, were mixed with

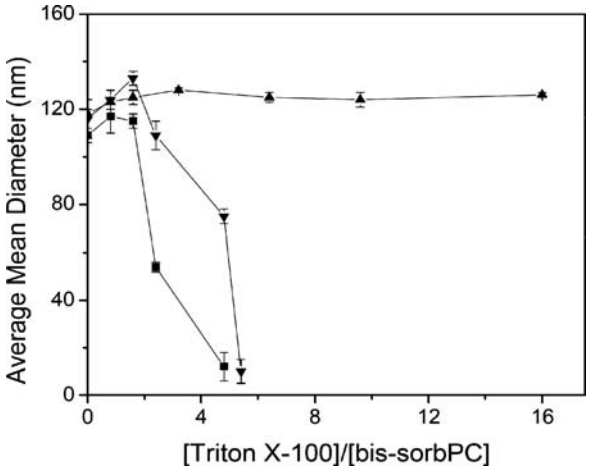

Fig. 22 Mean diameter of vesicles measured by dynamic light scattering as a function of added molar equivalents of Triton X-100. Polymerized bis-SorbPC/EGDMA *(filled triangles)*, unpolymerized bis-SorbPC/EGDMA *(filled squares)*, and polymerized bis-SorbPC *(inverted filled triangles)*. Reprinted with permission from [113]. Copyright 2006, American Chemical Society

bis-SorbPC and polymerized with UV light. These vesicles were more stable to Triton X-100 solubilization than poly(bis-SorbPC) vesicles lacking EGDMA (Fig. 22). UV polymerization of sorbyl lipid vesicles generates oligomers with marginal stability to surfactant solubilization [13, 81]; the addition of EGDMA apparently increases the extent of lipid cross-linking. Polymerized EGDMA/bis-SorbPC vesicles are permeable to small molecules but impermeable to globular proteins (e.g., Hb). These vesicles were used to deliver enhanced green fluorescent protein into cultured HeLa cells, presumably by endocytosis, demonstrating their potential utility for their delivering other types of cargo (e.g., enzymes) that could be used for intracellular sensing.

Lee and coworkers used polymerization-induced phase segregation to prepare porous vesicles that can be dispersed in organic solvents [114]. Mixed vesicles composed of BNPC (1,2-bis[9-(4-vinylbenzyloxycarbonyl)nonanoyl]-*sn*-glycero-3-phosphocholine), cholesterol, and divinylbenzene were thermally polymerized, followed by extraction of cholesterol and acid hydrolysis (Fig. 23) to remove the PC headgroups and acyl chains. The resulting vesicles contained nanometer-size holes, reflecting where cholesterol domains had been extracted, and were readily dispersible in organic solvents such as chloroform. This novel material could be useful as a chromatographic stationary phase or a catalyst support.

Yet another strategy for liposome stabilization is based on formation of a biomimetic, pseudocytoskeleton in the aqueous interior, consisting of a hydrophilic polymer network anchored to the bilayer through reactive lipid headgroups. An example of this strategy was reported by Stauch et al. [115]. *N*-Isopropylacrylamide and tetraEGDMA were encapsulated in egg PC vesicles that were doped with a lipid

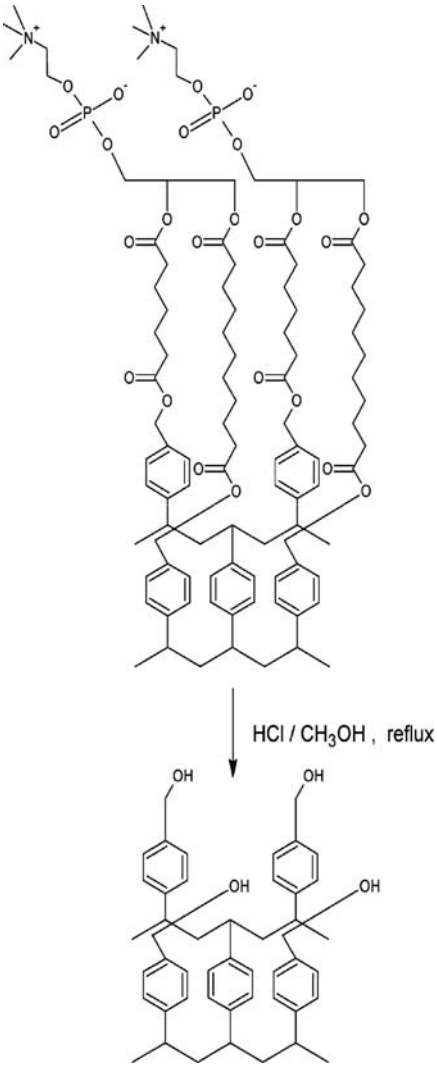

Fig. 23 Strategy for preparation of porous vesicles bearing hydroxyl groups from skeletonized vesicles via hydrolysis. Reprinted with permission from [114]. Copyright 2003, American Chemical Society

bearing a methacrylate-terminated PEG headgroup (1,2-distearyl-3-octaethylene glycol glycerol ether methacrylate, DOGM; Fig. 24). Photopolymerization initiated with DEAP produced a hydrophilic copolymer network in the vesicle interior that was anchored to the bilayer via DOGM. TEM micrographs are shown in Fig. 24. Vesicles with polymer-tethered membranes were more stable to solubilization by sodium cholate relative to vesicles that enclosed a polymer network but lacked DOGM, despite the fact that 98 mol% of the membrane was egg PC (which presumably retained some degree of fluidity).

Electrostatic association between a polyelectrolyte and oppositely charged lipid headgroups is an alternate approach designed to stabilize a liposome while

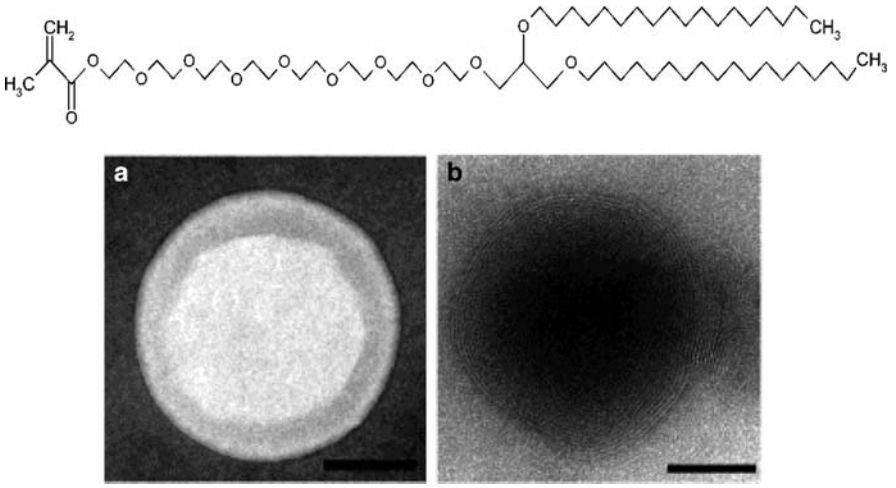

Fig. 24 Structure of DOGM (1,2-distearyl-3-octaethylene glycol glycerol ether methacrylate) and TEM micrographs of polymer-containing vesicles prepared by negative **a** and positive **b** staining. The *scale bar* represents 100 nm. Reprinted with permission from [115]. Copyright 2002, American Chemical Society

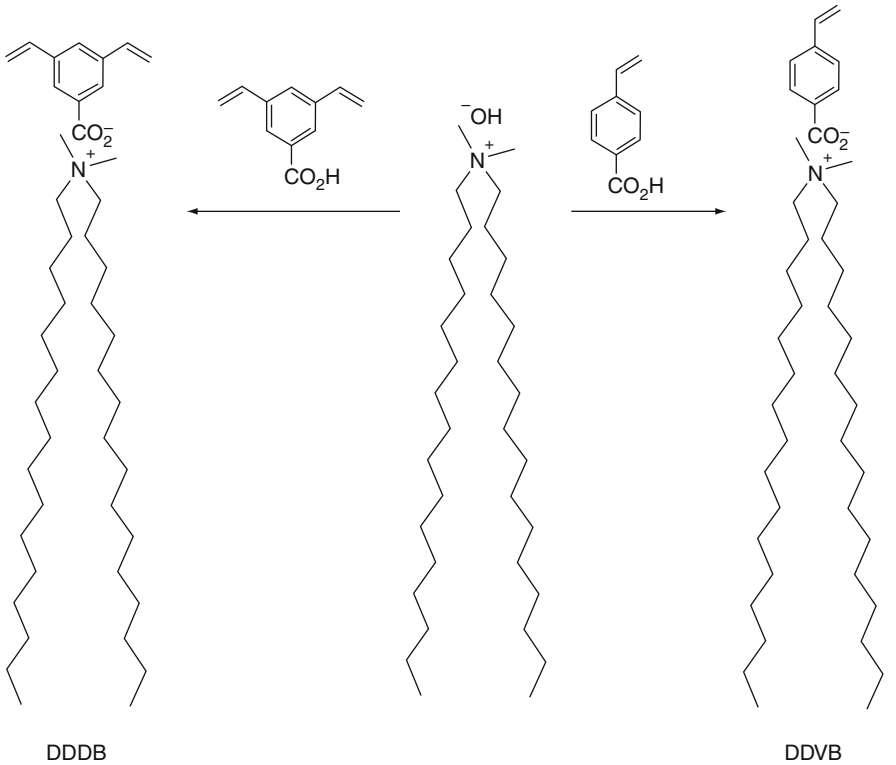

Fig. 25 Scheme for associating polymerizable anions with a cationic dual-chain surfactant to form DDDB and DDVB. Reprinted with permission from [116]. Copyright 2004, Wiley

maintaining lateral lipid mobility. In a study by Paul et al. [116], vesicles were formed from either DDVB, DDDB, or mixtures thereof (Fig. 25), then UV polymerized using 2,2-dimethoxy-2-phenyl acetophenone as the initiator. Vesicle stability in the presence of CTAB was monitored using light scattering. Cross-linked vesicles composed of poly(DDDB) were much more stable than linearly polymerized DDVB vesicles, and the relative stability of mixed vesicles was correlated to the mole fraction of DDDB.

5 Functionalization and Applications of Poly(Lipid) Films

In recent years, liposomes and supported membranes composed of fluid lipids have seen increased use as biolabeling and targeting agents, coatings for sensor transducers and biocompatible materials, nanoscale bioreactors, and separations media. Due to their enhanced stability, functionalized poly(lipid) materials have also been created and characterized for these applications.

5.1 Poly(Lipid) Bilayers Functionalized with Labels and Biomolecules

As discussed in Sect. 2, new types of polymerizable PE lipids conjugated to functional moieties have been synthesized and incorporated into HBMs [70, 71]. A number of other novel polymerizable lipids with fluorescent, metal chelating, and/or biotargeting functions have been reported. Campiglia and coworkers [117–119] prepared a series of mono- and bis-diacetylene lipids with iminodiacetate or ethylenediaminetriacetate (EDTA) headgroups (Fig. 26). In some cases, a fluorophore (e.g., pyrene) was also linked to the acyl chain terminus. Both Tb^{3+} and Eu^{3+} bind tightly to polymerized vesicles of DiynePC doped with the EDTA-bearing lipid, and the highly conjugated poly(lipid) backbone acts as a sensitizer to enhance the luminescence of chelated lanthanide ions. These vesicles have potential for use in bioassays where the relative instability of fluid-phase vesicles may be problematic.

Lipids with functional headgroups can be used to create novel poly(lipid)-based supramolecular assemblies for use in biological binding assays. For example, Ferguson et al. [120] synthesized diacetylene-based lipids with either inositol polyphosphate or biotin linked to the headgroup and incorporated these molecules into poly(diynePC) vesicles (Fig. 27a). Polymerized vesicles were tested in several different assays for proteins containing phosphatidylinositol polyphosphate (PIP_n) binding domains (Fig. 27b), and specific recognition was observed. Vesicles were immobilized to a streptavidin-coated substrate via the biotin headgroup, and proteins containing PIP_n binding domains bound more strongly to these vesicles than to monomeric PIP_n ligands. This work demonstrated that polymerization can be used to create a more stable alternative to unpolymerized vesicles for use in PIP_n binding assays.

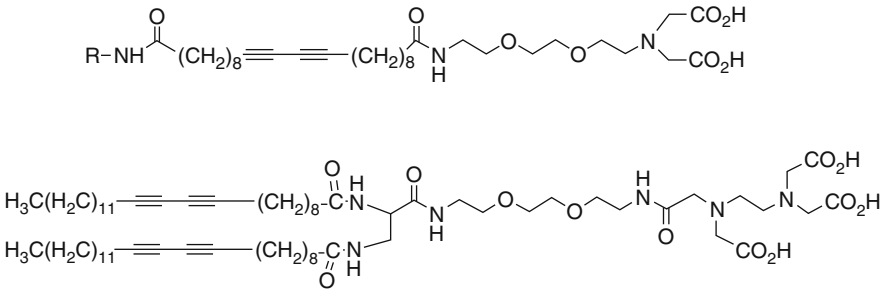

Fig. 26 Polymerizable diacetylene lipids with metal chelating headgroups. Reprinted with permission from [119] (copyright 2000, American Chemical Society) and [117] (copyright 2000, American Chemical Society)

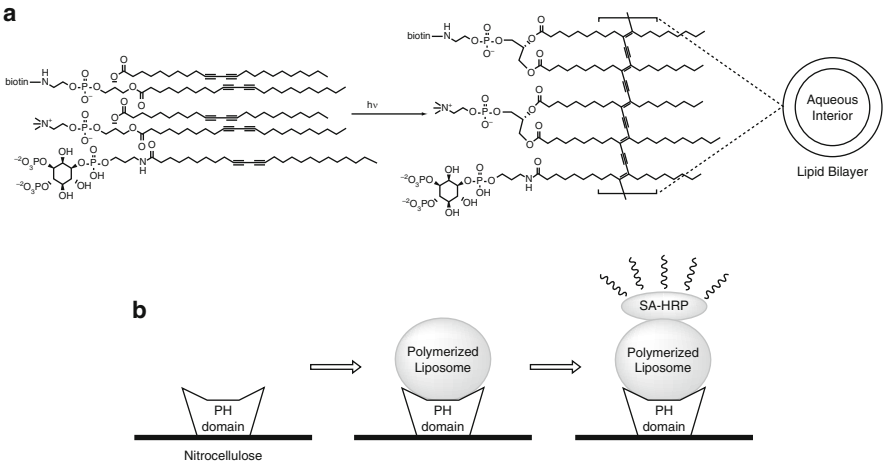

Fig. 27 **a** Poly(DiynePC) vesicles doped with DiynePE–biotin and Diyne–InsP_n. **b** Schematic of an assay using these vesicles. Proteins containing PIP_n binding domains are spotted on a nitrocellulose membrane, then the membrane is incubated with polymerized vesicles, followed by streptavidin–horseradish peroxidase (SAHRP) and chemiluminescent detection. Reprinted with permission from [120]. Copyright 2005, American Chemical Society

Adding a biospecific targeting agent to the surface of a polymerized lipid vesicle can be used to direct the delivery of an encapsulated drug to certain cells or tissues. Clark et al. [121] prepared poly(bis-DenPC) vesicles doped with 2,4-octadecadienoyl-polyethylene glycol-succinate (ODA-PEG-Su) and evaluated their potential as oral vaccine delivery vehicles. The ODA-PEG-Su component provided reactive succinates for functionalization of vesicles with UEA1, a lectin that binds to α-l-fucose residues displayed on intestinal M cells. The dienoyl groups allowed ODA-PEG-Su to be covalently anchored to the poly(bis-DenPC) bilayer, a strategy designed to prevent loss of the functionalized lipid from vesicles by exchange with

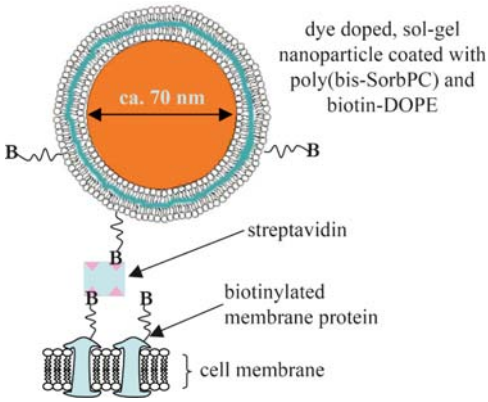

Fig. 28 Schematic of a poly(lipid)-coated silica nanoparticle. Fluorescent dyes are encapsulated in the sol–gel silica core; the nanoparticle is then coated with cross-linked bis-SorbPC doped with biotin-headgroup-conjugated DOPE (biotin–DOPE). A linkage through streptavidin is used to tag biotinylated membrane proteins

cellular membranes in vivo. Binding of polymerized vesicles to intestinal M cells in a mouse gut loop model was inhibited in the presence of α-l-fucose, demonstrating that specific targeting occurred.

Tan and coworkers have shown that a high concentration of fluorophores can be entrapped in sol–gel derived silica nanoparticles (NPs), ca. 70 nm in diameter, making them extremely bright labels for biodetection and imaging applications [122–124]. However, nonspecific adsorption of biological molecules, especially proteins, occurs on these particles. Senarath-Yapa et al. [125] addressed this problem by coating silica NPs with poly(bis-SorbPC) (Fig. 28). The coating has two major functions: to reduce nonspecific interactions, based on the inherently protein-resistant properties of the PC headgroup, and to permit functionalization of the particle by doping the coating with lipids bearing chemically reactive or bioactive headgroups. Both functions were demonstrated: (1) nonspecific adsorption of dissolved proteins to bare silica NPs and of bare NPs to cultured cells is significantly reduced by the poly(bis-SorbPC) coating; (2) functionalization of poly(lipid)-coated NPs with a biotin-conjugated lipid creates a probe that can be used to target both dissolved protein receptors as well as receptors on the membranes of cultured cells. Measurements performed on single NPs bound to PSLBs verified that the emission intensity of these NPs is significantly greater than that of single protein molecules labeled with several fluorophores.

Aspinwall and coworkers [95, 96] developed methods to create poly(PSLBs) patterned with spatially separated, chemically specific domains inside of fused silica separation capillaries. The process depicted in Fig. 12 was used to introduce functional lipids, such as 1,2-dioleoyl-*sn*-glycero-3-(*N*-(5-amino-1-carboxypentyl)iminodiacetic acid) (DOGS-NTA) charged with Ni^{2+}, into fluid DOPC segments between the UV-polymerized bis-SorbPC segments. The result is a capillary functionalized with segments that bind and/or capture proteins tagged with 6xHis (a moiety that is commonly used in protein purification). This process was extended to create multiple chemically unique domains. Fusion and photopolymerization of segments composed of bis-SorbPC doped with a functional lipid, followed by fusion/polymerization in adjacent segments, was performed

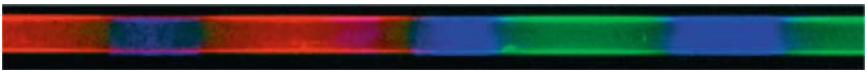

Fig. 29 A barcode of three different chemical functionalities formed in a silica capillary via spatially-selective polymerization. It consists of segments of poly(bis-SorbPC) doped with Rhodamine-capped DPPE (*red*), poly(bis-SorbPC) doped with NBD-capped DOPE (*green*), and DOPC doped with Ni^{2+}-charged DOGS-NTA. After the lipid pattern was formed, 6xHis-tagged Cerulean, a blue fluorescent protein, was injected into the capillary and bound selectively to the immobilized Ni^{2+} (*blue*). The capillary inner diameter is 50 µm. Reprinted with permission from [96]. Copyright 2007, American Chemical Society

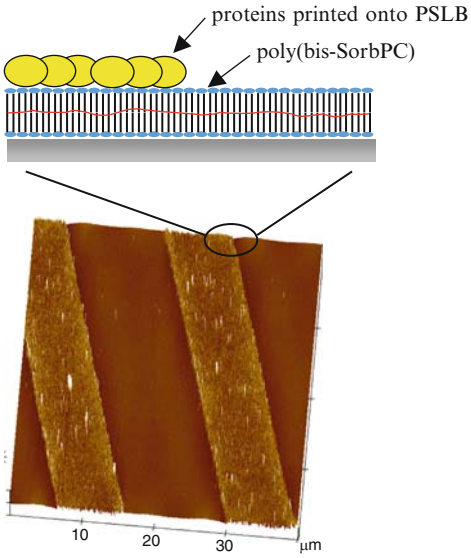

Fig. 30 AFM image (acquired in air) and schematic of a line pattern of BSA that was microcontact printed onto a dried poly(bis-SorbPC) PSLB. The image area is $40 \times 40\ \mu m^2$, with a height scale of 10 nm

sequentially. An example of a three-component pattern thus formed is shown in Fig. 29. The commercial availability of numerous lipids with functionalized headgroups suggests the utility of this approach for preparing capillary-based arrays that, when combined with microfluidics techniques, will be useful for high throughput chemical sensing applications.

Ross et al. [126] demonstrated a strategy for attaching proteins to the surface of planar supported bilayers that does not require doping with functionalized lipids. They used µCP to prepare protein patterns on dried poly(bis-SorbPC) PSLBs (Fig. 30) and found that the proteins remained firmly adsorbed when the printed bilayer was reimmersed in buffer, even in the presence of excess dissolved protein. The regions of the poly(PSLB) that were not printed retained their characteristic protein resistance when hydrated. For example, when dissolved avidin was incubated with a PSLB that had been printed with biotinylated BSA, avidin binding occurred only on the printed regions. This strategy was used to prepare patterns

of biospecifically bound protein multilayers, illustrating the potential of this technically simple method for creating planar supported protein arrays for high throughput bioassays.

5.2 *Incorporation of Transmembrane Proteins*

Supported lipid membranes and membrane arrays functionalized with TMPs have been fabricated by numerous research groups (see for example [5, 37, 127–135] and references therein). Lipid polymerization could be a useful strategy to enhance the operating lifetime of these materials when incorporated into biosensing and drug screening devices. A key issue that must be addressed is the potentially adverse effects that lipid polymerization may have on TMP structure and activity, which can be separated into two major subtopics:

1. Is the structure and activity of the protein affected by exposure to the conditions encountered during lipid polymerization? Methods commonly used to polymerize reactive lipids may expose reconstituted TMPs to free radicals, intense UV and/or visible light, temperatures in excess of 50°C, and/or high concentrations of salts. The susceptibility of a particular TMP to these conditions may be protein-specific. For example, irradiation with visible light causes irreversible photobleaching of Rho; thus photoinitiation using eosin Y/triethanolamine [56] would be a poor choice to polymerize a lipid bilayer containing this protein.
2. Is the protein functional in a poly(lipid) matrix? Polymerization of lipids in the acyl chain region of a bilayer significantly attenuates the lateral diffusion of fluorescent lipid monomers [13]. The prevailing view is that a lipid bilayer must be fluid for reconstituted TMPs to be bioactive [4, 136], and lateral mobility is certainly required for many types of reactions involving membrane-bound receptors (e.g., aggregation of TMP antigens induced by antibody binding). However, for some major classes of TMPs, bioactivity involves a conformational change, as in ligand activation of a GPCR, and accommodating this conformational change does not necessarily require lateral diffusion of lipid monomers. A growing body of evidence does show that the material properties of bilayers, such as thickness, elastic stretching and bending moduli, and intrinsic lipid curvature, modulate the conformational changes of TMPs via hydrophobic coupling between the bilayer-spanning portion of the protein and the surrounding lipids [137, 138]. Lipid polymerization will alter the elastic moduli of a bilayer, but it is not clear that this will prevent the bilayer from accommodating the conformational change of an incorporated TMP.

Recent studies that reported incorporation of pore-forming peptides and proteins into BLMs composed of poly(lipids) were discussed in Sect. 3. In both of these examples, a conformational change was not required for channel activity, and the bilayer was not completely polymerized. Reconstitution of TMPs into solid- and polymer-supported membranes composed solely of polymerized lipids has been reported by two groups in recent years.

Feng et al. [139] studied the activity of TM reconstituted into the PEM/HBM assembly described in Sect. 2.1. TM is a type I TMP that is a receptor for thrombin and mediates protein C activity in anticoagulant and antiinflammatory pathways. TM functionalization represents a promising strategy to control thrombus formation on the surface of a biomaterial that comes into direct contact with blood, such as the inner surface of an arterial graft. TM was incorporated into vesicles of monoacrylatePC (Fig. 1) that were then fused onto an amphiphilic terpolymer/PEM/glass coverslip (see Fig. 2). The eosin Y/triethanolamine method [56] was used to polymerize the lipids, after which the supported assembly could be removed from solution for characterization purposes.

The activity of TM-functionalized membranes was assessed by measuring the rate of protein C activation by the thrombin-TM complex. Lipid polymerization was found to reduce TM activity by ca. 30%, and this was attributed to two factors: exposure of the protein to free radicals during polymerization and reduced lateral mobility of lipids (and possibly TM) in the polymerized membrane. Michaelis–Menten analysis showed that the reduced activity was associated with an increase in the Michaelis constant, K_m. The surface coverage of TM reconstituted into planar membranes and their rate of protein C activation could be adjusted by varying the TM/lipid ratio used for vesicle fusion. At a TM surface coverage of 170 fmol cm^{-2}, the rate was comparable to that of several types of endothelial cell monolayers (Fig. 31). Inhibition of thrombin formation was also used to assess the activity of TM-functionalized membranes. When poly(lipid) HBMs containing TM were incubated with prothrombin, protein C, and coagulation factors Xa and Va, the rate of thrombin formation declined significantly, with near complete inhibition observed at high TM surface coverages. Overall, this work clearly demonstrated that TM retains considerable activity when reconstituted into a linearly polymerized lipid film. It also illustrates the potential for creating molecularly engineered antithrombogenic materials based on artificial proteo-lipid membranes.

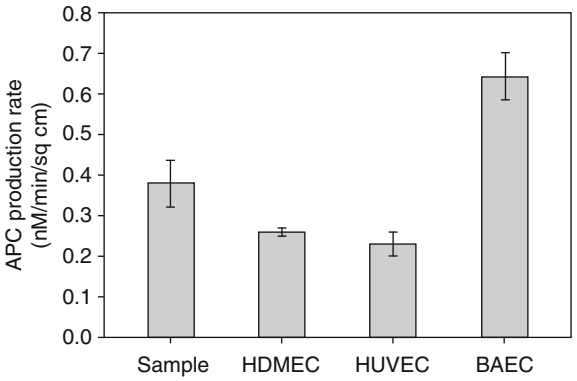

Fig. 31 Rate of surface-mediated protein C activation for TM reconstituted into a poly (acrylatePC) HBM at a protein surface coverage of 170 fmol cm^{-2} (sample) compared to confluent endothelial cell monolayers (HDMEC, human dermal microvascular endothelial cells; HUVEC, human umbilical vein endothelial cells; BAEC, bovine aortic endothelial cells). Reprinted with permission from [139]. Copyright 2002, American Chemical Society

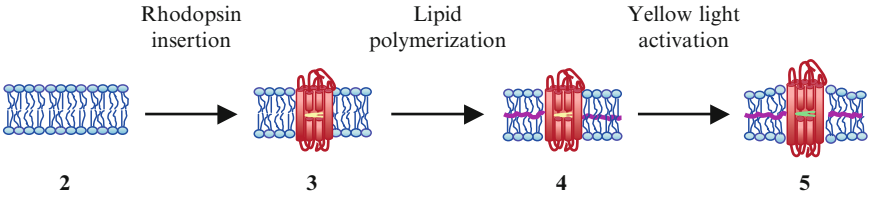

Fig. 32 Illustration of the major steps in formation and photoactivation of a poly(PSLB) with incorporated Rho. The numbers 2–5 correspond to the points in a PWR experiment at which angular scans are acquired (e.g., see corresponding curves in Fig. 33): A PSLB is formed on the SiO_2 waveguide surface (2); Rho is incorporated into the PSLB (3); the lipids are photopolymerized with UV light (4); and Rho is photoactivated with yellow light (5). Reprinted with permission from [141]. Copyright 2008, American Chemical Society

Subramaniam et al. [140, 141] studied the photoactivity of Rho, the rod cell photoreceptor, reconstituted into cross-linked PSLBs. Rho is a model for GPCRs, a large family of TMPs that play key roles in cellular signal transduction and thus are pharmacologically important targets for drug discovery [142]. Several research groups have shown that GPCRs can be reconstituted into planar supported membranes with retention of activity, which has spawned efforts to develop GPCR-based biosensors and biochips [129–135].

Photoactivation of Rho produces a metastable equilibrium between two intermediates, MI and MII [143]. Formation of MII involves a conformational change that elongates Rho along the axis normal to the membrane plane (Fig. 32) along with a significant increase in partial molar volume [144]. The interaction of Rho with the surrounding lipids modulates the extent of this conformational change [137], thus making Rho an appropriate model for studying the effect of lipid polymerization on GPCR activation.

PWR spectroscopy was used to characterize the photochemical activity of Rho in PSLBs composed of lipids with one or two dienoyl groups located at different positions in the acyl chains, having different headgroups, and differing degrees of cross-linking [140, 141]. In PWR, a Kretschmann configuration is used to excite *s*- and *p*-polarized modes in a single-mode silica waveguide [145]. MII formation causes local deformation of the bilayer and infusion of lipid molecules from the surrounding Gibbs border [134], as depicted schematically in Fig. 32. These changes increase the optical thickness of the proteo-lipid membrane, which is measured as shifts in the resonance angles that excite the guided modes. An example set of data is shown in Fig. 33.

PSLBs with varying degrees of cross-linking were prepared from bis-SorbPC, mono-SorbPC, and mixtures thereof (Fig. 6) [140, 141]. A surfactant dilution method was used to insert Rho into PSLBs prior to UV-initiated polymerization. Angle-resolved XPS measurements on poly(bis-Sorb) PSLBs containing Rho showed that the N 1*s* signal was independent of the take-off angle, establishing that the protein was inserted into the bilayer (i.e., uniformly distributed throughout its thickness) rather than merely adsorbed on its surface [80]. The PWR angular shifts upon photoactivation were nearly equivalent in polymerized and unpolymerized

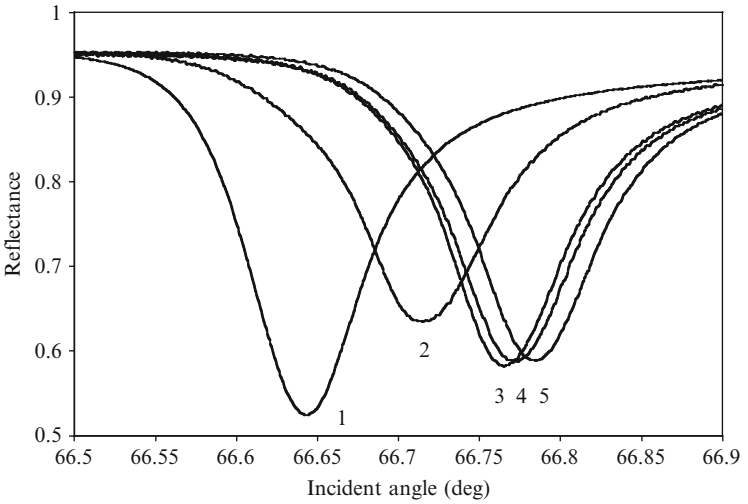

Fig. 33 *s*-Polarized PWR curves acquired with only buffer in the PWR flow cell (1), after bis-SorbPC PSLB formation (2), after Rho incorporation (3), after UV polymerization (4), and after yellow light activation of Rho (5). Reflectance was measured at 632.8 nm. Reprinted with permission from [140]. Copyright 2005, American Chemical Society

sorbyl PSLBs, as well as fluid DOPC. Thus the extent of MII formation was unaffected by lipid polymerization as well as the density of cross-links. Among the lipids examined, bis-DenPC (Fig. 6) was the least favorable for maintenance of Rho activity – after polymerization, the protein was essentially inactive [141]. It is hypothesized that formation of two cross-linked networks in poly(bis-DenPC), one in each monolayer near the glycerol backbone/polar headgroup, stiffens the bilayer such that it cannot deform to accommodate the hydrophobic mismatch resulting from elongation of Rho to form the MII intermediate. In contrast, polymerization of sorbyl lipids generates a cross-linked network in the more disordered center of the bilayer, and these polymers appear to retain sufficient elasticity to accommodate the membrane deformation that accompanies MII formation, as depicted in Fig. 32.

Overall, these studies were the first to demonstrate that the activity of a TMP can be maintained in a highly cross-linked poly(PSLB). The location of the polymerizable moiety is clearly an important consideration. These findings should provide guidance for designing robust poly(lipid) bilayers functionalized with TMPs for use in membrane-based biochips and biosensors.

5.3 Separations Media Based on Polymerized Lipids

CE is a widely used bioanalytical separations technique. However, strong, sometimes irreversible nonspecific adsorption of proteins occurs on the surface of a bare fused silica capillary in contact with a neutral buffer. Thus to separate proteins by

CE, a protein-resistant coating is usually applied to the inner capillary wall. The inherent protein resistance of the PC moiety [76,79] suggests that fused lipid coatings would be useful for this purpose; however, supported PC lipid bilayers are unstable under typical CE operating conditions, requiring frequent regeneration [146].

Two research groups have evaluated poly(lipids) as stable alternatives to fluid lipids for suppressing nonspecific interactions in CE. Wang and Lucy [147] subjected DOPC vesicles to thermally initiated radical polymerization using AIBN (2,2′-azobis(2-methylpropionitrile)), which generated mostly lipid dimers and decreasing concentrations of oligomers up to pentamers. Oligomerized DOPC vesicles were pumped through the capillary, forming an adsorbed coating that was shown to be much more stable than an unpolymerized coating. Separation of proteins in neutral pH buffer at low ionic strength was performed with high efficiency and recoveries >90% were observed for several analytes. However, over the course of 60 consecutive runs, efficiencies declined and peak tailing increased, indicating that lipid desorption eventually occurred (Fig. 34).

To prepare more stable poly(lipid) coatings, Mansfield et al. [148] used vesicle fusion and redox-initiated polymerization to deposit poly(bis-SorbPC) on the inner surface of capillaries. These coatings generated a higher electroosmotic flow than observed with unpolymerized lipid coatings (e.g., egg PC), but this allowed separation of both cationic and anionic proteins in a single run, albeit with lower separation efficiencies. Poly(bis-SorbPC)-coated capillaries were found to be extremely stable to harsh chemical conditions, including exposure to surfactants and dry storage for periods in excess of a year. These studies demonstrate the potential

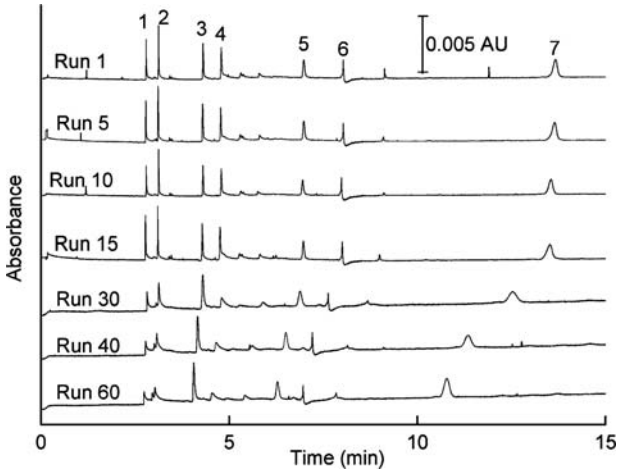

Fig. 34 Consecutive protein separations performed on a capillary coated with oligomerized DOPC. Peaks: (1) lysozyme, (2) cytochrome *c*, (3) ribonuclease A, (4) α-chymotrypsinogen A, (5) myoglobin, (6) hemoglobin, and (7) carbonic anhydrase. The sharp spikes seen in the electrophoretogram are artifacts due to air bubbles. The separation quality begins to degrade visibly between runs 15 and 30. Reprinted with permission from [147]. Copyright 2005, American Chemical Society

of poly(lipid)-based materials for CE separations of biomacromolecules that non-specifically interact with fused silica. Furthermore, the stability of functionalized lipids when doped into poly(bis-SorbPC) [95, 96] suggests that separations based on bioaffinity are feasible.

6 Concluding Remarks

Although the polymerization of lipid supramolecular assemblies is a relatively mature field of research, several significant improvements to existing technologies have been made in the past decade, and a number of novel poly(lipid) structures have been created for a diverse set of applications ranging from energy storage to biosensing. This review has focused on polymerization of membranes to achieve stability and introduce functionality. The latter is facilitated by the wide variety of mild (and in some cases reversible) attachment chemistries that have been developed to link both small molecule ligands and proteins to lipid headgroups. In addition, numerous functionalized lipids are commercially available, and several studies have shown that these lipids are stable when doped into poly(lipid) membranes, even when they are not covalently linked to the polymer network.

With respect to stability, it is important to emphasize that the requirements will be different for different types of applications. Just as beauty is in the eye of the beholder, chemical, mechanical, and thermal stability are defined by the end user. Exposure to different types of destabilizing conditions reveals different levels of membrane defect density and degradation [149]. Among the most severe tests are drying and exposure to solvents and surfactants. If these conditions will not be encountered during usage of a poly(lipid) assembly, then an approach less transformative than cross-linking polymerization may be more appropriate.

In addition to stability, polymerization of a lipid membrane is also likely to alter its elastic stretching and bending moduli, the lateral mobility of its constituents, and its permeability to ions and small molecules. In this regard, enhancing the stability of a membrane may be useful for an intended application but may not be the most important consideration. For example, to measure the conductivity of an ion channel incorporated into a BLM, a very high membrane resistance is required. If lipid polymerization to increase stability is achieved at the price of creating a leaky membrane, then nothing is gained.

Finally, we note that a growing body of evidence shows that the stability of a planar membrane can be enhanced by spreading it across a small aperture [97]. For example, a DiPhyPC bilayer suspended across a 150 nm radius orifice in a glass pipet remains intact when removed from buffer [150]. This suggests that it may be possible to form arrays in which fluid, stable bilayer patches are surrounded by a patterned substrate that anchors the membrane. Air stability can also be achieved by coating a PSLB with a hydrophilic polymer film (e.g., a biospecifically adsorbed protein layer [23, 149]). Both of these approaches maintain some degree of lateral lipid mobility in the membrane.

Acknowledgements The preparation of this manuscript was supported by grants from the National Science Foundation (CHE-0518702) and the National Institutes of Health (EB007047 and CA112427). Any opinions, findings, and conclusions or recommendations expressed in this material are those of the authors and do not necessarily reflect the views of the National Science Foundation or the National Institutes of Health.

References

1. Gennis RB (1989) Biomembranes: molecular structure and function. Springer, Berlin Heidelberg New York
2. Gruner SM (1989) J Phys Chem 93:7562
3. Ringsdorf H, Schlarb B, Venzmer J (1988) Angew Chem Int Ed Engl 27:113
4. Sackmann E (1996) Science 271:43
5. Tanaka M, Sackmann E (2005) Nature 437:656
6. McConnell HM, Watts TH, Weis RM, Brian AA (1986) Biochem Biophys Acta 864:95
7. Szoka F, Papahadjopoulos D (1980) Annu Rev Biophys Bio 9:467
8. Hayward JA, Chapman D (1984) Biomaterials 5:135
9. Gros L, Ringsdorf H, Schupp H (1981) Angew Chem Int Ed 20:305
10. Cremer PS, Boxer SG (1999) J Phys Chem B 103:2554
11. Ross EE, Rozanski LJ, Spratt T, Liu S, O'Brien DF, Saavedra SS (2003) Langmuir 19:1752
12. Liu S, O'Brien DF (2002) J Am Chem Soc 124:6037
13. Sisson TM, Lamparski HG, Kolchens S, Elayadi A, O'Brien DF (1996) Macromolecules 29:8321
14. McBee TW, Saavedra SS (2005) Langmuir 21:3396
15. Albrecht O, Johnston DS, Villaverde C, Chapman D (1982) Biochem Biophys Acta 687:165
16. Regen SL, Kirszensztejn P, Singh A (1983) Macromolecules 16:335
17. Regen SL, Singh A, Oehme G, Singh M (1982) J Am Chem Soc 104:791
18. Regen SL, Czech B, Singh A (1980) J Am Chem Soc 102:6638
19. Hub HH, Hupfer B, Koch H, Ringsdorf H (1980) Angew Chem Int Ed Engl 19:938
20. Akimoto A, Dorn K, Gros L, Ringsdorf H, Schupp H (1981) Angew Chem Int Ed Engl 20:90
21. Graff A, Winterhalter M, Meier W (2001) Langmuir 17:919
22. Lasic DD (1994) Angew Chem Int Ed Engl 33:1685
23. Holden MA, Jung SY, Yang TL, Castellana ET, Cremer PS (2004) J Am Chem Soc 126:6512
24. Kim JM, Patwardhan A, Bott A, Thompson DH (2003) Biochim Biophys Acta Biomembr 1617:10
25. O'Brien DF, Armitage B, Benedicto A, Bennett DE, Lamparski HG, Lee YS, Srisiri W, Sisson TM (1998) Acc Chem Res 31:861
26. Mueller A, O'Brien DF (2002) Chem Rev 102:727
27. Armitage BA, Bennett DE, Lamparski HG, O'Brien DF (1996) Adv Polym Sci 126:53
28. Bader H, Dorn K, Hupfer B, Ringsdorf H (1985) Adv Polym Sci 64:1
29. Nakaya T, Li YJ (1999) Prog Polym Sci 24:143
30. Okada S, Peng S, Spevak W, Charych D (1998) Acc Chem Res 31:229
31. Miller SA, Ding JH, Gin DL (1999) Curr Opin Colloid Interf Sci 4:338
32. Plant AL (1999) Langmuir 15:5128
33. Cornell BA, Braach-Maksvytis VLB, King LG, Osman PDJ, Raguse B, Wieczorek L, Pace RJ (1997) Nature 387:580
34. Song XD, Swanson BI (1999) Anal Chem 71:2097
35. Schmidt C, Mayer M, Vogel H (2000) Angew Chem Int Ed Engl 39:3137
36. Marra KG, Winger TM, Hanson SR, Chaikof EL (1997) Macromolecules 30:6483
37. Devadoss A, Burgess JD (2002) Langmuir 18:9617
38. Kasemo B (2002) Surf Sci 500:656

39. Heyse S, Stora T, Schmid E, Lakey JH, Vogel H (1998) Biochem Biophys Acta Biomembr 1376:319
40. Conboy JC, McReynolds KD, Gervay-Hague J, Saavedra SS (2002) J Am Chem Soc 124:968
41. McBee T, Wang L, Ge C, Beam B, Moore AL, Gust D, Moore TA, Saavedra SS, Armstrong NR (2006) J Am Chem Soc 128:2184
42. Liu J, Conboy JC (2004) J Am Chem Soc 126:8894
43. Tamm LK, McConnell HM (1985) Biophys J 47:105
44. Reimhult E, Hook F, Kasemo B (2003) Langmuir 19:1681
45. Parikh AN, Beers JD, Shreve AP, Swanson BI (1999) Langmuir 15:5369
46. Meuse CW, Krueger S, Majkrzak CF, Dura JA, Fu J, Connor JT, Plant AL (1998) Biophys J 74:1388
47. Raguse B, Braach-Maksvytis V, Cornell BA, King LG, Osman PDJ, Pace RJ, Wieczorek L (1998) Langmuir 14:648
48. Naumann R, Schiller SM, Giess F, Grohe B, Hartman KB, Karcher I, Koper I, Lubben J, Vasilev K, Knoll W (2003) Langmuir 19:5435
49. Terrettaz S, Mayer M, Vogel H (2003) Langmuir 19:5567
50. Janshoff A, Steinem C (2006) Anal Bioanal Chem 385:433
51. Atanasov V, Knorr N, Duran RS, Ingebrandt S, Offenhausser A, Knoll W, Koper I (2005) Biophys J 89:1780
52. Bayerl TM, Bloom M (1990) Biophys J 58:357
53. Song XD, Shi J, Swanson B (2000) Anal Biochem 284:35
54. Buranda T, Huang J, Ramarao GV, Ista LK, Larson RS, Ward TL, Sklar LA, Lopez GP (2003) Langmuir 19:1654
55. Mornet S, Lambert O, Duguet E, Brisson A (2005) Nano Lett 5:281
56. Orban JM, Faucher KM, Dluhy RA, Chaikof EL (2000) Macromolecules 33:4205
57. Kim K, Shin K, Kim H, Kim C, Byun Y (2004) Langmuir 20:5396
58. Kim HK, Kim K, Byun Y (2005) Biomaterials 26:3435
59. Kim K, Byun Y, Kim C, Kim TC, Noh DY, Shin K (2005) J Colloid Interf Sci 284:107
60. Krishna OD, Kim K, Byun Y (2005) Biomaterials 26:7115
61. Hughes AV, Howse JR, Dabkowska A, Jones RAL, Lawrence MJ, Roser SJ (2008) Langmuir 24:1989
62. Winger TM, Ludovice PJ, Chaikof EL (1999) Langmuir 15:3866
63. Marra KG, Kidani DDA, Chaikof EL (1997) Langmuir 13:5697
64. Chon JH, Marra KG, Chaikof EL (1999) J Biomater Sci Polym Ed 10:95
65. Liu S, Sisson TM, O'Brien DF (2001) Macromolecules 34:465
66. Liu H, Faucher KM, Sun XL, Feng J, Johnson TL, Orban JM, Apkarian RP, Dluhy RA, Chaikof EL (2002) Langmuir 18:1332
67. Cui W, Barr G, Faucher KM, Sun XL, Safley SA, Weber CJ, Chaikof EL (2004) Transplan Proc 36:1206
68. Jordan SW, Faucher KM, Caves JM, Apkarian RP, Rele SS, Sun X-L, Hanson SR, Chaikof EL (2006) Biomaterials 27:3473
69. Wilson JT, Cui W, Sun X-L, Tucker-Burden C, Weber CJ, Chaikof EL (2007) Biomaterials 28:609
70. Sun XL, Liu H, Orban JM, Sun L, Chaikof EL (2001) Bioconjug Chem 12:673
71. Sun X-L, Cui W, Kai T, Chaikof EL (2004) Tetrahedron 60:11765
72. Kyun Kim H, Kim K, Byun Y (2005) Biomaterials 26:3435
73. Johnston DS, Sanghera S, Pons M, Chapman D (1980) Biochem Biophys Acta 602:57
74. Lei JT, Sisson TM, Lamparski HG, O'Brien DF (1999) Macromolecules 32:73
75. Conboy JC, Liu S, O'Brien DF, Saavedra SS (2003) Biomacromolecules 4:841
76. Ross EE, Spratt T, Liu S, Rozanski LJ, O'Brien DF, Saavedra SS (2003) Langmuir 19:1766
77. Ross EE, Bondurant B, Spratt T, Conboy JC, O'Brien DF, Saavedra SS (2001) Langmuir 17:2305
78. Tegoulia VA, Rao W, Kalambur AT, Rabolt JF, Cooper SL (2001) Langmuir 17:4396
79. Glasmastar K, Larsson C, Hook F, Kasemo B (2002) J Colloid Interf Sci 246:40

80. Michel R, Subramaniam V, McArthur SL, Bondurant B, D'Ambruoso GD, Hall HK, Brown MF, Ross EE, Saavedra SS, Castner DG (2008) Langmuir 24:4901
81. Lamparski H, O'Brien DF (1995) Macromolecules 28:1786
82. Ratnayaka SN, Wysocki RJ, Saavedra SS (2008) J Colloid Interf Sci 327:63
83. Halter M, Nogata Y, Dannenberger O, Sasaki T, Vogel V (2004) Langmuir 20:2416
84. Derosa M, Gambacorta A, Gliozzi A (1986) Microbiol Rev 50:70
85. Fang Y, Frutos AG, Lahiri J (2002) Chembiochem 3:987
86. Groves JT, Boxer SG (2002) Acc Chem Res 35:149
87. Phillips KS, Wilkop T, Wu JJ, Al-Kaysi RO, Cheng Q (2006) J Am Chem Soc 128:9590
88. Morigaki K, Baumgart T, Offenhausser A, Knoll W (2001) Angew Chem Int Ed Engl 40:172
89. Morigaki K, Schonherr H, Frank CW, Knoll W (2003) Langmuir 19:6994
90. Morigaki K, Kiyosue K, Taguchi T (2004) Langmuir 20:7729
91. Okazaki T, Morigaki K, Taguchi T (2006) Biophys J 91:1757
92. Morigaki K, Schonherr H, Okazaki T (2007) Langmuir 23:12254
93. Morigaki K, Baumgart T, Jonas U, Offenhäusser A, Knoll W (2002) Langmuir 18:4082
94. Mahajan N, Lu RB, Wu ST, Fang JY (2005) Langmuir 21:3132
95. Ross EE, Mansfield E, Huang Y, Aspinwall CA (2005) J Am Chem Soc 127:16756
96. Mansfield E, Ross EE, D'Ambruoso GD, Keogh JP, Huang Y, Aspinwall CA (2007) Langmuir 23:11326
97. Reimhult E, Kumar K (2008) Tibtech 26:82
98. Benz R, Elbert R, Prass W, Ringsdorf H (1986) Eur Biophys J 14:83
99. Shenoy DK, Barger WR, Singh A, Panchal RG, Misakian M, Stanford VM, Kasianowicz JJ (2005) Nano Lett 5:1181
100. Daly SM, Heffernan LA, Barger WR, Shenoy DK (2006) Langmuir 22:1215
101. Meier W, Graff A, Diederich A, Winterhalter M (2000) Phys Chem Chem Phys 2:4559
102. Stanish I, Singh A (2001) Chem Phys Lipids 112:99
103. Lawson GE, Lee Y, Singh A (2003) Langmuir 19:6401
104. Wu J, Lizarzaburu ME, Kurth MJ, Liu L, Wege H, Zern MA, Nantz MH (2001) Bioconjugate Chem 12:251
105. Lawson GE, Lee YW, Raushel FM, Singh A (2005) Adv Funct Mater 15:267
106. Akama K, Awai K, Yano Y, Tokuyama S, Nakano Y (2000) Polym Adv Technol 11:280
107. Monfardini C, Veronese FM (1998) Bioconjugate Chem 9:418
108. Spratt T, Bondurant B, O'Brien DF (2003) Biochim Biophys Acta Biomembr 1611:35
109. Stanish I, Lowy DA, Lee Y, Fang J, Wong E, Ray RI, Singh A (2004) J Phys Chem B 108:127
110. Stanish I, Lowy DA, Tender LM, Singh A (2002) J Phys Chem B 106:3503
111. Stanish I, Lowy DA, Hung CW, Singh A (2005) Adv Mater 17:1194
112. Gomes J, Sonnen AFP, Kronenberger A, Fritz J, Coelho MAN, Fournier D, Fournier-Noel C, Mauzac M, Winterhalter M (2006) Langmuir 22:7755
113. Cheng Z, D'Ambruoso GD, Aspinwall CA (2006) Langmuir 22:9507
114. Im JY, Kim DB, Lee SH, Lee YS (2003) Langmuir 19:6392
115. Stauch O, Uhlmann T, Frohlich M, Thomann R, El-Badry M, Kim YK, Schubert R (2002) Biomacromolecules 3:324
116. Paul GK, Indi SS, Ramakrishnan S (2004) J Polym Sci A Polym Chem 42:5271
117. Roy BC, Fazal MA, Arruda A, Mallik S, Campiglia AD (2000) Org Lett 2:3067
118. Nadi S, Santos M, Haldar MK, Roy BC, Mallik S, Campiglia AD (2005) Inorg Chem 44:2234
119. Roy BC, Peterson R, Mallik S, Campiglia AD (2000) J Org Chem 65:3644
120. Ferguson CG, James RD, Bigman CS, Shepard DA, Abdiche Y, Katsamba PS, Myszka DG, Prestwich GD (2005) Bioconjugate Chem 16:1475
121. Clark MA, Blair H, Liang L, Brey RN, Brayden D, Hirst BH (2001) Vaccine 20:208
122. Lian W, Litherland SA, Badrane H, Tan WH, Wu DH, Baker HV, Gulig PA, Lim DV, Jin SG (2004) Anal Biochem 334:135
123. Santra S, Wang KM, Tapec R, Tan WH (2001) J Biomed Opt 6:160
124. Santra S, Zhang P, Wang KM, Tapec R, Tan WH (2001) Anal Chem 73:4988
125. Senarath-Yapa MD, Phimphivong S, Coym JW, Wirth MJ, Aspinwall CA, Saavedra SS (2007) Langmuir 23:12624

126. Ross EE, Joubert JR, Wysocki RJ, Nebesny K, Spratt T, O'Brien DF, Saavedra SS (2006) Biomacromolecules 7:1393
127. Giess F, Friedrich MG, Heberle J, Naumann RL, Knoll W (2004) Biophys J 87:3213
128. Salafsky J, Groves JT, Boxer SG (1996) Biochemistry 35:14773
129. Fang Y, Frutos AG, Lahiri J (2002) J Am Chem Soc 124:2394
130. Heyse S, Ernst OP, Dienes Z, Hofmann KP, Vogel H (1998) Biochemistry 37:507
131. Bieri C, Ernst OP, Heyse S, Hofmann KP, Vogel H (1999) Nat Biotechnol 17:1105
132. Martinez KL, Meyer BH, Hovius R, Lundstrom K, Vogel H (2003) Langmuir 19:10925
133. Alves ID, Salamon Z, Varga E, Yamamura HI, Tollin G, Hruby VJ (2003) J Biol Chem 278:48890
134. Alves ID, Salgado GFJ, Salamon Z, Brown MF, Tollin G, Hruby VJ (2005) Biophys J 88:198
135. Neumann L, Wohland T, Whelan RJ, Zare RN, Kobilka BK (2002) Chembiochem 3:993
136. Boxer SG (2000) Curr Opin Chem Biol 4:704
137. Brown MF (1994) Chem Phys Lipids 73:159
138. Andersen OS, Koeppe RE (2007) Ann Rev Biophys Biomol Struct 36:107
139. Feng J, Tseng PY, Faucher KM, Orban JM, Sun XL, Chaikof EL (2002) Langmuir 18:9907
140. Subramaniam V, Alves ID, Salgado GFJ, Lau PW, Wysocki RJ, Salamon Z, Tollin G, Hruby VJ, Brown MF, Saavedra SS (2005) J Am Chem Soc 127:5320
141. Subramaniam V, D'Ambruoso GD, Hall HK, Wysocki RJ, Brown MF, Saavedra SS (2008) Langmuir 24:11067
142. Howard AD, McAllister G, Feighner SD, Liu QY, Nargund RP, Van der Ploeg LHT, Patchett AA (2001) Trends Pharmacol Sci 22:132
143. Ridge KD, Palczewski K (2007) J Biol Chem 282:9297
144. Hubbell WL, Altenbach C, Hubbell CM, Khorana HG (2003) Advances in protein chemistry: membrane proteins. Elsevier, San Diego, p 243
145. Salamon Z, Macleod HA, Tollin G (1997) Biophys J 73:2791
146. Cunliffe JM, Baryla NE, Lucy CA (2002) Anal Chem 74:776
147. Wang CZ, Lucy CA (2005) Anal Chem 77:2015
148. Mansfield E, Ross EE, Aspinwall CA (2007) Anal Chem 79:3135
149. Han JH, Taylor JD, Phillips KS, Wang XQ, Feng PY, Cheng Q (2008) Langmuir 24:8127
150. White RJ, Ervin EN, Yang T, Chen X, Daniel S, Cremer PS, White HS (2007) J Am Chem Soc 129:11766

Adv Polym Sci (2010) 223: 43–85
DOI:10.1007/12_2008_11

Published online: 5 March 2009

Polymer Stabilized Lipid Membranes: Langmuir Monolayers

A.P. Siegel and C.A. Naumann

Abstract Polymer-tethered membranes combine fascinating structural, dynamic, and viscoelastic properties. Many important insights into these peculiar supramolecular systems can be obtained from studies on polymer-tethered monolayers. This chapter discusses recent experimental findings on polymer-tethered monolayers at the air–water interface. In particular, Langmuir monolayers which are comprised of pure lipopolymers and of binary phospholipid–lipopolymer mixtures are considered. Thermodynamic data as well as structural data based on a host of experimental techniques including X-ray and neutron reflectrometry, infrared reflection absorption spectroscopy, and sum frequency generation spectroscopy provide information on how lipopolymers organize at the air–water interface. This information is followed by a review of the viscoelastic properties of these systems, including the remarkable gelation transition that can be observed in lipopolymers and mixed phospholipid–lipopolymer monolayers. The diffusion properties are also discussed at length, and show that lipid diffusivity is critically dependent on the strength of inter-polymer interactions of lipopolymers.

Keywords Diffusion, Langmuir monolayer, Lipopolymer, Phospholipid, Viscoelasticity

Contents

A.P. Siegel and C.A. Naumann (✉)
Department of Chemistry and Chemical Biology, Indiana University Purdue University at Indianapolis 402 N. Blackford St., Indianapolis, Indiana 46202, USA
e-mail: canauman@iupui.edu

1 Introduction

Recent advances in the understanding of assembly and disassembly of biomolecules have led to the design of polymer-tethered membranes. One particularly attractive design of polymer-tethered membranes is based on phospholipid–lipopolymer mixtures. In phospholipid–lipopolymer mixed monolayers, the tethering concentration can be adjusted accurately through the molar concentration of lipopolymers. Importantly, by changing the lipopolymer–lipid mixing ratio, polymer-tethered membranes can be obtained with a wide range of fascinating structural and dynamic properties. Because many of these intriguing properties of polymer-tethered membranes can be observed on Langmuir monolayers, the current contribution summarizes recent advances in the design and characterization of lipopolymer-based polymer-tethered monolayers at the air–water interface.

Lipopolymers and phospholipids are amphiphiles with distinct structural properties. While the hydrophobic moieties show great similarities, the hydrophilic headgroups are structurally distinct. Most importantly, unlike phospholipids, the hydrophilic moiety of lipopolymers consists of a comparably bulky polymer chain, which is end-tethered through a hydrophilic linker to the two-pronged lipid tail of the molecule. The lipid/polymer hybrid character of lipopolymers results in unique molecular properties, which also critically determine the properties in lipopolymer–lipid mixed monolayers. Because the study of lipopolymers at the air–water interface provides important clues about properties of lipopolymer–lipid mixed monolayers, the first half of this chapter (Sect. 2) summarizes reported experimental results obtained from Langmuir monolayers of lipopolymers. Section 2.1 discusses film balance and neutron reflectometry experiments on lipopolymer monolayers, which have provided important structural information. Insight into the fascinating viscoelastic properties of lipopolymer monolayers is given in Sect. 2.2, where recent interfacial rheology experiments are described. Section 2.3 addresses the lateral diffusion properties of lipopolymers at the air–water interface, which offer valuable information about the diffusion properties of polymer-tethered membranes. The second half of this chapter (Sect. 3) focuses on experimental findings obtained from lipopolymer–phospholipid mixed monolayers at the air–water interface. Section 3.1 contains an overview over structural properties of such mixed Langmuir monolayers. Section 3.2 discusses corresponding viscoelastic properties. Finally, Sect. 3.3 summarizes the key data from lipid lateral diffusion studies in lipopolymer–phospholipid mixed monolayers.

2 Lipopolymer Langmuir Monolayers

2.1 Structural Properties

The structural properties of lipopolymers at the air–water interface have been traditionally explored using film balance techniques and neutron/X-ray reflectometry. The film balance method is an attractive tool to study the assembly of lipopolymers at the air–water interface as a function of molecular surface density (area per molecule). In this case, Langmuir monolayers of lipopolymers are constructed by simply adding these amphiphiles to the air–water interface. Here one or two movable barriers are employed to compress or expand the monolayer. The resulting changes in surface density of amphiphiles at the air–water interface are monitored using a film pressure sensor. This method provides valuable thermodynamic information because the pressure–area $(\pi - A)$ isotherm of a Langmuir monolayer can be determined. Complementary, neutron/X-ray reflectometry allows insight into the scattering length density profile of the monolayer perpendicular to the air–water interface with high resolution.

Baekmark et al. first investigated the pressure–area isotherms of lipopolymers at the air–water interface using lipopolymers with poly(ethylene glycol) (PEG) covalently linked to a phospholipid 1,2-distearoyl-*sn*-glycero-3-phosphoethanolamine (DSPE) [1]. Figure 1 contains structural information of widely studied lipopolymers together with corresponding structures of some phospholipids. The three main types of polymeric moieties of lipopolymers are poly(ethylene glycol) (PEG) (named by their approximate weight) linked to phospholipids and poly(2-methyl-2-oxazoline)$_n$ $(PMOx_n)$, and poly(2-ethyl-2-oxazoline)$_n$ $(PEOx_n)$ linked to di-octadecanoyl-glycerol (DiC_{18}). Figure 2 illustrates a typical pressure–area-isotherm of the lipopolymer DSPE–PEG2000.

Figure 2 shows that the $\pi - A$ isotherm for DSPE–PEG2000 is characterized by two plateaus. In this figure, the plateaus, or transitions, are labeled π_{low} and π_{high}. By following scaling arguments of polymer physics, Baekmark et al. originally interpreted these plateau regions as "pancake to mushroom" transitions for π_{low} and "mushroom-to-brush" transitions for π_{high} [1]. Interestingly, monolayer experiments of polystyrene–poly(ethylene oxide) diblock copolymers reveal identical low-pressure transition behavior but no transition at higher film pressure [3]. In that case, it was argued that in the low-pressure regime, the PEG chains desorb from the air–water interface in a temperature-independent fashion, which also agrees with the desorption properties of pure PEG at the air–water interface [4, 5].

Several experimental results have been reported which show that the high-pressure transition is qualitatively different to the low pressure counterpart in that it exhibits properties of a first order phase transition. For example, it was shown that the pressure of the high-pressure transition, π_{high}, is dependent on temperature, thus meeting an important criterion of a first order transition [2, 6]. Figure 3 displays a close-up of the high-pressure transition region of $\pi - A$ isotherms for DSPE–PEG2000 taken at different temperatures, showing very clearly that the high

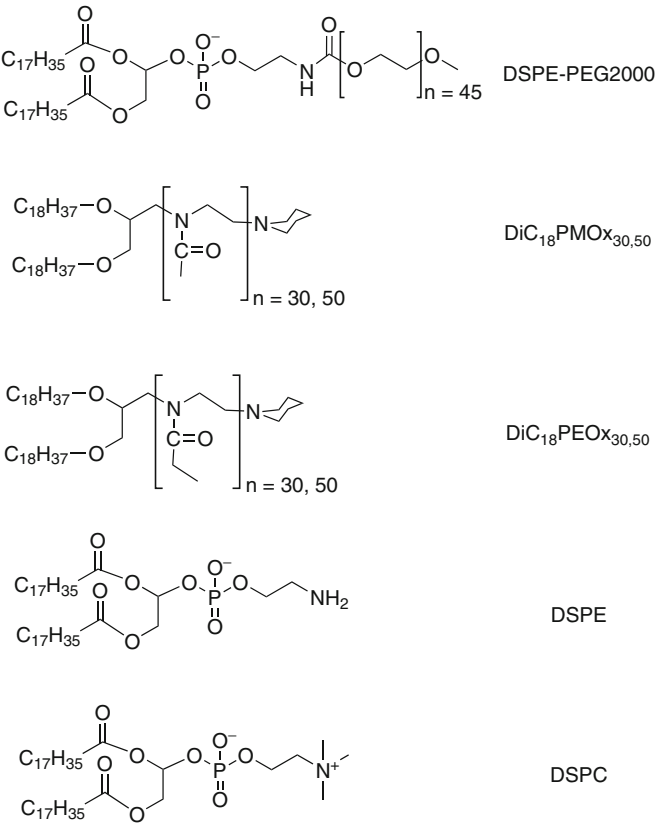

Fig. 1 Commonly investigated lipopolymers and lipids: 1,2-distearoyl-*sn*-glycero-3-phosphatidylethanolamine-*N*-[poly(ethylene glycol)$_{45}$] (DSPE-PEG2000), 1,2-dioctadecanoyl-*sn*-glycero-[poly((2-methyl-2-oxazoline)$_n$)] ($DiC_{18}PMOx_{30,50}$), 1,2-dioctadecanoyl-*sn*-glycero-[poly((2-ethyl-2-oxazoline)$_n$)] ($DiC_{18}PEOx_{30,50}$), 1,2-distearoyl-*sn*-glycero-3-phosphoethanolamine (DSPE) and 1,2-distearoyl-*sn*-glycero-3-phosphocholine (DSPC)

pressure transition is temperature dependent. The temperature dependence of the high-pressure transition region has also been shown on lipopolymer systems involving $DiC_{18}PMOx$ and $DiC_{18}PEOx$ [6].

To obtain more insight into the nature of the high-pressure transition, a series of film balance experiments were conducted, where the impact of the lipid and polymer moieties on this transition were investigated systematically. For example, $\pi - A$ isotherms were measured for PEG lipopolymers with saturated lipid tails of varying lengths [2]. Interestingly enough, the C_{16} chain DPPE–PEG2000 displayed a 10 mN m^{-1} higher π_{high} relative to the C_{18} chain DSPE–PEG2000, and the C_{14} chain DMPE–PEG2000 never displayed π_{high} at all, thus indicating a sensitive relationship between acyl chain length of the lipid moiety and π_{high}. In order to explore further the importance of the lipid tail to the high-pressure transition,

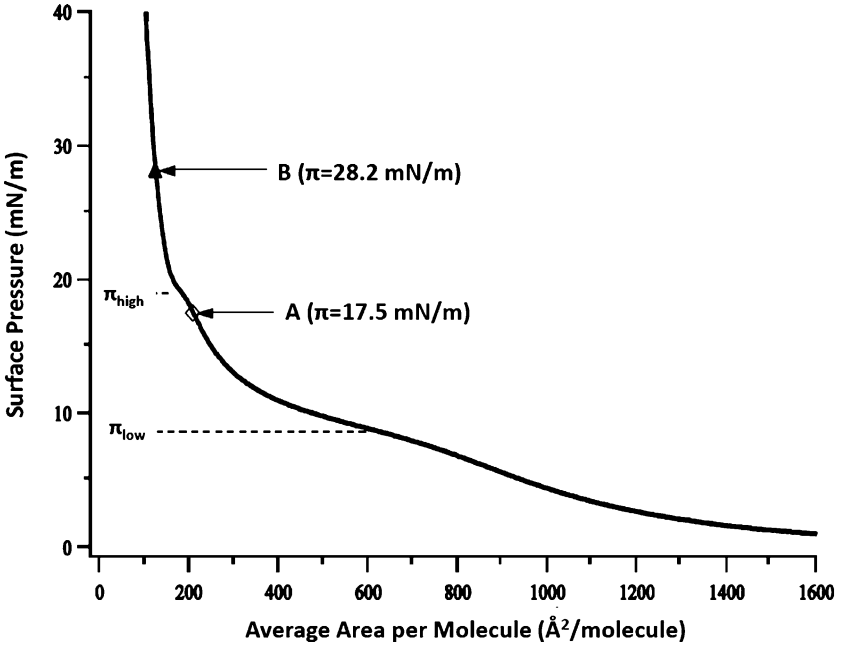

Fig. 2 Pressure–area isotherm of DSPE–PEG2000 at room temperature showing two plateaus indicative of a low-pressure transition (π_{low}) and a high-pressure transition (π_{high}). The points A and B represent film pressures where interfacial rheology experiments were conducted [2] (reproduced with permission from the American Chemical Society)

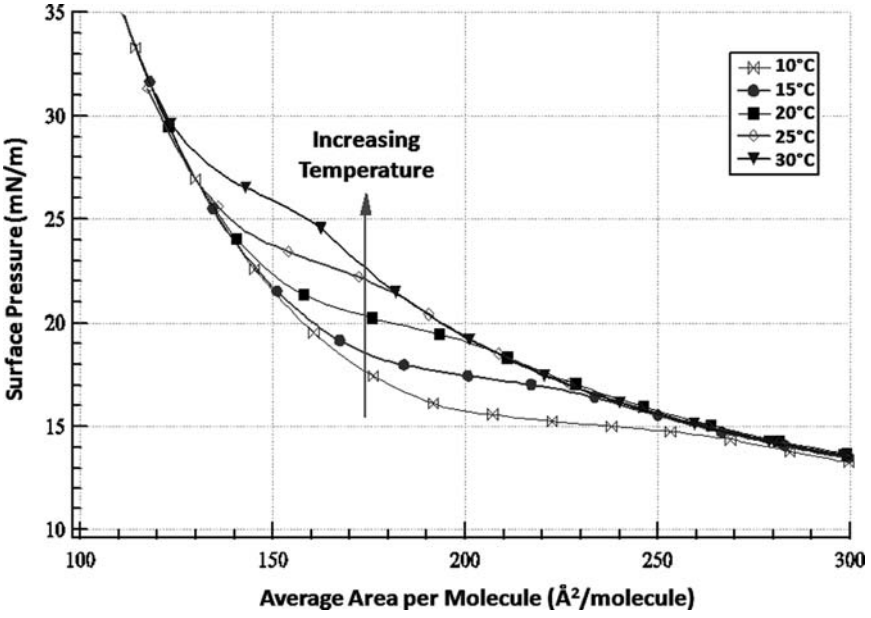

Fig. 3 Close-up of pressure–area isotherms of DSPE–PEG2000 near the high pressure transition at different temperatures [2] (reproduced with permission from the American Chemical Society)

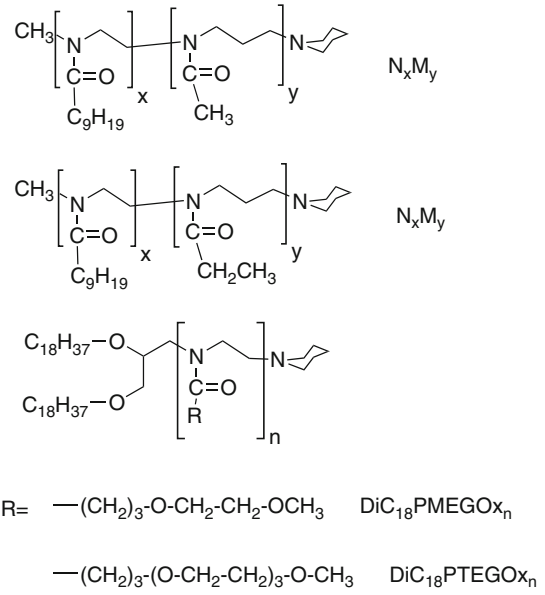

Fig. 4 Molecular structure of diblock copolymers and side-chain modified lipopolymers whose pressure–area isotherms are presented in Figs. 6 and 7, respectively. Diblock copolymers are poly(2-*n*-nonyl)-poly(2-methyl or 2-ethyl-2-oxazoline) (N_xE_y and N_xM_y), where x and y denote the block sizes of the hydrophobic nonyl and hydrophilic oxazoline blocks. Side-chain modified lipopolymers, which contain short oligo-EG sidechains in each monomer of the lipopolymer to create a bottle-brush-like structure, are di-octadecanoyl-glycerol 2-(3′-methoxymonoethylene glycol)propyl-2-oxazoline ($DiC_{18}MEGOx_n$) and di-octadecanoyl-glycerol 2-(3′-methoxytriethyleneglycol)propyl-2-oxazoline ($DiC_{18}TEGOx_n$) (adapted from [7, 8])

pressure isotherms were undertaken with the partially unsaturated 1,2-dioleoyl-*sn*-glycero-3-phosphoethanolamine–PEG2000 (DOPE–PEG2000), and compared to DSPE–PEG2000 [7]. No high pressure transition was found in the pressure–area isotherm of the unsaturated-lipid lipopolymer Langmuir monolayer. This finding is interesting because DOPE is known to have a substantially lower gel–liquid phase transition temperature than the saturated DPPE and DSPE. Another interesting study compared the pressure–area isotherms of lipopolymers and diblock copolymers, where the diblock copolymer, while containing a lipophilic moiety, did not contain the geometry of two acyl chains attached to a glycerol backbone [7]. The copolymers used, poly(2-*n*-nonyl)-poly(2-methyl or 2-ethyl-2-oxazoline) (N_xM_y or N_xE_y), are shown in Fig. 4. By contrast to lipopolymers, pressure–area isotherms of diblock copolymers in general, and of this type in particular, do not display any high pressure phase transition, thus indicating the crucial role of the saturated lipid moiety for the high-pressure transition to occur. In addition, the ethyloxazoline copolymers, N_xE_y, also show the low pressure transition which is attributed to polymers desorbing from the surface.

Triblock copolymers consisting of 135–800 monomers of PEG end capped with $C_{12}H_{25}$ or $C_{16}H_{33}$ lipid moieties have also been investigated [9]. Upon compression, $\pi - A$ isotherms of $C_{12}H_{25}{-}PEG_{135}{-}C_{12}H_{25}$, for example, exhibit not only the first transition, π_{low}, but apparently also a second transition at π_{high}. With a molecular weight of about 6,000, $C_{12}H_{25}{-}PEG_{135}{-}C_{12}H_{25}$ is fairly similar to DSPE–PEG5000, the results of which are reported above, except the lipid tails are on either end of the polymer from each other, instead of both together on one end. However, unlike lipopolymers, these molecules are not stable above the high pressure transition; if left on a trough for up to 12 h the pressure gradually decreases, indicating desorption of the triblock into the subphase [9]. Moreover, while the $\pi - A$ isotherms show the second plateau on compression of the monolayer, no similar plateaus are seen on expansion; rather the isotherm shows that some fraction of molecules are desorbed at the higher pressure. Finally, when the rate of compression was varied, the apparent π_{high} varied, with the fastest compressing monolayers undergoing the transition at the highest pressure. The low pressure transition, in contrast, displayed no changing behavior on compression and expansion or on varying rates of compression. Changing the rate of compression for lipopolymers, by contrast, does not change the pressure at which a plateau is reached, although compressing lipopolymers quickly may change the initial reading of the area per lipopolymer at which the plateau is reached until the system equilibrates [6].

Collecting all the experimental evidence obtained so far on the high pressure transition in $\pi - A$ isotherms leads to indications that this is a first order phase transition strongly related to the existence of dual lipid tails. Furthermore, the less pronounced the plateau of the high-pressure transition, the lower the gel–liquid phase transition temperature of the corresponding lipid (without attached polymer chain). This correlation suggests that there is a critical relationship between high-pressure transition and the lipids' ability to exhibit acyl chain condensations. And, in fact, in 1999 the high-pressure transition was described as an acyl chain condensation and not, as had been earlier suggested, as a mushroom-brush transition [6, 10]. The experimental evidence provided for this conclusion was based on infrared reflection absorption spectroscopy (IRRAS) data taken on lipopolymers at the air–water interface below, at, and above π_{high} (and at temperatures found to optimize the signal to noise ratio). In this experimental set-up, an infrared beam is reflected off the monolayer at the water surface and the absorbances of these reflections are recorded. After subtracting for the absorbance of a pure water surface, the data are Fourier-transformed into normalized infrared spectra, showing, of particular interest, the symmetric and asymmetric CH_2 stretches (the 2,900 cm^{-1} range) and also the C–O–C stretches (around 1,150 cm^{-1}). IRRAS data were obtained on DSPE–PEG2000, PMOx and PEOx systems [6] and on DSPE–PEG5000 and partially deuterated DSPE–PEG5000 [10]. The IRRAS data showed two trends. First, the maximum reflection-absorbance for both the symmetric and asymmetric CH_2 vibrations shifted to smaller wavenumbers as the monolayers were compressed, and this shift was most dramatic during the compression associated with π_{high}. The decrease seen was 4–7 times stronger than would be expected from simply compressing the monolayer, and was seen rather as an indicator that the CH_2 groups become more

ordered during the transition. As noted by Baekmark et al., the absolute values for these CH_2 stretches are quite similar to IRRAS data on liquid condensed phospholipid monolayers [6]. The IRRAS spectra on DSPE–PEG5000 with the lipid moiety containing either hydrogen or deuterium were particularly informative because by subtracting the two spectra it was possible to show that this decrease in the maximum absorbance trend seen on all the lipopolymer systems studied was due to the CH_2 stretches of the lipid, and not the CH_2 stretches in the polymers [10]. Second, the C–O–C stretches for the PEG IRRAS spectra above and below the transition pressure contained a broad band shape, indicative of an amorphous, and not ordered state. Consequently, these authors concluded from their data that the high pressure transition involves a dramatic ordering in the conformation of the acyl chains without an accompanying ordering of the polymeric moiety.

While the PEG and polyoxazoline lipopolymers all showed increased acyl chain order upon compression, many differences appear in the manner of their transitions, suggesting a fascinating interplay between polymer and lipid moieties in the assembly of lipopolymers at the air–water interface. To explore the influence of the polymer moiety on $\pi - A$ isotherms, several film balance experiments have been conducted where the polymer moiety of lipopolymers was modified systematically. Figure 5 shows a close-up around π_{high} of a study on DSPE–PEG lipopolymers of different chain length, and thus of different molecular weight [11]. The $\pi - A$ isotherms suggest a qualitative difference between the short-chain DSPE–PEG750 and DSPE–PEG1000 on one hand and DSPE–PEG2000, DSPE–PEG3000, and DSPE–PEG5000 on the other. For example, there is a notably larger shift in the area per molecule and transition pressure when comparing DSPE–PEG1000 (22

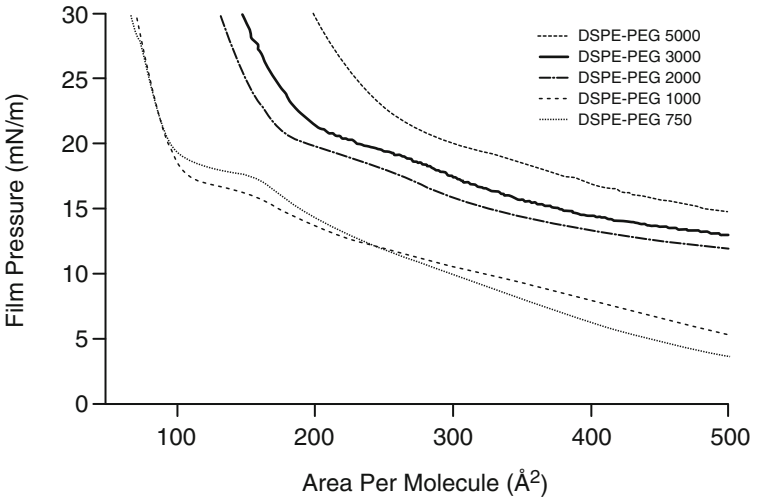

Fig. 5 Pressure–area isotherms of DSPE–PEG750, DSPE–PEG1000, DSPE–PEG2000, DSPE–PEG3000 and DSPE–PEG5000 around the high pressure transition [11] (reproduced with permission from the American Chemical Society)

monomers) and DSPE–PEG2000 (45 monomers), vs DSPE–PEG2000 and DSPE–PEG3000 (67 monomers). Based on these data, it was proposed that the PEG chains of the three longer chain lipopolymers are in a coiled, but slightly elongated conformation close to the high pressure transition, whereas those of the two shorter chain lipopolymers resemble a rodlike, fibrillar structure [11].

There is also experimental evidence that the nature of the polymer moiety may have a significant effect on the high-pressure transition as well. Comparisons of film balance experiments on $DiC_{18}PMOx_{35}$, $DiC_{18}PEOx_{31}$, and DSPE–PEG2000, which all have the same length lipid moiety, show that the high-pressure transition varied significantly between the polyoxazoline and PEG systems, with the polyoxazoline systems undergoing the transition at a much higher surface pressure. In addition, film balance experiments were performed comparing $DiC_{18}PEOx_{31}$ and dioctadecylamine [poly(ethyloxazoline)$_{35}$] ($DODA-PEOx_{35}$), which is nearly the same as $DiC_{18}PEOx_{31}$ other than the fact that the 18 C chains are connected to the polymer through an amine group instead of a glycerol group. The high-pressure transition varied significantly, with the amine system undergoing a transition nearly 10 mN m^{-1} again higher and about 15% more compressed than the $DiC_{18}PEOx_{31}$ system, so that $\pi_{high}^{PEG2000} < \pi_{high}^{PMOx35} < \pi_{high}^{PEOx31} < \pi_{high}^{DODA35}$ [12]. Overall, these data indicate that the location of the high-pressure transition depends on the subtle interplay of several factors, including the polymer structure and molecular weight and the nature of the hydrophobic anchor.

Using a synthetic approach to understanding the nature of the acyl chain condensation, a number of novel oxazoline lipopolymers were synthesized with the same lipid backbone, two 18 carbon chains attached to glycerol, but with polymers characterized by having different sidechains including a methoxymonoethylene glycol and an isopropylmethoxymonoethylene glycol on the ethyl end of the ethyloxazoline polymer ($DiC_{18}PMOGOx_{21}$ and $DiC_{18}PTEGOx_{18}$) [8]. These polymers are collected in Fig. 4. The thinking was that bulky side chains on the polymer would force physical distance between each lipopolymer, and thus inhibit the ability of the lipid moiety of each lipopolymer to condense with the lipid moiety of a neighboring lipopolymer, and be another way to explore the importance of lipid–lipid interactions on the high pressure transition region. This proved to be correct, as Fig. 6 shows that the oligo–EO substituted lipopolymers ($DiC_{18}PMOGOx_{21}$ and $DiC_{18}PTEGOx_{18}$) did not exhibit the high pressure transition at all before film collapse, and thus did not undergo the acyl chain condensation.

Additional film balance experiments on diblock and triblock copolymers have been shown to be helpful in evaluating the properties of the low pressure transition, π_{low}, at the air–water interface. Many $\pi - A$ isotherms of diblock and triblock copolymers have been published: one excellent example is Gonçalves Da Silva's polystyrene–polyethylene glycol diblock copolymers published in 1996 which showed not only the absence of a high pressure transition in these non-lipid amphiphiles, but also that the low pressure transition occurred at a constant area/monomer of PEG regardless of the size of the PEG polymer [3]. This is also more evidence that the pressure relates to submersion, monomer by monomer, of the PEG from the surface. Reviewing film balance studies on polyoxazoline-containing

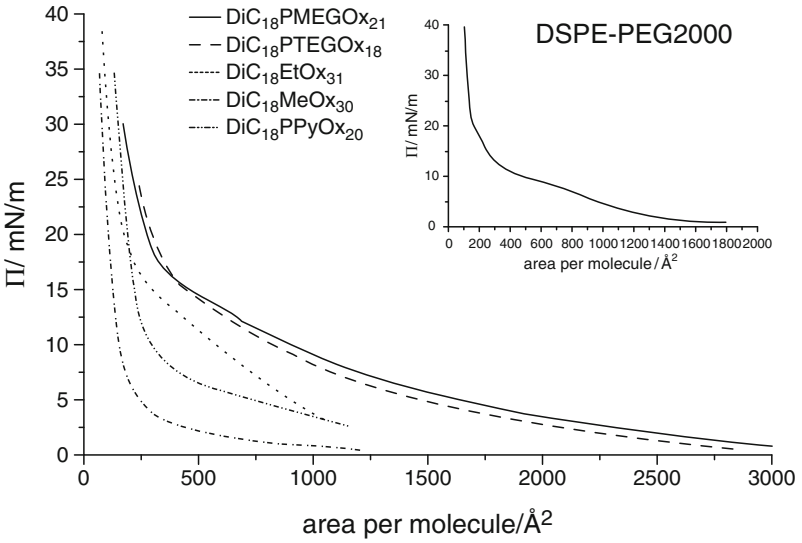

Fig. 6 $\pi - A$ isotherms of $DiC_{18}PPyOx_{20}$, $DiC_{18}PMOx_{30}$, $DiC_{18}PEOx_{31}$, $DiC_{18}PTEGOx_{18}$ and $DiC_{18}PMEGOx_{21}$ at room temperature, with the isotherms of DSPE–PEG2000 included for comparison (*inset*) [8] (reproduced with permission from Wiley)

lipopolymers, and diblock, and triblock copolymers confirmed that the low pressure transition can be found in the presence of amphiphilic PEOx, but not with the more hydrophilic PMOx (Fig. 7) [7]. It is recalled that the PEG lipopolymers, like the PEOx lipopolymers, display a strong degree of amphiphilicity at the air–water interface and also undergo the low pressure transition.

To obtain more information about the structural properties of lipopolymers at the air–water interface, several groups have pursued X-ray and neutron scattering experiments. Using X-ray and neutron reflectometry, Wurlitzer et al. confirmed acyl chain condensation above π_{high} but also found that the surface of the monolayer was rougher, less planar [13]. In particular, just below the surface there was a range of 15 Å where lipid tails, ether linkers between the lipid tails and the glycerol backbone, and PMOx monomers can be found. The first eight carbons of the PMOx chain were deuterated in order to better show the location of the polymer within the subphase, and they showed these first eight carbons in the same location as the ether linkers but the hydrogenated PMOx carbons, further down the chain, also had great density at this same height, just below the surface. The acyl chains and ether linkers do not penetrate further down than this and the deuterated carbons only extend another 10–15 Å further, but the hydrogenated PMOx carbons extend down to below 100 Å from the interface. Wurlitzer et al. hypothesized that the energy associated with the elastic effect of forcing the polymers closer together led to a partial immersion of the hydrophobic acyl anchors into the aqueous medium [13, 14].

Grazing incidence X-ray diffraction and specular X-ray diffraction studies by Ahrens et al. agree that some form of lipid condensation takes place at the

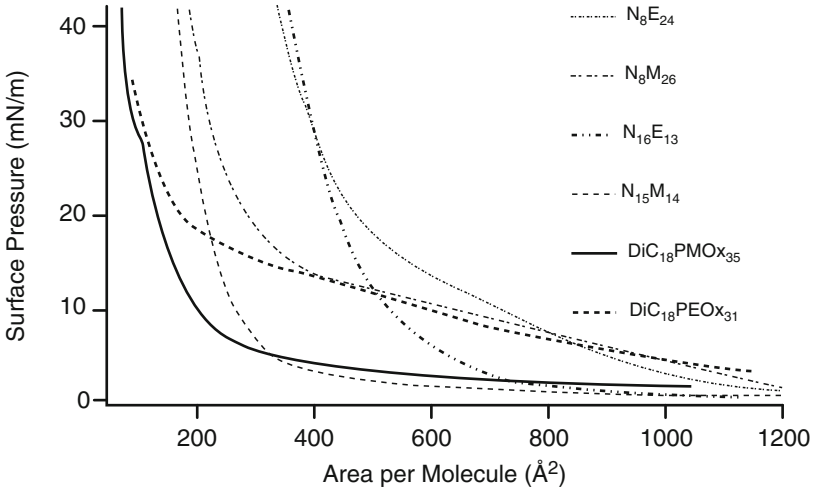

Fig. 7 $\pi - A$ isotherms of diblock copolymers with isotherms of lipopolymers $DiC_{18}PMOx_{35}$ and $DiC_{18}PEOx_{31}$ included for reference. Note the ethyloxazoline systems display low pressure transitions which the methyloxazolines do not, and the diblocks do not display high pressure transitions [7] (reproduced with permission from the American Chemical Society)

high-pressure transition, and also provide evidence of a possible superstructure [15, 16]. Looking at DSPE–PEG2000, Ahrens et al. found tilt angles of the acyl chains between 14° and 18° with respect to the surface normal for pressures above π_{high}, with tilt angles decreasing upon compression. The packing density for the samples based on the calculated lattice constants, however, was not in agreement with the bulk density of the lipids, but in fact showed the lipid tails much more closely packed (but not quite as densely packed as phospholipids in the absence of polymers) [15,16]. This finding corresponds to the IRRAS data from Baekmark and Wiesenthal, which found CH_2 stretches very similar to stretches for phospholipids packed closely together, although they could not be homogeneously so condensed because the average area per lipopolymer was much too large for a continuously condensed lipid surface. Ahrens, et al. suggested this was possible using a theory of surface micellization, whereby some aggregate of lipopolymers collects and the lipid tails within each aggregate condense together during the high-pressure transition. For evidence, grazing incidence X-ray diffraction showed that lattice constants *increased* upon compression above π_{high}, creating superstructures spaced 134–160 Å apart [16]. These investigators transferred the monolayers onto mica and found surface stripes of about the same periodicity using atomic force microscopy. However, it is difficult to compare fixed, dry monolayers which are necessarily subject to substrate interactions, with fluid monolayers on a water surface. Another group looking at X-ray grazing-incidence diffraction and reflectivity of lower molecular weight DSPE–PEG chains found little coherence for DSPE–PEG90 and DSPE–PEG350, but for DSPE–PEG750 found clusters of about 43 lipopolymers

within which the acyl chains were perpendicular to the surface, and showed good hexagonal packing [17].

Israelachvili considered the possibility of Langmuir monolayers of any sort of amphiphiles forming surface micelles in 1994 [18]. In his model, there is a critical micellar area (CMA or A_c), below which few micelles form and the concentration of the system is nearly equal to the concentration of discrete molecules, but above which, the concentration of micelles increases while the concentration of discrete molecules is constant. Below A_c, the total average area per molecule, A, will be the same as the area per molecule of the discrete molecules, defined A_1. If A_0 is defined as the hard-disk excluded area of a molecule in a micelle, and N is the number of molecules in a micelle, then the $\pi - A$ isotherm for a system forming surface micelles can be written as

$$\pi = \frac{kT}{N}\left[\frac{1}{A - A_0} + \frac{(N-1)}{(A_1 - A_0)}\right]. \tag{1}$$

The significant finding from this is that, for a hypothetical system, surface micellar formation for N even as small as 25 molecules leads to a plateau on a $\pi - A$ isotherm, and conversely, a plateau on a $\pi - A$ isotherm may indicate surface micellar formation. Israelachvili considers the case of fluid alkane chains connected to repelling hydrophilic head groups which are all in the plane of the monolayer, noting that micellar formation would enable the headgroups to increase the distance between them, and lower the interaction energy per molecule. Counterbalancing this, there is a maximum aggregation size related to the fully extended length of the hydrocarbon chain, l_c, above which micelles are not energetically favored, since the headgroups would presumably be repelled by the interior of a micelle even more than by nearby other headgroups. The shape of such micelles, Israelachvili goes on to suggest, would be either small circles or ribbons with a half width less than l_c.

Langmuir monolayers of diblock and triblock copolymers have been thoroughly studied, and through analyses of $\pi - A$ isotherms and neutron reflectometry data, it has been shown that many combinations of copolymers form surface micelles. Based on the density at different heights below the air–water interface of polystyrene and PEG in block copolymers, Dewhurst concluded that the polystyrene moieties aggregate into a cluster, with PEG forming a cushion underneath and a corona around the polystyrene center, akin to flower-like micelles [19]. Naturally, the nature of lipopolymers, with their acyl chain condensation, would lead to a different geometry than diblock copolymer micellization. However, trends observed by Deschenes et al. lead to the prediction that the size of the micelles is controlled by the ratio of hydrophobic to hydrophilic block area, with higher hydrophobic areas aggregating into planar morphologies, and lower ratio hydrophobic areas (different than, but similar to lipopolymers) forming cylinders, wormlike or dendritic structures [20]. The experimental findings from di- and triblock copolymers are interesting because there is some experimental evidence that lipopolymers may assemble into micellar structures at the air–water interface. For example, as already noted, Ahrens and Helm reported the formation of stripe-like structures on lipopolymer monolayers

after the monolayers had been transferred to mica [16]. Similarly, neutron reflectometry data, in combination with film balance and interfacial rheology results, have been interpreted in terms of a surface micellization of lipopolymers [7].

Up to this point, the information about the monolayers has looked at the structural properties as if the lipopolymer monolayers were static and fixed above a body of water. However, a truly remarkable aspect of these monolayers is their fascinating fluidity and visoelastic properties, and the range of distinct fluid and viscoelastic behavior they exhibit under different conditions and with different lipopolymers. These properties can be studied by analyzing the viscosity and elasticity of the monolayer, as discussed in Sect. 2.2, as well as by investigating the lateral diffusion of individual lipopolymers within the monolayer, as discussed in Sect. 2.3.

2.2 *Viscoelastic Properties of Lipopolymers in Langmuir Monolayers*

To obtain information about the viscoelasticity of lipopolymers at the air–water interface, Langmuir monolayers of lipopolymers were studied using interfacial rheology. Initial experiments were conducted using a custom-built interfacial needle shear rheometer, as described before [2, 21] and illustrated in Fig. 8. In this experimental setup, a trough is constructed with a Langmuir monolayer as noted in previous experiments, but in addition, a magnetic rod is stabilized at the air–water interface and subjected to an oscillatory magnetic field gradient, which is provided by a pair of Helmholtz coils surrounding the trough [21]. The position of the rod is tracked using an inverted microscope and a linear photodiode array. From the rod's position (strain) relative to the applied current in the coils (stress), it is possible to determine δ, the phase lag between the strain and the stress, as well as the amplitude ratio, AR, which is defined as the ratio of strain to stress. If it is assumed that the contribution from the underlying subphase is negligible compared with the interface, which is true in practice, these parameters define the dynamic surface modulus $G_s{}^*$, from which can be determined the storage modulus, $G_s{}'$ and the loss modulus, $G_s{}''$. These pioneering experiments on PEG lipopolymers revealed a remarkable change of viscoelastic properties in the range of the high-pressure transition [2]. As illustrated in Fig. 9, below this transition, the monolayer is fluid and the loss modulus, G'' (a measure of the viscosity of the film), is larger than the storage modulus, G' (corresponding to the elasticity of the film). In contrast, above the high pressure transition, the monolayer becomes elastic with $G' > G''$, thus suggesting the formation of a physical gel. Originally, this physical gel formation was interpreted in terms of two types of associative interactions: microcondensation of acyl chains to form small clusters, and water molecules acting as intercalators mediating the interaction between PEG chains via hydrogen bonding [2].

In a following study, it was confirmed that the gelation transition was not limited to PEG lipopolymers because comparable viscoelastic properties were observed on monolayers of polyoxazoline lipopolymers as well [12]. This called into question

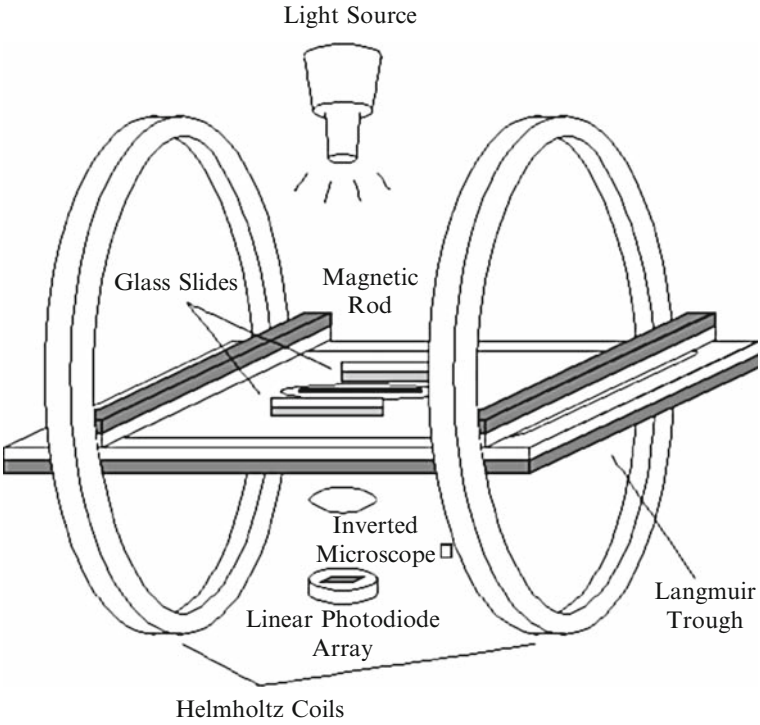

Fig. 8 Design of an interfacial stress rheometer. Here a magnetized rod is subjected to an oscillatory force generated by the Helmholtz coils. The motion of the rod is detected using a microscope and photodiode array. Differences between the applied force and resulting phase and magnitude of the displacement give information on the viscoelastic properties of the monolayer. Both the storage modulus G' and the loss modulus G'' can be determined [2, 21] (reproduced with permission from the American Chemical Society)

the initial model whereby intercalated water molecules via hydrogen bonding were the basis for the elasticity of the monolayer. To uncover the nature of the viscoelastic transition, additional interfacial rheology experiments were conducted where the polymer and lipid moieties of lipopolymers were altered systematically [7, 11]. These studies were conducted using an oscillating ring rheometer. For example, the molecular weight of the PEG moiety of PEG lipopolymers was changed (MW: 750, 1,000, 2,000, 3,000, 5,000) [11]. As illustrated in Fig. 10, these experiments showed that the gelation transition shifts to smaller areas per molecule and that there is a qualitative difference between higher MW species (MW: 2,000, 3,000, 5,000) and lower MW species (MW: 750, 1,000). In the first case, G' exhibits a power law-like behavior above the gelation transition. In the second case, a breakdown of the gel is observed after an initial power law-like behavior [11]. Interestingly, the strength of the gel (prior to collapse) was found to follow the trend G′(DSPE–PEG750)< G′(DSPE–PEG1000)< G′(DSPE–PEG2000)> G′(DSPE–PEG3000)> G′(DSPE–PEG5000). This result showed that the strength of the physical gel can

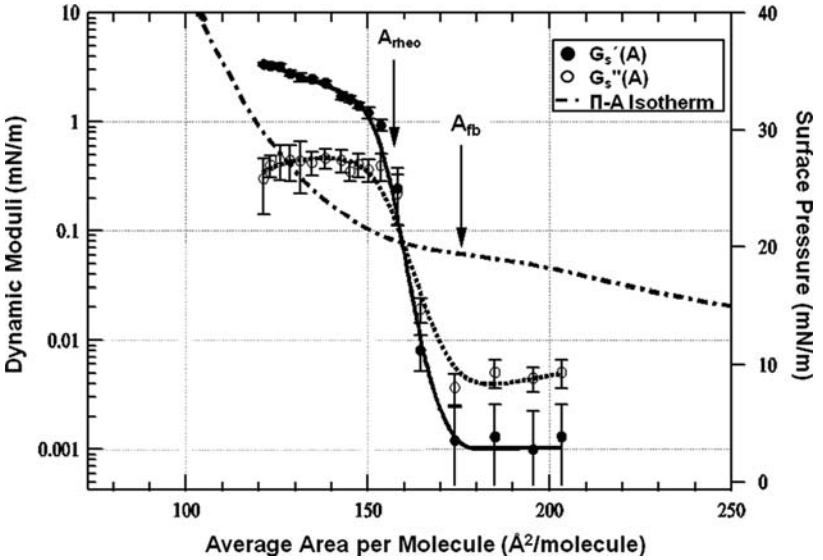

Fig. 9 Dynamic moduli vs area isotherm for DSPE–PEG2000, with $\pi - A$ isotherm also shown, pointing out that the viscoelastic transition point, where storage modulus $G_s' =$ loss modulus G_s'' is only slightly above the plateau of the high-pressure transition [2] (reproduced with permission from the American Chemical Society)

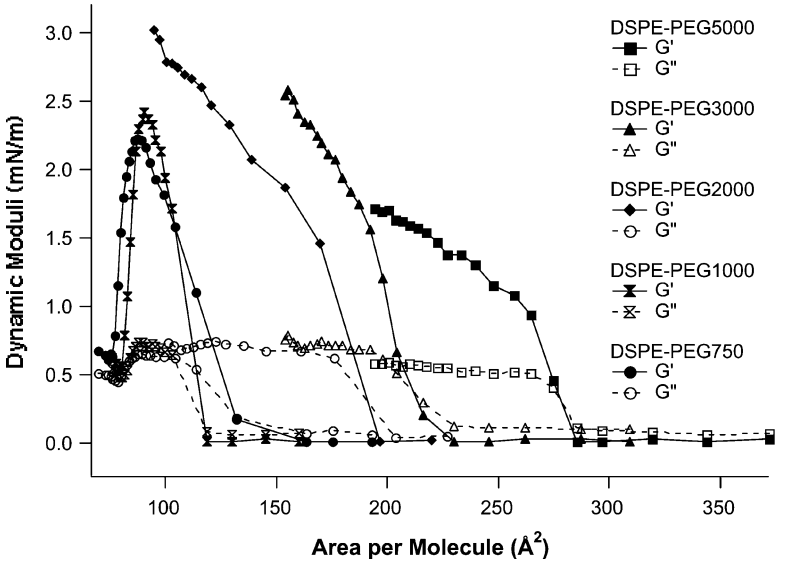

Fig. 10 Storage modulus, G_s', and loss modulus, G_s'', of DSPE–PEG750, DSPE–PEG1000, DSPE–PEG2000, DSPE–PEG3000, and DSPE–PEG5000 plotted vs area per molecule. All lipopolymers show a viscoelastic transition [11] (reproduced with permission from the American Chemical Society)

be regulated by changing the PEG molecular weight of lipopolymers. When PEG chains of PEG lipopolymers are shorter or longer than PEG2000, the strength of the polymer gel is weakened. These data are significant because they emphasize that polymer and lipid moieties of lipopolymers are equally important in the regulation of the high-pressure and gelation transitions. Furthermore, these results showed that both types of transitions are critically dependent on the area mismatch between lipid and polymer moieties of lipopolymers.

To explore the role of molecular structure of amphiphiles on the physical gelation transition, additional interfacial rheology experiments were conducted using polyoxazoline-based diblock copolymers and PEG lipopolymers with lipid anchors of various acyl chain lengths [7]. Figure 11 illustrates that only lipopolymers, and not diblock copolymers, exhibit a gelation transition. Interestingly, when $DiC_{18}PEOx_{31}$ and $DiC_{18}PMOx_{35}$ transitions are compared by area per molecule, as opposed to film pressure, they exhibit the gelation transition at the same area per molecule, about 90 $Å^2$.

Also, in contrast to DPPE–PEG2000 and DSPE–PEG2000, which have acyl chains of C_{16} and C_{18}, respectively, no rheological transition was observed for lipopolymers with relatively short acyl chains (C_{14}), DMPE–PEG2000. It should be recalled that no high pressure film balance transition was found for DMPE–PEG2000 either, thus suggesting a direct relationship between high-pressure and gelation transitions [7]. High pressure transitions and rheological transitions are not limited to PEG and polyethyloxazoline systems: DiC_{18} linked to glycerol which is also attached to a sugar-based polymeric moiety, namely three end-linked lactose units, also displayed the transition from a fluid to an elastic film [22]. Finally,

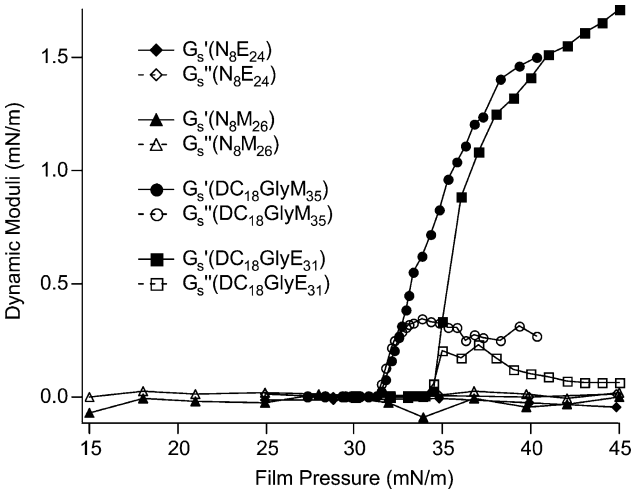

Fig. 11 Storage modulus, G_s', and loss modulus, G_s'', of N_8E_{24}, N_8M_{26}, $DiC_{18}PMOx_{35}$, and $DiC_{18}PEOx_{31}$ plotted vs film pressure (which increases as area per molecule decreases). Lipopolymers do show a viscoelastic transition but diblock copopolymers do not [7] (reproduced with permission from the American Chemical Society)

there is no rheological transition pressure for unsaturated acyl chains, just as there was high-pressure film balance transition [7]. Overall, these experiments confirmed that a high-pressure film balance transition is necessary for a rheological (gelation) transition to occur.

In another experiment it was shown that, while necessary, a high pressure film balance transition is not sufficient to cause this gelation to occur. The lipopolymer composed of lipids and polyethyloxazoline connected through an amine headgroup, $\mathrm{DODA-PEOx_{35}}$ underwent a high pressure film balance transition. However, it showed a loss modulus consistently higher than the storage modulus at all surface areas measured, and thus never displayed a rheological gelation transition [12]. Saturated phospholipids without polymer chains also never display rheological transitions, even though they obviously undergo acyl chain condensation [7]. In summary, the strength of the network, as characterized by its elasticity, is dependent on the strength of molecular interactions within the lipid moiety, but the lipid must be covalently connected to a polymer for gelation to occur. In particular, the strongest rheological transition occurs for DSPE–PEG2000; shortening or desaturating the lipid chain minimizes the rheological transition (and diblocks at the air–water interface without the dual acyl chains do not undergo the rheological transition to gels at all); changing the connecting head group can disrupt the rheological transition; and substituting PMOx for PEOx in otherwise identical systems does not affect the rheological transition, but both exhibit a transition at more concentrated areas per molecule than PEG lipopolymers. Cataloging the various lipopolymeric rheological transitions to an elastic monolayer does not, however, by itself, bring an understanding of the underlying phenomenon causing this behavior.

Polymers are known to become elastic upon interdigitation and entanglement, which might explain the elasticity of the monolayers above the viscoelastic transition. However, such a process is highly unlikely in a lipopolymer monolayer at the air–water interface given the short lengths of the polymeric chains involved. An alternative possible explanation is that hydrogen bond bridges between the head groups during lateral compression to higher pressures store the elastic energy, as proposed in the earlier work of Naumann and Schneider [2,22]. However, it has been shown that there is no attractive interaction potential between PEG chains [23, 24]. In addition, studies of PEG star copolymers in different pH solutions showed that it is unlikely there are hydrogen bond bridges between the PEG moieties, at least during lateral compression [25].

To understand further the nature of the rheological transition, a series of experiments were performed by our lab monitoring the time evolution of viscoelastic properties in PEG lipopolymer monolayers at film pressures near the gelation transition (previously unpublished data). In particular, the DSPE–PEG series with PEG molecular weights from 750 to 5,000 were measured at particular film pressures slightly less than and slightly more than the rheological transition pressure (accuracy of dynamic moduli is around $\pm 5\%$). The storage and loss modulus of a monolayer of pure DSPE–PEG2000 just below the rheological transition pressure, at $20.1\,\mathrm{mN\,m^{-1}}$, started out with the loss modulus higher than the storage modulus (non-gel state) at time $= 0$, but after 30 min, these values switched, and by 1 h,

the storage modulus was significantly higher and remained so for the duration of the experiment (4 h) (Fig. 12b). Similar behavior was observed when storage and loss of DSPE–PEG2000 were tracked at slightly higher pressures as well (data not shown). Thus, for DSPE–PEG2000, the longer the system was tracked by a rheological probe, the higher the storage modulus.

As illustrated in Fig. 12, however, the behavior of DSPE–PEG2000 was notably different than the behavior exhibited by either the longer chained lipopolymers or the shorter chained lipopolymers. DSPE–PEG750 had a very different response. When dynamic moduli were monitored over time at a pressure of 19.5 mN m^{-1}, corresponding to slightly *above* the expected rheological transition pressures, the storage modulus started out higher, in a gel state, but over 2–3 h, the storage modulus decayed until the loss modulus was higher, or liquefaction occurred. It is recalled that for these length chains, at pressures more than 10 mN m^{-1} above the rheological transition pressure, the gel state also collapsed and the monolayer liquefied [11]. When the time study was performed below the transition pressure, the low-weight monolayers stayed in the non gel state, and did not achieve the gel state within the time period studied, unlike the behavior of DSPE–PEG2000 (data not shown). Looking at the other end of the PEG spectrum, the DSPE–PEG5000 at 20.5 mN m^{-1}, just below the rheological transition pressure, stayed in the non gel state for the full 4 h, but at 22.0 mN m^{-1}, the DSPE–PEG5000 started out well into the gel-state with storage more than twice as high as loss modulus, but over a time period of less than 2 h, the monolayer liquefied and the situation was reversed. In summary, DSPE–PEG2000, over time, quickly developed into the gel state from just below the rheological transition pressure, but shorter and longer lipopolymers not only did not develop into the gel state from just below the rheological transition pressure, but decayed from the gel state to a liquid state at pressures just above the rheological transition pressure.

The results obtained from the study of the time evolution of viscoelastic properties are exciting because they show that the behavior of the DSPE–PEG2000 is reminiscent of the rheological behavior of star polymers [26, 27]. In those systems, concentrations of star polymers in good solvent swell upon heating and form jammed clusters which cause the solution to become elastic. This condition is thermally reversible. The conditions necessary are dense star solutions, a high number (>64) of arms for the star polymer, and intermediate (that is, better than Θ but not necessarily athermal) or good solvent [26]. Jamming of polymeric micelles of diblock copolymers, again in 3D have also been observed [28, 29]. Renou et al. noted that the transition which can be obtained by varying the temperature can also be obtained by increasing the volume fraction [29]. Here the diblock micelles first form upon increasing concentration, and then upon further compression act as dynamic (as opposed to covalently linked) star polymers and jam together while retaining their soft boundaries, thus leading to elastic behavior. At some increased concentration, these micelles form a crystalline structure.

The similarity between viscoelastic properties of lipopolymer monolayers and star polymers suggests that the gelation transition in lipopolymer monolayers might be caused by a jamming transition of micelles as well. Such a model is attractive because the ability to form surface micelles should be strongly connected to the

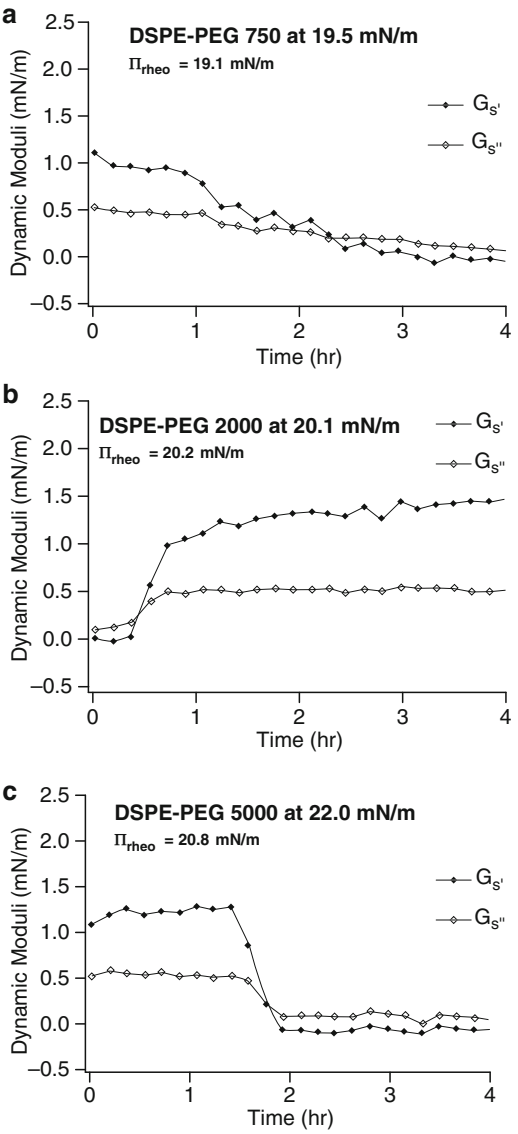

Fig. 12 a–c Time evolution of viscoelastic properties near the gel point for DSPE–PEG750, DSPE–PEG2000, and DSPE–PEG5000. **a** DSPE–PEG750, short-chain lipopolymer, starts out above the viscoelastic transition point at 19.5 mN m^{-1} but after 1 h, a gradual breakdown of the gel can be observed. After 2.5 h the loss modulus becomes higher than the storage modulus. **b** DSPE–PEG2000 starts out below the viscoelastic transition point, at 20.1 mN m^{-1}, and within 30 min has undergone gelation leading to a notably higher storage modulus and a slightly higher loss modulus. **c** DSPE–PEG5000, a long-chain lipopolymer, starts out above the viscoelastic transition point at 22.0 mN m^{-1} but within 2 h, the viscoelastic gel has broken down leading to similar results as **a**

ability of lipopolymers to exhibit a gelation transition. The data obtained from star polymers and diblocks indicate that the gelation transition requires the jamming of such surface micelles. Unlike other models, the jamming model is able to explain the importance of a long saturated lipid tail that can undergo acyl chain condensation in order to obtain a gelation transition. Within this model, it can also be rationalized that the length of the polymer chains will affect the ability of the lipopolymers to form jammed surface micelles. Polymers which are shorter will aggregate into surface micelles with shorter, less soft polymer shells less able to accommodate and form jams, so that increasing compression can cause the elastic monolayer to collapse. Monolayers of longer polymers, such as DSPE–PEG5000, may form surface micelles with insufficient aggregation numbers, which may lead to increased micelle interpenetration or deformability, thus enabling surface micelles to avoid lateral stress more easily, and thus present themselves as less elastic and more likely to rearrange and break down over time. It will be interesting to compare the viscoelastic behavior of mixtures of lipopolymers and phospholipids, since if they form micelles, there would be fewer polymeric moieties for the same number of condensed acyl chains in a mixture. This will be discussed in depth below in Sect. 3.2.

2.3 Diffusion Properties of Lipopolymers in Langmuir Monolayers

Another method of investigating monolayers is to study the diffusion of lipopolymers within the monolayer as a function of surface density (area per molecule). The manner in which the lipopolymers diffuse can shed light on how they organize and their usefulness in mixed lipopolymer phospholipid bilayers. Diffusion analysis can be accomplished through wide-field single molecule fluorescence microscopy. It must be remembered that determining diffusion data from fluid monolayers at the air–water interface is experimentally quite challenging, since the possibility of water flow affects the diffusion measurements. Unless properly accounted for, surface flow can introduce large margins of error. The specifics of a single molecule imaging set-up for monolayer experiments at the air–water interface have been reported elsewhere [30, 31], but in essence, lipopolymers are labeled with tetramethyl rhodamine isothiocyanite (TRITC) through thiourea coupling, and added to a lipopolymer monolayer at a mol concentration of 1×10^{-8} mol%. Then, after the lipopolymers are assembled on the monolayer at the desired area per molecule, an excitation source coupled to an intensified CCD camera with a synchronized shutter creates instantaneous micrographs of the position of the fluorescent particles, and the data are transferred to image recording and single molecule tracking software. From this, the positional change of single fluorescently-labeled molecules is analyzed for each successive frame using a constant time lag. By tracking two to four molecules per frame, it is possible to determine relative positional changes and obtain flow-corrected square displacements, r^2. When enough of such data are collected, these can be averaged to determine the mean squared displacement, and if the data fit a normal diffusion curve, a diffusion coefficient, D, can be determined.

By using the described single molecule imaging approach, the diffusion properties of $DiC_{18}PMOx_{30}$ and $DiC_{18}PMOx_{50}$ were determined at eight different surface concentrations, from fairly dilute up to just below the high-pressure transition concentration, at which level the diffusion decreases nearly to zero [31]. PMOx systems were chosen since they do not undergo a low pressure transition, and two different length polymers were utilized for the purpose of comparing diffusion coefficients of lipopolymers with different length polymers. The lateral diffusion was found to be Brownian at all concentrations studied, and the diffusion coefficient, D is plotted vs area per molecule, A, for both $DiC_{18}PMOx_{30}$ and $DiC_{18}PMOx_{50}$ in Fig. 13.

Interestingly, the lipopolymers exhibit two different diffusion regimes, labeled as Regions I and II. In Region I, in the case of weak interpolymer interactions, D is independent of A, but the plateau or Region I value depends on the number of polymeric units, N. In Region II, D scales proportionally with A, and is also dependent on N.

The diffusion properties in Region I are well described by the Rouse model, which predicts the self-diffusion coefficient will scale as 1/N, the number of monomeric units. Applied to the two lipopolymers of interest, the Rouse model predicts the ratio

$$\frac{D_{\text{diC18PMOx30}}}{D_{\text{diC18PMOx50}}} = \frac{50}{30} = 1.67. \tag{2}$$

This Rouse ratio is in excellent agreement with our diffusion data in Region I, which provide

$$\frac{D_{\text{I,30}}}{D_{\text{I,50}}} = \frac{9.7}{5.7} = 1.7. \tag{3}$$

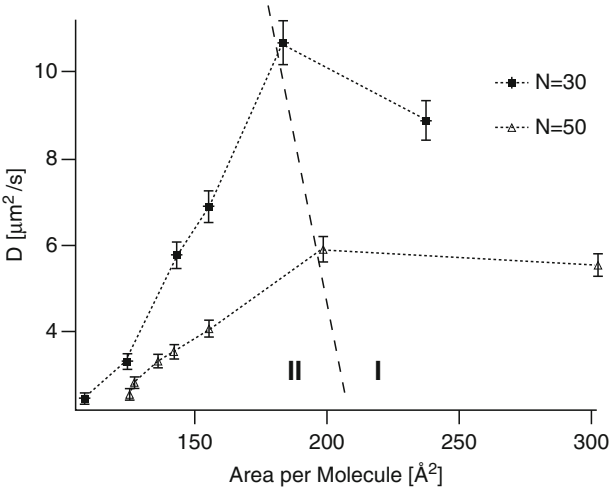

Fig. 13 Single molecule tracking data of dye-labeled PMOx lipopolymers as a function of area per molecule. The plots of the lateral diffusion coefficient, D, vs area per molecule for $DiC_{18}PMOx_{30}$ and $DiC_{18}PMOx_{50}$ show two different diffusion regions (labeled I and II). Unlike in Region II, D follows Rouse scaling in Region I [31] (reproduced with permission from the American Chemical Society)

Obviously, the diffusion data in Region II do not obey Rouse scaling because the diffusion coefficient is now dependent on lipopolymer surface concentration. Due to the higher surface density of lipopolymers in this region, more significant interpolymer interactions can be expected. The diffusion properties of polymers in bulk at elevated concentrations are characterized by chain entanglement and reptation. Here the self diffusion of reptating chains can be expressed by $D \sim c^{-\alpha}N^{\beta}$, with $\alpha = 1.75$ and $\beta = 2$ [32, 54, 55]. The data shown in Fig. 13 for the lipopolymers do not fit these coefficients well; the best fit for α for $diC_{18}PMOx_{30}$ is 4.9, and for $diC_{18}PMOx_{50}$ it is 2.4, and the best fit for β is 1.6 [31]. This disagreement is not surprising because it is hard to visualize lipopolymers with their lipid tails constrained to a surface involved in a two- or three-dimensional reptation and because the chains are too short to exhibit significant entanglement.

Another model for understanding the diffusion of lipopolymers at the air–water interface in Region II is the free area model, useful for describing the motion of phospholipids on a Langmuir monolayer and many systems where the diffusing particles can be approximated by hard spheres, disks or cylinders [38]. In this model, a particle can diffuse in any direction that is free, or in other words, in any direction that is empty of another particle. As would be expected, more crowded or concentrated systems diffuse more slowly. Assuming the particles are at a constant temperature and that other energetic considerations can be described within a constant, D_o, this type of diffusion can be expressed as

$$D = D_o \exp\left(-\frac{\gamma A_{\min}}{A_{\text{free}}}\right), \tag{4}$$

where γ is a scaling constant to be found, $A_{\min}$ is the minimum free area per lipopolymer required for diffusion, A_{free} is the average free area per lipopolymer given by $A_{\text{free}} = A_{\text{lipo}} - A_{\min}$, and A_{lipo} is the area per molecule, as graphed in Fig. 13 [31]. If $A_{\min}$ is estimated by extrapolating the D vs A_{lipo} plot to $D = 0$, both lipopolymer curves depicted above show an excellent agreement with this model in Region II when $\ln(D/D_o)$ is plotted against $(A_{\min}/A_{\text{free}})$, and this graph is shown as Fig. 14.

In addition, the slopes of the lines are well within the expected range for the free area model of $0.5 \leq \gamma \leq 1$, with values of 0.77 and 0.66. The good agreement between diffusion data and free-area model indicates that the lipopolymer lateral diffusion is dependent on the strength of interpolymer interactions and that the polymer moieties behave like rigid spheres or cylinders during the diffusion process (nondraining behavior). Figure 14 provides a few interesting implications for lipopolymer–lipid mixtures. First, lipopolymers characterized by significant interpolymer interactions can simply be considered diffusion obstacles for phospholipids, as confirmed in polymer-tethered monolayers and bilayers [39, 40]. Second, if the lipopolymers behave as hard cylinders in fluid conditions under appropriate conditions such as explored in this section, it is reasonable to expect that they can be modeled as hard cylinders in mixed phospholipid–lipopolymer monolayers, explanation of which will be the subject of the second half of this chapter.

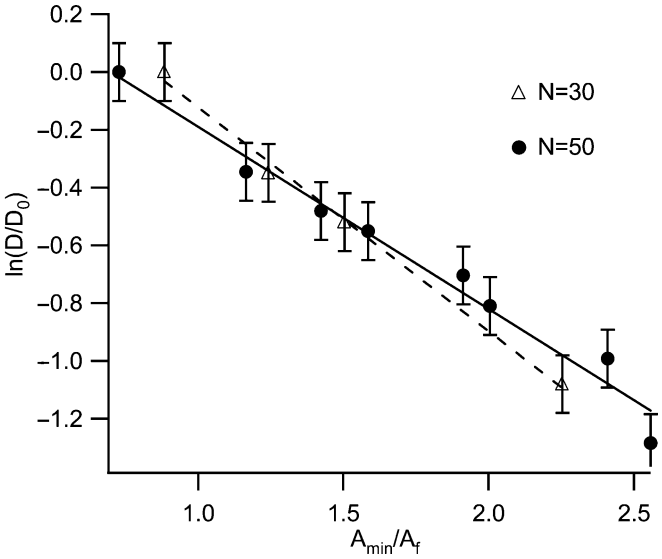

Fig. 14 Plot of $\ln(D/D_0)$ vs $A_{\min}/A_f$, for $n = 30, 50$ in diffusion Region II. The *dashed and solid lines* represent the best linear fits for $n = 30$ and $n = 50$, respectively. The excellent agreement between data points and fits shows that D of end-tethered PMOx chains in diffusion region II is well described by the free area model [31] (reproduced with permission from the American Chemical Society)

It is worth noting that the observed diffusion behavior of lipopolymers at the air–water interface shows some similarity to corresponding results on diblock copolymers, which are arranged in 2D. Lower molecular weight diblocks were found to follow Rouse scaling, whereas their higher molecular weight counterparts were better described by processes of activated reptation and block retraction [33–37]. Furthermore, temperature-dependent studies on diblocks organized in polymerosomes also showed that the self diffusion can be interpreted by a free volume theory [33].

3 Lipopolymer–Phospholipid Monolayer

3.1 Structural Properties

Although the first section of this chapter was concerned with structural and dynamic information on monolayers of lipopolymers, before investigating lipopolymer–phospholipid mixtures, it is reasonable to consider the structural information that exists concerning pure phospholipid monolayers at the air–water interface. Film balance experiments, X-ray and neutron reflectometry, and molecular dynamics simulations have provided insight into the structural properties of these biologically

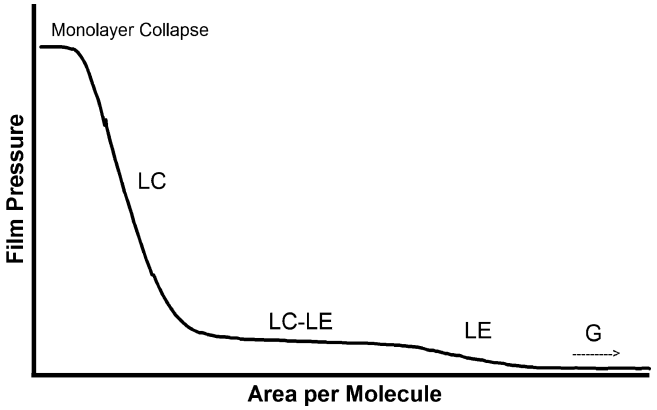

Fig. 15 Conceptual $\pi - A$ isotherm for DPPC showing the different phases: G for gas, LE for liquid expanded, LC–LE for the transition region where both liquid expanded and liquid condensed exist, and LC for the liquid condensed region

important amphiphiles. Figure 15 illustrates a $\pi - A$ isotherm of the saturated phospholipid DPPC, which exemplifies the typical phase properties of saturated lipids in a monolayer at the air–water interface (data from our laboratory).

At high area per molecule, the monolayer is first incomplete and is described as being in a gassy state, but after completion exists in the liquid-expanded (LE) state. Upon further compression, a plateau is reached, in the range of 50–70 $Å^2$, followed by a sharp increase in surface pressure after the phospholipids are all in the liquid-condensed (LC) state. Molecular dynamics simulations suggest that the head groups do not change orientations or order when transitioning from LE to LC [41]. In particular, the phosphate–nitrogen tilt angle is roughly parallel to the surface of the water and is not affected by compression of the monolayer through the phases from LE to LC; and the methyl groups on the choline prefer to sit at the air–water interface in both phases. In contrast, the lipid tails change from disordered in the LE phase to hexagonal packing in the LC phase [41], and thus the plateau represents a conformational change very similar to the acyl chain condensation described for lipopolymers by [6]. This is interesting because it shows the great similarity between the phase transitions of the phospholipids and the lipopolymers: in both, the systems start out widely spread, then upon compression, both undergo acyl chain condensation. Therefore, it is reasonable to project that mixtures of phospholipids and lipopolymers will also undergo similar processes. On the other hand, at high lipopolymer molar concentrations, significant repulsive interpolymer interactions are likely to occur, which should cause high lateral stress in the mixed monolayer with possible consequences for structural and dynamic properties. Here it cannot be excluded that lipopolymers with a very hydrophilic polymer moiety, such as polymethyloxazoline, and those with an amphiphilic polymer moiety, such as PEG and polyethyloxazoline, cause different structural and dynamic properties. The current section will provide an overview over the existing knowledge on mixed lipopolymer–phospholipid Langmuir monolayers.

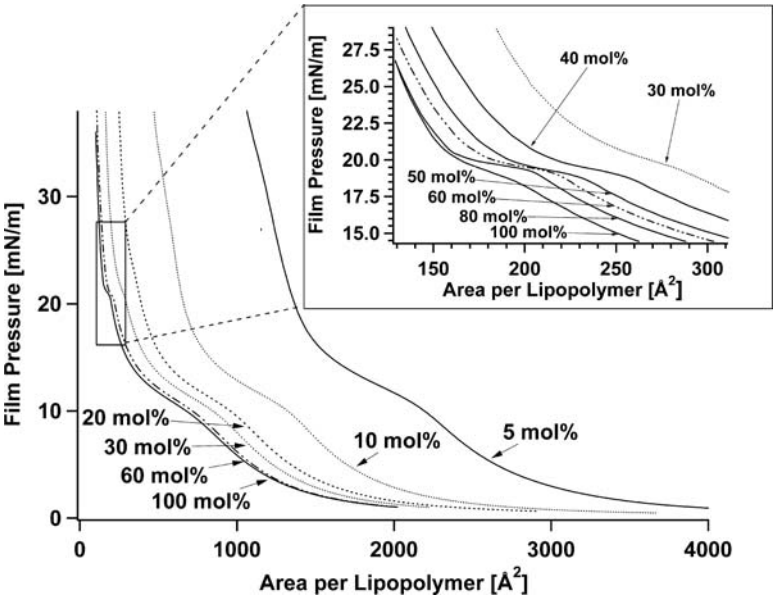

Fig. 16 $\pi - A$ isotherms of different DMPC–DSPE–PEG2000 mixtures for lipopolymer molar concentrations of 5–100 mol%. At ≥ 30 mol%, the $\pi - A$ isotherms show the high-film transition at ~ 19 mN m^{-1} (*see inset*). At lower mol%, the transition becomes much less noticeable and shifts to higher film pressures [42] (reproduced with permission from the American Chemical Society)

Several film balance studies have been reported on lipopolymer–phospholipid mixed monolayers at the air–water interface. Figure 16 displays the $\pi - A$ isotherms of a binary DMPC/DSPE–PEG2000 mixed monolayers ranging from 5 to 100 mol% DSPE–PEG2000 [42]. The isotherm of the lowest concentration of lipopolymer, 5 mol%, is to the right of all the other isotherms, since that mixture contains a large fraction of phospholipid (95 mol%) which is not taken into consideration in this pressure–"area of lipopolymer" isotherm. The analysis of these data provides several interesting results. First, for concentrations larger than 30 mol% lipopolymer, the isotherm of the mixture is nearly identical to the isotherm of the pure lipopolymer. Second, all of the isotherms, even as low as 5 mol% DSPE–PEG2000, show the same low film pressure plateau around 9 mN m^{-1}. As discussed before, this plateau is related to the desorption of the PEG polymers from the air–water interface, which possibly is assisted by the presence of choline headgroups of DMPC. Third, the high pressure transition is still visible at nearly the same pressure for lipopolymer concentrations of 30 mol% and higher. It has been pointed out that the observed disappearance of the high-film pressure transition at lower lipopolymer molar concentrations could be related to the inability to force the polymer chains into a more stretched configuration. Under such circumstances, lipopolymers are expected to be too far away from each other to undergo acyl chain condensation [42]. These data are interesting because they suggest that phospholipids act as templating molecules

for lipopolymers in a binary phospholipid–lipopolymer mixed monolayer. Such an interpretation is in good agreements with epifluorescence microscopy studies on this binary mixture, which found no evidence for large-scale phase separations between DMPC and DSPE–PEG2000 at any lipopolymer molar concentration studied [42]. This result is particularly notable if one considers that binary mixtures of phospholipids with a comparable mismatch in acyl chain length are known to exhibit pronounced phase separations [43, 44].

It is also instructive to analyze the behavior of mixtures where both phospholipids and lipopolymers contain the same sized 18 carbon lipid tails, such as mixtures of DSPC and DSPE–PEG2000. $\pi - A$ isotherms of these mixtures are qualitatively similar to the isotherms of DMPC/DSPE–PEG2000 mixtures. The high pressure transition can be seen with mixtures as low as 10 mol% lipopolymer, but at this concentration it occurs at a higher surface pressure [45]. By plotting the area per molecule vs mole fraction of DSPE–PEG2000 for a constant surface pressure at 6.1 mN m^{-1} (below the first transition point) and at 14.8 mN m^{-1} (above the first transition point), Xu et al. also obtained several other interesting results, as shown in Fig. 17. They found that at the low surface pressure, 6.1 mN m^{-1}, an exactly linear relationship existed between area per molecule and mole fraction, indicating there is additivity in molecular area with increasing PEG–lipid. In other words, both PEG–lipid and lipid compete equally for space at the air–water interface in that regime. At the higher pressure, however, increasing the fraction of PEG–lipids up to about 5 mol% does not increase the average area per molecule proportionately. The authors concluded that in this regime, at very low concentrations, the area per molecule is dominated by the headgroup area of the phospholipid at the interface, but at around 5 mol% lipopolymer the area per molecule value for a given pressure begins to become dominated by the area occupied by the lipopolymer in the water subphase. Moreover, this effect is most marked during a transition which starts about 5 mol% and continues to around 20 mol%. Above 20 mol% lipopolymer, the area per molecule is again a straight line proportional to the concentration of DSPE–PEG2000, as can be seen in Fig. 17. This elegant experiment shows that for low pressures, phospholipids and lipopolymers mix homogeneously at the air–water interface, and lipopolymers act essentially the same as phospholipids, but at higher pressures, the polymer moiety plays a significant role in determining the surface pressure. Xu et al. also looked at $\pi - A$ isotherms of pure PEG-2000, unconnected to a lipid anchor, and determined that it submerges from the air–water interface at pressures a little less than 5 mN m^{-1}, lending support to the concept that the first transition is the submersion of the polymers from the surface.

Xu et al. also considered the hydration of the polymer moiety of PEG lipopolymers at different surface pressures and concentrations [45]. From $\pi - A$ isotherms of pure PEG, they determined that each PEG monomer is fully hydrated with about three water molecules. Upon increasing the concentration of PEG lipopolymers at the air–water interface, they determined that the water is gradually squeezed out. This finding leaves the possibility that the high-pressure plateau of lipopolymers is at least partially accompanied by a dehydration process in the polymer moiety. Thus, the energetic factors contributing to the second transition and the acyl chain conden-

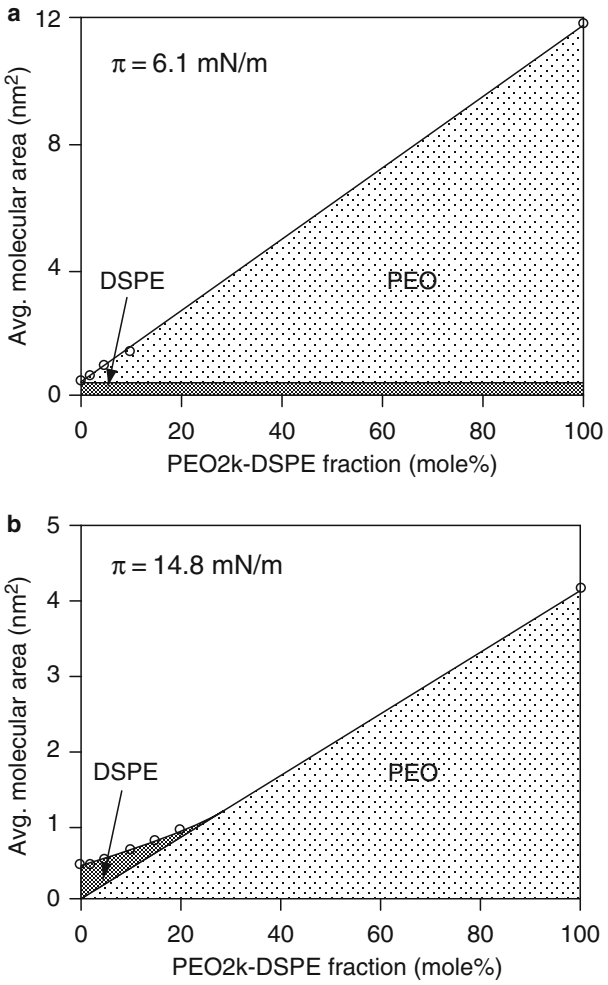

Fig. 17 a, b Area occupied per PEG2000 molecule grafted to DSPE as a function of mol% of DSPE–PEG2000 in the lipid mixture at surface pressures of **a** 6.1 mN m^{-1} and **b** 14.8 mN m^{-1} [45] (reproduced with permission from the American Chemical Society)

sation include not only the enthalpic gain of the lipids becoming aligned but also the entropic loss of the dehydration of the PEG chains and the entropic loss due to the lipid ordering. This dehydration has been reported as a suggestion that water acts as a poor solvent for lipopolymers at higher pressures [6]. Finally, through comparison of pure PEG $\pi - A$ isotherms with mixed monolayer systems, Xu et al. considered whether it was appropriate to label the high pressure transition a mushroom to brush transition. If a brush is said to be present when there are no remaining monolayers at the air–water interface, and the surface area per monomer is determined through the $\pi - A$ isotherm of the PEG2000 in the pancake conformation, then it is a simple

matter to calculate the area per molecule when the last PEG monomer will desorb from the surface. Xu et al. calculated that the transition to brush occurs at areas slightly smaller than the first transition, but much larger than the second, high pressure transition. The mushroom-brush nomenclature, however, may not be the best terminology if the systems are, as discussed in Sect. 2.3, in jammed micelles or other aggregates.

$\pi - A$ isotherms of mixtures have also been taken at different temperatures as well, in an effort to understand the stability of these monolayers and the entropic factors associated with the mixing [46]. There, a two-dimensional Clausius–Clapeyron equation was used to find the heat of mixing, and from this, the entropy associated with the low pressure transition. Unfortunately, these authors did not extend their analysis to mixtures at the high pressure transition to compare their findings with the predictions of Xu et al. Majewski et al. earlier published $\pi - A$ isotherms of DSPE with 0–9% DSPE–PEG2000 with nearly identical results to those reported by Xu et al. [47]. For example, 9 mol% lipopolymer also displayed a high pressure transition. Their work is particularly interesting because the film balance experiments were accompanied by complementary neutron reflectometry studies which will be discussed below.

Different experimental methods have been used to obtain information on how the phospholipids and lipopolymers pack together in a binary mixture. Using neutron reflectometry, Majewski et al. determined the scattering length density profile of the monolayer perpendicular to the air–water interface for mixtures of DSPE with 0–9 mol% DSPE–PEG2000 at high surface pressures, around 40–45 mN m^{-1} well above π_{high} [47]. Reflectivity curves and corresponding scattering length density profiles from this study are depicted in Fig. 18.

Majewski et al. found that for the system of pure DSPE at this high pressure of 42 mN m^{-1}, the lipid tails obtain their greatest density around 25 Å below the surface (the air–lipid interface), the head group is evident by a change in density around 40 Å below the surface, and this is followed by a return to the density of water at around 50 Å below the surface. The reflectometry curves in the presence of 1.3 and 4.4 mol% DSPE–PEG2000 are qualitatively similar to that of pure DSPE. In particular the 1.3 mol% PEG trace shows great similarity, with only a slightly greater depth for the location of the head group to 45 Å below the surface, and the trace has largely returned to the density of water around 55 Å below the surface. For the 4.5 mol% PEG trace, the acyl chain peak is less pronounced, but the depletion layer signifying the headgroup is still very prominent. In addition, there is a contribution to the density from the polymeric chain beyond 55 Å even down to 110 Å below the surface. The situation for the 9 mol% PEG trace, however, is quite different. The acyl chain peak is much less pronounced, with a peak perhaps one third the height of the pure DSPE system. Next, unlike the other mixtures, there is no corresponding dip in the scattering length density signifying the headgroup, but the trace instead displays a slow trailing off of density. This is interpreted as showing a roughening of the acyl chains over a larger depth, as well as PEG existing in the area of the headgroup. The contribution from PEG beneath the headgroup reaches a minimum around 65 Å below the surface and then slowly returns to the density of water at

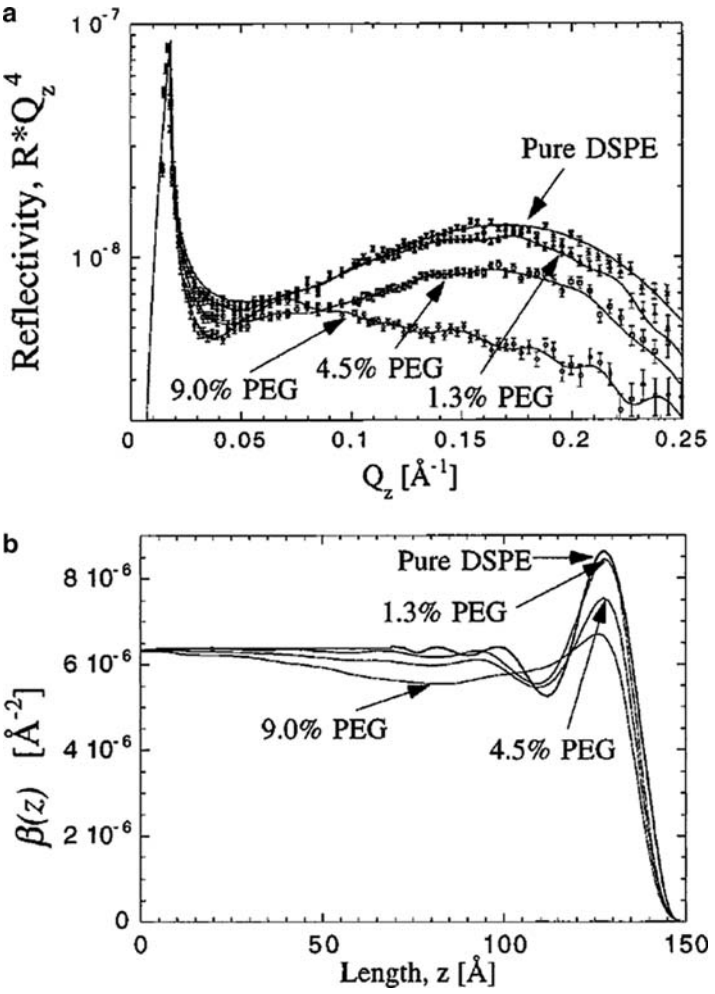

Fig. 18 **a** Neutron reflectometry data for lipid/PEG–lipid monolayers on a pure D_2O subphase. The four reflectivity curves correspond to a pure DSPE monolayer and to mixtures of DSPE and DSPE–PEG2000. In this set of data, all of the DSPE and DSPE–PEG2000 lipid hydrocarbon chains were fully deuterated (*case 1*). *Full lines* represent free form fits to the individual measurements. **b**. Corresponding scattering length densities ($\beta(z)$) obtained from the fits shown in **a** [47] (reproduced with permission from the American Chemical Society)

around 145 Å below the surface. Majewski interprets the 4.5 and 9 mol% systems as evidence of mushroom and brush conformations. In the first, here called mushroom conformation, the monolayer acts essentially as a phospholipid monolayer, but with some density beneath the headgroups. In the second, here called brush conformation, there is roughening of the lipid layer as seen by the lowering and spreading out of the acyl chain peak, and there is no expected depletion layer as the polymeric brushes are crowded in among the headgroups, and forced to stretch out further from the surface than in the lower mol% system [47]. The film balance data

support the notion that DSPE–PEG2000 has different polymer conformations at 4.5 and 9 mol% lipopolymer at 42 mN m^{-1}. The 4.5 mol% mixture does not show the high pressure transition and thus the PEG chains of the lipopolymers appear to be in roughly the same conformation as a pure lipopolymer at a lower pressure, for example, at about 15 mN m^{-1}. By contrast, the 9 mol% system appears very similar to pure lipopolymer systems above the high-pressure transition, at about 30 mN m^{-1}.

Gutberlet et al. obtained neutron and X-ray reflections from surface monolayers of phospholipid–lipopolymer mixtures of DMPC and diC_{18}−$PMOx_{30}$ at three surface pressures, 4, 17, and 30 mN m^{-1} and systems of 0, 25, and 50 mol% diC_{18}−$PMOx_{30}$. They found a linear increase in layer thickness with increasing film pressure for all three lipopolymer molar concentrations and concluded that the polyoxazoline layer thickness develops rather continuously as a function of the lateral pressure, at least up to 30 mN m^{-1} [48]. Unfortunately, Gutberlet et al. did not publish a $\pi - A$ isotherm for their mixtures. The pure PMOx system starts to transition at around 29 mN m^{-1} at 20°C [6], and introducing lipids to lipopolymers either does not change the pressure at which the high pressure transition occurs, or it increases the high pressure transition for low concentrations of lipopolymers [12] so it may well be that these data are looking at monolayers which, although at different pressures, are all in the same conformation, which would explain the linearity of change in layer thickness.

Another technique that has been used to characterize a lipopolymer–phospholipid monolayer at the air–water interface is sum frequency generation (SFG) spectroscopy [49]. SFG is useful for analyzing monolayers at the air–water interface because the conformation of the molecules at the surface can be analyzed and compared to the IR peaks of functional groups on molecules with well known conformations. For example, the OH stretches will display information on how the water interacts with the mixture: a 3,200 cm^{-1} band is seen when water is hydrogen bonded to other molecules in a coordinated fashion; a 3,400 cm^{-1} is observed when water is loosely coordinated or hydrogen bonded with other molecules at the surface; and a band around 3,700 cm^{-1} is found for pure liquid water at the air–water interface. In addition, the CH_2 and CH_3 stretches can give information on the conformation and tilt angle of the lipid tails. Ohe et al. took data on monolayers of DSPE with varying concentrations of DSPE–PEG2000 from 0 up to 16.7 mol%, at 5, 15, and 35 mN m^{-1}, corresponding to the states below, between and above the two transition pressures [49].

These authors showed that pure DSPE displayed very low contributions of OH bands at any of the three surface pressures, corresponding to little water at the surface (as would be expected, since the top layer is all acyl chains), but there were small bands at 3,200 and 3,400, though none at 3,700. On increasing the mole fraction of DSPE–PEG2000 in the monolayer, however, both the 3,200 and 3,400 cm^{-1} bands became more pronounced at all surface pressures, increasing with mol fraction. This reconfirms that the PEG headgroups at the surface are surrounded by a hydration shell and thus there are tightly coordinated waters hydrogen bonded to the PEG. In fact, the ice-like band, 3,200 cm^{-1}, becomes more pronounced on increasing pressures or increasing DSPE–PEG2000 mol% concentration. Interest-

ingly, for concentrations of 1.3 and 4.5% DSPE–PEG2000 at all surface pressures, as well as for all concentrations at the low $5\,\mathrm{mN\,m^{-1}}$ pressure, the relative proportion of ice-like band and liquid-like bands are roughly equal, with the ice-like band having a somewhat greater amplitude than the liquid-like band. Comparing SFG data at 5 and $15\,\mathrm{mN\,m^{-1}}$ shows that increasing lipopolymer concentrations beyond 4.5 mol% does little to increase the $3,400\,\mathrm{cm^{-1}}$ liquid-like stretch, but it does increase the ice-like $3,200\,\mathrm{cm^{-1}}$ band up to 16.7 mol%. At $35\,\mathrm{mN\,m^{-1}}$, there is very little change in either OH stretch from 4.5 to 16.7 mol%, and even pure DSPE–PEG2000 shows little change in the magnitude of the OH stretches compared to 4.5 mol%. Ohe et al. interpreted this data to show that, at higher pressures (above $5\,\mathrm{mN\,m^{-1}}$) and higher concentrations (above 4 mol%), there was no corresponding increase in water as would be expected from water hydrogen bonded to the PEG, but instead the PEG in those systems must be increasingly dehydrated relative to the PEG in the lower pressure or lower concentration monolayers. Thus, energetic factors must be responsible for squeezing the water out of the monolayer. This analysis agrees in principle with the findings of Xu et al. with regard to dehydration, which were obtained from film balance studies [45].

The CH_2 and CH_3 stretches were also analyzed at the same variations of pressures and concentrations [49]. Typically, CH_3 can display a band at $2,950\,\mathrm{cm^{-1}}$ which is the overlap of an asymmetric stretching at $2,960\,\mathrm{cm^{-1}}$ and Fermi resonance bands at $2,940\,\mathrm{cm^{-1}}$ and a stretch at $2,870\,\mathrm{cm^{-1}}$ corresponding to a CH_3 symmetric stretching band. In addition, there is a CH_2 symmetric band at $2,850\,\mathrm{cm^{-1}}$ which corresponds to a system with gauche isomers. The gauche isomer is slightly energetically less stable, but is found in liquid or noncondensed systems. For pure DSPE–PEG2000, at $15\,\mathrm{mN\,m^{-1}}$ there is a slight band showing evidence of gauche isomers. At $35\,\mathrm{mN\,m^{-1}}$, this band has disappeared, and there is no evidence of gauche isomers. This is in agreement with the findings in [6]. Interestingly, in the mixed monolayers, Ohe et al. found no evidence of the $2,850\,\mathrm{cm^{-1}}$ band, that is, no gauche isomers are seen, at any concentrations or pressures [49]. By comparing the line amplitude of the symmetric and asymmetric stretches of the terminal methyl groups in the different mixtures, it is also possible to draw conclusions about the tilt angle of the terminal methyl groups. At the low surface pressure of $5\,\mathrm{mN\,m^{-1}}$, tilt angle increases with increasing concentration of DSPE–PEG2000 to nearly 90° at greater than 10 mol% DSPE–PEG2000. This result can be well understood: There is a decrease in the density of lipid tails and therefore terminal methyl groups with increasing concentration of lipopolymer and this causes the lipid tails to be less upright, and thus the tilt angle becomes larger. The situation is different for the 15 and $35\,\mathrm{mN\,m^{-1}}$ pressures. For $35\,\mathrm{mN\,m^{-1}}$, initially the tilt angle increases slightly with increasing mol fraction of lipopolymer, but by 10 mol%, the tilt angle has reached a plateau of around 47° and it stays there up to 16 mol%. Ohe interprets these data for the $35\,\mathrm{mN\,m^{-1}}$ system to show that the PEG groups are completely submerged at this pressure and the acyl groups of the DSPE–PEG2000 interact much as the DSPE itself, so a change in relative concentration does not change the tilt angle of the terminal methyl groups of either substituent. For the intermediate, $15\,\mathrm{mN\,m^{-1}}$ system, the tilt angle increases more

strongly with increasing mole fraction of DSPE–PEG2000 to about 10 mol%, where it has increased to 58° or so. Thereafter, it appears to level off somewhat, or perhaps increase slightly. This, Ohe interprets, arises because the PEG at this pressure are not completely submerged and thus the acyl chains are in an intermediate state. These authors label the 15 mN m^{-1} conformation "mushroom" and the 35 mN m^{-1} conformation "brush." It is clear from Ohe's work that the methyl groups on the end of the acyl chains behave differently in the different mixtures at the different pressures, and there is a change which occurs around 10 mol% lipopolymer where the acyl chains act in a different manner than below that concentration. Ohe also goes on to explain Majewski's result regarding the decrease in the mole fraction of acyl chains at increasing mol% of DSPE–PEG2000 as being due to the tilting of the acyl chains, at least in the region up to 10 mol% lipopolymer. This work again confirms that low concentrations of lipopolymers at high pressures in mixtures act like pure lipopolymers at low pressures and concentrations, but this must be read carefully in light of others' findings on tilt angles of lipopolymeric systems [15].

3.2 Viscoelastic Properties of Lipid–Lipopolymer Mixtures

To this point, the structural data have indicated that mixed monolayers at low pressures act like low pressure phospholipid monolayers, and mixed monolayers at medium and high pressures act like lipopolymer monolayers in different conformations, depending on the concentration of lipopolymer and the surface pressure studied. Film balance and interfacial rheology experiments on pure lipopolymer monolayers also suggest that the gelation transition occurs at or slightly above the high-pressure transition observed in $\pi - A$ isotherms. Corresponding experiments on mixed phospholipid–lipopolymer monolayers will show that the gelation transition may also occur further away from the plateau of the high-pressure transition. Before looking at the viscoelastic properties of mixtures, the viscoelastic properties of phospholipids and lipopolymers should be recalled. Monolayers of phospholipids, even in liquid condensed phases, never become elastic, which is to say the storage modulus is never greater than the loss modulus, but both do increase significantly if the monolayer is compressed to a small enough area per molecule [2]. Monolayers of lipopolymers are fluid below a rheological transition pressure which is nearly the same as the high transition pressure found via a plateau in $\pi - A$ isotherms, and elastic above the rheological transition pressure. As discussed before, the observed elasticity is probably due to the formation of small, two dimensional micellar structures which jam into each other at the air–water interface. As illustrated in Fig. 19, the rheological response of mixtures of DSPE–PEG2000 and DMPC show a very interesting trend [42]. For lipopolymer concentrations of 60 mol% or higher, the rheological response is nearly identical to that of pure lipopolymer, when looked at as a function of area per lipopolymer. The response is liquid below a transition pressure, and elastic above the pressure, and continues to be elastic at all higher pressures. In fact, the rheological transition point is the same, about 165 $Å^2$, independent of

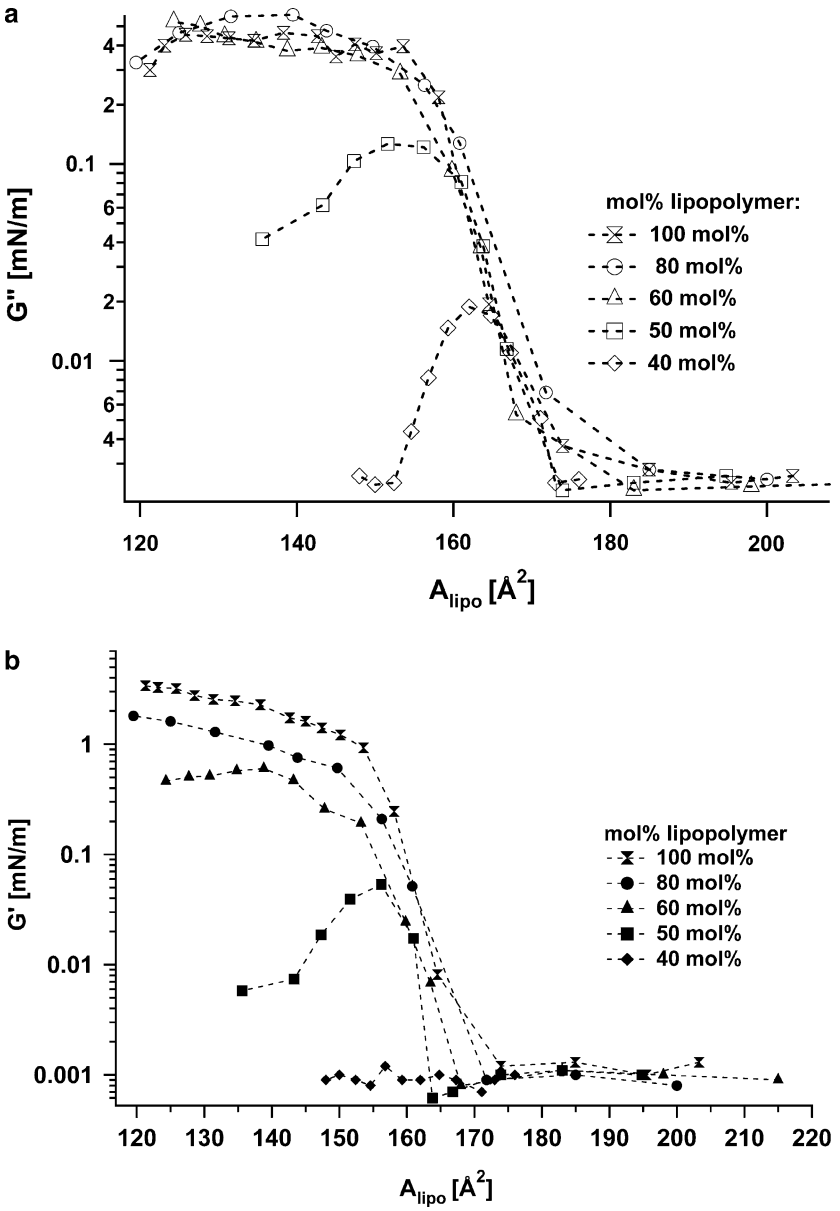

Fig. 19 a, b Viscoelastic response of the DSPE–PEG2000 monolayer as a function of amount of DMPC incorporated. Loss modulus **a** and storage modulus **b** are shown vs A_{lipo}, and are essentially independent of amount of phospholipids incorporated for mol% lipopolymer >40%. No viscoelastic transition occurs for mol% lipopolymer <40% [42] (reproduced with permission from the American Chemical Society)

the amount of phospholipids incorporated, with the only difference being that the higher mol% have a stronger elastic modulus response. This should be contrasted with the film balance studies, where high pressure transitions were seen as low as 9 mol% for DSPE/DSPE–PEG2000 systems. At 40–50 mol% DSPE–PEG2000 with DMPC, there is a rheological transition at about $A_{\text{rheo}} = 165$ Å^2 for the loss modulus, but not for the storage modulus at 40 mol%, and the increase in the storage modulus at 50 mol% never exceeds the loss modulus so the monolayer does not become elastic at any area. This is interesting because unlike the structural studies which show similar behavior down to 9 mol% lipopolymer, here a significant difference is found even at 50 mol% lipopolymer. Clearly, there are conditions where no gelation transition can be observed, even though a high-pressure transition is found.

To evaluate further the viscoelastic properties in lipid–lipopolymer mixed monolayers, the frequency dependence of the magnitude of the dynamic modulus $|G_s^*(\omega)|$ was determined as well, where $G_s^*(\omega) = G_s'(\omega) + i\ G_s''(\omega)$ [42]. Here two different situations were considered. First, $|G_s^*(\omega)|$ at different frequencies was monitored at 50 mol% DSPE–PEG2000 as a function of area per lipopolymer (Fig. 20a) Second, $|G_s^*(\omega)|$ at different frequencies was determined for different lipopolymer molar concentrations at a constant area per lipopolymer (Fig. 20b). Overall, the data in Figs. 19 and 20 indicate that increasing amounts of phospholipids weaken the ability to form gels and reduce the strength of such physical networks, thus supporting the notion of phospholipids acting as templating molecules in the mixed phospholipid–lipopolymer monolayer.[1] These data also show that, in many significant ways, dilute mixtures of lipopolymers at high surface pressures act like pure lipopolymers at low surface pressures.

As illustrated in Fig. 21, Naumann et al. also explored the reversibility of the gelation transition [42]. Here the loss modulus was tracked in a DMPC/DSPE–PEG2000 mixed monolayer with 40 mol% DSPE–PEG2000 during compression and subsequent expansion of the monolayer. Both curves are almost identical, thus suggesting a thoroughly reversible process. Interestingly, as can be seen by referring back to Sect. 2.2., the viscoelastic response for 40 mol% DSPE–PEG2000 is also remarkably similar to the behavior of the loss modulus at different A_{lipo} for monolayers of pure $DiC_{18}PEOx_{31}$, DSPE–PEG750, and DSPE–PEG1000, which underwent a comparable collapse.

To obtain more insight into the relationship between high-pressure film balance and gelation transitions, Naumann et al. also determined the location of the gelation transition in the $\pi - A$ isotherms of the DMPC/DSPE–PEG2000 mixed monolayer at various lipopolymer molar concentrations [42]. As shown in Fig. 22, unlike for pure lipopolymer systems, viscoelastic and high-pressure film balance transitions typically do not overlap. Furthermore, below 80 mol% lipopolymer, the gelation transition is clearly outside the plateau region of the corresponding $\pi - A$ isotherm

[1] Interestingly enough, the storage modulus of diblock copolymers is weakened by increasing the mol fraction of one of the substituents of the diblock, unfunctionalized PEG chains [47]. This is similar to the current situation if a DSPE-PEG2000 lipopolymer is considered a short diblock copolymer and the mixed-in phospholipid is considered one of the substituents of the diblock.

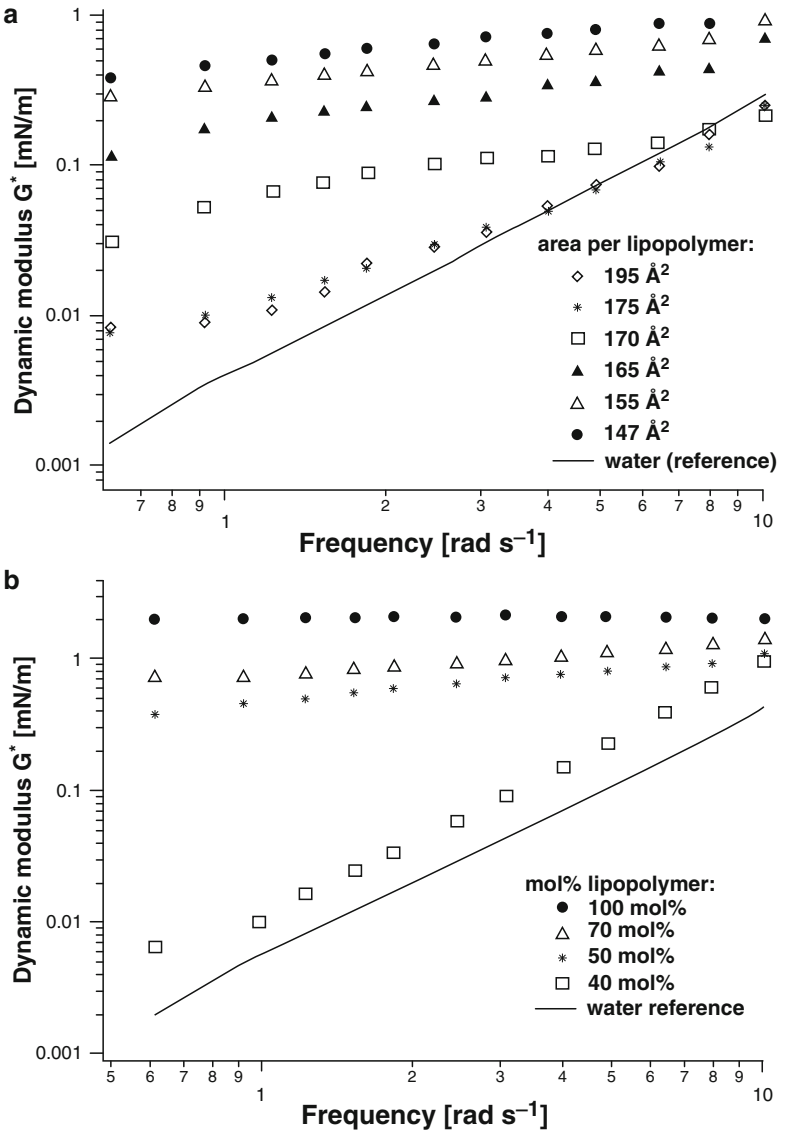

Fig. 20 a, b Frequency dependence of the magnitude of the dynamic modulus **a** for different A_{lipo} at a constant mol% = 50 mol% lipopolymer and **b** for different mol% at a constant $A_{\text{lipo}} = 150$ Å^2. At high A_{lipo} and low mol% no network forms but at low A_{lipo} and high mol% there is clear evidence of gel formation. *Solid line* represents response of the needle at the clean water surface [42] (reproduced with permission from the American Chemical Society)

and does not cause any change in the slope of the isotherms. This result clearly indicates that the high film pressure and gelation transitions describe two related, but different, transition phenomena. It also supports the notion that the high-pressure

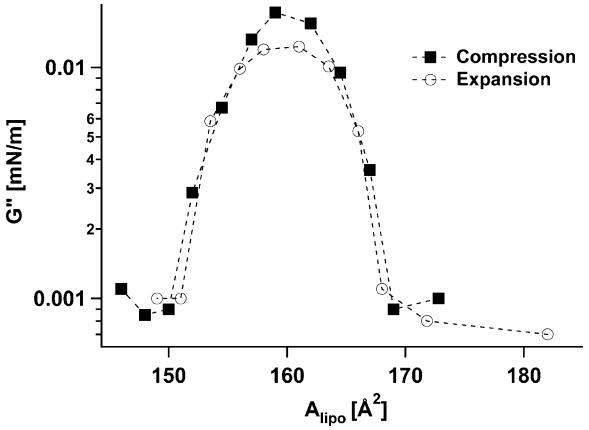

Fig. 21 Loss modulus vs A_{lipo} plotted for 40% lipopolymer during compression and expansion of bilayer shows reversibility of the viscoelastic transition. Also, the gel exhibits a collapse at smaller A_{lipo} (and higher pressures) than pure lipopolymer [42] (reproduced with permission from the American Chemical Society)

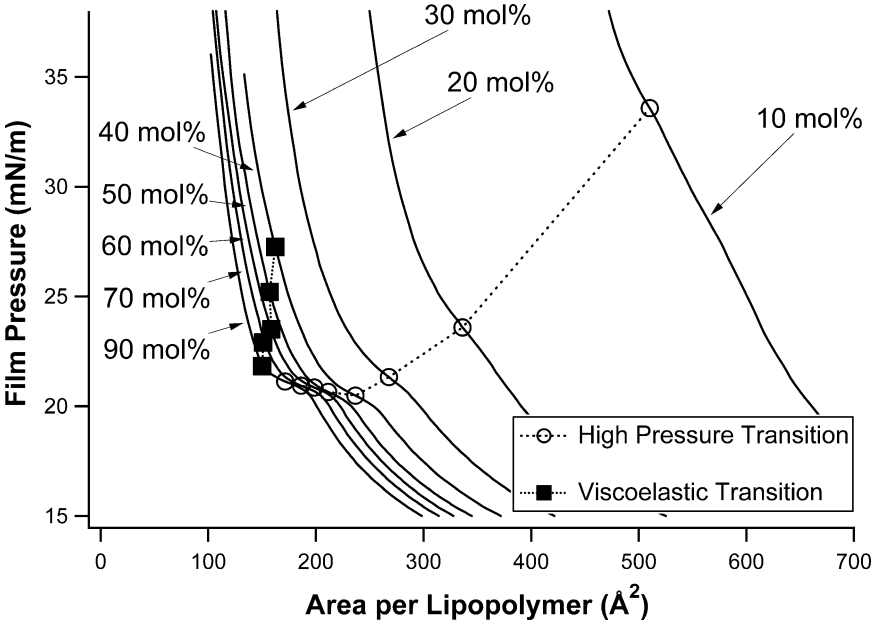

Fig. 22 $\pi - A$ isotherms of mixtures of DMPC/DSPE–PEG2000 from 10 to 100 mol% DSPE–PEG2000, where the film balance transitions are plotted for each isotherm and the viscoelastic transitions are plotted for 40–100 mol%. The transitions only coincide at 100% DSPE–PEG2000. The different trends underlie the fact that the high pressure transition and viscoelastic transition signify different physical phenomena [42] (modified, with permission from the American Chemical Society)

transition is associated with the formation of surface micelles and that the gelation transition requires not only formation but also the jamming of such micelles. Figure 22 also shows that π_{high} is well pronounced and largely constant between 30 and 100 mol% lipopolymer, but becomes less obvious and increases with decreasing lipopolymer concentrations below 30 mol%. This changing behavior between high and low lipopolymer molar concentrations can be understood in terms of the changing location of the main lateral pressure in the lipopolymer–phopsholipid mixed monolayer at high film pressure. At elevated lipopolymer molar concentrations, the main lateral pressure is localized in the polymer moiety of lipopolymers. In contrast, with decreasing lipopolymer content at medium to low lipopolymer molar concentrations, the lateral stress builds up increasingly in the lipid moieties of lipids and lipopolymers.

As an interesting side note, the viscoelastic properties of phospholipid monolayers mixed with hydrophobically modified PEG polymers (HMPEG) have also been studied [56]. A hydrophobically modified PEG polymer is a PEG polymer linked to an *n*-butyl group linked to an 18 carbon straight chain thence linked to another long PEG polymer, all through the use of peptide bonds. In this study, the PEG polymers were three or six times as long as PEG2000 and each molecule contained three to five C_{18} groups interspersed between PEG polymers. These should behave somewhat like lipopolymers, but these HMPEG are covalently linked to each other, and are investigated for the degree of protection hydrophobically modified PEG polymers can afford to liposomes to enable them to evade immune recognition and protect against complement binding. Pressure–area isotherms of mixtures of these HMPEG with phospholipids show a plateau around 10 mN m^{-1} and then an increase up to the film breaking at pressures greater than 50 mN m^{-1} with no high pressure plateau. Similarly, analysis of the storage and loss modulus show that these systems do not exhibit the elastic behavior or rheological transitions such as those found with lipopolymer monolayers (Auguste et al. 2008).

3.3 Diffusion Properties of Lipid–Lipopolymer Mixtures

The diffusion properties of mixtures of phospholipids and lipopolymers should be discussed in light of the diffusion properties of pure phospholipids and pure lipopolymers. Wide-field single molecule fluorescence microscopy studies on phospholipid (DMPC and DMPG) monolayers at the air–water interface showed that the lateral diffusion of phospholipids obeys the two-dimensional free area model [50]. As was noted in Sect. 2.3, pure lipopolymers at appropriate A_{lipo} also obey the free area model in terms of their diffusion characteristics [31]. Previously, the lateral diffusion of phospholipids in mixed phospholipid–lipopolymer mixed monolayers has been determined using fluorescence recovery after photobleaching (FRAP) and wide-field single molecule fluorescence microscopy [39, 51]. The diffusion results from these experiments are summarized in Fig. 23. We found that for lipopolymer molar concentrations up to 10 mol% corresponding to area per lipopolymer

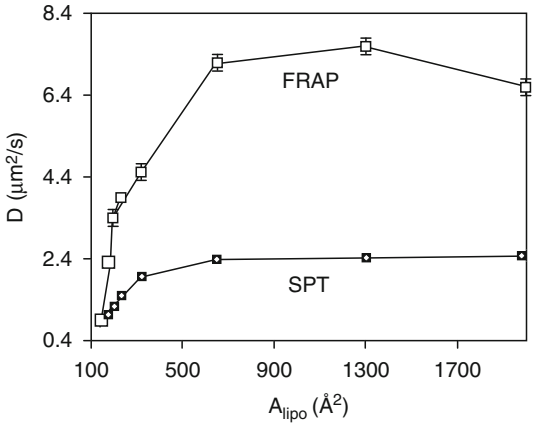

Fig. 23 Lateral diffusion coefficient D as a function of A_{lipo} using FRAP and single molecule fluorescent microscopy methods [39] (reproduced with permission from the American Chemical Society)

of a little over 600 Å^2, with a constant A_{lipid} of 65 mN m^{-1}, the diffusion coefficients were fairly constant. Then, from 10 to 30 mol%, still with A_{lipid} constant, the diffusion coefficients decrease with decreasing A_{lipo} down to 230 Å^2. These data suggest that the lateral diffusion of phospholipids becomes increasingly obstructed in the presence of significant inter polymer interactions between lipopolymers. The observed differences in diffusion coefficients for a given A_{lipo} between FRAP and single molecule imaging in Fig. 23 have been attributed to the different time and length scales of both techniques [39]. In addition, tracking inaccuracies associated with the tracking of photolabile dyes exhibiting on–off blinking should be considered. Despite these discrepancies, both experimental techniques are able to identify the different diffusion regimes described above.

To explore the impact of the high-pressure transition on lipid lateral diffusion, Ke and Naumann also determined the lipid lateral diffusion at constant 30 mol% lipopolymer but decreasing A_{lipo} down to 150 Å^2 [39]. Here, three different diffusion regimes could be identified. In the first regime, the diffusion is independent of the concentration of lipopolymer. This behavior is quite similar to the situation of pure lipopolymers at low pressures, as discussed above. The change-over to the second regime occurs around 600–650 Å^2. This corresponds in terms of the $\pi - A$ isotherms to around the end of the low pressure transition. Naumann et al. considers how squeezed a lipopolymer would be at an $A_{\text{lipo}} = 650$ Å^2, if this represents a polymer squeezed into a tube, following the calculations of de Gennes [52]. For a polymer in a thick tube, the relationship is

$$L = \frac{R_F^2}{d}. \tag{5}$$

This represents the length of the polymer if it is not squeezed, but constrained to a certain diameter d. The Flory radius for a polymer in a mushroom configuration is defined by the number of segments N, (in this case 45) and the length of the monomeric unit, a, (in this case, 3.5 Å) and is written as

$$R_F = aN^{3/5} = 34.3 \text{ Å}. \tag{6}$$

The diameter, d, is calculated from the area per lipopolymer using the familiar relation Area $= \pi r^2$. Substituting 650 Å^2 for Area gives $d = 28.8$ Å, and from (5), $L = 40.9$ Å. Free polymers in solution would have a value of $L = R_F$. According to (6), this solution of 30% lipopolymers where $A_{lipid} = 65$ Å^2 yields $L/R_F = 1.36/1$, or slightly stretched. Thus, it appears that around the density when the polymers start to interact with each other and become stretched, they cause the diffusion of lipids on the monolayer to slow down proportionally [51]. In other words, the lipopolymers start to act like obstacles instead of fellow-phospholipids. The second transition, from the second to the third diffusion regime, appears at around $A_{lipo} = 180$ Å^2. This is a significant concentration because it is around the high pressure transition seen on $\pi - A$ isotherms and the rheological transition pressure of pure lipopolymers. Not surprisingly, the lateral diffusion of lipids is obstructed below this point.

Further analysis of the relationship of the single molecule fluorescent microscopy diffusion coefficients is presented in Fig. 24 [39]. To follow the free area model, a plot of $\ln(D/D_o)$ vs (a_{min}/a_f) or, to simplify matters, a plot of ln(D) vs $1/a_f$ must be a straight line at different A studied. This is uniformly the case for phospholipids such as DMPC, but for lipopolymer mixtures, only the points which were taken at $A_{lipo} > 180$ Å^2 agree with the free area model. This corresponds to points a, b, and c, but not point d.

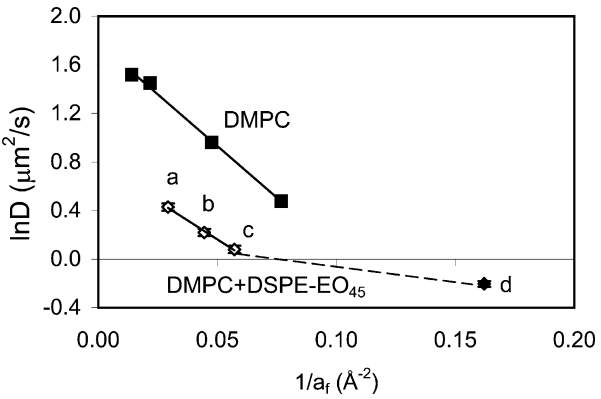

Fig. 24 Plots of ln(D) vs $1/a_f$ for DMPC and the requirements for molecules obeying the free area model, for pure DMPC and 70 mol%DMPC + 30 mol%DSPE–PEG2000. The *straight solid line* indicates that DMPC obeys the free area model. In case of the binary lipid/lipopolymer mixture, the free area model is only valid between points a–c, but not between c–d [39] (reproduced with permission from the American Chemical Society)

4 Conclusion

Overall, existing experimental findings highlight a fascinating relationship between structural, viscoelastic, and diffusion properties in mixed phospholipid–lipopolymer mixed monolayers. The various experimental findings provide strong evidence that these properties can be tuned via the lipopolymer molar concentration. At low lipopolymer molar concentrations, where no polymer–polymer interaction occurs, these peculiar amphiphiles act like their phospholipid cousins. At intermediate lipopolymer molar concentrations, moderate interlipopolymer interactions can be observed, which may have profound effects on membrane organization and dynamics, however, within the context of a fluid monolayer. At elevated lipopolymer concentrations, interlipopolymer interactions become quite strong and may lead to phenomena such as surface micellization/physical gelation and pronounced obstructed diffusion. Clearly, a fundamental understanding of properties on pure lipopolymer monolayers provides important insight into the observed behavior on phospholipid–lipopolymer mixed monolayers. Furthermore, at the air–water interface, phospholipids seem to act as templating molecules, thus providing a tool of regulating lipopolymer–lipopolymer interactions. Although the findings obtained from monolayer systems at the air–water interface cannot generally be applied to polymer-tethered bilayers, they are often quite useful for the characterization and understanding of their bilayer counterparts. Prominent examples are the obstructed diffusion of lipids and membrane proteins and the coupling of obstructed diffusion of phospholipids in polymer-tethered bilayers [40, 53].

Acknowledgments This work was supported by grants from the Petroleum Research Fund and the National Science Foundation.

References

1. Baekmark TR, Elender G, Lasic DD, Sackmann E (1995) Conformational transitions of mixed monolayers of phospholipids and polyethylene oxide lipopolymers and interaction forces with solid surfaces. Langmuir 11:3975–3987 (correction) (1996) Langmuir 12:4980–4980
2. Naumann CA, Brooks CF, Fuller GG, Knoll W, Frank CW (1999) Viscoelastic properties of lipopolymers at the air-water interface: a combined interfacial stress rheometer and film balance study. Langmuir 15:7752–7761
3. Goncalves da Silva AM, Filipe EJM, d'Oliveira JMR, Martinho JMG (1996) Interfacial behavior of poly(styrene)-poly(ethylene oxide) diblock copolymer monolayers at the air-water interface. hydrophilic block chain length and temperature influence. Langmuir 12:6547–6553
4. Kim MW, Cao BH (1993) Additional reduction of surface tension of aqueous polyethylene oxide (PEO) solution at high polymer concentration. Europhys Lett 24:229
5. Cao BH, Kim MW (1995) Molecular weight dependence of the surface tension of aqueous poly(ethylene oxide) solutions. Faraday Discuss 98:245–252
6. Baekmark TR, Wiesenthal T, Kuhn P, Albersdorfer A, Nuyken O, Merkel R (1999) A systematic infrared reflection-absorption spectroscopy and film balance study of the phase behavior of lipopolymer monolayers at the air-water interface. Langmuir 15:3616–3626

7. Foreman MB, Coffman JP, Murcia MJ, Cesana S, Jordan R, Smith GS, Naumann CA (2003) Gelation of amphiphilic lipopolymers at the air-water interface: 2D analogue to 3D gelation of colloidal systems with grafted polymer chains. Langmuir 19:326–332
8. Luedtke K, Jordan R, Hommes P, Nuyken O, Naumann CA (2005) Lipopolymers from new 2-substituted-2-oxazolines for artificial cell membrane constructs. Macromol Biosci 5:384–393
9. Barentin C, Muller P, Joanny JF (1998) Polymer brushes formed by end-capped poly(ethylene oxide) (PEO) at the air-water interface. Macromolecules 31:2198–2211
10. Wiesenthal T, Baekmark TR, Merkel R (1999) Direct evidence for a lipid alkyl chain orderng transition in poly(ethylene oxide) lipopolymer monolayers at the air-water interface obtained from infrared reflection absorption spectroscopy. Langmuir 15:6837–6844
11. Coffman JP, Naumann CA (2002) Molecular weight dependence of viscoelastic properties in two-dimensional physical polymer networks: amphiphilic lipopolymer monolayers at the air-water interface. Macromolecules 35:1835–1839
12. Naumann CA, Brooks CF, Fuller GG, Lehmann T, Ruehe J, Knoll W, Kuhn P, Nuyken O, Frank CW (2001a) Two-dimensional physical networks of lipopolymers at the air/water interface: correlation of molecular structure and surface rheological behavior. Langmuir 17:2801–2806
13. Wurlitzer A, Politsch E, Huebner S, Krueger P, Weygand M, Kjaer K, Hommes P, Nuyken O, Cevc G, Loesche M (2001) Conformation of polymer brushes at aqueous surfaces determined with X-ray and neutron reflectometry. 2. High-density phase transition of lipopolyoxazolines. Macromolecules 34:1334–1342
14. Krueger P, Loesche M (2004) Characterization of floating surface layers of lipids and lipopolymers by surface-sensitive scattering. In: Haberlandt R, Michel D, Poppl A, Stannarius (eds) Molecules in interaction with surfaces and interfaces. Lecture Notes in Physics, vol. 634. Springer, Berlin Heidelberg New York, pp 395–438
15. Ahrens H, Baekmark TR, Merkel R, Schmitt J, Graf K, Raiteri R, Helm CA (2000) Hydrophilic/hydrophobic nanostripes in lipopolymer monolayers. ChemPhysChem 1:101–106
16. Ahrens H, Graf K, Helm CA (2001) Observation of a superstructure X-ray peak within lipopolymer monolayers on the water surface. Langmuir 17:3113–3115
17. Kuhl TL, Majewski J, Howes PB, Kjaier K, von Nahmen A, Lee KYC, Ocko B, Israelachvili JN, Smith GS (1999) Packing stress relaxation in polymer-lipid monolayers at the air-water interface: an X-ray grazing-incidence diffraction and reflectivity study. J Am Chem Soc 121:7682–7688
18. Israelachvili J (1994) Self-assembly in two dimensions: surface micelles and domain formation in monolayers. Langmuir 10:3774–3781
19. Dewhurst PF, Lovell MR, Jones JL, Richards RW, Webster JRP (1998) Organization of dispersions of a linear diblock copolymer of polystyrene and poly(ethylene oxide) at the air-water interface. Macromolecules 31:7851–7864
20. Deschenes L, Bousmina M, Ritcey AM (2008) Micellization of PEO/PS block copolymers at the air/water interface: a simple model for predicting the size and aggregation number of circular surface micelles. Langmuir 24:3699–3708
21. Brooks CF, Fuller GG, Frank CW, Roberston CR (1999) An interfacial stress rheometer to study rheological transitions in monolayers at the air-water interface. Langmuir 15:2450–2459
22. Schneider MF, Lim K, Fuller GG, Tanaka M (2002) Rheology of glycocalix model at air/water interface. Phys Chem Chem Phys 4:1949–1952
23. Witten TA, Pincus PA (1986) Colloid stabilization by long grafted polymers. Macromolecules 19:2509–2513
24. Lin EK, Gast AP (1996) Self consistent field calculations of interactions between chains tethered to spherical interfaces. Macromolecules 29:390–397
25. Lee AS, Butun V, Vamvakaki M, Armes SP, Pople JA, Gast AP (2002) Structure of pH-dependent block copolymer micelles: charge and ionic strength dependence. Macromolecules 35:8540–8551
26. Loppinet B, Stiakakis E, Vlassopoulos D, Fytas G, Roovers J (2001) Reversible thermal gelation in star polymers: an alternative route to jamming of soft matter. Macromolecules 34:8216–8223

27. Stiakakis E, Vlassopoulos D, Loppinet B, Roovers J, Meier G (2002) Kinetic arrest of crowded soft spheres in solvents of varying quality. Phys Rev E 66:051804
28. Kapnistos M, Vlassopoulos D, Fytas G, Mortensen K, Fleischer G, Roovers J (2000) Reversible thermal gelation in soft spheres. Phys Rev Lett 85:2072–2075
29. Renou F, Benyahia L, Nicolai T (2007) Influence of adding unfunctionalized peo on the viscoelasticity and the structure of dense polymeric micelle solutions formed by hydrophobically end-capped PEO. Macromolecules 40:4626–4634
30. Murcia MJ, Garg S, Naumann CA (2007) Single molecule fluorescence microscopy to determine phospholipid lateral diffusion. In: Dopico A (ed) Methods in membrane lipids. Humana, Totowa, pp 277–294
31. Luedtke K, Jordan R, Furr N, Garg S, Forsythe K, Naumann CA (2008) Two-dimensional center-of-mass diffusion of lipid-tethered poly(2-methyl-2-oxazoline) at the air-water interface studied at the single molecule level. Langmuir 24:5580–5584
32. Leger L, Hervet H, Rondelez F (1981) Reptation in entangled polymer solutions by forced Rayleigh light scattering. Macromolecules 14:1732–1738
33. Lee JCM, Santore M, Bates FS, Discher DE (2002) From membranes to melts, rouse to reptation: diffusion in polymersome versus lipid bilayers. Macromolecules 35:323–326
34. Dalvi MC, Lodge TP (1994) Diffusion in block copolymer melts: the disordered region and the vicinity of the order-disorder transition. Macromolecules 27:3487–3492
35. Ehlich D, Takenaka M, Hashimoto T (1993) Forced Rayleigh scattering study of diffusion of block copolymers. 2. Self-diffusion of block copolymer chains in lamellar microdomains and disordered melts. Macromolecules 26:492–498
36. Lodge TP, Dalvi MC (1995) Mechanisms of chain diffusion in lamellar block copolymers. Phys Rev Lett 75:657–660
37. Hammersky MW, Hillmeyer MA, Tirell M, Bates FS, Lodge TP, von Meerwall ED (1998) Block copolymer self-diffusion in the gyroid and cylinder morphologies. Macromolecules 31:5363–5370
38. Almeida PFF, Vaz WLC (1995) Lateral diffusion in membranes. In: Lipowsky R, Sackmann E (eds) Handbook of biological physics, structure and dynamics of membranes, vol. 1A. Elsevier, Amsterdam
39. Ke PC, Naumann CA (2001) Hindered diffusion in polymer-tethered phospholipid monolayers at the air-water interface: a single molecule fluorescence imaging study. Langmuir 17: 5076–5081
40. Deverall MA, Gindl E, Sinner E-K, Besir H, Ruehe J, Saxton MJ, Naumann CA (2005) Membrane lateral mobility obstructed by polymer-tethered lipids studied at the single molecule level. Biophys J 88:1875–1886
41. Duncan SL, Larson RG (2008) Comparing experimental and simulated pressure-area isotherms for DPPC. Biophys J 94:2965–2986
42. Naumann CA, Brooks CF, Wiyatno W, Knoll W, Fuller GG, Frank CW (2001) Rheological properties of lipopolymer-phospholipid mixtures at the air-water interface: a novel form of two-dimensional physical gelation. Macromolecules 34:3024–3032
43. Vaz WLC, Melo ECC, Thompson TE (1989) Translational diffusion and fluid domain connectivity in a two-component, two-phase phospholipid bilayer. Biophys J 56:869–876
44. Leidy C, Wolkers WF, Jorgensen K, Mouritsen OG, Crowe JH (2001) Lateral organization and domain formation in a two-component lipid membrane system. Biophys J 80:1819–1828
45. Xu Z, Holland NB, Marchant RE (2001) Conformations of short-chain poly(ethylene oxide) lipopolymers at the air-water interface: a combined film balance and surface tension study. Langmuir 17:377–383
46. Chou TH, Chu I-M (2003) Thermodynamic characteristics of DSPC/DSPE-PEG2000 mixed monolayers on the water subphase at different temperatures. Coll Surf B Biointerf 27:333–344
47. Majewski J, Kuhl TL, Gerstenberg MC, Israelachvili JN, Smith GS (1997) Structure of phospholipid monolayers containing Poly(ethylene glycol) lipids at the air-water interface. J Phys Chem B 101:3122–3129

48. Gutberlet T, Wurlitzer A, Dietrich A, Politsch E, Cevc G, Steitz R, Losche M (2000) Organization of tethered polyoxazoline polymer brushes at the air/water interface. Phys B Condens Matter 283:37–39
49. Ohe C, Goto Y, Noi M, Arai M, Kamijo H, Itoh K (2007) Sum frequency generation spectroscopic studies on phase transitions of phospholipid monolayers containing poly(ethylene oxide) lipids at the air-water interface. J Phys Chem B 111:1693–1700
50. Ke PC, Naumann CA (2001) Single molecule fluorescence imaging of phospholipid monolayers at the air-water interface. Langmuir 17:3727–3733
51. Naumann CA, Knoll W, Frank CW (2001) Hindered diffusion in polymer-tethered membranes: a monolayer study at the air-water interface. Biomacromol 2:1097–1103
52. De Gennes PG (1987) Polymers at an interface: a simplified view. Adv Colloid Interf Sci 27:189–209
53. Deverall MA, Garg S, Lüdtke K, Jordan R, Rühe J, Naumann CA (2008) Transbilayer coupling of obstructed lipid diffusion in polymer-tethered phospholipid bilayers. Soft Matter 4:1899–1908
54. Alexander S (1977) Adsorption of chain molecules with a polar head a scaling description. J Phys 38:983–987
55. de Gennes, PG (1971) Reptation of a Polymer Chain in the presence of Fixed Obstacles. J Chem Phys 55:572–579
56. Auguste DT, Kirkwood J, Kohn J, Fuller GG, Prud'homme RK (2008) Surface Rheology of Hydrophobically modified PEG polymers associating with a Phospholipid monolayer at the air-water interface. Langmuir 24:4056–4064

Adv Polym Sci (2010) 224: 87–111
DOI:10.1007/12_2009_27

Published online: 21 October 2009

Polymer-Tethered Bimolecular Lipid Membranes

Wolfgang Knoll, Katja Bender, Renate Förch, Curt Frank, Heide Götz, Claudia Heibel, Toby Jenkins, Ulrich Jonas, Asmorom Kibrom, Ralf Kügler, Christoph Naumann, Renate Naumann, Annette Reisinger, Jürgen Rühe, Stefan Schiller, and Eva-Kathrin Sinner

W. Knoll (✉)
AIT Austrian Institute of Technology, Vienna, Austria
and
Institute of Materials Research and Engineering, Singapore
e-mail: Wolfgang.Knoll@ait.ac.at

E.-K. Sinner
Institute of Materials Research and Engineering, Singapore
e-mail: sinnere@imre.a-star.edu.sg

K. Bender
Department of Forensic Medicine, University of Cologne, Cologne, Germany
e-mail: katja.bender@uk-koeln.de

R. Förch, H. Götz, C. Heibel, A. Kibrom, R. Kügler, R. Naumann, A. Reisinger
Max-Planck-Institute for Polymer Research, Mainz, Germany
e-mail: {foerch,goetz,heibel,kibrom,naumannr,reisinger}@mpip-mainz.mpg.de,
ralf.kuegler@emdchemicals.com

C. Frank
Department of Chemical Engineering, Stanford University, Stanford, CA
e-mail: curt.frank@stanford.edu

T. Jenkins
Dept. of Chemistry, University of Bath, United Kingdom
e-mail: a.t.a.jenkins@bath.ac.uk

U. Jonas
Institute of Electronic Structure and Laser, Foundation for Research and Technology-Hellas
Heraklion, Crete, Greece
e-mail: jonas@mpip-mainz.mpg.de

C. Naumann
Nanoscale Imaging Center, Purdue University, Indianapolis, IN
e-mail: canaumann@iupui.edu

J. Rühe
Dept. of Microsystem, Engineering, University of Freiburg, Freiburg, Germany
e-mail: ruehe@imtek.uni-freiburg.de

S. Schiller
FRIAS, Freiburg, Germany
e-mail: stefan.schiller@frias.uni-freiburg.de

Abstract This contribution describes the assembly and structural and functional characterization of various types of polymer-supported lipid bilayer membranes. We start with the description of the polymer-cushioned membrane that can be prepared by first attaching (covalently) polymer coils (as tethers or cushions) from solution to a reactive solid support, followed by the covalent coupling of a lipid monolayer containing reactive anchor lipids. Alternatively, a lipopolymer monolayer (if needed mixed with "normal" lipids) is pre-organized at the water-air interface in a Langmuir trough and then transferred to a solid substrate which is again pre-functionalized by a reactive coating. A special case discussed is the use of glycolipopolymers for the assembly of the proximal tethered monolayer. From all these interfacial architectures the final structure, the supported bilayer, is obtained by the fusion of vesicles forming the distal monolayer of the membrane.

For some of these polymer-tethered lipid bilayers a few key performance indicators are discussed. In particular, we describe structural parameters obtained from surface plasmon resonance spectroscopy and compare those to important functional features, i.e., the electrical capacitance and resistance of the membrane. Furthermore, the ability of the polymer tethers to swell in water and evidence for the resulting lateral mobility of the lipid molecules in the membrane as an indicator for the fluid nature of the tethered bilayers are presented.

Next, the use of polyelectrolyte multilayers, prepared by the layer-by-layer deposition protocol, as well as the use of polymer cushions prepared by plasma-polymerization is introduced. Evidence for the proper structural and functional characteristics of the corresponding tethered bilayers is derived from neutron reflectivity and from IR data, and by the observation of the functional incorporation of proteins.

And finally, the very promising application of hydrogels as cushions but also as protective coatings for the tethered membrane architectures, eventually allowing even for operations in air, is presented and discussed.

Keywords Tethered lipid bilayer membrane · Polymer cushion · Lipopolymer · Glycolipopolymer · Polyelectrolyte multilayers · Plasma polymers · Hydrogels · Self-assembly · Surface plasmon resonance spectroscopy · Electrochemical impedance spectroscopy · Neutron reflectometry · Fluorescence recovery after photo bleaching (FRAP)

Contents

1 Introduction

Approximately 20% of the open reading frames in complex organisms encode membrane-associated proteins [1]. Despite their abundance and key roles in vital processes, e.g., cell adhesion, recognition, motility, energy production, transport of nutrients, etc., our knowledge of the structure–function relationship for membrane proteins is rather limited, and lags far behind that of soluble proteins [2–4]. This is largely due to the complexity of the biological membrane as is schematically sketched in Fig. 1 [5]: the multicomponent nature of the biomembrane with the lipid bilayer constituting the matrix into which a variety of proteins is embedded as functional and structural elements still represents a major challenge for the experimental characterization of the fundamentals of membrane structure

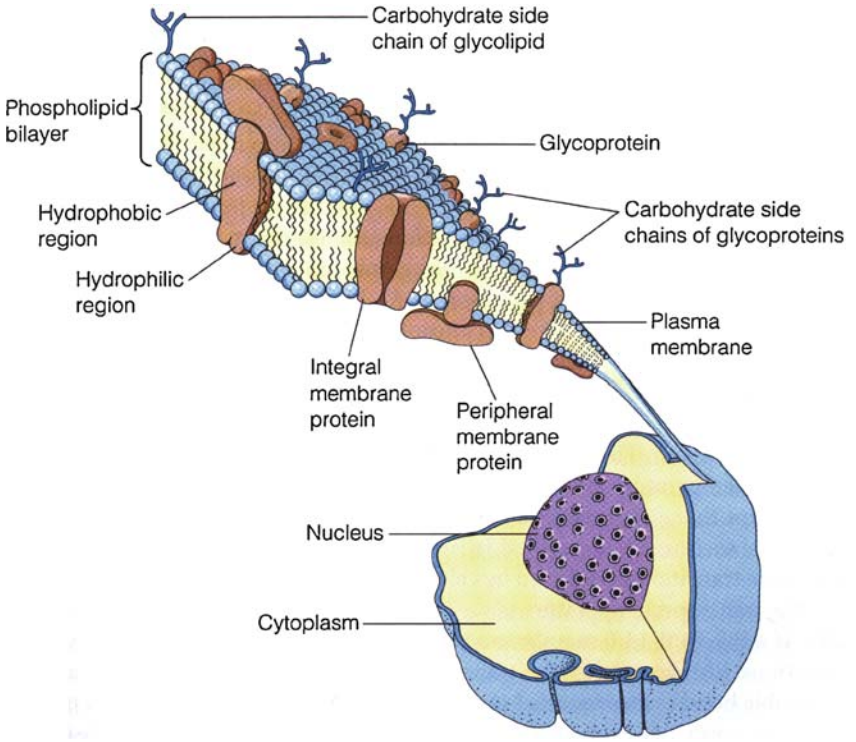

Fig. 1 The complexity of the architecture of a biological membrane (from [5], with permission)

and processes. With the limited set of biophysical tools that we have available, it is nearly impossible to probe adequately the physical–chemical properties and mechanisms underlying membrane protein function [6].

Similarly unsatisfying is the situation with respect to the implementation of platforms for bio-sensors that are able to address the many important interactions between ligands and membrane integral receptors. This is even more surprising as 50% of the interesting drug targets are transmembrane receptor proteins, and as current sensing platforms for monitoring membrane proteins and processes are lacking in versatility and flexibility, and are not suitable for "layman" use.

As a consequence of this unacceptable situation, the interest in model systems suitable for the construction and study of complex lipid/protein membrane architectures increased steadily over the years [7]. The classical portfolio of model membranes used for biophysical and interfacial studies of lipid (bi)layers and lipid/protein composites includes Langmuir monolayers assembled at the water/air interface, (uni- and multi-lamellar) vesicles in a bulk (liposomal) dispersion, the bimolecular lipid membrane (BLMs), and various types of solid supported membranes [8]. All these have their specific advantages but also suffer from serious drawbacks.

The supported membranes [9] seem to offer the best options for very detailed biophysical studies of membrane structure, order, and dynamics, allowing at the same time for experimental strategies aimed at elucidating the much-needed correlation of these parameters with the functional performance of incorporated (or surface-associated) proteins or protein aggregates [10]. By virtue of the fact that the (fluid) lipid bilayer in this platform is weakly coupled to a solid support, the resulting largely enhanced stability allows for the use of a variety of surface analytical tools for structural characterizations, ranging from X-ray and neutron reflectometry (NR), optical techniques, including ellipsometry, surface plasmon- and waveguide spectroscopies, vibrational spectroscopies, to fluorescence based techniques, scanning probe methods, and many more. Additionally, functional aspects, e.g., the behavior of membrane integral units diffusing in the (liquid-crystalline) two-dimensional matrix of the lipid bilayer, the binding of ligands to membrane-integral receptors, or the translocation of ions across the hydrophobic barrier of the bilayer could be studied in parallel and interpreted on the basis of the simultaneously monitored structural data [11].

However, the fact that in these systems the bilayers are only weakly physisorbed to the substrate, i.e., are only floating on top of a very thin water layer, can eventually lead to delamination and the destruction of the membrane architecture. Hence, attempts were made to stabilize further the lipid matrix and the incorporated proteins by chemically tethering either one of them to the solid support [12]. In some cases this was done via flexible spacers that coupled the membranes by "anchor lipids" to the substrates while simultaneously decoupled the membranes sufficiently from the solid surface, thus preventing the incorporated proteins from being denatured by their strong interaction with the polar groups of the hydrophilic support [13]. Here, in the present contribution, we summarize some of the various concepts based on polymer layers used as "cushions" that allow for the stable coupling and, if needed, even covalent binding of the lipid bilayer membrane to the solid support giving the whole architecture its robustness and long term stability [14].

We introduce different strategies developed for the build-up of polymer supported membranes and describe their properties as they can be characterized in great detail by a variety of surface analytical techniques [15].

2 Assembling Polymer: Cushioned Membranes

Many questions pertaining to membrane processes in general and ligand/membrane receptor interactions in particular can be addressed by a novel model membrane system, i.e., polymer-supported or polymer-tethered lipid bilayers [12, 14]. The basic structural unit for this sensor platform is the tethered lipid bilayer membrane [16] displayed in Fig. 2D. The essential architectural elements of this supramolecular assembly include the solid support, e.g., an optical or electrical transducer (device), the polymeric tether system which provides the partial covalent and, hence, very stable attachment of the whole membrane to the substrate surface, and the fluid lipid bilayer, functionalized if needed by embedded proteins.

All strategies for the build-up of stable polymer-tethered BLMs are based on the mere self-assembly of specifically custom-tailored molecules. Two fundamentally different strategies can be taken as depicted in Fig. 2 and are described in detail below. The first is based on a sequential adsorption/binding of the polymer cushion from solution to a solid support that was prefunctionalized by a reactive layer exposing chemical groups that can covalently couple to the corresponding binding partners of the polymer [17]. Onto this surface-attached polymer cushion a lipid monolayer, typically preorganized at the water-air interface, can then be bound by means of mixed reactive "anchor" lipids [18]. This is schematically shown in Fig. 2A. The result is a polymer-tethered lipid monolayer (Fig. 2B) which can be converted to the desired target architecture – the polymer-supported bilayer (Fig. 2D) – either by the fusion of vesicles from a liposomal dispersion, or by the transfer of the distal layer via the Langmuir/Blodgett- or the Langmuir/Schaefer-techniques from the water/air interface, or by a simple adsorption and self-organization step of lipid molecules from solution.

Alternatively, a Langmuir monolayer of lipo(glyco-) polymers, spread and organized (by compression to the desired lateral packing density) at the water/air interface, can be transferred to and triggered to react with a suitable functional coating deposited prior to the transfer onto a solid substrate by a self-assembly step from solution (Fig. 2C; see also Fig. 6a) [16, 19, 20]. An additional advantage of this preorganization is the possibility to add other lipids or functional components to the lipopolymer monolayer by simply spreading mixtures that are then transferred to the support. Again, the final polymer-tethered bilayer is completed by the deposition of the distal layer (Fig. 2D).

An example of the broad range of surface-analytical techniques that can be applied in order to monitor the build-up of these architectures and then further to characterize the structural and functional properties of the resulting complex lipid bilayer membranes is presented in Fig. 3 [21]. Shown in Fig. 3a is the com-

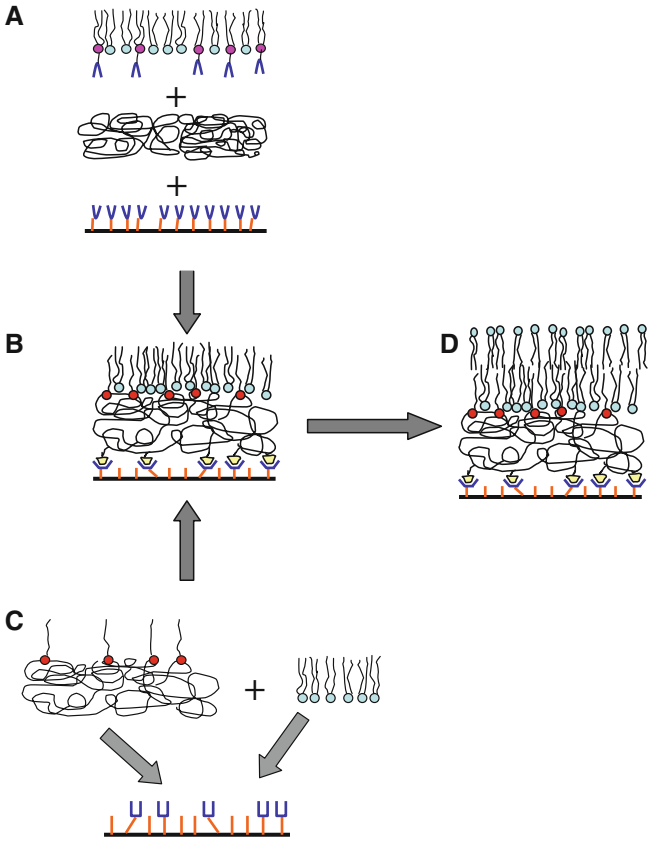

Fig. 2 The construction of a polymer-cushioned lipid bilayer membrane. (**A**) Architecture constructed in a sequential way: first, onto the functionalized substrate a polymer layer (cushion) is deposited by adsorption from solution and covalent binding, followed by the (partial) covalent attachment of a lipid monolayer containing some "anchor lipids" as reactive elements (**B**) able to couple the whole monolayer to the polymer cushion. (**C**) Alternatively, a lipopolymer monolayer, organized, e.g., at the water-air interface can be co-spread with regular low-mass amphiphiles and then transferred as a mixed monolayer onto a solid support, prefunctionalized with reactive groups, able to bind covalently to the polymer chains of the lipopolymer molecules, (**B**). (**D**) By a fusion step (or a Langmuir Schaefer transfer) the distal lipid monolayer completes the polymer-tethered membrane architecture

bination set-up of a surface-plasmon spectrometer in the classical Kretschmann configuration, using a prism as the plasmon coupling element. The interfacial architectures of interest can then be optically characterized in situ and in real time at the interface between a 50 nm thin Au layer needed for the resonant excitation of the surface plasmon modes in contact with the sample electrolyte solution (Fig. 3a). Two modes of operation are typically applied, i.e., the angular scan (Fig. 3b) and/or the kinetic scan (Fig. 3c). In the angular scan mode, a series of reflectivity scans are taken after each preparation step and analyzed in terms of an additional optical

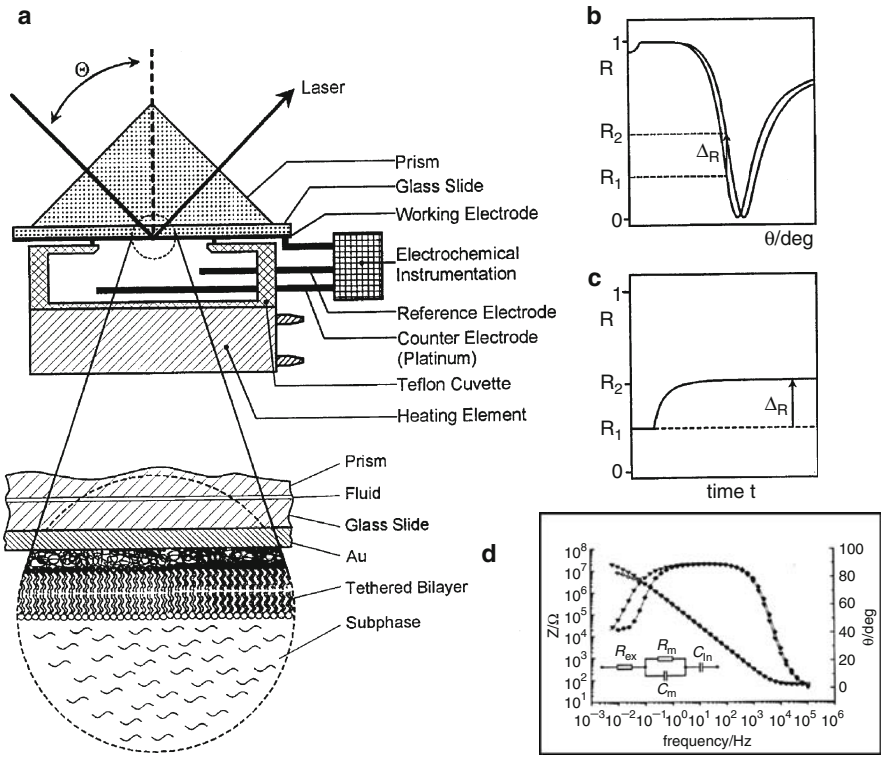

Fig. 3 (**a**) Experimental set-up based on a surface plasmon spectrometer combined with an electrochemical/impedance spectroscopic module for the simultaneous characterization of structural and functional features of tethered BLMs. The enlargement shows the solid/solution interface with the thin Au layer used for surface plasmon excitation, the tethering layer and the lipid bilayer in contact to the aqueous buffer phase; (**b**) typical angular surface plasmon resonance scans before and after the formation of the distal lipid layer (on top of the self-assembled proximal tethered lipid monolayer) by vesicle fusion; (**c**) kinetic mode of the fusion process recorded by monitoring the change of the reflected intensity at a fixed angle of incidence (cf. **b**) as a function of time; (**d**) schematics of an impedance spectroscopic experiment, i.e., recording the (amplitude and phase of the) current response upon the application of a small-amplitude AC voltage

thickness. Knowing the refractive index of this layer then allows the determination of its corresponding geometrical thickness. If monitored at a fixed angle of incidence, the time-dependent change of the reflectivity can be analyzed to yield kinetic information of the assembly steps, of the association or dissociation of any molecules binding to the membrane or integral receptors, etc.

The Au layer – which is a prerequisite for surface-plasmon optics – can be used simultaneously as the working electrode in a regular three-electrode electrochemical set-up (also shown in Fig. 3a) with the reference and the counter electrode being immersed in the flow-cell attached to the Au coated substrate. In this way, various electrochemical techniques, e.g., cyclic voltammetry or impedance spec-

troscopies, can be applied to the membrane samples, yielding in addition to the structural properties obtained from the surface-plasmon optical studies also functional parameters of the interfacial architectures. This then allows for very detailed studies of the structure–function relationship of these model membranes and of any reconstituted proteins.

2.1 Sequential Build-Up of Polymer-Membrane Architectures

A specific example of the concept of the sequential preparation of a polymer-tethered lipid bilayer membrane is given in Fig. 4 [17]. A mono-chloro-silane derivative with a reactive ester endgroup in the ω – position self-assembles via adsorption from solution to a substrate that is prepared by first evaporating a 50 nm thin Au-layer needed for the surface-plasmon optical characterization of the resulting architectures, followed by sputter-coating a thin SiO_2 layer required for the covalent coupling of the silane groups of the reactive coupling layer (Fig. 4a). The corresponding surface-plasmon angular reflectivity spectra, taken prior to and after the deposition of the silane monolayer are shown in Fig. 5A, B, respectively.

Next, onto this reactive substrate a polymer monolayer of poly(ethyloxazoline)-*co*-poly(ethyleneimine) adsorbs from solution and partially reacts via the amine groups to the reactive ester moieties to form a covalently attached cushion (Fig. 4b). The corresponding angular SPR scan of the covalently bound polymer taken after its deposition from solution and after an extended overnight soxhlet extraction of the sample (to remove all unreacted and, hence, merely physisorbed polymer) is shown in Fig. 5C. Finally, a (partially) reactive monolayer of lipid molecules or other amphiphiles, in our case a simple monolayer of a reactive ester derivative of a long chain fatty acid, is organized as a monolayer and transferred to and reacted with the surface-attached cushion, thus generating the desired polymer-tethered lipid monolayer (Fig. 2B; the corresponding SPR scan is shown in Fig. 5D).

2.2 Lipo-Polymer Layers as Support for Tethered Membranes

The schematics of the alternate strategy, i.e., the preorganization of a lipopolymer layer at the water-air interface and the subsequent transfer of this complex monolayer to a solid support, prefunctionalized by a reactive monolayer, are shown in Fig. 6a [19, 22]. Compared to the illustration in Fig. 2B, here the coil character of the polymer of each individual lipopolymer is emphasized. The covalent coupling concept using benzophenone groups is displayed in Fig. 6b. The versatility of the proton abstraction reaction upon UV light excitation of the benzopheneone group allows for a broad range of lipopolymers to be coupled to the substrate. Two examples, both based on poly(ethyloxazoline) as the polymer chain, although with different molecular structures as the amphiphile, are given in Fig. 7c, d, respec-

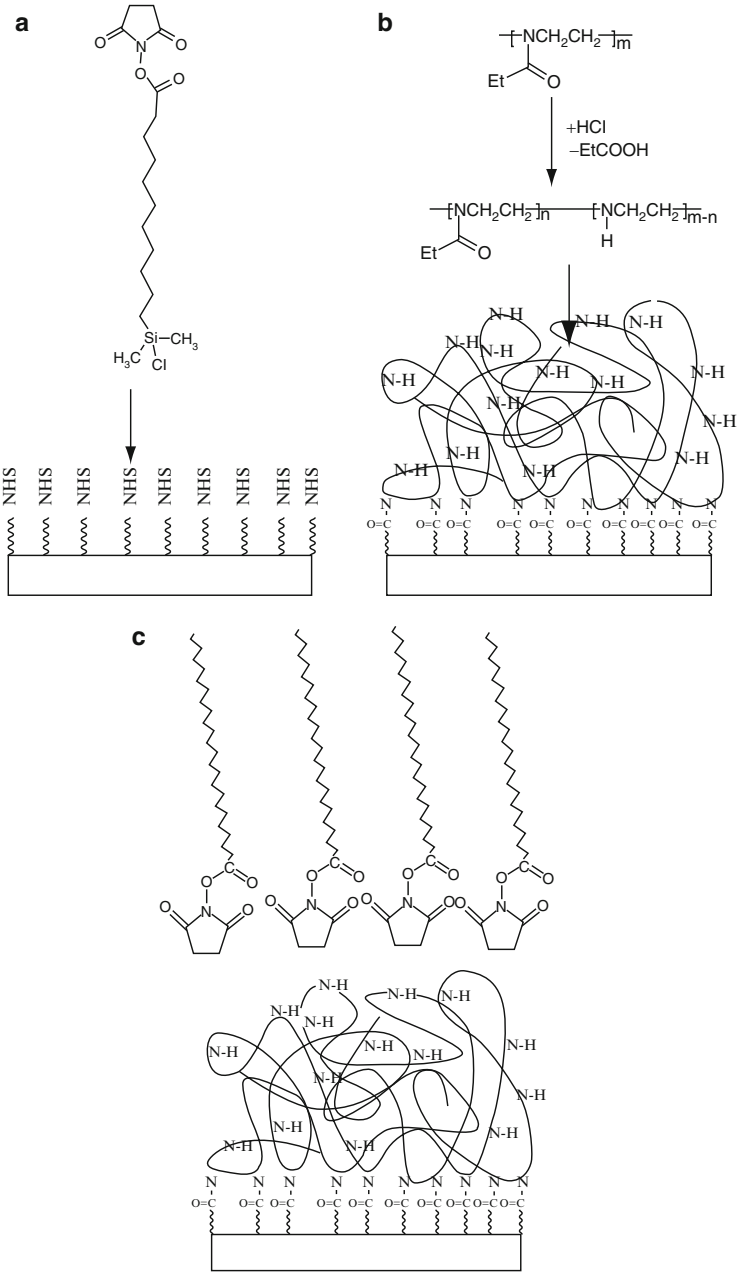

Fig. 4 (**a**) The reactive-ester analogue of a carboxy-terminated monochloro-silane derivative self-assembles onto a glass substrate to result in a reactive monolayer. (**b**) Onto this, an ethyleneimine-containing polymer coil, obtained by the partial conversion of a polyoxazoline precursor polymer binds covalently after adsorption from solution to give a stable polymer cushion for the binding of a monolayer of a reactive amphiphile, a reactive ester derivative of a fatty acid in the example given in (**c**)

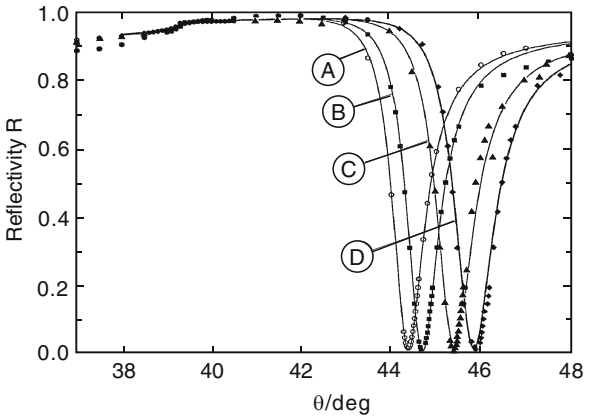

Fig. 5 Surface-plasmon resonance curves, i.e., reflectivity-vs-incident angle scans of the bare substrate, a Ag coated glass slide with a thin SiO_2 layer evaporated on top (A), after the self-assembly of a reactive monochlorosilane derivative (cf. Fig. 4a) (B), after the adsorption (from solution), covalent binding, and soxhlet extraction of the polymer cushion (C), and after the deposition of a model lipid monolayer (a layer of reactive ester derivatives of a fatty acid) (D)

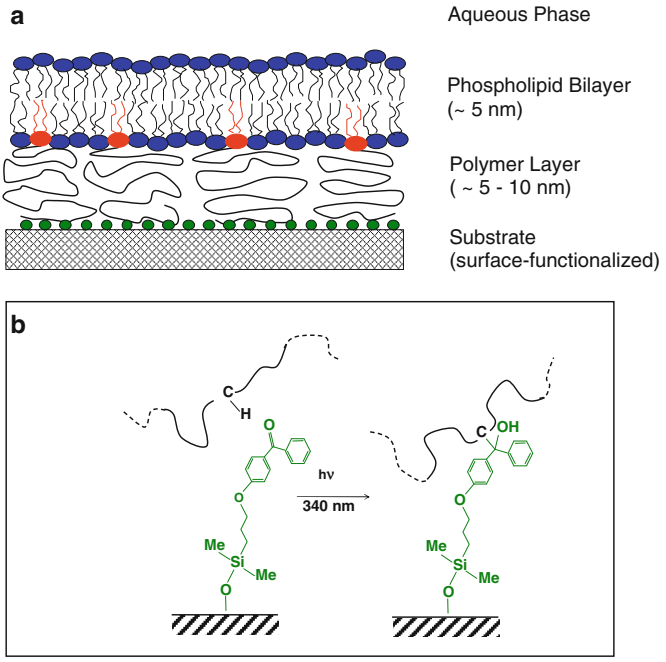

Fig. 6 (**a**) Schematics of a polymer-tethered lipid bilayer on a solid support; the architecture is composed of a proximal mixed monolayer of lipopolymers and regular low-mass lipids, covered by a monolayer of "normal" lipids obtained by vesicle fusion. The lipopolymers are covalently attached to the benzophenone-derivative coated substrate by a proton-abstraction reaction as depicted in (**b**)

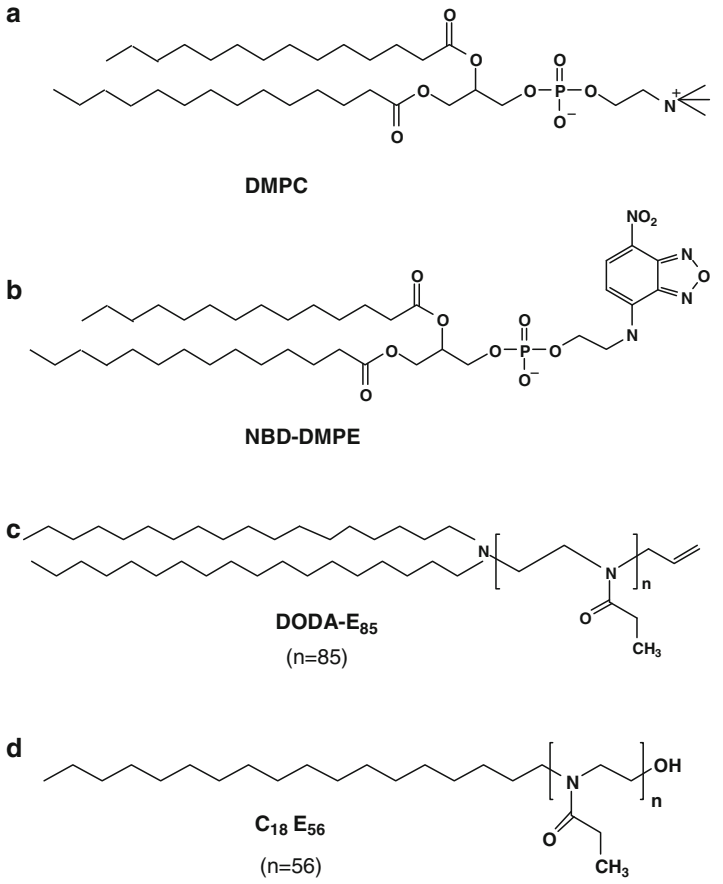

Fig. 7 A series of different lipids used for the build-up of polymer-tethered interfacial architectures: (**a**) DMPC stands for dimyristoylphosphatidylcholine, a classical synthetic lipid; (**b**) NBD-DMPE is a fluorescently labeled dimyristoylphosphatidyethanolamine derivative; and DODA-E_{85} (**c**) and $C_{18}E_{56}$ (**d**) are ethyloxazoline-lipopolymers of different structure

tively. It was shown that, this way, very stable polymer-tethered lipid monolayers (and from there lipid bilayers) could be assembled. The fact that the proximal lipopolymer layer is preorganized at the water-air interface allows for an excellent control of its composition and its packing density, thus controlling the grafting density as an important parameter determining the properties on the bilayer membrane but also that of incorporated proteins.

2.3 Lipo-Glycopolymers as Building Blocks for Tethered Membrane Architectures

As has been pointed out above, the study of dynamic membrane processes such as membrane protein function requires a fluid and electrochemically insulating lipid bilayer combined with a sufficiently extended cytoskeleton analog compartment, the polymer cushion, as reservoir and space for cytoplasmatic protein subunits. The biopolymer analogs presented in this section allow for the construction of a membrane mimic exhibiting such advanced properties. Recent efforts utilizing polymer tethers to overcome the limitation of small molecule tethered bilayers were disappointing due to the collapse of the polymer film in brush like states or its adoption of coiled conformations [23]. Clearly, the lateral interaction of the tether plays an important role in stabilizing the spacer in an elongated conformation. The inspiration for a new tethered membrane system utilizing lipo-glycopolymers (LGP) was derived from observations of the biological glycocalix surrounding the cell with carbohydrates creating a high osmotic pressure keeping cells apart, but also allowing for hydrogen bond mediated interchain stabilization. The lipo-glycopolymer presented here consisted of dioctadecylamine (DODA) as the lipid part and a polyacrylate backbone with β-O-3 linked glucose units. It was synthesized by controlled radical polymerization of protected D-glucose-2-propenoate with a DODA-modified nitriloxide initiator [20]. Despite a narrow molecular mass distribution of the glycopolymer (DI$\sim$1.17), deviations in length of the polymer tether and nanoscopic surface roughness of the substrate surface posed severe challenges for the covalent surface immobilization of a coherent lipid membrane architecture. In order to allow for a covalent immobilization of the surface proximal tether while maintaining an integral hydrophobic lipid layer, the LGP was oriented at the air-water interface of a Langmuir trough, allowing its oriented transfer by the Langmuir–Blodgett technique to a sensor surface in an elongated conformation. Since a polar protic solvent is used to solubilize and transfer the LGP the reactive surface layer used to immobilize the LGP must not be composed of electrophilic groups often used to immobilize carbohydrates. For the covalent attachment of the LGP we introduced a covalent immobilization scheme utilizing an azide based photochemical surface attachment scheme in order to assemble the complex supramolecular architectures with a defined orientation from the aqueous solution to the surface. The attraction of the scheme is given by its versatility for additional applications, e.g., for designing new protein nano-arrays in bionanotechnological applications. The photoreactive SAM was synthesized on the surface via a two step process. First a mixed SAM composed of 1-mercaptohexane and amino terminated C_{12}-spacered disulfide is prepared and subsequently modified with 5-azido-2-nitro-benzoic acid chloride (ANB) introducing the photoreactive moiety. (C_{12}-spacers have shown better binding reliability than C_6-spacers, most likely due to quenching of the azide via radiative decay channels and energy dissipation through the closer vicinity of the C_6-spacered azide to the metal surface.) It is interesting to note that LGP still reaches decoupling distances close to the the-

Table 1 EIS data (membrane capacitance and resistance) and SPR data (thickness measurements) obtained from LGP based bilayers

	$R_{II}\,(M\Omega\,cm^2)$	$C_{II}\,(\mu F\,cm^{-2})$	$d\,(nm^{-1})$
Mixed SAM	1.4 ± 0.5	2.0 ± 0.1	2.5 ± 0.2
Lipo-glycopolymer, monolayer	6.5 ± 0.5	2.1 ± 0.2	11.5 ± 1.5
Lipid bilayer	10.4 ± 1.0	1.6 ± 0.2	14.5 ± 2
Lipid bilayer + valinomycin	0.01 ± 0.002		

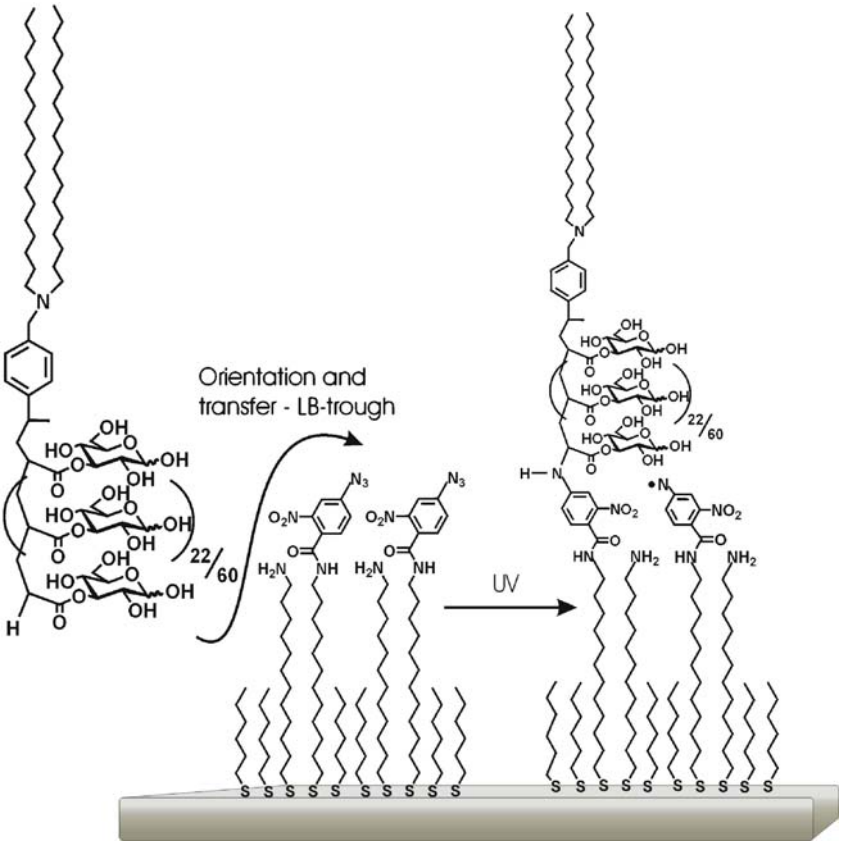

Fig. 8 Lipo-glycopolymer membranes, prepared in three steps: a preoriented lipo-glycopolymer monolayer is transferred onto a photo-reactive SAM and covalently linked to the surface prior to the bilayer formation via vesicle fusion

oretical maximum (Table 1) underlining the stabilizing effect of the carbohydrate interactions (Fig. 8). Vesicle fusion onto these LGP monolayers utilizing diphytanylphosphatidyl choline completed the lipid bilayer. Highly insulating tethered membranes with large decoupling distances of more than 10 nm from the surface (Table 1) were created and investigated by using surface plasmon resonance spectroscopy (SPS) and electrochemical impedance spectroscopy (EIS) (results are shown in Table 1). The impedance measured for the LGP-tethered membranes

varied from 1 to 3 $M\Omega cm^2$ even though single experiments achieved values of larger than 10 $M\Omega cm^2$. These data are comparable with those of known BLMs.

In order to test the functionality and reservoir properties of the new tethered lipid bilayers, the ion carrier valinomycin was used to study the selective transport of potassium ions. The data, shown in Table 1, confirmed the formation of a fluid and insulating tBLM. The addition of 0.1 M potassium ions resulted in a drop in resistance of up to three orders in magnitude corresponding well to literature values [13].

3 Important Basic Properties of Tethered Membranes: The Swelling of the Cushion and the Lateral Mobility of the Lipids

Among the various membrane properties that might need to be optimized for a particular "application" of the tethered membrane architecture and/or of any incorporated proteins we discuss only two key performance parameters, i.e., (1) the ability of the tethering system to swell by the up-take of a sufficient amount of water into the interstitial space between the lipid bilayer and the solid support, and (2) the high lateral mobility of the individual lipid molecules in the two opposing leaflets of the bilayer membrane.

The proper function of a membrane is intimately linked to the liquid-crystalline character of its lipid bilayer matrix. Among other factors, this depends crucially on the existence of sufficient water reservoirs on both sides of the bilayer membrane. (The lipid bilayer is a thermotropic and lyotropic smectic liquid-crystal.) While this is naturally given on the distal side of the tethered membrane architecture by the aqueous phase of the flow cell, the coupling of the membrane to the substrate on the proximal layer imposes serious restrictions on the amount and free accessibility, e.g., for ions of the aqueous phase between the bilayer and the solid substrate. In this context, the tethering system not only couples and thus stabilizes mechanically the whole architecture to the support; foremost it has to decouple the lipid bilayer from the strong interactions of the headgroups with the polar support. This way:

- The liquid-crystalline character of the lipid bilayer can be maintained
- Sufficient space for any cytoplasmatic protein subunits protruding out of the membrane can be accommodated
- A sufficiently large reservoir for the electrolyte phase can be engineered

All these requirements can be fulfilled by polymers of the proper design and chemical nature as presented above.

3.1 Swelling and Drying of the Polymer Tethers

The degree of swelling of the tethering system, i.e., the amount of water that can be accommodated by the polymer cushion, can be followed by surface-plasmon optics. Figure 9 gives an example of the swelling of a polymer-tethered lipid monolayer in

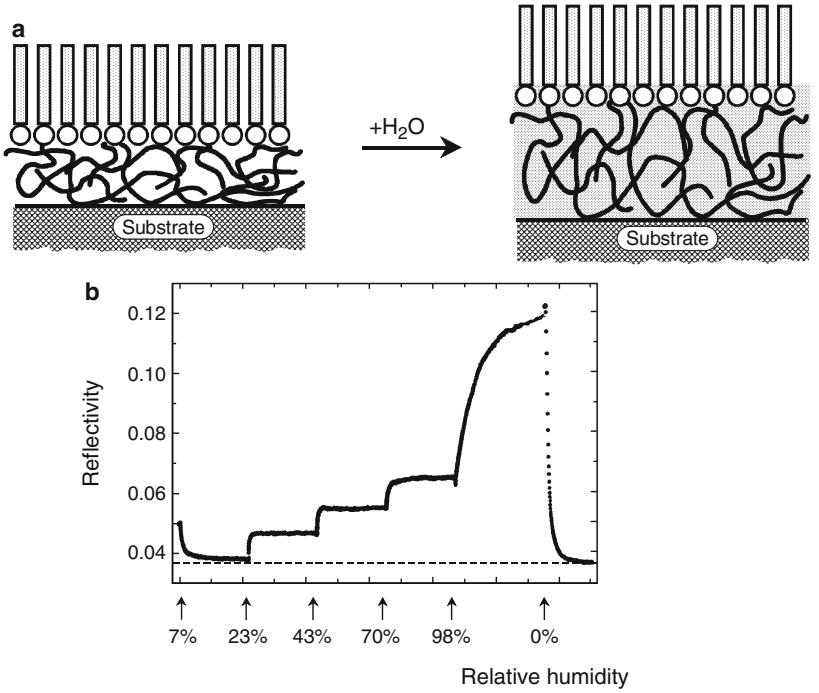

Fig. 9 The polymer-tethered lipid monolayer (**a**) can swell by the up-take of significant amounts of water; (**b**) surface-plasmon optical evidence of the swelling behavior of a polymer-cushioned monolayer by the exposure to air of different humidity (% relative humidity as indicated). Upon exposure to dry air the tethered monolayer collapses to its water-free thickness (however, can swell again if exposed to humid air (not shown))

air at different relative humidity. The concept of the measurement is schematically given in Fig. 9a. Any incorporation of water molecules into the tether leads to an increase of the (optical) thickness of the whole interfacial architecture resulting in a shift of the surface-plasmon resonance angle that can be easily probed (Fig. 3b, c). (Since the chemical potential of water at 100% relative humidity is identical to that of liquid water, the thickness increase, i.e., water uptake at 100% humidity, is equivalent to the swelling of the membrane in bulk water; however, it can be detected with much better contrast if measured in air.) A kinetic drying/swelling protocol as recorded by surface-plasmon optics is given in Fig. 9b. The polymer-tethered monolayer was prepared at ambient conditions and then exposed to air of 7% relative humidity (as indicated in Fig. 9b). This resulted in a partial drying of the tether with the concomitant decrease of its thickness to a new equilibrium value. Upon raising the relative humidity, the tethered membrane increasingly swells again to the corresponding new equilibrium. The whole process is fully reversible: the exposure of the membrane to dry air leads to the complete loss of the water in the tether giving the architecture a stable shelf life. Not shown is a further reswelling upon repeated exposure to humid air.

3.2 *Lateral Mobility of Lipids in a Tethered Bilayer Membrane*

Another important feature of a tethered membrane that we briefly discuss is the lateral mobility of its lipid constituents. The example that we present refers to a tethered mixed monolayer (the respective architecture corresponds to the one given schematically in Fig. 6a) composed of the lipopolymer DODA-E_{85}, presented in Fig. 7c, and the regular lipid DMPC (Fig. 7a) [19]. The diffusion coefficient can be quantitatively determined by a technique originally introduced for vesicular systems, i.e., by fluorescence recovery after photo-bleaching (FRAP). A particularly simple version of this method is based on the fluorescence microscopic observation of the (time dependent) behavior of an area on the tethered bilayer surface that was first depleted of its fluorescently labeled lipid molecules by a bleach pulse (Fig. 10). While prior to the pulse the homogeneous intensity background indicates a homogeneous lipid bilayer (Fig. 10a, $t = 0$ s), the bleach pulse generates a dark hole that – for a fluid system – already at $t = 12$ s (Fig. 10b) starts to become fuzzy at the edges by the diffusion of fluorescently labeled lipid molecules that migrate from the unbleached area into the dark spot. With increasing time lapsed, the dark spot gradually

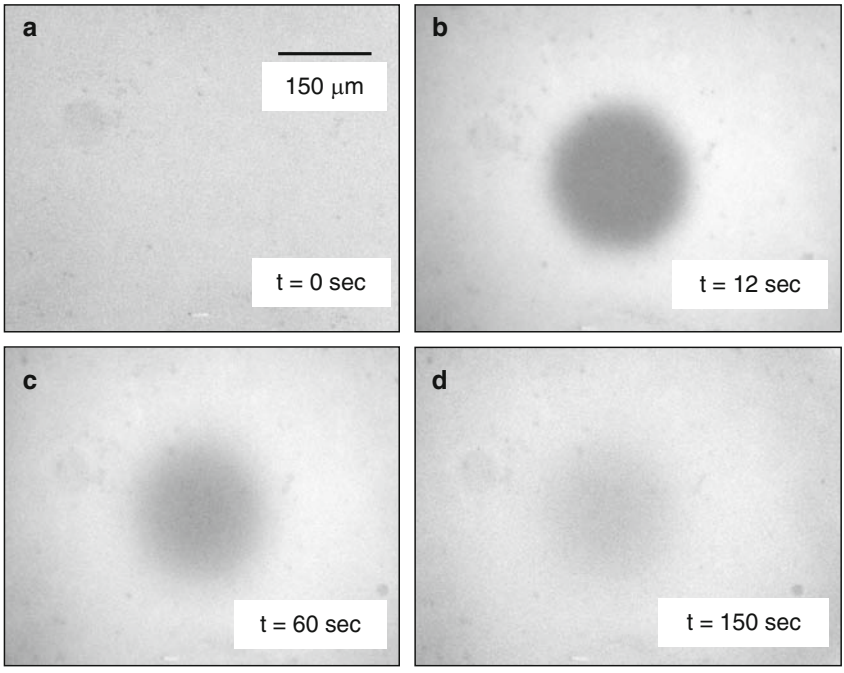

Fig. 10 Time-lapse fluorescence microscopy images of a tethered lipopolymer membrane prior to the exposure to a laser pulse ((**a**), $t = 0$ s), that burns a nonfluorescent (*black*) hole into the membrane. The following images were taken after 12 s (**b**), 60 s (**c**), and 150 s (**d**), respectively. Note the gradual refilling of the bleached area by lateral diffusion of unbleached labeled lipid molecules from the unexposed membrane areas

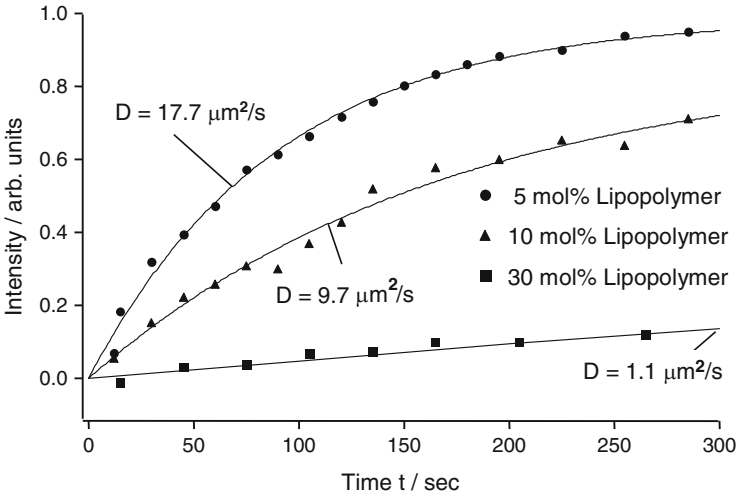

Fig. 11 Time-dependent recovery of the fluorescence after bleaching a hole into the lipopolymer-tethered membranes composed of DMPC and an increasing amount of the lipopolymer DODA-E_{85}, as indicated. The intensities were obtained by integrating the fluorescence across the hole area (cf. some of the corresponding fluorescence micrographs given in Fig. 10)

becomes refilled (Fig. 10c, d, respectively) and disappears eventually at a later time provided the recovery is 100% (i.e., for an infinite and freely accessible reservoir of unbleached molecules).

By recording fluorescence micrographs like those presented in Fig. 10, integrating the emitted fluorescence intensity across the bleached spot area, and plotting the resulting values as a function of time after the bleach pulse, one obtains a recovery curve that yields the diffusion coefficient as a fitting parameter. This is shown in Fig. 11 for three different lipopolymer-tethered bilayer membranes varying in composition as indicated. All diffusion coefficients obtained are values typical for fluid membranes as they are also found in vesicle membranes that are known to be in a liquid-crystalline state. The other interesting finding is the fact that an increasing fraction of lipopolymer molecules acting as membrane anchors (Fig. 6a) obviously slows down the lateral diffusion of the lipid molecules although they are not themselves part of the tethering system. They need, however, to migrate around those obstacles on their random walk within the two-dimensional matrix of the lipid bilayer.

4 Polyelectrolyte Multilayers as Supports for Tethered Membranes

Among the various strategies for the construction of polymer-tethered model membranes, the concept of simply using electrostatic interactions between the membrane with its partially charged lipids and a polyelectrolyte layer as cushion

was expected to be a particularly promising concept [24]. All preparation steps involved in this approach are based on mere self-assembly processes, leading to a convenient all water-based protocol for the build-up of model membranes. In the following some structural features of these assemblies are reported [25].

The polyelectrolyte multilayers employed in these studies consisted of alternating layers of poly(ethyleneimine) (PEI) and poly(4-styrenesulfonicacid) sodium salt (PSS) and were prepared via adsorption from solution as described by Decher et al. [26] on functionalized Au- or SiO_x substrates. The lipids used for the preparation of the bilayers were dimyristoyl-L-α-phosphatidylglycerol (DMPG, negatively charged in aqueous solution) and DMPC. Uni-lamellar lipid vesicles were prepared via the extrusion technique.

The polyelectrolyte-tethered bilayers were investigated by means of time dependent surface plasmon spectroscopy, impedance spectroscopy, FRAP, as well as NR [27]. The NR data given in Fig. 12 were first calculated based on a model that included the substrate and a box for the polyelectrolyte multilayer (A), and an additional box for the lipid bilayer (C). However, in order to fit the experimental NR curve, a top layer had to be added that was approximated by a uniform coating with average scattering length density b/V shown in the inset of Fig. 12. The thickness of

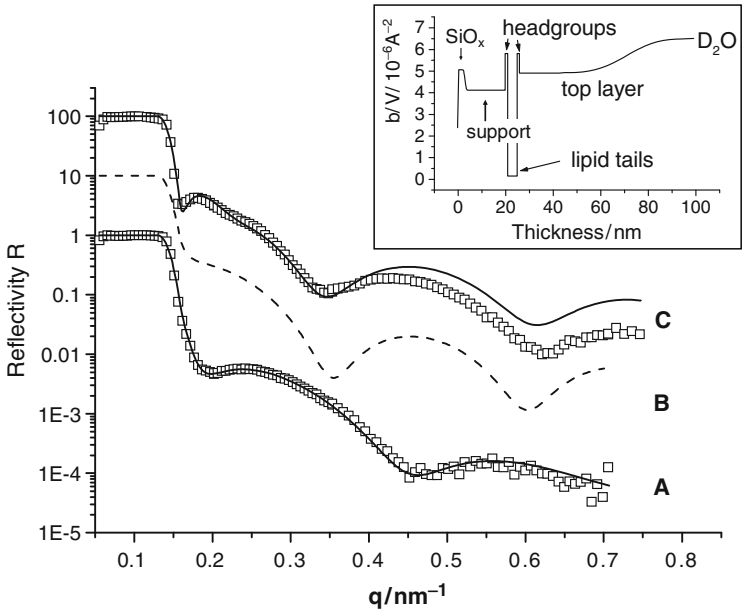

Fig. 12 Neutron reflectometry (NR) data of the polyelectrolyte multilayer (4 PSS/4 PAH) – coated solid support without lipid bilayer (**A**), and with a DMPC/DMPG (10:1) mixed membrane on top (**C**). The curves are shifted relative to each other for clarity. *Solid lines* represent model calculations of the data with scattering length densities, b/V, corresponding to the blank multilayer support (**A**), and to the tethered bilayer plus a nonspecific top layer (**C**), as given in the *inset*. The *dotted line* (**B**) represents a simulation of a lipid bilayer without an additional nonspecific layer on top

the top layer was well defined by the visible modulation in the reflection data with a short period in q and was found to be in the order of the radius of (un)fused liposomes. The modulation was strongly damped, indicating a very rough interface facing towards the aqueous phase (C). A simulation without the additional nonspecific top layer did not describe the data in an acceptable way (dotted curve B in Fig. 12).

5 Plasma-Polymer Layers as Cushions for Lipid Membrane Architectures

Lipid bilayer membranes tethered to plasma-polymerized films as hydrophilic supports were another concept introduced recently [28]. The plasma polymerization of maleic anhydride (MAH-PP), e.g., has led to the synthesis of thin polymeric coatings that appear to be suitable to act as a reservoir for an aqueous phase and a cushion for lipid bilayers [29]. A crucial requirement for the use of such polymers as water containing supports for lipid bilayer membranes is their adhesion to the substrate. In a previous study [30] covalent binding of MAH-PP films to gold supports was achieved by a self assembled alkylthiol adhesion layer. The previous work has shown that maleic anhydride, when polymerized at a low duty cycle, can behave as a polyelectrolyte. The thin polymer layers were found to have a very low electrical resistance $\left(\text{ca. } 100\,\Omega\text{cm}^2\right)$ after immersion and subsequent hydrolysis/swelling in aqueous buffer.

The schematics of the preparation protocol for plasma-polymer-tethered bilayers are given in Fig. 13: mixed vesicles containing a negative and a zwitterionic lipid were fused in a Ca^{2+} containing buffer solution onto decylamine derivatized MAH-PP films. The MAH-PP layer appears to form a sub-membrane architecture, which exhibits some of the properties required for biomimetic membrane supports by acting as a polyelectrolyte cushion for the fluid bilayer membrane.

Liposome fusion and the incorporation of membrane proteins were studied using EIS and surface plasmon spectroscopy with the chemical composition of the plasma polymer film being monitored using Fourier transform infrared spectroscopy (FTIR). A typical FTIR spectrum of the derivatized MAH-PP given in Fig. 14 shows peaks typical for the amide I $\left(1{,}730\,\text{cm}^{-1}\right)$ and the carboxyl groups $\left(1{,}680\,\text{cm}^{-1}\right)$ in the derivatized MAH-PP. It is remarkable to note that, after 15 h of reaction, anhydride groups are still observable within the polymer (at 1,780 and $1{,}860\,\text{cm}^{-1}$, respectively (cf. the succinic anhydrate spectrum given in (c) for comparison.)), suggesting that the amino-derivatization occurs only within the uppermost surface layers. In comparison, the peaks representing the amide and carboxyl groups are missing in the FTIR spectrum of the unmodified MAH-PP. A good surface coverage of the decylamine on the surface is also reflected in the significant increase in hydrophobicity of the surface. The average advancing contact angle of the functionalized MAH-PP was $\theta_A = 93 \pm 2°$, with the receding angle being $\theta_R = 82 \pm 6°$, as compared to the untreated MAH-PP which gave an average θ_A of $62 \pm 2°$ (receding angle $47 \pm 2°$).

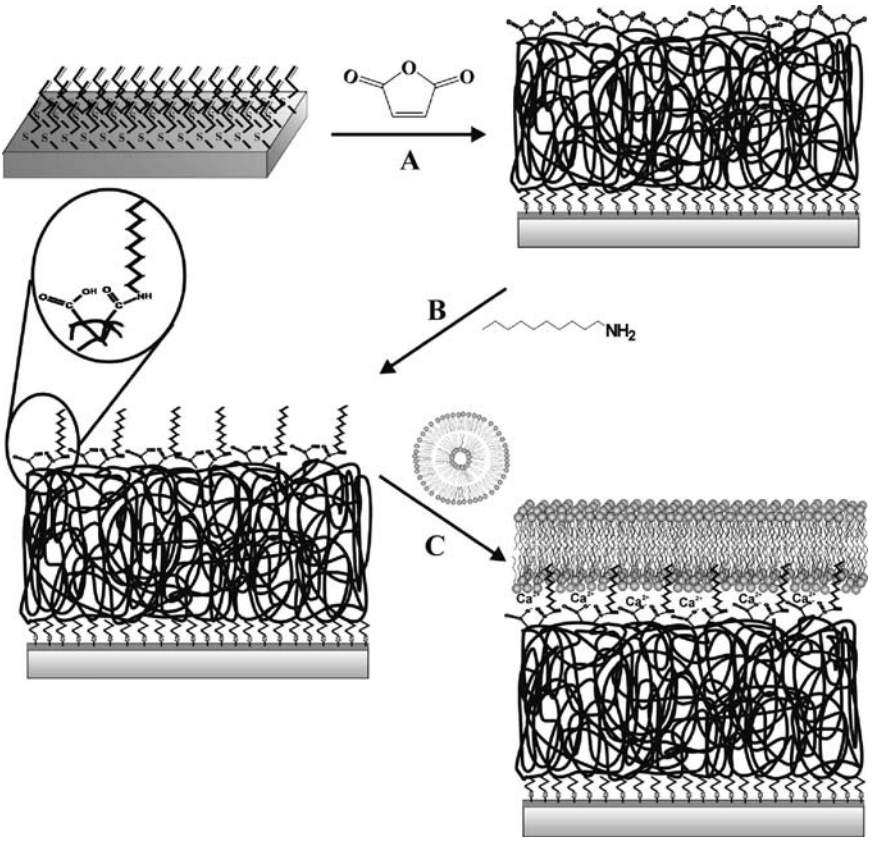

Fig. 13 Simplified schematic of the decylamine functionalized MAH-PP supported lipid membrane. (**B**) plasma polymerization of the MAH monomer on a self-assembled layer of allylmercaptane on an gold electrode. (**B**) Functionalization of the MAH-groups with decylamine (aminolysis). (**C**) Vesicle fusion in Ca^{2+} containing buffer for completion of the lipid membrane

The protein-functionalization of a decylamine modified MAH-PP supported biomimetic membrane was tested by the incorporation of cytochrome c oxidase (CcOX) from *Paracoccus denitrificans*. CcOX is part of the respiratory chain and is responsible for the active transport of protons against the gradient of the electrochemical potential across the lipid membrane. This reaction is driven by the enzymatic reduction of dioxygen where electrons are derived from the coenzyme cytochrome c. This process has been studied using mitochondria or CcOX reconstituted in liposomes and by the incorporation into tethered lipid membranes.

Adding CcOX solubilized in dodecylmaltoside (0.48 nM cell concentration) to the bilayer on the modified plasma polymer resulted in an increase in thickness

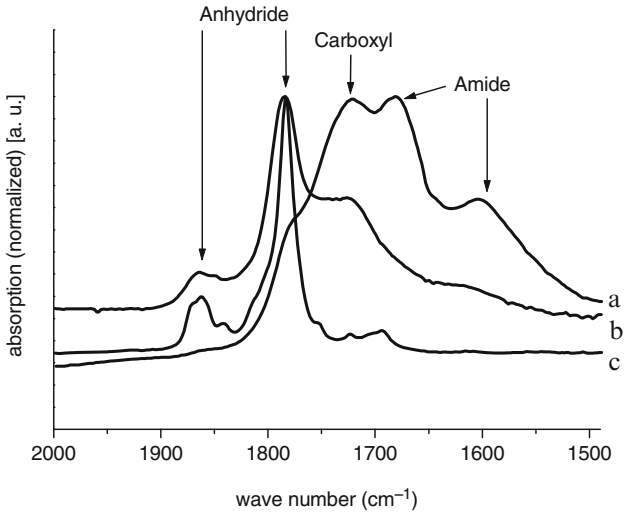

Fig. 14 FTIR spectra of the decylamine functionalized MAH-PP after 15 h of aminolysis (a). In comparison the spectra of an unfunctionalized MAH-PP film of equal quality (b) and of succcinic anhydride (c)

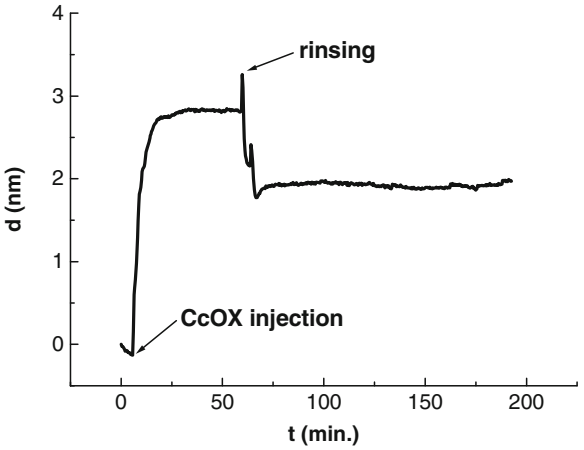

Fig. 15 SPR kinetics of the incorporation of cytochrome c oxidase (CcOX) into a plasma–polymer supported membrane

of about 2 nm as shown in Fig. 15. This finding gives evidence for the successful incorporation of the protein into the lipid bilayer, with the activity of the CcOX in the bilayer being tested by adding reduced cytochrome which showed a reduction of the membrane resistance.

6 Hydrogels as Tethers and as Mimics of the Mucosa

A completely different approach for the construction of protein-functionalized polymer-tethered membranes starts with the immobilization of the protein to be investigated as the unit that tethers the membrane to the top layer of the polymer. This can be achieved by using a hydrogel as the support layer with mesh sizes smaller than the size of the protein. The gel is firstly modified with a binding motif such as a nitrilo-triacetic acid (NTA) functionality to which the proteins can be bound by chelating via Ni^{2+} ions the his-tags engineered to their C- or N-terminus. This is schematically shown in Fig. 16. Since the protein is too big to penetrate the gel, it stays on the surface. A similar approach had been successfully applied before, however, on a short spacer layer rather than a polymer [31]. The detergent micelle solubilizing the protein is then replaced by a surface-dialysis step resulting in the formation of a largely defect-free electrically isolating protein-lipid layer tethered to the hydrogel. The sealing properties of these bilayer lipid membranes were sufficient to allow for a detailed investigation of electron and ion transport processes mediated, e.g., by CcOX [32]. An interesting additional aspect of hydrogels as supports is the possibility to manipulate their properties by external stimuli, e.g., by pH or temperature changes, thus providing a responsive support system [33].

Hydrogels are not only interesting new architectures for the tethering of lipid bilayer membranes to a solid support - they offer another exciting feature, i.e., acting as a stabilizing coating covering and thus protecting the whole interfacial structure (Fig. 16). However, the real potential of such a hydrogel-sandwiched membrane is the possibility to operate the lipid bilayer in air! Of course, typical analytes that will be monitored with the tethered membrane platform in a sensor configuration will be applied via an aqueous solution. However, from a general point of interest and, in particular, in view of the growing interest in developing a bio-electronic nose sensor, we proposed to start research into the detection of gaseous, air-borne analytes.

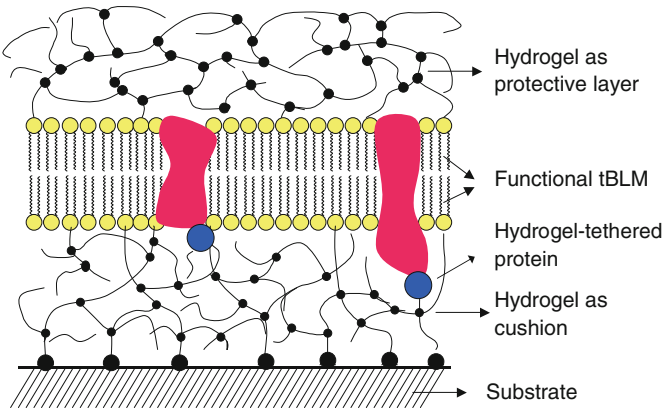

Fig. 16 Hydrogel used as cushion and as a protective coating for membranes when operating in (humid) air

The need for such sensors is unquestioned whether one is concerned with environmental pollution control, general air management, e.g., in airplanes or other closed rooms, or with the detection of bio-hazards, the food industry, the cosmetic industry – the list of potential customers is endless.

However, because lipid membranes with any (odorant) receptors incorporated [34] are only stable and work properly in an aqueous environment, we proposed strategies for the stabilization and protection of functional biomimetic membranes in air (of a certain minimal humidity). One of the envisaged strategies mimics the natural protection system of our nasal membranes, i.e., the mucosa [35]. We proposed the use of hydrogel structures composed of various chemical species (polar/charged synthetic polymers, polysaccharides, polypeptides, etc.) that are coupled to the tethered membrane (Fig. 16). This strategy will allow for the storage of sufficient amounts of water in order to keep the membrane/protein structure in a fully hydrated form, however, is stable even against dry air. This attempt, i.e., forming an artificial mucosa, is very promising based on the recent research of amphiphilic block-copolymers as membrane mimics [36].

7 Conclusions

The polymer-tethered lipid bilayer membrane on a solid support is a promising model system that mimics in many aspects a fluid biomembrane for biophysical studies of general lipid bilayer properties as well as of functional features of integrated proteins. At the same time, it offers the mechanical stability and chemical robustness that is needed for practical applications, e.g., for screening drugs that target membrane-integral receptors or for the construction of a membrane chip. Compared to other strategies for coupling lipid bilayers to a solid substrate, e.g., the mere supporting (floating) of the bilayer on top of an ultra thin water layer or the tethering of the architecture via a few anchor lipids with a short spacer unit to the substrate, the use of a thick polymer cushion offers the advantage of a clear separation of the liquid-crystalline lipid bilayer and its incorporated proteins form the potentially destructive interference with the substrate surface. This allows for maintaining the fluid character of the lipids in the bilayer leaflet, for the native reconstitution of even proteins with major cytoplasmatic subunits protruding out of the membrane and it provides a sufficiently large reservoir for water, ions, and other molecules interacting with the membrane and its constituents.

It has been shown that the chemical nature of the polymer cushion can be very flexible with examples ranging from polyelectrolytes to carbohydrate-containing macromolecules and cross-linked hydrogels. So far, the cushion has played only a rather passive role in that it was almost exclusively used as a structural element in the build-up of the tethered membrane architectures. The real potential, however, lies in the fact that these polymer systems could play a crucial functional role for these

artificial membranes: the responsive character of a suitably derivatized hydrogel is a first example [33]. Other features that could be tailored into the polymer support include:

- Active components needed for various signal transduction pathways
- Elements that mimic properties of the cytoskeleton or the glycocalix associated with biological membranes
- Artificial functional elements allowing for the implementation of specific sensing concepts, e.g., chromophores with ion specific emission properties.

Another most interesting aspect concerns the mechanical coupling of the polymer cushion with the membranes and their incorporated proteins. This could lead to interfacial architectures that show interesting features of structure formation by the coupling of the specific entropy driven properties of polymers in general with the self-organization capability of lipid bilayer structures. Experiments along these lines are under way.

Acknowledgements Part of this work was supported by the Deutsche Forschungsgemeinschaft (DFG) through the Priority Program SPP 1234 "Intelligente Hydrogele," by the European Union through Contract No. 043431, "FuSyMem," by the US National Science Foundation through the MRSEC "Polymer Interfaces and Macromolecular Assemblies" and the Science and Research Councel (SERC) of Singapore. We thank numerous colleagues that contributed though their encouraging support and many helpful discussions.

References

1. Liu JF, Rost B (2001) Protein Sci 10:1970–1979
2. White SH, Ladokhin AS, Jayasinghe S, Hristova K (2001) J Biol Chem 276:32395–32398
3. White SH, Wimley WC (1999) Annu Rev Biophys Biomol Struct 28:319–365
4. Popot JL, Engelman DM (2000) Annu Rev Biochem 69:881–922
5. Mathews CK, van Holde KE (1995) Biochemistry, 2nd edn. Benjamin/Cummings, Menlo Park, CA
6. White SH, Wimley WC, Ladokhin AS, Hristova K (1998) Methods Enzymol 295:62–87
7. In focus: structure and properties of soft organic-aqueous interfaces, Biointerphases 3 (2008) pp FC1–93
8. Chan YHM, Boxer SG (2007) Curr Opin Chem Biol 11:581–587
9. Tamm LK, McConnell HM (1985) Biophys J 47:105
10. Tanaka M, Sackmann E (2005) Nature 437:656
11. Knoll W, Morigaki K, Naumann R, Sacca B, Schiller S, Sinner E (2004) In: Wolfbeis OS, Mirsky VM (eds) Ultrathin electrochemical chemo- and biosensors, chap 10. Springer, Berlin, pp 239–253
12. Spinke J, Yang J, Wolf H, Liley M, Knoll W (1992) Biophys J 63:1667–1671
13. Schiller S, Naumann R, Lovejoy K, Kunz H, Knoll W (2003) Angew Chem Int Ed 42:208–211
14. Sinner E, Knoll W (2001) Curr Opin Chem Biol 5:705–711
15. Köper I, Schiller S, Giess F, Naumann R, Knoll W (2006) In: Leimannova Liu A (ed) Advances in planar lipid bilayers and liposomes, Chap 2, pp 37–53
16. Shen WW, Boxer S, Knoll W, Frank CW (2001) Biomacromolecules 2:70–79
17. Heibel C, Maus S, Knoll W, Rühe J (1998) In: Frank CW (ed) Organic thin films – structure and applications. American Chemical Society, Washington, DC, pp 104–118

18. Beyer D, Elender G, Knoll W, Kühner M, Maus S, Ringsdorf H, Sackmann E Angew Chem Int Ed (1996) 35:1682–1685
19. Naumann CA, Prucker O, Lehmann T, Rühe J, Knoll W, Frank CW (2002) Biomacromolecules 3:25–27
20. Götz H, Harth E, Schiller S, Frank C, Knoll W, Hawker CJ (2002) J Polym Sci A Polym Chem 40:3379–3391
21. Knoll W, Frank CW, Heibel C, Naumann R, Offenhäusser A, Rühe J, Schmidt EK, Shen WW, Sinner A (2000) Rev Mol Biotechnol 74:137–158
22. Hausch M, Zentel R, Knoll W (1999) Macromol Chem Phys 200:174–179
23. Munro JC, Frank CW (2004) Langmuir 20:3339–3349
24. Cassier T, Sinner A, Offenhäuser A, Möhwald H (1999) Colloids Surf Biointerfaces 15: 215–225
25. Kügler R, Knoll W (2002) Bioelectrochemistry 56:175–178
26. Decher G (1997) Science 277:1232–1237
27. Stamm M, Hüttenbach S, Reiter G (1991) Torema Physica B 173:11–16
28. Bender K, Fraser S, Förch R, Jenkins ATA, Köper I, Naumann R, Schiller S, Knoll W (2005) In: Mutlu M, Dinescu G, Förch R, Martin-Martinzen JN, Vyskocil J (eds) Plasma polymers and related materials. Hacettepe University Press, Turkey, pp 32–42
29. Jenkins ATA, Hu J, Wang YZ, Schiller S, Foerch R, Knoll W (2000) Langmuir 16:6381–6384
30. Schiller S, Hu J, Jenkins ATA, Timmons RB, Sanchez-Estrada FS, Knoll W, Foerch R (2002) Chem Mater 14:235–242
31. Giess F, Friedrich M, Heberle J, Naumann R, Knoll W (2004) Biophys J 87:3213–3220
32. Ataka K, Giess F, Knoll W, Naumann R, Haber-Pohlmeier S, Richter B, Heberle J (2004) J Am Chem Soc 126:16199–16206
33. Smith HL, Jablin MS, Vidyasagar A, Saiz J, Watkins E, Toomey R, Hurd AJ, Majewski J (2009) Phys Rev Lett 102:228102
34. Robelek R, Lemker E, Wiltschi B, Kirste V, Oesterhelt D, Sinner EK (2007) Angew Chem Int Ed 46:605–608
35. Huang Y, Leobandung W, Foss A, Peppas NA (2000) J Control Release 65:63–71
36. Taubert A, Napoli A, Meier W (2004) Curr Opin Chem Biol 8:598–603

Adv Polym Sci (2010) 224: 113–165
DOI:10.1007/12_2008_10

Published online: 5 March 2009

Biomimetic Block Copolymer Membranes

Violeta Malinova, Serena Belegrinou, Dirk de Bruyn Ouboter, and Wolfgang Peter Meier

Abstract Amphiphilic block copolymer membranes, classified as vesicles, are nano-aggregates receiving a lot of scientific interest due to their wide range of potential applications extending from biomedicine (e.g., drug delivery, imaging, nanoreactors) to material science (biosensors, electronics). This chapter summarizes the principles of vesicle formation, various membrane-forming copolymer systems and their properties as well as common techniques for vesicle preparation and characterization. Copolymer membranes with responsiveness to external stimuli are particularly attractive for use in drug delivery and are, therefore, also discussed. In addition, the chapter reviews recent examples of vesicles encapsulating proteins, enzymes and therapeutics as prospective systems for bio-applications.

Keywords Amphiphilic block copolymers, Membranes, Nanoreactors, Polymersomes, Self-assembly, Stimuli-responsive vesicles

Contents

V. Malinova, S. Belegrinou, D. de Bruyn Ouboter, and W.P. Meier (✉)
Department of Chemistry, University of Basel, Klingelbergstrasse 80, CH-4056, Switzerland
e-mail: W.Meier@unibas.ch

List of abbreviations

ADP	Adenosine diphosphate
AFM	Atomic force microscopy
AMD	Atomistic molecular dynamics
Apy	4-Aminopyridine
ATP	Adenosine triphosphate
BSA	Bovine serum albumin
CALB	*Candida Antarctica* lipase B
CG	Coarse-grain
CMC	Critical micelle concentration
CWC	Critical water concentration
d	Membrane thickness
DFT	Density functional theory model
DLS	Dynamic light scattering
DMF	Dimethylformamide
Dox	Doxorubicin
DPD	Dissipative particle dynamics
DPPC	Dipalmitoylphosphatitylcholine
DPPG	Dipalmitoylphosphatidylglycerol
DSC	Differential scanning calorimetry
DTNB	$5,5'$-Dithiobis-2-nitrobenzoic acid
EPD	External potential dynamics
FF–TEM	Freeze-fracture transmission electron microscopy
fPVs	Functionalized protein-containing vesicles
FRAP	Fluorescence recovery after photobleaching
FTIR	Fourier Transform Infrared Spectroscopy
HBPO	Hyperbranched poly(3-ethyl-3-oxetanemethanol)
ICAM-1	Intercellular adhesion antibodies-1
IPN	Interpenetrating polymer network
ITO	Indium–tin–oxide

Kc	Membrane bending rigidity
LCMs	Large compound micelles
LCST	Lower critical solution temperature
LCVs	Large compound vesicles
LFA	Lipofectamine
LSCM	Laser Scanning Confocal Microscopy
M_n	Number average molecular weight
MVVs	Multivesicular vesicles
M_w	Weight average molecular weight
NIR	Near infrared
P2VP	Poly(2-vinylpyridine)
P4VPMeI	Poly(4-vinylpyridinum) methyl iodide
P4VPQ	Poly(*N*-methyl-4-vinyl pyridinium)
PAA	Poly(acrylic acid)
PAM	Poly(acrylamide)
PAMPA	Poly[*N*-(3-aminopropyl)methylacrylamide hydrochloride]
PAMPS	Poly(sodium-2-acrylamido-2-methylpropanesulfonate)
PAzoM	Poly{6-[4-(4-methylphenyl-azo) phenoxy]hexyl acrylate}
PB	Poly(butadiene)
PBO	Poly(butylene oxide)
PC	Phosphatidylcholine
PCEMA	Poly(2-cinnamoylethyl methacrylate)
PCL	Poly(caprolactone)
PDEA	Poly(2-(diethylamino)ethyl methacrylate)
PDI	Polydispersity index
PDMAEMA	Poly(2-(dimethylamino) ethyl methacrylate)
PDMS	Poly(dimethyl siloxane)
PDPA	Poly(2-(diisopropylamino)ethyl methacrylate)
PEE	Poly(ethyl ethylene)
PEG	Poly(ethylene glycol)
PEO	Poly(ethylene oxide)
PFG–NMR	Pulsed field gradients nuclear magnetic resonance
PGMA	Poly(glycidyl methacrylate)
PH	$3,3',3''$-Phosphinidynetris-benzenesulfonic acid
PI	Poly(isoprene)
PIAT	Poly(isocianopeptide)
PLL	Poly-L-lysine
PMATC	Poly(*p*-methacrylamido)acetophenone thiosemicarbazone
PMOXA	Poly(methyl oxazoline)
PMPC	Poly(2-(methacryloyloxy)ethyl phosphorylcholine
PNIPAM	Poly(*N*-isopropylacrylamide)
PO	Poly-L-ornithine
PPO	Poly(propylene oxide)

PPS	Poly(propylene sulfide)
PS	Poly(styrene)
P*t*BA	Poly(*tert*-butyl acrylate)
PTMSPMA	Poly(3-(trimethoxysilyl)propyl methacrylate
SAXS	Small-angle X-ray scattering
SCFT	Real-space self-consistent field theory
SDS	Sodium dodecyl sulfate
SEM	Scanning electron microscopy
SFM	Scanning force microscopy
SLS	Static light scattering
TAX	Taxol
TEM	Transmission electron microscopy
TEMT	Transmission electron microtomography
T_g	Glass transition temperature
THF	Tetrahydrofuran
TIRFM	Total internal reflection fluorescence microscopy
TMSPMA	3-(Trimethoxysilyl)propyl methacrylate
ULVs	Unilamellar vesicles
WAXS	Wide-angle X-ray scattering
θ	Contact angle
τ	Membrane tension

Similarly to natural amphiphiles (e.g., lipids), synthetic block copolymers comprised of two or more chemically incompatible blocks can microphase separate in solution into aggregates of multiple morphologies. Upon manipulation of the relative block lengths and environmental parameters such as solvent composition, presence of additives and temperature, spheres, micelles, large compound micelles (LCMs), rods, tubules, lamellae, vesicles, large compound vesicles (LCVs), etc. can be prepared. Already for a few decades these structures have attracted scientific interest because of their wide range of potential applications extending from cosmetics and drug delivery to electronics.

Of particular interest are the amphiphilic block copolymer membranes, classified as vesicles (hollow spheres with walls composed of polymer bilayers) which resemble the natural cellular bilayer and can be used in biomedicine (as artificial cells and nanoreactors), drug delivery and nanotechnology. Due to the similarity in vesicle formation and bilayer morphology with liposomes, block copolymer vesicles are called "polymersomes" [1]. Recent progress in polymer physics and chemistry facilitated the design and synthesis of amphiphilic block copolymer membranes, thus making them an active area of research. At first we discuss here the principles of vesicle formation, emphasizing on the factors that control their size and stability. Next we describe different membrane forming copolymer systems and several techniques most commonly used for their characterization. At last potential applications of amphiphilic block copolymer membranes are accented.

1 General Aspects of Block Copolymer Membrane Formation

The membrane formation process in block copolymer systems is based on the principles which have long been known for lipids. Therefore, we review here briefly thermodynamic, geometric and kinetic factors influencing the membrane formation. For more details the reader is referred to the corresponding literature.

Polymers composed of covalently bonded hydrophilic and hydrophobic fractions (blocks) segregate at the nanometer scale when exposed to a selective solvent for at least one part of the molecule. In water, such lyotropic ("lyo-" = solvent, "-tropic" = induced by) behavior is mainly caused by the hydrophobic effect [2]. In order to minimize entropically unfavorable contacts with water molecules the hydrophobic part of the polymer chain tends to segregate and self-associate with neighbors, whereas the hydrophilic part has high affinity to the polar (aqueous) medium. Vesicles may also be formed in nonpolar media, as a result of mutual attraction of polar groups.

The self-assembly process in block copolymer systems leading to vesicle formation has been concisely reviewed by Antonietti and Forster [3]. They consider the vesiculation in terms of a bilayer formation, which will next bend (close) to form a vesicle. Classically, the shape (geometry) of self-assembled structures is determined by the size of the hydrophobic block and described by a packing parameter $P = v/al_c$, in which v is the volume of the densely packed hydrophobic segment, a is the area occupied by the hydrophilic group, and l_c is the chain length of the hydrophobic segment [4]. Hence, when $P < 1/3$, spherical micelles are formed, and when $1/3 < P < 1/2$, cylindrical micelles are observed, whereas $1/2 < P < 1$ corresponds to vesicles. If $P = 1$, flat lamellae (planar bilayers) are formed, and finally for $P > 1$, inverted structures are expected. These trends are well established for small surfactants and lipids and are generally valid also for amphiphilic block copolymers, although it is more convenient to use the volume or weight fraction f of the hydrophilic block $(0 < f < 1)$ to describe their shape. In fact, decreasing the lengths of the hydrophilic blocks at constant hydrophobic blocks lengths causes a transition from spherical to worm-like micelles and finally to vesicular structures [5, 6]. It is proposed that a starting point for generating polymersomes in water is a ratio of hydrophilic block to total mass: $f \approx 35 \pm 10\%$ [1]. Molecules with $f > 45\%$ can be expected to form micelles, whereas molecules with $f < 25\%$ can be expected to form inverted structures. This rule has not been exhaustively probed for different chain chemistry and molecular weights (MWs); however, copolymers with average MWs ranging from ~2,000 to 20,000 Da following the rule showed the ability to form polymersomes.

Apart from geometrical constraints, the most important parameter for determining the vesicle shape is the spontaneous curvature of the bilayer membrane [7]. Changes of this parameter (e.g., induced by temperature) control the vesicular morphology and may lead to transitions resulting in several shape classes. Vesicle morphologies will be discussed in more detail in Sect. 3. At low concentrations lamellar (sheet-like) aggregates are formed in solution. After they grow in size, the energy loss due to surface tension effects will cause the aggregate closure into a

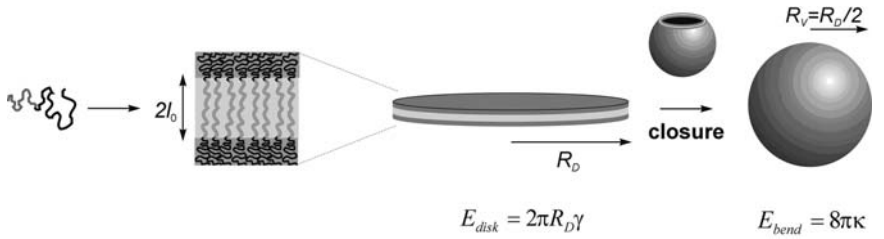

Fig. 1 Schematic illustration of the formation of bilayers and their closure to vesicles. Antonietti M, Foerster S (2003) Adv Mater 15:1323. Copyright Wiley. Reproduced with permission [3]

vesicular form (Fig. 1). Bending of the bilayer to a closed shell requires a bending energy, E_{bend}. For a particular disk area, the disk radius will be twice as large as the vesicle radius, and therefore, the balance of line tension and bending energy defines the minimum aggregate number corresponding to the 'minimal vesicle size'. Thus, the resulting (minimal) vesicle radius will be $R_{\text{V}} = 2k/\gamma$, where k and γ are the bending modulus and surface tension, respectively. Evidently, vesicles will preferentially appear in a system for which the bilayer bending elasticity is low and the surface tension is high.

Beyond the thermodynamic control, the kinetics of chain rearrangement can dramatically influence the phase behavior leading to kinetically trapped structures, which do not necessarily correspond to an absolute free energy minimum of the system. Thus, the formation of block copolymer vesicles, from a kinetic point of view, can be a result of a transition from rod-like aggregates via flat, nonclosed lamellar structures. The kinetics of such transitions has been explored in [8]. The transition steps are represented as follows:

$$\text{rod} \underset{k_{1\text{b}}}{\overset{k_{1\text{f}}}{\rightleftarrows}} \text{lamella} \underset{k_{2\text{b}}}{\overset{k_{2\text{f}}}{\rightleftarrows}} \text{vesicle}$$

where $k_{1\text{f}}$ represents the rate constant of the formation of lamellae from rods and $k_{1\text{b}}$ the reverse rate constant. Analogously, $k_{2\text{f}}$ refers to the rate constant of vesicle formation from lamellae and $k_{2\text{b}}$ to the reverse rate constant. Equations presenting the relation between the rate constant and the concentration of the three morphologies could be applied to calculate the concentrations of the individual species in solution [9]. Experimental investigations on the mechanism of the morphological changes including vesicle formation have been performed for PS_{310}-*b*-PAA_{52} [10]. It has been found that the rod to vesicle transition occurs slower (the time constant is two orders of magnitude longer) than the reverse, even though it takes place at higher water content. Shen and Eisenberg developed a phase diagram for the PS_{310}-*b*-PAA_{52} copolymer in a dioxane/water mixture that showed the region of stability of vesicles [11]. They have shown that a gradual increase in the water content of the solvent mixture transfers the aggregates from a region of spherical micelles to a region where spheres coexist in equilibrium with rods, to a region

where only rods exist, followed by a region of rod and vesicle coexistence, and then finally to a region where all of the aggregates are converted to vesicles. The authors also proved that the morphological transitions are reversible by decreasing and subsequently increasing the dioxane content. A high ratio of water to dioxane in the solvent mixture can kinetically trap the morphology of the aggregates by affecting the mobility of the copolymer chains. In general, copolymers with crystalline and glassy blocks have to overcome a higher energy barrier to achieve self-assembly. The use of mixed solvents (i.e., one component serving as a fluidizer) lowers the T_g of the hydrophobic blocks and provides polymer chains with the necessary mobility to assemble. For example, stability of vesicles was experimentally verified for poly(styrene)-*b*-poly(acrylic acid) (PS-*b*-PAA) in dioxane–tetrahydrofurane (THF)–water or dimethylformamide (DMF)–THF–water mixtures [12,13]. In such systems containing polymers as PS with high glass transition temperatures, vesicles are only obtainable after addition of an organic solvent, which fluidizes the membrane. While when water is added to the system, the aggregates become 'frozen', which, in fact, facilitates their further imaging and characterization.

2 Computer Modeling and Simulations

Despite the large number of experimental papers concerning block copolymer vesicles, some questions related to the equilibrium nature of such morphologies still remain unclear. It is crucial to understand to what extent vesicles would be stable under given conditions as well as to be able to design polymer aggregates of particular properties simply by using a computer modeling. Unlike the extensive theoretical studies dedicated to lipid vesicles, computational analyses of polymer-based vesicular assemblies are far more complex and demand a lot of additional input. Several computer simulations have been available to study the formation of polymer vesicles based mainly on particle models. Anderson and Wilson [14] used atomistic molecular dynamics (AMD) to describe the organization of amphiphilic polynorbornene-*g*-poly(ethylene oxide) graft copolymer at the air/water interface. With the help of this method, they constructed density profiles that could be directly compared to experimental neutron reflectivity data over a wide range of polymer surface concentrations. The simulation gave a reflectivity profile in excellent agreement with experiments at low surface concentrations. In general, computer simulations at atomistic level are necessary to gain insight into detailed interactions such as hydrogen bonding, polymer–solvent interactions, and specific conformational effects (e.g., *cis/trans* isomerization). A few coarse-grain (CG) models have been developed to simulate block copolymer systems on length scales that are far larger than scales accessed using atomistic models [15–18]. CG models represent a group of atoms by a single sphere. In view of this simplification, the full chemical details of the molecules cannot be retained. However, effective interactions among the spheres have been chosen to mimic some key features of the real polymer chain. Recently, the CG MD model was further elaborated and applied

to compute the morphologies and physical properties of PEO–PEE assemblies in water [19–22]. The model replicated the experimentally observed phase behavior of hydrated PEO–PEE diblock copolymers. With hydrophilic-to-hydrophobic block length ratios (f_{EO}) ranging from about 0.3 to 0.7, the diblock copolymers self-assembled in water into either a bilayer ($f_{EO} \sim 0.3$–0.4), a cylindrical micelle ($f_{EO} \sim 0.5$), or a spherical micelle ($f_{EO} \sim 0.5$) [20]. Simulations done on the triblock copolymer PEO–PEE–PEO in water have shown assembly into "tube"-like structures [22]. Formation of such structures has indeed been experimentally observed for PMOXA–PDMS–PMOXA [23]. Srinivas et al. [20] used the CG model to study the effects of block length on different physical properties of the bilayer such as the area elastic modulus, the hydrophobic core thickness and the lateral chain mobility. Scaling of the hydrophobic core thickness agreed with experimental results reported on bilayers in the same block length regime as was accessible to simulation [24].

Dissipative particle dynamics (DPD) is similar to the MD models, but here dissipative and random forces acting between particles are considered in addition to the usual conservative interactions [25]. By using DPD simulations, starting from both a randomly dispersed system and a bilayer structure of the amphiphile, Yamamoto et al. [17, 26] observed a spontaneous vesicle formation. The groups of Ortiz and Lipowsky [27] combined DPD with a new CG model for investigations on PEO–PEE. DPD allowed the system size to increase sufficiently to simulate entire vesicles while still maintaining the diblock molecular weight within the experimental range. In order to obtain a physically realistic description of the system, the PEO–PEE model required an introduction of a density-based atomistic-to-CG mapping. With these changes, the resulting DPD model for PEO–PEE gave values for the membrane area elastic modulus and the power-law scaling of the hydrophobic core thickness that were again in excellent agreement with the experimental values. Additionally, mechanisms of vesicle content release via vesicle rupture induced by osmotic swelling were explored with this model.

In general, the vesicle formation observed in these simulations is based on the following process. The amphiphilic block copolymers aggregate rapidly from the homogeneous initial state into small spherical micelles; then the spherical micelles grow to larger micelles by collision (cylindrical micelles, open disk-like micelles); the large disk-like micelles finally close up and form vesicles; the micelle growth process and the closure process are slower than the first spherical micelle formation process. This mechanism is also supported by Monte Carlo simulations [28] and experiments with lipid systems [29, 30]. Recently, He and Schmid [31] studied the dynamics of vesicle formation in an initially homogeneous dilute solution of amphiphilic diblock copolymers, using the external potential dynamics (EPD) [32] method. They suggested a new pathway of spontaneous vesicle formation which differs from the conventional one (mentioned above). In summary, the mechanism includes the following steps: copolymers from the solution slowly aggregate to micelles; the latter grow and become semivesicles (bigger spherical micelles with a solvent-retaining core), finally, solvent particles diffuse into the semivesicles, and

they become full vesicles. The authors also discussed different contributing mechanisms and proposed a simple method to control vesicle formation.

Simulations for amphiphilic diblock copolymer solutions have also been lately performed with density functional theory model (DFT) [33–35]. By solving the time evolution equations for concentrations T. Uneyama [33] showed that a polymer vesicle is spontaneously formed from the homogeneous state. Moreover, the vesicle formation mechanism obtained by this simulation agreed with the results of other simulations based on the particle models as well as experiments. The author demonstrated that changing parameters such as the volume fraction or the Flory-Huggins interaction parameter could result in formation of spherical micelles, cylindrical micelles, or bilayer structures. It is believed that with the constant progress in computer technologies, computer modeling will become a standard tool for designing polymer aggregates of particular properties.

3 Vesicle Morphology

Besides the thermodynamic and kinetic regulations (mentioned above) determining the final structure of the block copolymer assemblies, it has been suggested that the aggregation of block copolymers depends on the chain stretching in the core [36, 37], the interfacial energy, and repulsion among corona chains [10, 37, 38]. Additionally, the size and shape of the morphologies can be controlled experimentally through variations in the copolymer composition (i.e., block lengths) [39]), the initial copolymer concentration, the nature and composition of the solvent mixture (including water content) [40], the temperature, the presence of additives (e.g., ions [41], homopolymers [42], surfactants [43,44]), and the polydispersity. The influence of these factors in PS-*b*-PAA and PS-*b*-PEO systems has been described mainly by Eisenberg's group [45], but input came also from other groups [24,42,46,47]. Therefore, we will only briefly comment on these factors and direct the reader to recent publications in the field.

The effect of polydispersity of block copolymers on the aggregation behavior is less elaborated. Polydispersity index (PDI) is defined as the ratio of weight average molecular weight (M_w) to the number average molecular weight, (M_n) and is a measure of the width of the molecular weight distribution. Investigations conducted with PS-*b*-PAA system showed a decrease of the vesicle size with increase of the polydispersity index of the PAA block [48]. Most likely, segregation of the smaller hydrophilic chains to the inside of the vesicle bilayer takes place, whereas the longer chains would form the outer surface. It is suggested that, under the same conditions, individual monodisperse copolymers yield different vesicular morphologies than their polydisperse mixtures. However, detailed studies are needed to investigate the effect of polydispersity on the aggregation behavior, especially in order to take advantage of the new and complex polymer architectures. Yang and coworkers investigated theoretically the aggregation behavior of polydisperse diblock copolymers in dilute solution using a 2D real-space self-consistent field

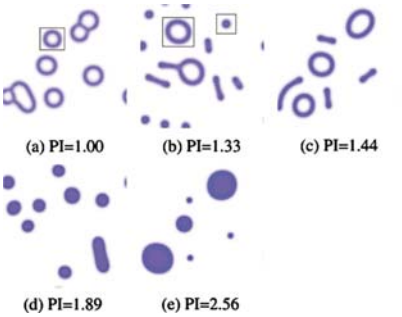

blends	copolymer 1 (%)	copolymer 2 (%)	PI of block A
1	A_3B_{24}(50)	A_3B_{24}(50)	1.00
2	A_2B_{24} (75)	A_6B_{24}(25)	1.33
3	A_1B_{24} (50)	A_5B_{24} (50)	1.44
4	A_1B_{24} (67)	A_7B_{24} (33)	1.89
5	A_1B_{24} (78)	$A_{10}B_{24}$ (22)	2.56

Fig. 2 Aggeragate morphologies in dilute solution of amphiphilic diblock copolymer blends as prepared in the table with an increase of PI of hydrophilic block A. Reprinted with permission from [49]. Copyright (2006) American Chemical Society

theory (SCFT) [49]. For simplicity, the polydispersity was artificially acquired by mixing binary amphiphilic diblock copolymers where the hydrophilic or hydrophobic blocks were composed of two different lengths while the other block length was kept constant. In both cases (i.e., polydisperse hydrophilic block or polydisperse hydrophobic block) the increase in PI led to a variety of morphology changes from vesicles to mixture of vesicles and micelles and finally to micelles (Fig. 2). Based on the obtained results the authors proposed that the long blocks would rather segregate to the outside while short ones to the inside surface of the vesicle. Such length segregation existing in polydisperse block copolymers would lead to decrease of the size of aggregates, in agreement with experimental and theoretical results.

So far, detailed studies about the influence of the size of polymer blocks on the aggregation processes have been performed for PS-*b*-PAA [39], PB-*b*-PEO [47], PEO-*b*-PCL [50], and PEO-*b*-poly(γ-methyl-ε-caprolactone) systems [51].

The block copolymer molecular mass (related strongly to the block lengths) determines the thickness of the vesicular membranes was experimentally proved for a series of PEO-*b*-PBD polymers [24]. Microscopy images evidenced an increase in the wall thickness upon increasing the polymer molecular mass in the range from 3,600 to 20,000 g mol^{-1}.

The chemical composition and architecture of the polymer also play important roles in the self-assembling process. Most of the polymers producing vesicular morphology consist of linear block copolymer chains, but amphiphilic macrocyclic systems containing cyclodextrines [52], cryptands [53], calixarenes [54], etc. as well as dendritic polymers [55–57] are also known to form vesicles. Interestingly, M. Maskos reported that even the end groups of a polymer chain have a certain influence on the aggregate morphology [58]. He observed important differences in the phase diagram of $PB_xPEO_y - COOK$ containing a PEO-sided carboxyl end group and $PB_xPEO_y - H$ having a PEO-sided hydroxyl end group. Generally, the resulting morphology of the nanoparticles in water was 'quasi-shifted' towards a higher ratio of PB for the $PB_xPEO_y - COOK$ as compared to $PB_xPEO_y - H$ and the characteristic dimensions Dc (diameter of a sphere, cross-section of a cylinder or bilayer) were

slightly larger for the carboxyl-terminated diblock copolymers. Both observations indicated a slightly increased stretching of the PEO corona chains as compared to the hydroxyl-terminated block copolymers, which could be explained by a repulsion of the carboxyl end groups and the PEO at the experimental pH = 7. In addition, no pronounced effect of the PEO-sided end group was found in methanol in this part of the phase diagram, most likely due to more favored interaction of PEO and methanol as compared to water.

In a number of publications it has been shown that the solution conditions (i.e., polymer concentration, water content in the solvent mixture, nature of the common solvent, pH) have a critical impact on the vesicular morphology, as well as vesicle size. Eisenberg and coworkers observed that in PS_{410}-*b*-PAA_{25} system vesicles are preferentially formed at higher polymer concentrations as compared to concentrations at which micelles and rods are present [59]. The phase diagrams for polymer solutions of various PS-*b*-PAA polymers revealed the same tendency [11, 39]. The most common experimental method for vesicle preparation is first dissolution of the polymer in a good solvent, common for all constituting blocks, followed by addition of water, which acts as a precipitating solvent for the hydrophobic blocks (see Sect. 6). The formation of the first colloidal particles (micelles) occurs at a critical water concentration (CWC), the value of which is an individual property of the studied system. With increases in the water content, changes in the morphology of the aggregates can be observed, typically from micelles to rods and further to vesicles. On the other hand, the polarity of the common solvent in the polymer solution influences the repulsion between the hydrophilic blocks thus controlling the coiling of all blocks comprising the polymer chain. Consequently, depending on the solvent nature aggregates of various shapes and sizes may be observed. In the case of ionic hydrophilic blocks a morphology control owing to the solvent dielectric constant can be expected. In general, the existence of various morphologies in different solvents could be explained by applying the χ parameter which is in turn related to solubility parameter (δ) and the dielectric constant (ε), and describes the strength of the polymer–solvent interaction [37]. The solvent influence on the aggregation process was also investigated for PS-*b*-P4VPMeI (poly(4-vinylpyridinum methyl iodide)) and PS-*b*-PEO amphiphilic block copolymer systems [60, 61]. Furthermore, these studies demonstrated that a precise alteration of the shapes and sizes of colloidal aggregates is possible by controlling the interactions in the hydrophilic part of the vesicle membrane.

Different types of forces like electrostatic interactions [62, 63], hydrogen bonding [64–67], or donor–acceptor interactions (e.g., metal–ligand coordination bond) [68, 69] have been found to facilitate vesicle formation. For instance, the phase behavior of a system consisting of two oppositely charged block ionomers is strongly affected by the additional energy contributions from electrostatic interactions. Thus, just by mixing different diblock polymers, complex superstructures with adjustable properties for special applications can be produced [70]. Recently, Gao and coworkers [71] demonstrated a controlled vesicle formation in a poly(ethylene oxide)-*block*-polybutadiene (PEO-*b*-PB)/poly(acrylic acid) (PAA) solution based on the interpolymer hydrogen-bonding complexation between PAA and PEO. The

authors proved that the change in the vesicular morphology from unilamellar vesicles (ULVs) to multivesicular vesicles (MVVs) is dependent on the PAA content.

It has been shown that the addition of small (micro and millimolar) amounts of acids, bases or inorganic salts to the polymer solutions could also induce drastic changes in the aggregate morphology [72, 73]. This is especially valid for systems where the hydrophilic block is ionic (e.g., PS-*b*-PAA) [41]. Obviously, due to the simplicity in experimental preparations and low costs such additives are advantageous over other factors (i.e., block length ratio, solvent composition) inducing various polymer morphologies.

It should be mentioned here that the actual vesicle size is usually affected by the preparation procedures. Consequently, this allows for tailoring of vesicle size by experimental conditions and preparation methods, as will be further discussed.

Block copolymer systems can form vesicles of a wide range of sizes; varying from a few nanometers to a few micrometers. Those in the range of 100–1,000 nm have been explored extensively. Various types of vesicle morphologies are represented in Fig. 3.

Shapes of vesicular aggregates range from tubular to spherical, from more exotic large compound (LCV) and starfish vesicles to "simpler" extended lamellae. Both unilamellar [75] and multilamellar ('onions') [47, 76] vesicles have been observed. One of the possible morphologies formed in solution are tubular vesicles, also known as tubes (rods) [77, 78]. Soft, water-filled polymer tubes of nanometer-range diameters and several tens of millimeters in length have been prepared via self-assembly of amphiphilic ABA triblock copolymer in aqueous media (Fig. 4). The tubes were mechanically and chemically stable and could be loaded with water-soluble substances [23].

Haluska et al. observed a spontaneous formation of large pores in the membrane of PB-*b*-PEO polymers [79]. The high-genus morphology was persistent with time and could be explained in terms of bending elastic energy. Recently, such unusual perforated block copolymer vesicles with highly folded membranes have also been detected by Chen et al. [80]. By using electron microscopy analyses (TEM and SEM) together with transmission electron microtomography (TEMT), the authors

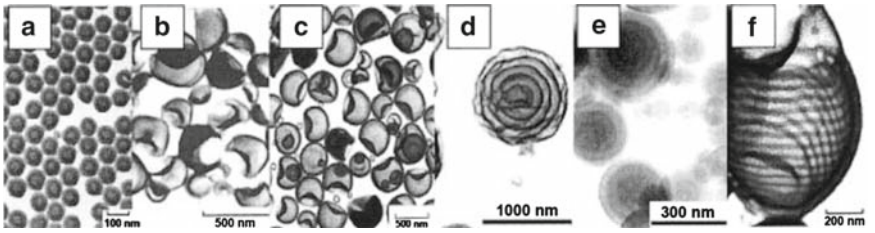

Fig. 3 a–f Representative micrographs of various types of vesicles. **a** Small uniform vesicles (PS_{410}-*b*-PAA_{13}). **b** Large polydisperse vesicles (PS_{100}-*b*-PEO_{30}). **c** Entrapped vesicles (PS_{200}-*b*-PAA_{20}). **d** Hollow concentric vesicles (PS_{132}-*b*-PAA_{20}). **e** Onions (PS_{260}-*b*-$P4VPDecI_{70}$). **f** Vesicles with tubes in the wall (PS_{100}-*b*-PEO_{30}). Burke S, Shen H, Eisenberg A (2001) Macromol Symp 175:273. Copyright Wiley. Reproduced with permission [74]

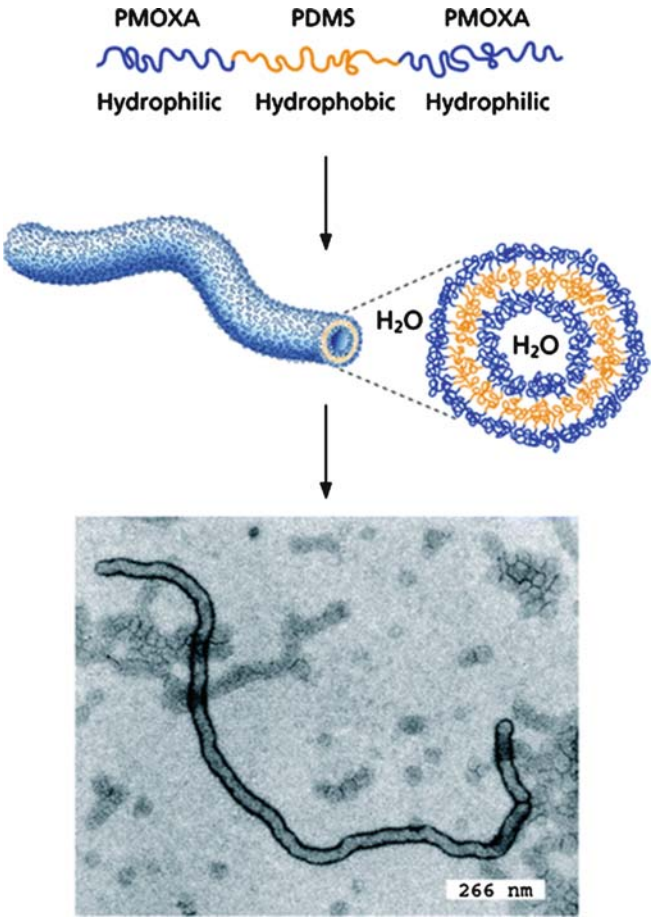

Fig. 4 Self-assembly of ABA triblock copolymers in aqueous solution; a TEM image of a polymer nanotube; *scale bar*: 266 nm [23]. Reproduced with permission of The Royal Society of Chemistry

revealed that poly-(ethylene oxide)-*block*-poly(3-(trimethoxysilyl)propyl methacrylate) (PEO_{45}-*b*-$PTMSPMA_{180}$) forms in solution perforated vesicles with holes on vesicle surface which are interconnected inside (Fig. 5).

4 Chemical Composition and Architecture of Vesicle-Forming Block Copolymers

As mentioned above, the chemical composition, functionality and supramolecular architecture are the key factors affecting the self-assembled structures. In order to aggregate into vesicular objects block copolymers need to have at least two

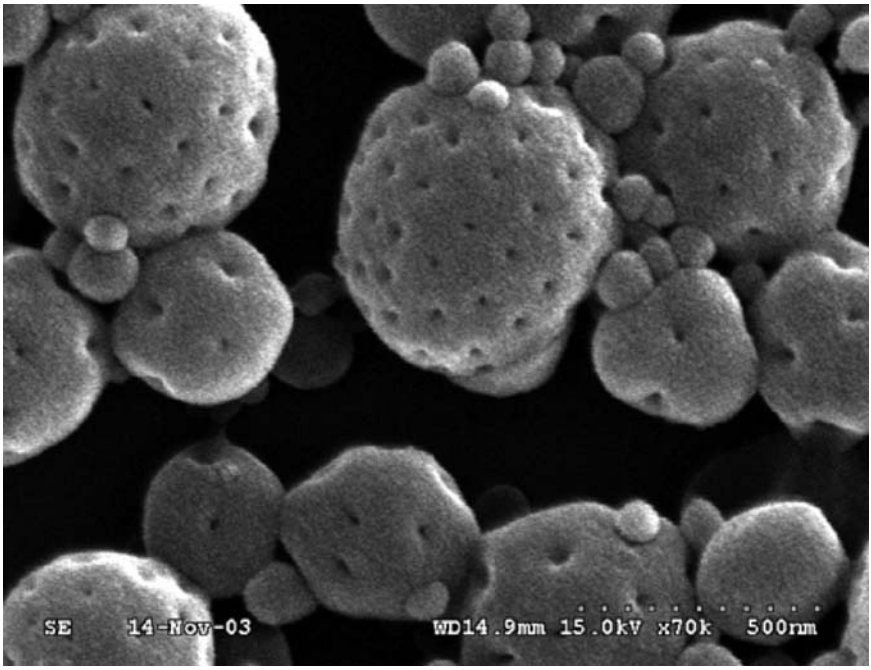

Fig. 5 SEM image of PEO45-*b*-PTMSPMA180 vesicles in a mixture of methanol and water. Reprinted with permission from [80]. Copyright (2007) American Chemical Society

incompatible blocks that have a different solubility in the liquid where vesicle formation takes place. Moreover, the volume ratio of the different blocks has to permit arrangement of block copolymers in a membrane-like structure. Common methods and polymerization techniques applied to synthesize desired polymer architectures are described in detail in specialized reviews [81,82]. Within the last few years the number of amphiphilic polymers reported to form vesicular aggregates has increased significantly. Table 1 summarizes examples of polymers that self-assemble into vesicles in aqueous media. Besides the conventional AB linear type systems, more complex structures such as ABA [83], ABC [84], ABCA [85,86], and ABABA [87] were shown to form vesicles in aqueous media. Copolymer asymmetry can be used to direct thermodynamically driven assemblies in polymeric vesicles as was demonstrated with ABC triblocks [84] or with ABCA tetrablocks [85, 86]. Additionally, dendridic type [88], grafted polymers [89], and macrocyclic type polymers [52] have also been reported to form vesicular morphologies. Vesicles formed from biohybrid polymers are commented in detail in a distinct chapter by Schlaad et al. and therefore discussion is omitted here.

A variety of block copolymer systems are able to form vesicles in nonaqueous solutions (organic solvents) [62, 90–100]. However, such systems are not regarded as biomimetic systems and further discussion concerning them is left out.

The chemistry of the hydrophilic blocks will dictate the properties of the vesicles in water such as adhesiveness and ability to resist protein adsorption, which is a key

Table 1 Synthetic block copolymers containing hydrophobic and hydrophilic segments reported to form vesicular structures in water

Linear AB, ABA or ABC block copolymers		
Hydrophobic block (B)	Hydrophilic block (A) and (C)	Architecture and solvent conditions
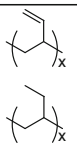		AB and ABA water [5]
	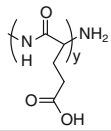	AB water/NaOH [102, 103]
	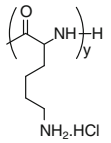	AB water/NaCl/NaOH [104]
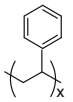		AB dioxane or DMF/water [105]
	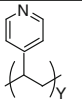	AB, ABA dioxane /water [106]
		AB DMF/water [61]
	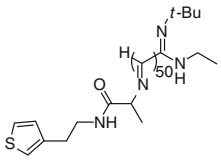	AB (rod-coil) THF/water [107]
	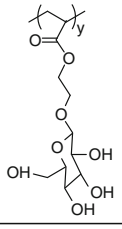	AB DMF or THF or Dioxane/water [108]
	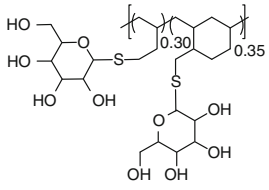	AB THF/water [109]

(continued)

Table 1 continued

Linear AB, ABA or ABC block copolymers		
Hydrophobic block (B)	Hydrophilic block (A) and (C)	Architecture and solvent conditions
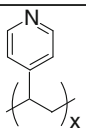	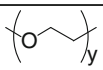	AB chloroform/water [110]
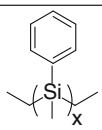	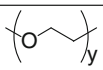	BABAB THF/water [87]
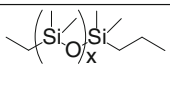	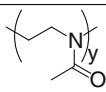 (A)  (C)	ABA ethanol/water [83] ABC ethanol/water [84] CBC THF/water [111]
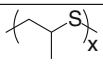	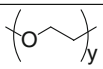	AB and ABA Water [112]
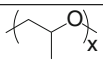	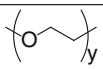	ABA water [75, 113]
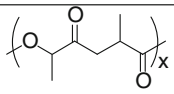	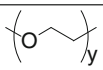	AB water [114]
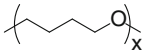		AB, ABA Water [47, 115]
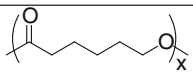	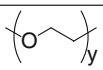	AB water [114]
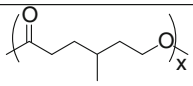	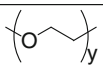	AB water [51]
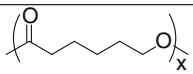	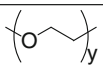 (A) 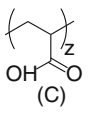 (C)	ABC MOPS buffer [116]

(continued)

Table 1 continued

Linear AB, ABA or ABC block copolymers		
Hydrophobic block (B)	Hydrophilic block (A) and (C)	Architecture and solvent conditions
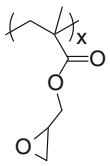	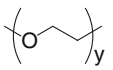	AB THF/water [117]
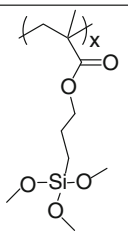	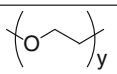	AB methanol/water [80, 118]
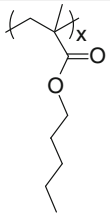	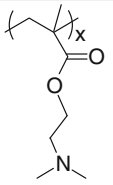	ABA water [119]
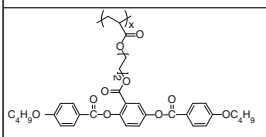	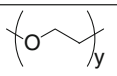	AB dioxane/water [120]
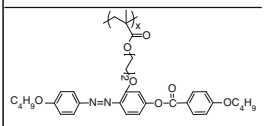		
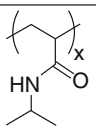	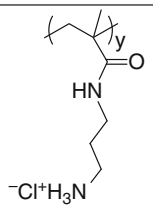	AB water [121]

(continued)

Table 1 continued

Linear AB, ABA or ABC block copolymers		
Hydrophobic block (B)	Hydrophilic block (A) and (C)	Architecture and solvent conditions
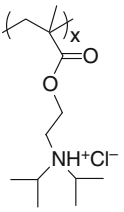	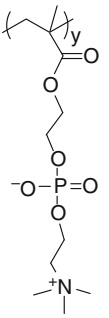	AB water [122]
Dendritic (comb-like) AB block copolymer		
Hydrophobic block (B)	Hydrophilic block (A)	Architecture and solvent conditions
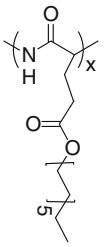	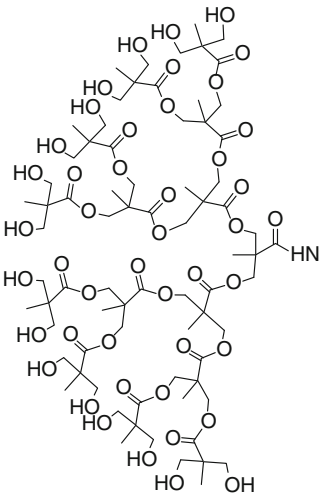	AB THF/water [88 , 123]
Graft copolymer		
Hydrophobic block (B)	Hydrophilic block (A)	Architecture and solvent conditions
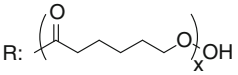 branches	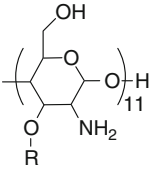 main chain	AB dioxane/water [89]

(continued)

Table 1 continued

Linear AB, ABA or ABC block copolymers		
Hydrophobic block (B)	Hydrophilic block (A) and (C)	Architecture and solvent conditions
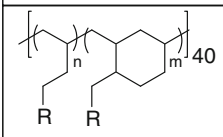	R (hydrophilic moieties) 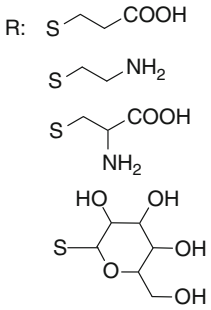	Water [124]

property for "stealth" drug delivery systems. As mentioned previously, amorphous and rubbery hydrophobic blocks will confer to the membranes the liquid-like character typical for lipid bilayers. Moreover, the apolar region of the membrane will dictate the permeability to solutes and water. Lipid membranes have characteristic permeabilities to different solutes and the presence or absence of unsaturation in the hydrocarbon chains or of cholesterol in the bilayer can contribute to small changes in permeability. In copolymers the presence of heteroatoms in the hydrophobic block such as oxygen (in polyesters and polyethers, e.g., PPO, PBO), silicon (in silicones) or sulfur (in poly(propylene sulfide)) can produce similar effects. In hydrocarbon block copolymer vesicles permeability dramatically drops when compared with lipid membranes due to the increased membrane thickness, but the presence of heteroatoms could introduce selectivity for certain molecules, such as glucose [101].

To explore vesicle applications polymersomes with improved resistance to rupture are needed. Stabilization of the vesicle structure has been achieved by cross-linking of the polymer shell. Some examples include the fixation of the vesicles through photopolymerization of unsaturated carbon–carbon double bonds in poly(ethylene oxide)-*b*-poly(butadiene) without [125,126] or in presence of a water-soluble initiator [127]; by using methacrylic ends of a telechelic triblock copolymer [83], or by using the thiophene rings of a coil–rod block copolymer [107]. The "click chemistry" method has been applied to cross-link block copolymers functionalized with alkynyl end groups forming the corona of the vesicles [128]. Other approaches suggested the use of cross-linking agents (additives) such as interpenetrating polymer networks (IPN) for stabilizing Pluronic L121 ($PEO_5 - PPO_{68} - PEO_5$) vesicles [129], primary alkyl diamines which reacted with the epoxy groups of poly-(ethylene oxide)-*b*-poly(glycidyl methacrylate) (PEO-*b*-PGMA) and cross-linked the vesicle walls [117], or poly(sodium-2-acrylamido-2-methylpropanesulfonate) (PAMPS) inducing the formation of ionically cross-linked vesicles due to interpolyelectrolyte complexation with an oppositely charged block [121], etc.

5 Membrane Properties

Membrane properties of polymer vesicles reflect the chemical composition, the block length ratio and the molecular weight of the block copolymers from which they are formed.

5.1 Polymer Membrane Thickness

It was found that the membrane thickness increases with increasing copolymer molecular weight (M_n) (Fig. 6). This dependence has been demonstrated via imaging of a series of PEE–PEO and PBD–PEO vesicles by Cryo-TEM [24]. Based on this data, an experimental scaling factor $a \approx 0.5$ was determined by fitting the membrane thickness (d) vs the hydrophobic molecular weight (M_h) : $d \sim (M_h)^a$. In general, block copolymers are expected to be in the strong segregation limit (SSL). In such a configuration, the classical strong segregation theory would predict $a \approx 0.67$. This scaling factor has been determined by Battaglia and Ryan for vesicles of butylene oxide and ethylene oxide block copolymers [115].

Besides the membrane thickness, the copolymer molecular weight affects also the lateral mobility of polymer chains within the membrane. Using fluorescence recovery after photobleaching (FRAP), Lee et al. [131] discovered that entanglements are responsible for the reduced mobility of copolymers with sufficiently high MW.

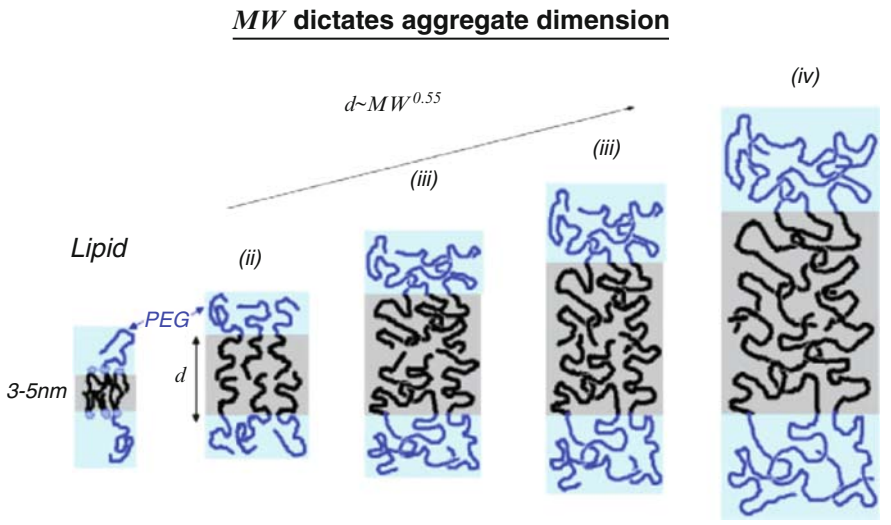

Fig. 6 Schematic scaling of polymersome membrane thickness with copolymer molecular weight. Ahmed F, Photos PJ, Discher DE (2006) Drug Dev Res 67:4. Copyright Wiley. Reproduced with permission [130]

In polymersomes with thicker membranes the limited mobility of high MW polymer chains is the reason for the better resistance to dissolution. Thus, while liposomes would normally be destroyed when exposed to SDS (sodium dodecyl sulfate) or other strong detergents, polymer vesicles would be more resistant to detergents since this process is obstructed by the restricted chain mobility. Combination of experimental data and theoretical modeling suggests that polymer vesicle dissolution is mediated by the diffusion of detergent molecules across the membrane [132].

5.2 Mechanical Properties of Polymer Vesicles

The membrane elastic behavior of PEO–PEE "giant" polymersomes has been studied by a micropipette aspiration method [5]. The results showed that the polymer membrane elasticity is comparable to fluid-state lipid membranes; however the vesicles could sustain a greater strain before rupture, proving an enhanced polymersome toughness, which originates from membrane thickness.

Measurements of lateral diffusivity [131] as well as apparent membrane viscosity [133, 134] have shown that membrane fluidity generally decreases with increasing MW (Fig. 7), as the most drastic decrease is detected when the chains are sufficiently long to entangle.

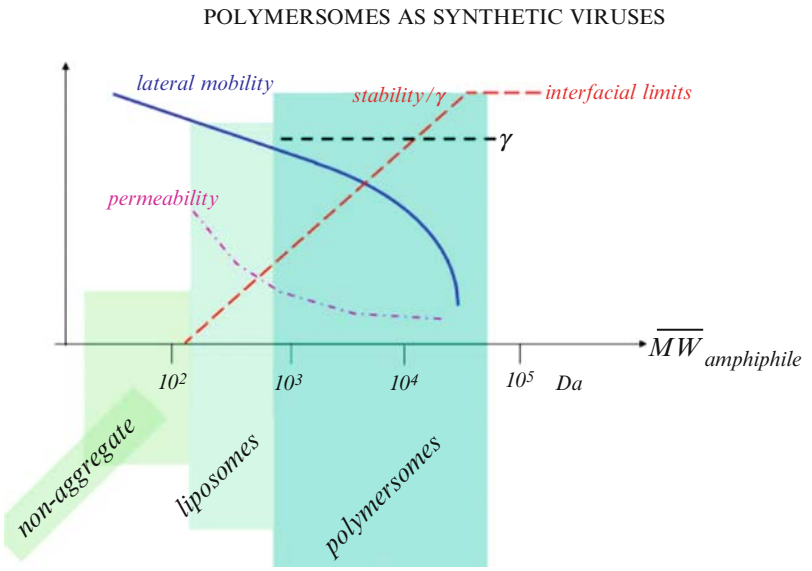

Fig. 7 Schematic plot of typical physical properties with the molecular weight of a vesicle's amphiphile. Ahmed F, Photos PJ, Discher DE (2006) Drug Dev Res 67:4. Copyright Wiley. Reproduced with permission [130]

Bermudez et al. [135] studied the effect of the membrane thickness d (and thus indirectly the molecular mass MW) of PEO–PEE vesicles on the membrane bending rigidity (Kc). The scaling between Kc and d was nearly quadratic, in agreement with the established theories for lipid bilayers, hence providing a way to alter the vesicle properties by choosing the polymer blocks.

The resistance of polymeric membranes to electromechanical stimuli has been investigated by Aranda-Espinoza et al. [136] who used for their studies the micropipette aspiration method in combination with electroporation. It appeared that the electromechanical stability also increases with membrane thickness as the robustness of the vesicle membranes can be orders of magnitude larger than that of phospholipid membranes [134]. Applying the 'black lipid membrane' technique, the membrane robustness of free standing ABA triblock copolymer films has been tested [137]. The measured rupture potential revealed a high membrane stability, which could even be enhanced by cross-linking of the terminal methacrylate groups within the membrane. Higher toughness and durability properties have been found for covalently cross-linked polymersomes in contrast to noncross-linked ones, which exhibit a fluid-like character [126].

One of the most important properties of amphiphilic membranes is their selective permeability to hydrophobic and hydrophilic molecules. Therefore, measurements assessing the permeability of specific molecules are of high significance to fully characterize the amphiphilic membranes. Moreover, understanding the transport of various species through the walls will facilitate vesicle exploitation. In general, it has been assumed that due to their increased membrane thickness and conformational freedom of the polymer chains, vesicles are far less permeable to water compared to liposomes. This assumption was supported by studies on the water permeability of PEE_{37}-*b*-PEO_{40} vesicles, which revealed the permeability coefficient ($P_f \sim 2.5 \pm 1.2\,\mu m\ s^{-1}$) to be at least 10 times less than that measured for phospholipid vesicles ($P_f \sim 25$–$100\,\mu m\ s^{-1}$) [5]. Further investigations showed that triblock $PMOXA_{15}$-*b*-$PDMS_{110}$-*b*-$PMOXA_{15}$ membranes have a water permeability about two orders of magnitude lower than for phospholipids vesicles [138]. However, a large enhancement in water permeability of up to 800 times that of pure polymer was achieved when a water-channel membrane protein Aquaporin Z was incorporated to the synthetic membranes.

Nuclear magnetic resonance echo experiments with pulsed field gradients (PFG–NMR) have proven to be a powerful approach to analyze the molecular exchange through vesicle membranes [139]. Leson et al. applied this technique to study the molecular exchange of water molecules through membranes of dispersed vesicles prepared from block copolymers with different hydrophobic sections (poly-2-vinylpyridine, polyisoprene, polybutadiene and polylactid) and PEO hydrophilic section [140]. A characteristic parameter of the exchange process is the activation energy for the membrane permeation. In the given case, it characterizes the energy barrier which an individual water molecule has to overcome when it penetrates through the hydrophobic region of the vesicle membrane. Calculations based on these parameters revealed a variation of the water permeability for the different

vesicle types. The authors attributed this to different membrane thickness and to different polarities of the hydrophobic sections; e.g., poly(2-vinylpyridine) in P2VP–PEO is more polar than poly(isoprene) in PI–PEO, which explains the higher permeability of P2VP–PEO membranes. It has also been noticed that the differences in permeability tended to decrease with increasing temperature.

A simple method to measure the membrane permeability to specific molecules has been presented by G. Battaglia and coworkers [141]. The authors encapsulated highly hydrophilic $3,3',3''$-phosphinidynetris-benzenesulfonic acid (PH) into poly(ethylene oxide)-*co*-poly(butylene oxide) (EB) vesicles and monitored its reaction with $5,5'$-dithiobis-2-nitrobenzoic acid (DTNB) penetrating the membrane from the exterior. The reaction rate (amount of the formed product as a function of time after DTNB addition) measured with UV/Vis was directly correlated to the permeability of the permeating molecule. A comparison of these results with the permeability of egg yolk phosphatidylcholine (PC) vesicles showed that EB membranes have a more selective permeability toward polar molecules than the phospholipids membranes. Also in this case the permeability appeared to depend on the membrane thickness as predicted by Fick's first law.

Interestingly, it has been found that the permeability of the vesicle membrane can be affected by small organic molecules, which change the thickness and the polarity profile of the bilayers. For example, ethanol influenced significantly the permeation characteristics of poly(isoprene-*b*-ethylene oxide) bilayer membranes [142]. Recently, Yan et al. used freeze-fracture transmission electron microscopy (FF–TEM) and pulsed-field gradient nuclear magnetic resonance (PFG–NMR) spectroscopy to investigate the effect of glycerol on the permeability of vesicle membranes of poly(ethyleneoxide)-*b*-poly(dimethylsiloxane)-poly(ethyleneoxide) $((\mathrm{PEO})_{15}-(\mathrm{PDMS})_{15}-(\mathrm{PEO})_{15})$ in water/glycerol mixed solvents [143]. In general, the results showed that the permeability of the vesicle membrane increases with increasing glycerol concentration in the solvent. Gradual substitution of water with glycerol led to significant structural transformations: small vesicles gradually swelled, and at glycerol content of 60% a complete disintegration of the vesicles into membrane fragments was observed. The authors assumed that the glycerol molecules lead to an increase of the polarity as well as of the flexibility of the hydrophobic block. This effect of small molecules on intermediate polarity might be of general importance for controlling the permeability of vesicle membranes.

The membrane permeability is affected also by the glass transition temperature of the hydrophobic block of polymer vesicles. For instance, the group of A. Eisenberg loaded a drug, doxorubicin, into a vesicular system based on poly(styrene-*b*-acrylic acid) (PS-*b*-PAA) and found that due to the much higher glass transition temperature (T_g) of PS than that of lipids, the rate of drug diffusion through the polymer membrane was slow [144]. The authors tuned the permeability of PS membrane by adding different amounts of dioxane to the external solutions of the vesicles, which plasticized the glassy vesicle membranes. It was shown that by varying the degree of plasticization of the vesicle wall, the extent of loading and release can be controlled independently. The same group investigated the proton diffusion across

the membranes of PS-*b*-PAA vesicles [145]. A pH gradient was created across the vesicle membrane with a pH inside (pH_{in}) of ca. 2.9 and a pH outside (pH_{out}) of ca. 8.5. The permeability of the PS wall was tuned by adding different amounts of dioxane (0–40 wt%) to the external solution. The diffusion coefficients of protons increased with increasing the dioxane content most likely due to plasticization of the PS membrane by dioxane.

5.3 Adhesion of Polymer Vesicles

The understanding of the adhesion behavior of polymersomes to biologically relevant surfaces such as the cellular membrane is essential for their potential applications (i.e., targeted drug delivery). To investigate the polymersome response to adhesion, amphiphilic copolymers have been modified with chemical moieties complementary to specific receptors and the adhesion forces driven by these receptor–ligand interactions have been measured. For example, Rigler and Meier quantified the binding of biotinylated nanocontainers to fluorescently labeled streptavidin by fluorescence cross-correlation spectroscopy [146]. Alternatively, the group of Hammer used the micropipette manipulation method to investigate the adhesion of biotin–lysine functionalized PEO–PBD vesicles to avidin-coated beads [147]. The results showed that the length of the biotin-containing diblock, the length of the surrounding nonfunctionalized diblock, and the density of the functionalized polymer all had an effect on the adhesion strength. The strongest adhesion was seen when the functionalized polymer was significantly longer than the surrounding nonfunctionalized polymer. This was likely because longer functionalized polymer has a better access to the opposing surface. The same group tried to better elucidate the mechanism and proposed a model to design functionalized polymersomes with predetermined ligand-induced adhesiveness [148]. In subsequent studies Hammer and coworkers measured the adhesiveness of micron-sized PEO-*b*-PB polymersomes functionalized with antiintercellular adhesion antibodies-1 (anti ICAM-1) that bind to vascular intercellular adhesion molecules-1 (ICAM-1), which could be useful for vascular targeting [149]. Micropipette aspiration was used to confirm a specific adhesion and measure the adhesion strength between an anti ICAM-1-coated polymersome and an ICAM-1-coated polystyrene microsphere at various surface densities of adhesion molecules. The adhesion strength increased linearly with the surface density of anti ICAM-1 molecules, in contrast to the adhesion measured between biotinylated vesicles and avidin-coated beads [147]. The difference in the dependence on functional groups density was likely due to the molecular presentation at the vesicle surface (molecular topology); in the described study, the anti ICAM-1 antibodies were effectively presented and, thus, a monotonic increase in adhesiveness with antibody density was observed.

Recently, Nam and Santore examined adhesive plaque formation dynamics of unilamellar PEG–PDMS copolymer membranes, driven by avidin–biotin binding [150]. With the help of dual micropipette aspiration the authors controlled the

membrane tension and studied the irreversible membrane–membrane contact and the limit of binding sites density. Furthermore, they found that the adhesion and spreading kinetics are dominated by configurational motions of the ligands and receptors, membrane deformation processes, and the underling ligand–receptor binding kinetics. The final calculations based on membrane tension (τ) and contact angle (θ) values indicated that the chemical driving force for adhesion greatly exceeds the mechanical resisting tension.

5.4 Fusion and Fission of Polymer Vesicles

Polymer vesicles have been designed to be tougher than liposomes and their fusion/fission behavior has never been included in the design stage [38]. In general, the contact and fusion of polymer vesicles is restricted due to a strong steric hindrance given by the solvated polymer brushes on the outer wall. Despite this barrier, fusion of polymersomes has been reported to occur at certain chemistry and conditions. For example, Luo and Eisenberg proposed a fusion/fission mechanism for PS–PAA diblocks in different dioxane/water mixtures to explain the appearance of intermediate morphologies where two vesicles closely interact or share a membrane wall [13]. The same group investigated [151] the effect of solvent composition on the fusion rate of vesicles from the same copolymers.

Real-time monitoring of fusion and fission has been reported for polymer vesicles generated from an amphiphilic multiarm copolymer with a hyperbranched poly(3-ethyl-3-oxetanemethanol) core and many oligo(ethylene oxide) arms (HBPO-star-PEO) [152, 153]. Sonication could partly break the hydrogen bonds and give rise to molecular packing defects on the membrane, which triggers the membrane fusion.

Recently, Su and coworkers observed a real-time fusion process of giant vesicles from amphiphilic poly(*N*-isopropylacrylamide)-*block*-poly{6-[4-(4-methylphenyl-azo) phenoxy] hexylacrylate} (PNIPAM-*b*-PAzoM) formed in H_2O/THF mixture [154]. The fusion of the vesicles was induced upon irradiation of light at 365 nm and visualized directly under an optical microscope (Fig. 8). Most likely the fusion derivation was preliminarily due to the perturbation by the photoinduced *trans*-to-*cis* isomerization of azobenzene units in the vesicles.

6 Experimental Methods for Preparation of Vesicles

In general, the methods reported for preparation of liposomes are also applicable to amphiphilic polymers forming vesicular structures. The preparation methods are divided in two main groups: solvent free techniques and solvent displacement techniques (cosolvent methods) comprising the use of organic solvents. In the first group, the amphiphile in its dry state is brought in contact with an aqueous medium and is subsequently hydrated to yield vesicles. This way no organic solvent is

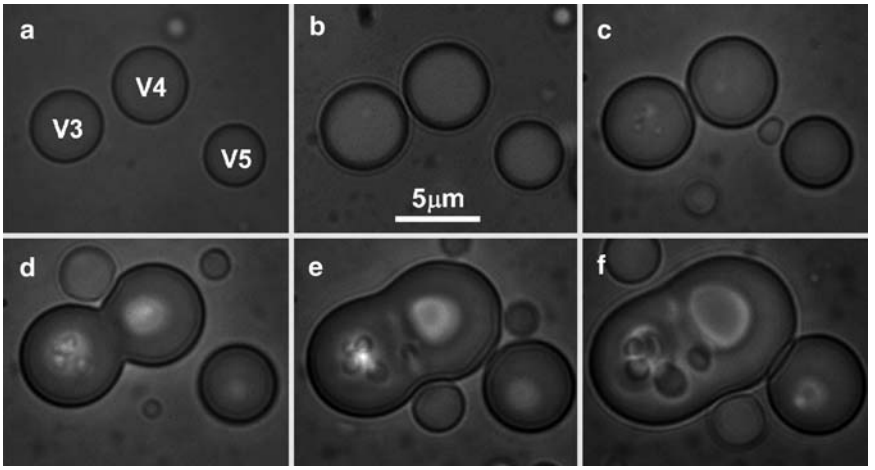

Fig. 8 a–f Fusion process of the PNIPAM-*b*-PAzoM vesicles in a 50 vol. % H_2O/THF mixture induced by irradiation of UV light (365 nm, 0.6 mW). Image **a** is the initial image of three vesicles denoted V3, V4 and V5, respectively, and after irradiation for different time intervals: **b** 16, **c** 33, **d** 42, **e** 58, **f** 80 min. The *scale bars* are the same of 5 mm for all graphs. Su W, Luo Y, Yan Q, Wu S, Han K, Zhang Q, Gu Y, Li Y (2007) Macromol Rapid Commun 28:1251. Copyright Wiley. Reproduced with permission [154]

present any more in the system, which can be mandatory for certain applications. In the second group of preparative methods, the block copolymer is first dissolved in an appropriate organic solvent and then the polymer solution is mixed with water under vigorous stirring. The organic solvent can be removed subsequently with an appropriate technique such as dialysis or freeze-drying. Even though sometimes solvent residues remain which may interfere in biological and galenical applications. Solvent residues further fluidize the membranes leading to decreased vesicle stabilities [155]. It is also possible to prepare vesicles by a so-called detergent method, where the polymer is dispersed in water with the help of a surfactant with high CMC (critical micelle concentration), which is then removed by dialysis or by using appropriate resins [156]. Each method can yield a variety of self-assembled superstructures (micelles, vesicles, tubes). As discussed above, several factors such as length of the individual blocks, polydispersity, additives (ions, homopolymers and surfactants), nature and composition of the solvent, water content as well as temperature provide control over the type of the self-assemblies [45].

Homogeneous in size vesicle dispersions can be achieved through vortexing, freeze–thaw cycles, extrusion and sonication, or a combination of these methods. These steps usually also lead to decrease of vesicle diameter and lamellarity [101, 157].

6.1 Solvent Free Preparation Methods (Film Rehydration, Electroformation)

The film rehydration method includes preparation of a thin copolymer film on a solid surface (e.g., glass, Teflon) in the first step [42, 77, 101, 133, 158]. This is achieved by dissolving the polymer in an appropriate solvent or solvent mixture, which is then evaporated by means of a rotary evaporator, high vacuum pump or nitrogen stream. In the second step, aqueous buffer or pure water is added which leads to swelling of the film. It is proposed that the swelling is caused by water permeation through defects in the polymer layers; this process being driven by hydration forces. Formation of vesicular aggregates by the film rehydration method is reported for amphiphilic copolymers comprising hydrophobes with sufficiently low T_g such as poly(ethyl ethylene) (PEE), poly(dimethyl siloxane) (PDMS), poly(propylene sulfide) (PPS), poly(butylene oxide) (PBO), and poly(propylene oxide) (PPO). As a general rule, the higher the MW of the macroamphiphiles the more difficult is the vesicular formation with this method at room temperature and hydration has to be combined with additional treatments such as freeze-thawing, heating and sonication. When block copolymers have low MWs, spontaneous formation of vesicles can occur in a short time and without any additional energetic input. Commonly, small multilamellar vesicles with a broad size distribution are obtained with the film rehydration method.

The method of solid rehydration (bulk swelling) resembles the film rehydration method; however, the amphiphile is directly hydrated as bulk powder. Therefore, longer or more vigorous agitation to completely hydrate the polymer is required [42, 103, 114].

Electroformation is a suitable technique to achieve homogenous unilamellar giant polymersomes with diameters above one micrometer [133, 157]. This method is similar to the film rehydration method, but, instead of using a solid surface, the polymer film is spread on a pair of electrodes, made of either indium–tin–oxide (ITO) coated glass plates [159, 160], platinum wires [161, 162] or gold wires [163]. After addition of buffer, an electric current is applied to facilitate hydration. The electric field affects the vesicle formation by decreasing membrane tension, by inducing periodic motions (mechanical stress) and by increasing interlayer repulsion through electroviscous/electrostatic effects (mainly in the case of charged amphiphiles).

Battaglia and Ryan [164] studied in detail the mechanism of different pathways for preparation of vesicles from poly(ethylene oxide)-*co*-poly(butylene oxide) with various molecular weights. The vesicle formation was observed both macroscopically (confocal laser scanning microscopy) and microscopically (small-angle X-ray scattering). Both methods have revealed that the amphiphilic block copolymers swell in water following two qualitatively different growth regimes. At first the complex kinetics of hydration were studied and modeled using a generalized random walk approach. Subsequently, the formation of vesicles was monitored in the

presence of an electrical field and compared with the formation by simple hydration. It was found that the final vesicle size is strongly dependent on the concentration gradient.

6.2 Solvent Displacement Techniques

The cosolvent method, also known as solvent injection method permits vesicle formation for glassy or crystalline block copolymers. As a rule, the amphiphilic copolymer is dissolved in an appropriate organic solvent or solvent mixture, the role of which is to lower the T_g below room temperature; next the solution is added dropwise to an aqueous buffer under vigorous stirring. Originally this method has been employed for PS–PAA and PS–PEO copolymers that self-assembled in vesicular structures by adding water to DMF or dioxane polymer solution [61, 105] and then further applied to many other polymer systems [165].

The cosolvent method is known to result in a dispersion of vesicles of a rather broad size distribution. The polydispersity can be reduced by repeated extrusion [83]. A drawback of the method is that organic solvent could remain in the vesicles and the surrounding liquid. To exclude residual solvent, the vesicle suspension is dialyzed or ultrafiltered.

In other reports, solvents immiscible with water were used to form polymeric vesicles. Feijen and coworkers reported on vesicle formation for diblock copolymers of PEO and polyesters or poly(carbonates) with both water-miscible and immiscible solvents [155]. In some cases it is very difficult to remove the organic solvent and experiments with vesicles formed in water-immiscible solvents are limited to some extent.

Interestingly, Förster and coworkers reported the use of inkjet printing technology to produce directly unilamellar polymer vesicles with a narrow size distribution. The average size of the vesicles depended on the initial polymer concentration in the organic (water-miscible) phase and the type of nozzle used [166].

Block copolymers can also assemble into vesicular objects when dispersed in an organic solvent selective for one of the blocks. Such systems that form vesicles in nonaqueous media can be exploited for nonbiological applications and will not be an object of discussion here. Information concerning their nature and self-assembly is available in reference [167].

7 Characterization Methods

In this section we briefly present several techniques commonly used to study vesicles. Owing to space limitations, we rather concentrate on the physicochemical properties that can be learned from those measurements and omit an exhaustive

characterization of each technique. The techniques reviewed here are those generally applied in colloid science and involve light scattering and various microscopies.

7.1 Scattering Methods

Turbidity measurements, practically realized by static and dynamic light scattering experiments, are the main tool to study polymer aggregation in solution. Light scattering has been extensively used to determine vesicle size and size distribution (size polydispersity), vesicle disruption by dilution [83] or detergent exposure [132] changes in the vesicular size with variation of pH [168], vesicular morphology and morphology evolution with thermal treatment [169], as well as the critical aggregation concentration [83]. The average hydrodynamic radius R_h determined by dynamic light scattering (DLS) measurements gives an indication of the size of colloidal objects. Laser light scattering is able to probe aggregates in the size range of 1–1,000 nm [170]. From static light scattering (SLS), structural properties are available such as weight averaged molecular weight (Mw), particle shape and size [83, 171], and particle–particle as well as particle–solvent interactions.

Combinatorial small-angle X-ray scattering (SAXS) and wide-angle X-ray scattering (WAXS) provide information about structural features of colloids. These scattering methods have been used to investigate phase behavior over a concentration gradient of block copolymers in water [172]. The small-angle neutron scattering (SANS) technique is unique for studies of chain conformations and interaction parameters in the one-phase region. It allows investigations of the morphology and thermodynamics of polymer blends and copolymers. Additionally, structure and self-assembly of block copolymers, and control of drug encapsulation by multilamellar vesicles have been studied [173].

7.2 Microscopy

Microscopy allows a direct visualization of polymersomes and many important aspects like size, morphology or homogeneity can instantly be revealed. Therefore, the method is a very powerful tool for polymersome's investigation.

Optical microscopy offers the possibility to visualize directly polymeric vesicles under 'physiological' conditions. It is not necessary to dry or stain specimens; instead, they can be kept in aqueous buffer. The major drawback of light microscopy compared to electron microscopy is the limited resolution, due to which it is mandatory to have polymersomes of large size: giant vesicles with diameters above one micron are best suited for such studies.

In some cases, polymersomes neither absorb light nor seem to get stained with chemical dyes. Therefore, contrast is so poor that the specimen remains essentially invisible and contrast has to be enhanced using other techniques. *Phase contrast*

microscopy is ideal for thin, unstained objects, which barely exhibit any light absorption in the visible part of the spectrum. By means of this technique a direct visualization of polymeric aggregates, providing information on the structural details [42,174] and the kinetics of transition between different aggregate morphologies [8] was possible. In addition, dynamics of morphological transformations can be continuously recorded [77].

Unlike transmission light microscopy, in *fluorescence microscopy* a sufficient contrast is achieved since only the emitted light from the specimen reaches the detector. There are several important advantages of fluorescence over transmission microscopy techniques: (1) specific labeling with fluorochromes gives the ability to distinguish between nonfluorescing materials; (2) multiple staining with different probes allows for visualization of individual target molecules; (3) fluorescence microscopy reveals the presence of fluorescent material with exquisite sensitivity – as few as 50 fluorescent molecules per milliliter are sufficient to be detected. Besides visualization of steady state structures, fluorescence microscopy permits to study dynamic processes of macromolecules such as diffusion, binding constants, enzymatic reaction rates and a variety of reaction mechanisms in time-resolved measurements.

In most cases, the amphiphilic polymers do not exhibit intrinsic fluorescence and therefore a dye needs to be encapsulated, or the vesicle membrane has to be stained. The first method requires encapsulation of a water-soluble fluorescent dye during vesicle formation followed by a subsequent exclusion of the dye from the extracellular space (e.g., by size exclusion chromatography, dialysis, ultrafiltration, or centrifugation). To stain the membrane either a fluorophore is covalently linked in a certain percentage to the membrane forming molecules, or a lipophilic probe is aggregated in the hydrophobic part of the membrane [116, 146, 175, 176].

Total Internal Reflection Fluorescence Microscopy (TIRFM) is another useful tool for studying the reactions of individual molecules adsorbed, adhered or bound to surfaces. Typical applications are membrane fusion of vesicles [177], conformational and orientation changes [178] and lateral mobility of molecules [179].

Confocal microscopy presents further improved possibilities (e.g., exquisite sensitivity) for vesicle investigation. By *Laser Scanning Confocal Microscopy (LSCM)* optical slices of the specimen are imaged with high contrast and high resolution [70, 116, 180, 181]. LSCM offers the ability to adjust magnification electronically simply by varying the area scanned by the laser. Here disadvantages are the limited number of excitation wavelengths available with common lasers (referred to as laser lines). Besides visualization of steady state structures, studies of dynamic processes are possible. Confocal microscopy is therefore an extremely powerful technique for studying vesicles (Fig. 9), however, the relatively high equipment costs limit its application as standard tool.

The most frequently applied technique for determination of the topography of structures on solid substrates are scanning force microscopy (SFM) methods [182], which allow for obtaining precise (with a few Å resolution) images. Presently, the atomic force microscopy (AFM) technique is a basic tool in laboratories for

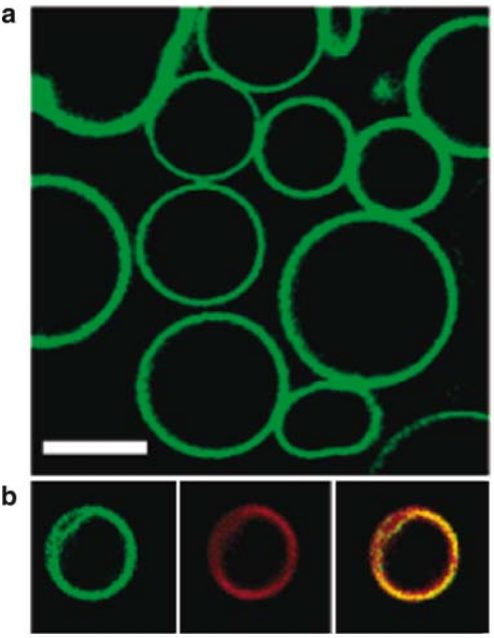

Fig. 9 Confocal LSM images of micron-size TAT-conjugated NIR polymersomes. **a** Fluorescein-Tat functionalized vesicles. **b** FITC-Tat functionalized vesicle surface with near-infrared fluorophores (NIRF) leaded within the membrane. Green = FITC, red = NIRF, yellow = fluorophore colocalization; scale bar = 10 μm. Reprinted with permission from [181]. Copyright (2007) American Chemical Society

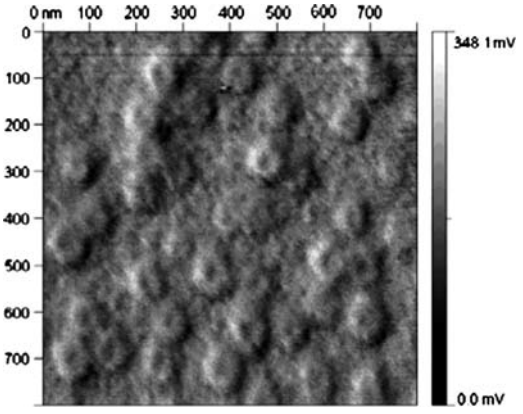

Fig. 10 Tapping mode AFM analysis of $PDMAEMA_4PBMA_{66}PDMAEMA_4$ vesicles on silicon substrate. Reprinted with permission from [119]. Copyright (2007) American Chemical Society

investigating the properties of thin films on solid substrates, but it has also proven useful in studies of shape and size of polymer vesicles (Fig. 10) [183–185].

Transmission Electron Microscopy (TEM) is perhaps the most used visualization method for studying polymer aggregates. Additionally, negative staining permits very high resolution imaging of surface details. *Cryo-TEM* offers another advantage: since specimens are rapidly frozen and viewed in a natural hydrated state

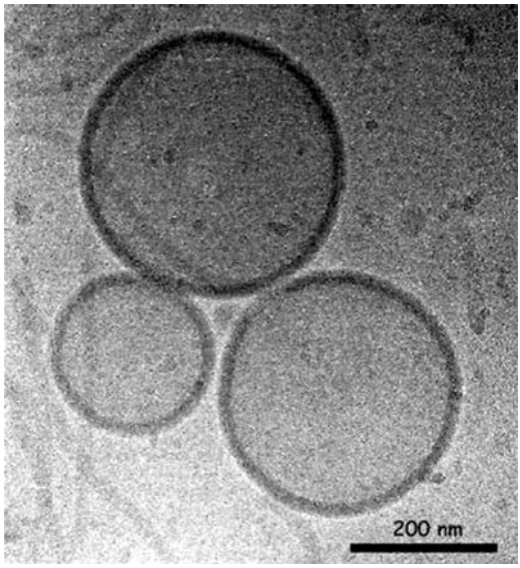

Fig. 11 Cryo-TEM image of PMOXA-*b*-PDMS-*b*-PMOXA vesicles prepared by film swelling in water; *scale bar*: 200 nm. Reprinted from [187] Kita-Tokarczyk K, Grumelard J, Haefele T, Meier W. Block copolymer vesicles-using concepts from polymer chemistry to mimic biomembranes. Polymer 46:3540, Copyright (2005), with permission from Elsevier

(aqueous suspension), a direct visualization of the aggregates is possible without the risk of artifacts that could occur in conventional TEM from drying and/or staining (Fig. 11). A good example to illustrate the power of Cryo-TEM for high-resolution imaging of polymer aggregates was presented by Won et al. The authors visualized vesicular and micellar aggregates in dispersions of PEO−PBD, PEO−PEE and PEO−PEE−PEO copolymers [186]. Furthermore, with the help of cryo-TEM, a spontaneous formation of vesicles and their transition to lamellar structures were observed [46]. A cryogenic scanning electron microscopy has also been used to characterize multilamellar vesicle structures [47].

Freeze-fracture reveals intravesicular details in three dimensions. Samples are frozen rapidly in liquid nitrogen and fractured to reveal internal structure. Additionally, lyotropic behavior of amphiphilic ABA triblock copolymers in water has been investigated using polarized light optical microscopy and freeze-fracture TEM [188].

UV and FTIR spectroscopies have been successfully applied to confirm the cross-linking in vesicles from PI-*b*-PCEMA [189, 190], based on the fact that absorption from CEMA (2-cinnamoylethyl methacrylate) disappears during the UV irradiation of a vesicle solution. *Fluorescence spectroscopy* is normally applied in studies of controlled encapsulation and release from polymersomes as well as for finding the position of particular components in a membrane [13]. The degree of ionization of the corona blocks has been studied in various diblock copolymer systems with ζ potential measurements [72,191]. Such measurements allow for the precise assessment of the influence of inorganic acid/base on the formation and sizes of the resulting vesicles. *Differential scanning calorimetry* (DSC) was used to investigate the self-assembly of PS-*b*-P4VP (4-vinyl pyridine) in the presence of perfluorooctanoic

acid (PFOA) in chloroform solutions [192]. From DSC results conclusions were drawn concerning the thermal changes in the system, namely, transitions between various morphologies and the influence of various additives on the behavior of the system. *Nuclear magnetic resonance techniques* can also be used successfully to determine membrane properties such as permeability, hydration limit (water content along the polymer chains forming the membrane) and diffusion coefficients of the vesicles [193–195].

8 Interactions of Amphiphilic Block Copolymers with Biological Membranes

Recently, scientific interest has been concentrated on interactions between amphiphilic block copolymers and lipid mono- and bilayers [196–200]. Understanding the nature of such interactions will open a route towards multiple applications in fields as biophysics, biomedicine, and biotechnology. Particular areas of scientific interest are, for instance, elucidation of the mechanism of membrane-sealing capabilities of block copolymers penetrating into lipids [198, 201] and how adsorption of amphiphilic block copolymers to liposomes enhances their stability [202, 203]. Furthermore, the interactions between polymers and biomembranes play a central role in the investigation of polymer-induced "flip-flop" within lipid membranes [200, 204, 205], and in the triggered generation of synthetic membrane channels and pores in lipid membranes [196].

In this research field most studies have been performed with poly(ethylene oxide)-*b*-poly(propylene oxide)-*b*-poly(ethylene oxide) triblock polymers (PEO−PPO−PEO) commonly referred to "poloxamers" (ICI) or "pluronics" (BASF) [197, 199, 202]. These noncytotoxic and nonionic polymers are biocompatible and therefore have emerged as potentially important materials in biotechnology and molecular medicine [206, 207]. For instance, the poloxamer known as P188 or F68 ($PEO_{76}-PPO_{29}-PEO_{76}$) has attracted special interest due to its membrane sealing capabilities [201, 208]. The work of several groups targeted at better understanding of the polymer mediated cell membrane sealing mechanism by modelling the outer leaflet of the cell membrane using a Langmuir lipid monolayer spread at the air–water interface [198, 199, 201]. Upon injection of P188 into the subphase of DPPC (dipalmitoylphosphatitylcholine) or DPPG (dipalmitoylphosphatidylglycerol) monolayers, and after attaining appropriate surface pressures, polymer adsorption to the lipid monolayers was observed. As the polymer did not adsorb at higher surface pressures, it was presumed that it will only insert into non-intact membranes. Increasing the surface pressure led to expulsion of the polymer from the lipid layer. This might represent a model for the self-healing process of membranes. As the cells heal and inner membrane lipid packing is regained, the polymer is "squeezed out" and therefore removed entirely [201]. It has been suggested that the hydrophobic PPO domain directs the poloxamer integration into lipid monolayers. Further experiments showed that increasing the absolute size of the PPO subunits

renders the polymer more bulky and therefore prevents insertion, however, once inserted, larger poloxamers are able to remain associated within the film even at much higher lipid packing densities [199]. The experimental observations were supported by Monte Carlo simulations [198]. Besides poloxamers, the interactions of other amphiphilic polymers with lipid monolayers have also been studied [209, 210]. For example, diblock copolymers with polar poly(*tert*-butyl acrylate) (P*t*BA) and nonpolar poly(styrene) (PS) blocks were anticipated to act as polymeric surfactants for the treatment of the dry-eye syndrome [210, 211]. This syndrome arises from instabilities in the tear film. Amphiphilic PtBA–PS-copolymers were designed to interact with the lipids present in the tear film in order to increase its stability. Experimental results indicated that a copolymer bearing a small hydrophilic and a large hydrophobic block is a likely candidate for strengthening the tear film [210].

Apart from Langmuir monolayers also lipid bilayers (i.e., liposomes) served as model systems to elucidate polymer–lipid interactions [197, 202, 203]. Normally, a lack of stability limits the liposome's applications in *vivo* and in vitro. This drawback could be overcome by conjugation of triblock copolymers into liposomes. Two different pathways to achieve steric vesicle stabilization were proposed: the copolymer chains are either directly involved in the vesicle formation process, thus the hydrophobic chains become an integral part of the bilayer, or alternatively, the copolymer is adsorbed onto preformed vesicles [203]. Besides stability, adsorption of polymers on liposomes also affects permeability. It was shown, for example, that there is a direct correlation between the poloxamer adsorption and the leakage rate of encapsulated carboxyfluorescin dye [202]. Evidently, the adsorbed polymers solubilize the lipid membrane and increase the permeability. Additionally, PEO−PPO−PEO copolymers, inserted into lipid vesicles, induce transient pores in the membrane, thus increasing its porosity, which enables controlled release of enclosed components [196]. A transmembrane permeation induced by pluronics was also verified for antitumor drugs like anthracycline [212]. As much as a pore formation and a membrane destabilization in lipid vesicles may sound contradictory to the previously described monolayer healing experiments, it has to be remembered here, that the experimental set-ups for monolayer and vesicle studies have different constraints and the results cannot be always directly compared.

Firestone et al. investigated the relationship between the molecular architecture of a series of poly(ethylene oxide)-*b*-poly(propylene oxide) (PEO−PPO) di- and triblock copolymers and the nature of their interactions with lipid bilayers [213]. The number of repeat units in the hydrophobic PPO block has been found to be a critical determinant for the polymer–lipid bilayer association. Further studies showed that temperature, polymer architecture and concentration also control the mode of interaction of PEO−PPO−PEO copolymers with lipid bilayers. Increasing either the number of repeat units in the PEO block or the polymer concentration promotes a greater degree of structural ordering [197].

It was also observed that nonionic amphiphilic ABA polymers (e.g., PEO−PPO−PEO) [200, 205], polycations (e.g., quaternized poly(4-vinylpyridine) [214] and hydrophobically modified poly(*N*-isopropylacrylamide) [204] are able to accelerate translocation from the inside leaflet to the outside leaflet ("flip-flop") within

lipid bilayer membranes. Driving forces and mechanisms of flip-flop catalyzed by nonionic and cationic polymers are different. The nonionic polymers bind to the biological membrane via incorporation of their hydrophobic blocks into the inner part of the lipid bilayer. On the other hand, external binding of cationic polymers is driven by electrostatic interactions between the positively charged polymer units and the negatively charged lipid headgroups within the outside leaflet. Polymer-induced flip-flop can influence other biologically important events in the biological membranes. It has been found that the flip-flop catalyzed by polymers is closely associated with the ability of polymers to increase the membrane permeability toward biologically active compounds. For instance, when bound to lipsosomes both Pluronics and polycations catalyze a pronounced acceleration of the transmembrane Dox permeation [205, 215–217].

Even though polymer–lipid interactions find already a number of biomedical applications, these systems still lack systematic investigations to achieve a better understanding of the ongoing mechanisms on molecular level. Without a doubt, this research will undergo further progress.

9 Vesicles Reacting to Environmental Stimuli

In contrast to lipids, polymer chemistry allows various chemical modifications to introduce functionality and make polymers responsible to environmental stimuli (pH, temperature, ions, light, etc.). In biosciences, responsiveness to external stimuli is a crucial factor, especially in drug release and construction of biomaterials.

pH varies inside the body and so is a suitable stimulus for in *vivo* applications. Principally, pH-sensitive polymeric vesicles contain polyelectrolyte blocks, i.e., weak acids (e.g., carboxylic acid) or weak bases (e.g., amino groups), which change their properties upon protonation or deprotonation. This way, the amphiphilic balance changes leads to increased/decreased vesicle stability. Bochert et al. [110] showed a pH-induced release of hydrophilic dyes from poly(2-vinylpyridine-*b*-ethylene oxide) (P2VP–PEO) block copolymer vesicles. P2VP has a pH-dependent solubility: it is insoluble in water at neutral and alkaline conditions, but soluble at pH values below 5. When the pH of the vesicular solution is lowered below 5 the P2VP block gets protonated, which results in a vesicular dissolution and release of the dye, respectively.

Du and coworkers [122] prepared vesicles from poly(2-(methacryloyloxy)ethyl phosphorylcholine-*b*-2-(diisopropylamino)ethyl methacrylate (PMPC-*b*-PDPA) directly in water without any cosolvents. These vesicles are stable at physiological pH and completely dissociate below pH 6. Moreover, they are very close analogues of conventional liposomes due to the biomimetic phosphorylcholine motif. Further research demonstrated that these polymersomes are efficient systems for pH-controlled encapsulation and delivery of DNA [218].

Bellomo et al. [219] reported that a polypeptide type copolymer composed of poly[*N*-2-{2-(2-methoxyethoxy)ethoxy}acetyl-L-lysine] as hydrophilic block and

poly(L-leucine–*co*–L-lysine) as hydrophilic/hydrophobic block forms pH responsive vesicles. At pH 10.6, the pH-sensitive block adopted a hydrophobic α-helical conformation, while protonation of the lysine residues at pH 3.0 caused a helix-to-coil transition which let to destabilization of the vesicular structure and release of the payload.

The group of Lecommandoux used different poly(L-glutamic acid)-based polymers to achieve vesicles with pH-responsive behavior [220–222]. For instance, poly(butadiene)-*b*-(glutamic acid) block copolymer formed vesicles by direct dissolution in a basic aqueous solution. The size of the aggregates was reversibly influenced by pH and ionic strength. Furthermore, the 1,2-vinyl bonds in the polybutadiene block can be cross linked by UV-light to produce shape-persistent stimuli-responsive nanocapsules. With another product, poly(L-glutamic acid)-*b*-poly(L-lysine), the same group prepared "schizophrenic" vesicles, stable at pH < 4 and pH > 10. At pH below 4, poly(L-glutamic acid) is the hydrophobic block and above pH 10, poly(L-lysine) acts as hydrophobic block. Between pH 5 and 9, both blocks are hydrophilic, leading to complete disruption of the vesicles.

A system with interesting properties is the poly(ethylene oxide)-*block*-poly[2-(diethylamino) ethyl methacrylate]-*stat*-[3-(trimethoxysilyl)propyl methacrylate] (PEO-*b*-P(DEA-*stat*-TMSPMA)) block copolymer. This self-crosslinkable copolymer formed vesicles which demonstrated pH-tunable membrane permeability [223].

Water-soluble poly(acrylic acid)-based nanocapsules with reversible pH- and ionic strength-dependent swelling transition were prepared by Meier et al. [224]. During this transition gated pores in the spherical polymer shells are opened (closed), which enables free molecular exchange between the interior of the hollow sphere and the bulk medium. This pH-switchable control of permeability can trigger release of encapsulated cargo from the polyelectrolyte spheres.

Discher and coworkers demonstrated an intelligent approach to shrink rapidly growing tumor by means of pH-sensitive vesicles [176]. The authors used poly(ethyleneglycol)-*b*-poly(lactic acid) vesicles loaded with anticancer drugs that disintegrated into membrane-lytic micelles within hours at 37°C and low pH. In contrast to the release mechanism relying on the systematic change in hydrophobic blocks polarity upon protonation/deprotonation, the release with this system was accomplished via hydrolytic degradation of the hydrophobic block at acidic pH. Hence, pH-triggered release within the endolysosomes was possible due to their acidic pH.

Temperature-responsive polymer vesicles are highly attractive systems for triggered release due to several reasons, first, local changes in the body temperature are easily achievable by applying coldness or heat, second, the deviation from normal body temperature (37°C) due to the presence of pathogens or pyrogens can be used to release the payload precisely at the site of disease. Most often one of the components of temperature-responsive vesicles is a polymer with lower critical solution temperature (LCST) such as poly(*N*-isopropylacrylamide) (PNIPAM) (LCST ∼32°C) or some other poly(*N*-alkylacrylamide) compounds [225, 226]. For instance, the group of McCormick prepared amphiphilic block copolymers consisting of hydrophilic poly[*N*-(3-aminopropyl)methylacrylamide hydrochloride] (PAMPA)

block and thermo-responsive poly(*N*-isopropylacrylamide) (PNIPAM) [121]. PNIPAM has an LCST of 32°C, above which it phase separates from solution. This fact makes the PAMPA-*b*-PNIPAM polymer capable of forming vesicles above the LCST within a narrow temperature range of 2–3°C. Vesicles are formed directly in water by varying the solution temperature. Additionally, the vesicles can be structurally "locked" by polyelectrolyte complexation using the oppositely charged poly(sodium 2-acrylamido-2-methylpropanesulfonate) (PAMPS) (Fig. 12). By further experiments, McCormick and coworkers demonstrated that similar thermally responsive vesicles formed from poly[2-(dimethylamino) ethyl methacrylate-*block*-(*N*-isopropylacrylamide)] (PDMAEMA-*b*-PNIPAM) copolymer in aqueous solution can be easily decorated with gold nanoparticles [227].

Related thermo-sensitive, cross-linked polymer vesicles were also formed by self-assembly of poly(2-cinnamoylethyl methacrylate)-*block*-poly(*N*-isopropylacrylamide) ($PCEMA_{61}-b-PNIPAM_{22}$) copolymer and subsequent photo-crosslinking of the PCEMA shells [228]. The vesicles can load a large amount of 4-aminopyridine (Apy) and release the compound at a tunable rate depending on temperature.

Qin et al. [229] produced a thermo-responsive PEO-*b*-PNIPAM block copolymer that forms vesicles above the LCST of 32°C. The PEO-*b*-PNIPAm vesicles are shown to be stable at body temperature and to encapsulate both hydrophilic drugs (e.g., Doxorubicin) and hydrophobic molecules into their membranes (e.g., PKH 26). Temperature-controlled quick release of both types of compounds below 32°C was possible.

The use of light as an external stimulus to control changes in the polymer properties has recently started being exploited [226].

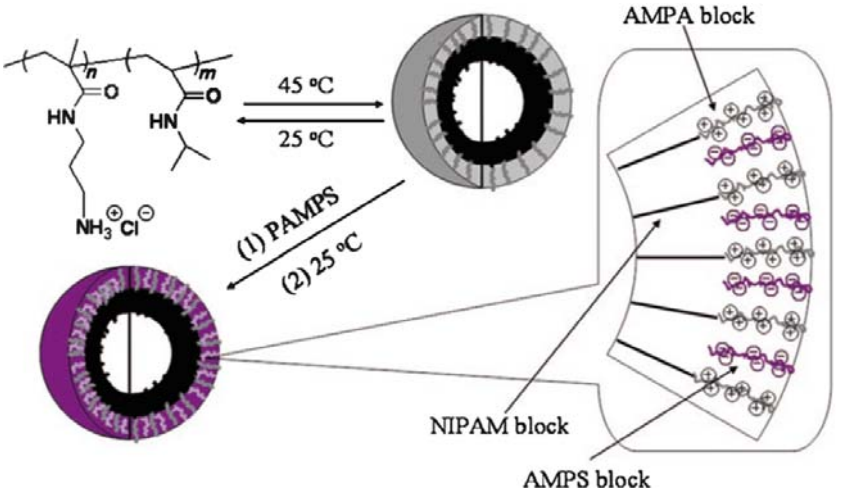

Fig. 12 Schematic illustration of the formation of vesicles from PAMPA-*b*-PNIPAM diblock copolymers and their subsequent ionic cross-linking. Li Y, Lokitz BS, McCormick CL (2006) Angew Chem Int Ed 45:5792. Copyright Wiley. Reproduced with permission [121]

Light-responsive polymeric vesicles can be designed by introducing polymer blocks with photoreactive groups. In particular, azobenzene derivatives are attractive for applications due to the readily induced and reversible isomerization of the azo bond between the *trans* (E) and *cis* (Z) geometrical isomers, which can be induced by light and heat. Upon isomerization azobenzene molecules undergo significant changes in the optical, mechanical and chemical properties. Zhao and coworkers demonstrated a reversible destabilization of vesicles from azobenzene-based polymers [230, 231]. The azobenzene moieties in the hydrophobic block change from hydrophobic to hydrophilic due to UV-induced trans–cis isomerization, leading to dissociation of the vesicles. However, reaggregation occurs by shifting from hydrophilic to hydrophobic after the reverse cis–trans isomerization upon visible light irradiation. They further explained the hydrophilicity shift as a result of the small dipole moment in the trans isomer and a significantly higher dipole moment in the cis isomer. Based on the same principle, Su et al. [232] demonstrated light-responsive vesicles from poly(acrylicacid)$_{299}$-*block*-poly{6-[4-(4-methylphenylazo)-phenoxy]hexyl acrylate}$_{19}$ (PAA$_{299}$-*b*-PAzoM$_{19}$) on a very specific block ratio. Interestingly, the vesicles changed their shape from spherical to ear-like during UV-light irradiation (Fig. 13).

With another polymer, poly(*N*-isopropylacrylamide)-*block*-poly{6-(4-(4-methyl-phenyl-azo)phenoxy)hexylacrylate} (PNIPAM-*b*-PAzoM), the same group showed photo-induced vesicle fusion upon UV irradiation [154]. Indeed, UV light has a rather low biomedical significance; therefore systems responsive to NIR light, which is characterized with deeper tissue penetration and minimal risk of damages to healthy cells, should be designed.

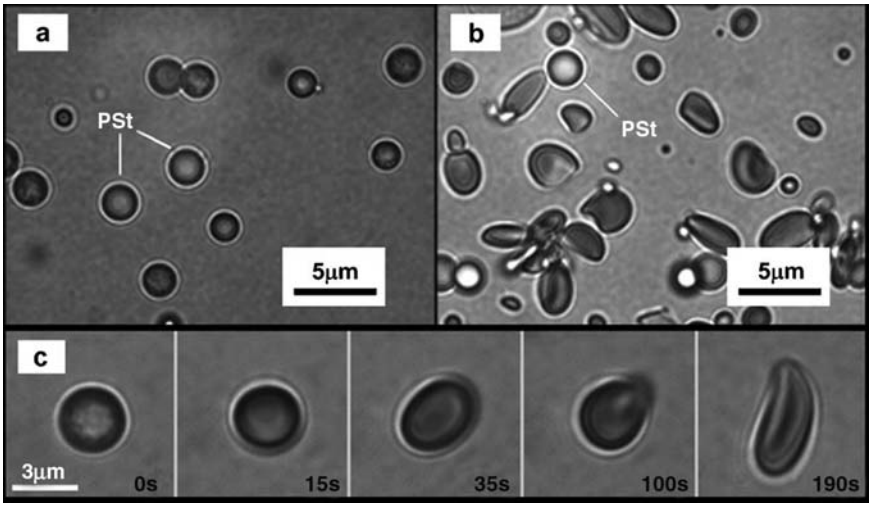

Fig. 13 a–c Photomicrographs of the vesicles containing azobenzene groups in 80:20 H_2O/THF mixture **a** before UV irradiation and **b** after irradiation for 600 s. Image **c** is a series of photomicrographs of an isolated vesicle under UV irradiation for different times, and the *scale bars* of 3 mm are the same for all of the graphs in image **c**. Su W, Han K, Luo Y, Wang Z, Li Y, Zhang Q (2007) Macromol Chem Phys 208:955. Copyright Wiley. Reproduced with permission [232]

Oxidative or reductive stress might also be interesting as stimuli for polymer vesicles since it can be produced by manpower (e.g., electric current) or by activated macrophages in inflamed tissues and cancer cells. Furthermore, the redox potential in the body varies depending on the side (e.g., extracellular and intracellular). The group of Hubbell [112] prepared a block copolymer from polyethylene glycol (PEG) and poly(propylene sulfide) (PPS) that forms vesicles in water. Upon exposure to oxidative agents, the thioethers in PEG-*b*-PPS-*b*-PEG vesicles were oxidized to poly(propylene sulphone) (polar), thus leading to hydrophilization of the originally hydrophobic block. Accordingly, it was observed that the vesicles destabilized upon incubation with H_2O_2. In further experiments the same authors coupled PEG to PPS using a disulfide bond [233]. The resulting PEG–SS–PPS vesicles appeared to be sensitive to the high intracellular concentrations of cysteine, but stable under the milder extracellular conditions. In cellular experiments a vesicle disruption and release of a payload due to cysteine induced cleavage of the disulfide bond was observed. Such a system might be interesting for cytoplasmic delivery.

The scientists have just started to explore the possibilities that responsive vesicular systems can offer. For example, combined with new targeting strategies, they can be developed towards very specific drug delivery vehicles. Following the results from environmentally-responsive micelles and translating their properties to membrane systems will be certainly one of the future trends in the field. For material science, the design and synthesis of vesicle forming polymers able to respond to minimal changes in physical/chemical parameters of their environment became challenging topics and will be further exploited to achieve control of self-assembly via molecular architecture.

10 Potential Applications of Polymer Membranes

Features such as mechanical stability, tunable properties, responsiveness to environmental stimuli, ability to encapsulate both hydrophilic and hydrophobic compounds, etc. make polymer membranes excellent candidates for use in medical, pharmaceutical, and environmental fields. Hence, polymer membranes have attracted a considerable attention in recent years. In this section, we review the potential applications of block copolymer vesicles.

10.1 Therapeutic Applications

Many of the polymer vesicles present in the literature are addressed to drug delivery applications. To achieve their potential as effective delivery vehicles, polymersomes must efficiently encapsulate therapeutic agents. Their ability to encapsulate molecules into either the aqueous lumen [144, 229, 234] of the vesicle (e.g., doxorubicin) or the hydrophobic core of the membrane (e.g., taxol (TAX)) has been

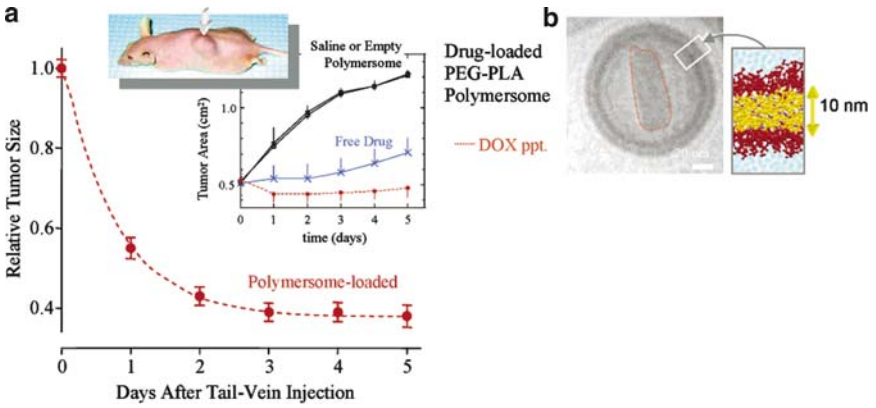

Fig. 14 a, b Drug loading, release, and antitumor activity of degradable polymersomes. **a** Cryo-TEM image of DOX- and TAX-loaded PEG–PLA-based nanopolymersome. **b** Solid tumors shrink after a single injection of (DOX + TAX)-loaded polymersomes. For treatment, either drug-loaded polymersomes (*red*), free drug (*blue*), empty polymersome or saline control was injected in the tail vein. Reprinted with permission from [176]. Copyright (2006) American Chemical Society

systematically studied [181, 235]. A beautiful example of combined delivery platform comes from Discher's labs [236]. The researchers developed an effective anticancer therapeutic device by loading both doxorubicin and taxol simultaneously to biodegradable polymersomes. The concept involves poly(ethyleneoxide)-*b*-poly(lactic acid) block copolymer vesicles, where doxorubicin is encapsulated in the hollow sphere, while taxol incorporates in the polymer membrane (Fig. 14). This formulation decreased the size of breast cancer tumors in mice considerably and showed a better performance than free drugs [176].

Drawing from work with lipoplexes, polymer vesicles were investigated for use as gene therapy vectors, and initial studies of DNA interaction with different catanionic vesicle systems were performed. For instance, Korobko and coworkers were able to release effectively genes in vitro [237,238]. This was achieved by encapsulating DNA to the lumen of cationic vesicles from poly(butadiene-*b*-*N*-methyl-4-vinyl pyridinium) (PB-*b*-P4VPQ). Additionally the authors demonstrated that these polymersomes are not limited to small DNA molecules, but successfully encapsulated DNA plasmid pUC18 within the aqueous lumen [238].

Recently, the group of Battaglia used poly(2-(methacryloyloxy)ethylphosphorylcholine)-*co*-poly(2-(diisopropylamino)ethyl methacrylate) (PMPC–PDPA) diblock copolymers to prepare biomimetic and pH-sensitive polymersomes for gene delivery [218]. These formulations encapsulated and released DNA in a pH-controlled manner. Notably, the pH drop was sufficient to trigger the transition from DNA-loaded vesicles to DNA–copolymer complexes.

Encapsulation and delivery of DNA has also been investigated with poly(amino acid) (poly(AA)) based polymer vesicles. Brown and coworkers synthesized an amphiphilic triblock copolymer from methoxy-poly(ethylene glycol) (mPEG), hydrophobic palmitic acid chains in block segments along a poly-L-lysine (PLL) or

poly-L-ornithine (PO) backbone, and a block segment of bare, cationic PLL or PO [239]. This triblock self-assembles to form vesicle structures capable of intercalating with DNA. Incubation of these DNA-containing vesicles with two different cell lines showed improved DNA transfection vs poly(AA) + DNA or DNA alone. Injection of the DNA-encapsulating poly(AA) vesicles in *vivo* has shown that gene transfer can be achieved in the lungs and liver [240]. However, measurements of cytotoxicity in cell culture indicated cell death at vesicle concentrations as low as 0.1 mg mL^{-1} of polymer, meaning that a more biocompatible polymer gene delivery vector is needed.

Initial work with degradable PEG–PLA vesicles has shown that the encapsulation and delivery of siRNA in vitro is comparable to levels achieved with the commonly used lipoplex of siRNA and Lipofectamine 2000 (LFA) [241].

So far, little work has been done to encapsulate therapeutic proteins. Hence, the encapsulation of recombinant insulin was a challenging test of therapeutic protein encapsulation in PEG-based polymersomes [241]. Encapsulation of insulin in neutral and biologically stable PEG–PBD polymersomes provides a promising method to increase therapeutic efficiency by maintaining protein structure.

Another possibility for therapeutic application of polymer vesicles has been presented recently [242]. Superoxide dismutase, an antioxidant enzyme, was encapsulated in the vesicular cavity and shown to remain functional in neutralizing superoxide radicals in situ. The polymer membranes were proven permeable to superoxide radicals by pulse radiolysis, and the encapsulation of the enzyme prolongs its lifetime (which is only minutes in the bloodstream, when non-shielded).

10.2 Active Targeting of Polymersomes

To bring the nanocontainer to a specific place where it should release its payload, targeting is a required approach. Hence, much work has been carried out to attach ligands or antibodies to the hydroxyl end-group of PEG-based assemblies [150, 181, 243]. Biotinylated nondegradable block copolymer assemblies have been shown to attach to surfaces coated with the biotin receptor avidin [146, 147, 150, 244]. Coupling chemistry has been applied to conjugate either an antihuman IgG, or antihuman serum to PEG-carbonate- or PEG-polyester-assembled polymer vesicles [149, 245]. HIV-derived Tat peptide attached to PEG–PBD polymersomes enhanced the cellular delivery of nanoparticles [246] and increased dendritic cell uptake in vitro [181].

Researches from Meier's and Hunziker's groups proposed targeting strategy involving biotin–streptavidin interactions [146,247]. First they prepared vesicles from biotinylated poly(methyloxazoline)–poly(dimethylsiloxane)–poly(methyloxazoline) triblock (PMOXA–PDMS–PMOXA) copolymers, next avidin was added to attach to the outside of the vesicles, and in the following step biotinylated ligands, poly(guanylic acid) sequences, were bound to the avidin's free sites (Fig. 15). The ligand was supposed to interact specifically with a cell receptor (scavenger receptor

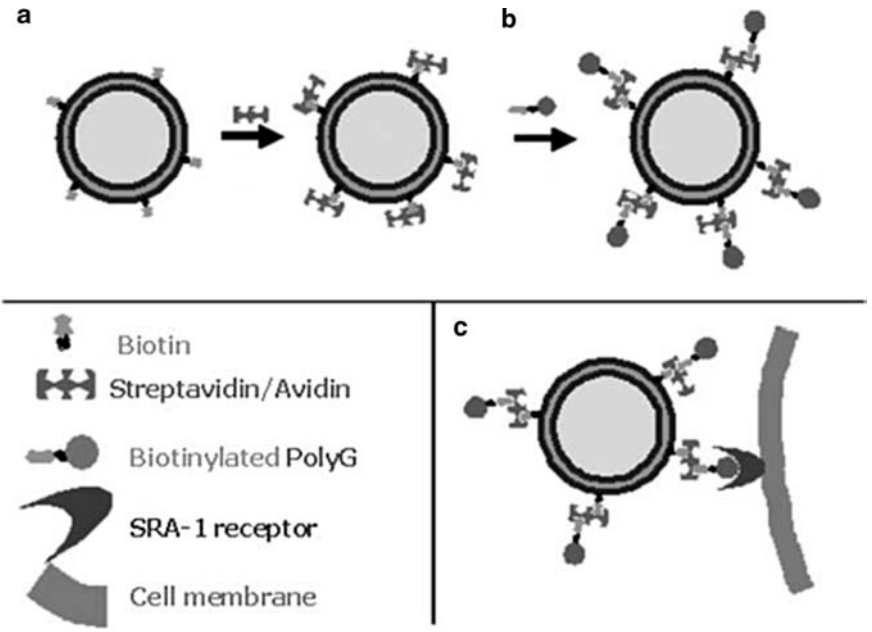

Fig. 15 a–c Schematic representation of the coupling of polyG with polymeric nanocontainers via biotin–streptavidin affinity interaction, **a** coupling of biotinylated nanocontainers with streptavidin, **b** subsequent incubation with biotinylated polyguanilic acid to render ligand-labeled nanocontainers, **c** schematic representation of the mode of action by receptor–ligand targeting. Reprinted from [187] Kita-Tokarczyk K, Grumelard J, Haefele T, Meier W. Block copolymer vesicles-using concepts from polymer chemistry to mimic biomembranes. Polymer 46:3540, Copyright (2005), with permission from Elsevier

A1), present in macrophages, responsible for cardiovascular disorders. Microscopy studies revealed a very good colocalization of receptors and ligands, while no such effect was observed with control cells, which did not possess the A1 receptor. Further loading of the above described biotin–avidin functionalized vesicles with fluorescent labels (calcein) allowed a microscopic observation of the binding and uptake of the vesicles by the cells [175]. Again, the vesicles preferred to attach to macrophages and they were observed to actually enter the cells by endocytosis. After some time, calcein was released which could be observed by fluorescence microscopy.

In recent studies Broz et al. [248] showed that the same receptor-targeted polymer vesicles described above can be used for safe encapsulation and highly efficient delivery of pravastatin and controlled intracellular release of encapsulated hydrophilic substances. With these formulations, it was possible to inhibit the endocytotic activity of macrophages defined by the uptake of known scavenger receptor ligands. Furthermore, the same authors presented the design of prototype PMOXA–PDMS–PMOXA artificial organelles based on certain design principles [249]. These include a size suited for cellular integration, a polymer membrane as a diffusion barrier for

separation of the microenvironment from the surroundings while allowing substance transfer of the chosen model substrate, an enzyme content allowing a specific biochemical reaction inside the organelle that can be observed from the outside (e.g., by fluorescence microscopy), protection of the content from undesired interference like proteases and inhibitors, and finally, lack of toxicity through choice of biocompatible materials. To test the cell-targeting properties of the ligand-functionalized protein-containing vesicles (fPVs) and their ability to specifically deliver their content into the target cells, Broz and coworkers incubated fPVs with several cell types, including fibroblasts, muscle cells, and hepatic endothelial cells. After 1 h of incubation no cellular uptake of fPVs by any of these cell types was observed. However, when incubated with THP-1 derived macrophages the fPVs were recognized and taken up by approximately 30% of macrophages. The authors observed for the first time that fPVs can also distribute to the Golgi and the endoplasmic reticulum.

The mechanisms behind the cell entry and release processes remain yet to be fully understood, however, from practical point of view the platform offers the possibility to target various cell receptors once appropriate ligands are attached to the vesicles.

10.3 Nanoreactors

Pioneering work in the incorporation of functional proteins into polymer bilayers was performed by Meier et al., who integrated membrane proteins into "black" block copolymer membranes [250]. This work proved that proteins could be incorporated into hyperthick triblock copolymer membranes while maintaining their functionality as measured by membrane conductance. Incorporation of proteins in "black" block copolymer films has been expanded for applications in sensors [251] and protein driven energy transduction [252] across polymeric biomembranes.

Recently, it has been shown experimentally that diverse channel proteins and enzymes can be inserted in polymer membranes and remain functional in such an artificial environment [253]. For example, the group of Meier prepared polymersome nanoreactors based on PMOXA–PDMS–PMOXA triblock copolymers (Fig. 16). In a series of experiments the authors demonstrated successful incorporation of the channel protein OmpF [254, 255], encapsulation of β-lactamase [254, 256], nucleoside hydrolase [255] and horseradish peroxidase [257] and trypsin [249]. It should be noted that functional nanoreactors can be achieved only by incorporation of channel proteins such as OmpF to the polymersomes, which control the membrane permeability by bringing substrates to the inside and transporting products to the outside medium. In a similar way, a more sophisticated nanocontainer was realized by incorporating the bacterial channel protein LamB that serves as a receptor for the λ-phage virus. The λ-phage virus recognizes its receptor, binds to the polymersome and injects its DNA through the channel to the inside of the vesicle [258]. To understand better how membrane proteins can be incorporated into hyperthick polymer membrane and maintain functionality, simulations using coarse-grained molecular dynamics were performed [22]. Simulations suggested that polymer chain flexibility

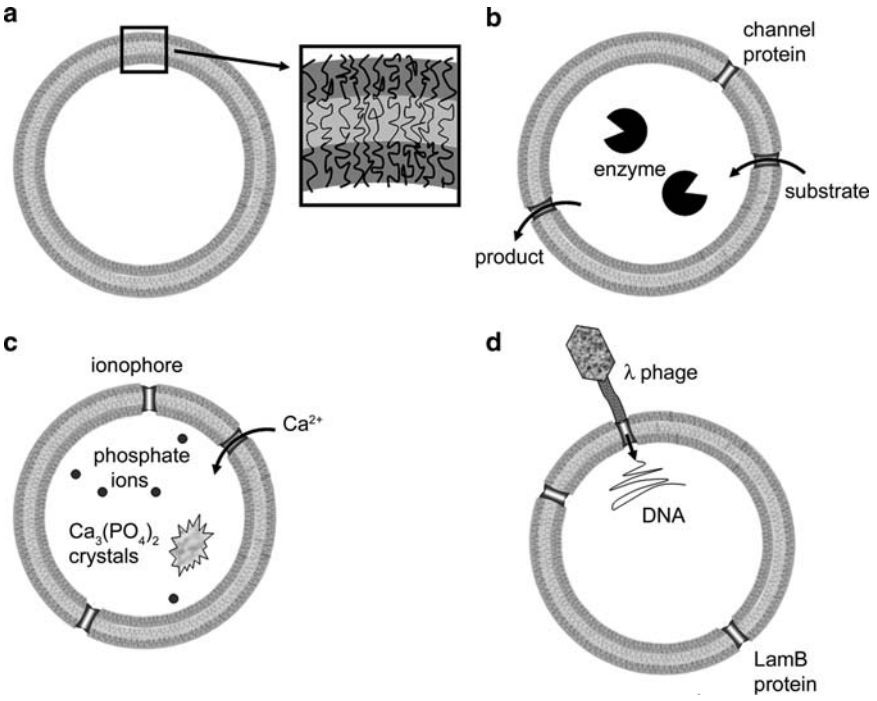

Fig. 16 a–d Schematic representation of polymer nanoreactors. **a** Cross section of triblock copolymer vesicle. **b** Polymersome with encapsulated enzyme and membrane-embedded channel protein. In the case described in the text, the substrate entering the vesicle is ampicillin, and the product of the hydrolysis is ampicillinoic acid. **c** Polymersome with embedded ionophores allowing Ca^{2+} ions to enter the vesicle ere they react with phosphate ions to form calcium phosphate crystals. **d** The LamB protein serves as a receptor to the l phage virus which can inject its DNA through the channel into the polymersome [259]. Reproduced with permission of The Royal Society of Chemistry

permits the integration of proteins with small membrane-spanning domains, but the flexibility of the hydrophilic chains can partially block the functional pore of the membrane protein, resulting in decreased functionality compared to when the proteins are incorporated in more natural lipid membranes.

Two membrane proteins were used in polymer vesicles for ATP production. In this very complex system, bacteriorhodopsin inserted in the polymer membranes pumped protons from the outside to the inside of vesicles when illuminated by light [260]. Next, those protons would turn on the ATP-ase (also inserted in the membrane), and when ADP is present, ATP production could be monitored in solution [261]. From the academic point of view, such platforms are excellent model systems for understanding the protein function.

Principally, encapsulation of proteins within the aqueous lumen of polymersomes can benefit from the extended circulation kinetics and controlled release properties of polymersomes. Neutral diblock (PEO–PDB, PEO–PEE), charged triblock (PEO–

PCL–PAA) as well as polyion complex vesicles showed the ability to encapsulate large, globular proteins such as FITC-labeled bovine serum albumin (FITC–BSA), myoglobin and hemoglobin [70, 116, 157, 262]. Because oxygen is capable of diffusing across the polymersome membrane at rates similar to lipid bilayers, polymersomes encapsulating hemoglobin have been shown to have oxygen affinities similar to those of human RBCs [262]. Furthermore, encapsulation of enzymes into polymer vesicles and controlled substrate permeability across polymeric membranes were exploited by several groups for applications in biocatalysis [101, 107, 263]–[266]. Encapsulation inside polymer vesicles can protect enzymes from harmful environmental factors like proteases and improve long-term storage. For example, *Candida antarctica* lipase B (CALB) was incorporated successfully in the bilayer and in the aqueous core of polystyrene–polyisocianopeptide (PS–PIAT) polymersomes and showed activity in both environments [265].

Hubbel and coworkers designed PEG–PPS–PEG polymersomes loaded with glucose oxidase [101]. PEG–PPS–PEG triblock copolymer is permeable to β-D-glucose. Glucose oxidase converts β-D-glucose to β-D-gluconolactone, generating hydrogen peroxide as a side product. The hydrogen peroxide produced diffuses through the polymer membrane and oxidizes the hydrophobic PPS block, resulting in vesicle destabilization. This concept for "self-destructing" polymeric vesicles is attractive for medical application since mM concentrations of glucose are available in the blood stream to trigger H_2O_2 release and low amounts of hydrogen peroxide do not harm patients. The encapsulation of glucose oxidase significantly improved its long-term storage in aqueous solution. A complex nanoreactor based on PS–PIAT diblock copolymer has been prepared by Vriezema et al. [266]. In this nanoreactor, a cascade reaction was sequentially catalyzed by three enzymes: glucose oxidase encapsulated in the vesicular cavity, horseradish peroxidase inserted in the polymer membrane and *C. antarctica* lipase B in the outside medium. The reaction turnover was dependent on the positional assembly of the enzymes; thus a removal of any enzyme from the system disturbed the cascade and no product could be obtained.

Polymer membranes have also been explored as scaffolds for bio-mineralization. PMOXA–PDMS–PMOXA vesicles were loaded with phosphate anions. Alamethicin, an ion channel peptide reconstituted in the vesicle membrane, allowed for cation (calcium) transport. After a certain incubation time, calcium phosphate crystals were seen inside the vesicles (Fig. 17), while no crystallization occurred in the outside medium [163].

Planar polymer films were recently mineralized with calcium phosphate [267]. Using the Langmuir monolayer technique, it was possible to control the particle growth by the polymer film properties at the air–water interface and the subphase parameters (pH, ion strength). Small changes it the growth conditions resulted in various particle shapes and dimensions. Such examples of controlled biomimetic mineralization are indeed very motivating for further studies of crystallization processes in synthetic membranes.

Polymer vesicles are also suitable to transport and target imaging agents such as fluorescent dyes and paramagnetic contrast agents. Hammer and coworkers encapsulated porphyrin-based near-infrared (NIR) fluorophores into PBD–PEO

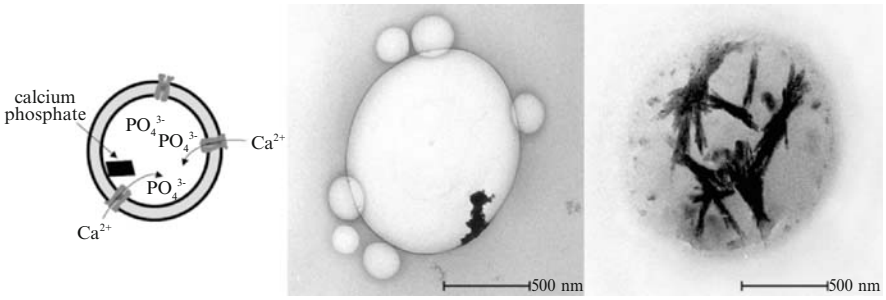

Fig. 17 Schematic representation of ion-channel controlled precipitation of calcium phosphate in block copolymer vesicles (*middle drawing*), and TEM micrographs (*right drawing*) of phosphate-loaded PMOXA–PDMS–PMOXA triblock copolymer giant vesicles after 1 and 24 h of incubation with $CaCl_2$ solution in the presence of the ionophore; *scale bar*: 500 nm [163]. Reproduced with permission of The Royal Society of Chemistry

block copolymer vesicles [268, 269]. High-loading capacity and direct injection of NIR-emissive polymersomes permitted the in *vivo* visualization of tumors in rats. Recently the same authors expanded their work to fully biodegradable emissive nanoparticles based on PEO-*b*-PCL and PEO-*b*-PMCL [270]. Coupling of targeting moieties to NIR-emissive polymersomes might allow early detection of tumors using noninvasive techniques. Lu et al. suggested a new approach to prepare fluorescent vesicles. They used polyacrylamide-*b*-poly(*p*-methacrylamido)acetophenone thiosemicarbazone (PAM-*b*-PMATC) block copolymer as the hydrophobic PMATC block has intrinsic fluorescence [271]. These fluorescent polymer vesicles could be potentially used as drug carriers and fluorescent tracers to determine the drug release behavior.

In the field of sensors, ion-binding block copolymers, which allow the formation of 'functionalized' vesicles, could be of special interest. Vesicles sensitive to magnetic field were obtained from aqueous dispersion of hydrophobic iron oxide nanoparticles and block copolymers of PGA and PBD [272]. Sachsenhofer and coworkers reported on the embedding of hydrophobic gold nanoparticles into PEO–PBD polymersomes [273]. Recently, polymer vesicles containing $Ru(bpy)_3^{2+}$ units in the wall with a high potential for application in catalysis were introduced [274].

11 Planar Polymer Membranes

Planar polymer films (either free-standing or at interfaces) are of particular interest, not only because they are preferred in many applications, but also because they allow for surface studies which could not be performed on vesicles. Langmuir monolayers from a vesicle-forming amphiphilic triblock copolymer were studied towards understanding the polymer interactions with a cation transporting peptide, alamethicin [275]. Planar solid supported block copolymer membranes are

attractive for engineering applications and for protein insertion in order to study membrane transport or diffusion. So far, amphiphilic membranes organized on solid surfaces are presented only in terms of grafted films. Recently researchers from Meier's group suggested a "grafting from" approach [185] to prepare amphiphilic methacrylate-based diblock copolymer membranes covalently bound to gold supports. Furthermore, they demonstrated a "grafting to" approach to form solid-supported amphiphilic ABA block copolymer membranes by fusion of charged polymer vesicles [276]. These concepts could be employed for applications such as sensor development, given the stability and robustness of the polymer self-organized film.

In summary, we believe to have presented an overview of recent achievements in the field of polymer membranes. Progress in the field is aroused by novel amphiphilic block copolymers, engineered transmembrane channel proteins, improved analytical methods to characterize the systems, and computational studies that help to understand polymer membrane properties.

Future research must focus on the design of tailor-made polymer membranes that suit special needs and on the understanding of their behavior in the living organism as well as of the exact mechanism of release. Various combinations of polymersomes with ligands, transmembrane proteins, receptors, and enzymes are needed to increase the potential of these nanosystems. Without doubt, improved knowledge of the nature of such formulations will offer a new paradigm towards their exploitation in fields such as biocatalysis (i.e., enantioselective bioreactors), biomedicine (i.e., imaging, medical therapy) and material science (biosensors). Certainly, more efforts have to be dedicated to cutting down production expenses and scaling-up the polymersome's production since those are important prerequisites that render polymersomes attractive for industrial applications.

References

1. Discher DE, Ahmed F (2006) Ann Rev Biomed Eng 8:323
2. Tanford C (1978) Science 200:1012
3. Antonietti M, Foerster S (2003) Adv Mater 15:1323
4. Israelachvilli JN, Mitchell DJ, Ninham BW (1976) J Chem Soc Faraday Trans 2 Mol Chem Phys 72:1525
5. Discher BM, Won Y-Y, Ege DS, Lee JCM, Bates FS, Discher DE, Hammer DA (1999) Science 284:1143
6. Hajduk DA, Kossuth MB, Hillmyer MA, Bates FS (1998) J Phys Chem B 102:4269
7. Doebereiner HG, Evans E, Kraus M, Seifert U, Wortis M (1997) Phys Rev E Statist Phys Plasmas Fluids Relat Interdisciplin Top 55:4458
8. Chen L, Shen H, Eisenberg A (1999) J Phys Chem B 103:9488
9. Dawson B (1973) Kinetics and mechanisms of reactions. Educational, London
10. Burke SE, Eisenberg A (2001) Polymer 42:9111
11. Shen H, Eisenberg A (1999) J Phys Chem B 103:9473
12. Luo L, Eisenberg A (2001) J Am Chem Soc 123:1012
13. Luo L, Eisenberg A (2001) Langmuir 17:6804
14. Anderson PM, Wilson MR (2004) J Chem Phys 121:8503

15. Goetz R, Gompper G, Lipowsky R (1999) Phys Rev Lett 82:221
16. Termonia Y (2002) J Polym Sci B Polym Phys 40:890
17. Yamamoto S, Maruyama Y, Hyodo S-a (2002) J Chem Phys 116:5842
18. Maiti PK, Lansac Y, Glaser MA, Clark NA, Rouault Y (2002) Langmuir 18:1908
19. Srinivas G, Shelley JC, Nielsen SO, Discher DE, Klein ML (2004) J Phys Chem B 108:8153
20. Srinivas G, Discher DE, Klein ML (2004) Nat Mater 3:638
21. Srinivas G, Klein ML (2004) Mol Phys 102:883
22. Srinivas G, Discher DE, Klein ML (2005) Nano Lett 5:2343
23. Grumelard J, Taubert A, Meier W (2004) Chem Commun:1462
24. Bermudez H, Brannan AK, Hammer DA, Bates FS, Discher DE (2002) Macromolecules 35:8203
25. Warren PB (1998) Curr Opin Colloid Interf Sci 3:620
26. Yamamoto S, Hyodo S-a (2003) J Chem Phys 118:7937
27. Ortiz V, Nielsen SO, Discher DE, Klein ML, Lipowsky R, Shillcock J (2005) J Phys Chem B 109:17708
28. Bernardes AT (1996) J Phys II 6:169
29. Leng J, Egelhaaf SU, Cates ME (2002) Europhys Lett 59:311
30. Leng J, Egelhaaf SU, Cates ME (2003) Biophys J 85:1624
31. He X, Schmid F (2006) Macromolecules 39:2654
32. Maurits NM, Fraaije JGEM (1997) J Chem Phys 107:5879
33. Uneyama T (2007) J Chem Phys 126:114902
34. Uneyama T, Doi M (2005) Macromolecules 38:5817
35. Uneyama T, Doi M (2005) Macromolecules 38:196
36. Yu K, Eisenberg A (1996) Macromolecules 29:6359
37. Yu Y, Zhang L, Eisenberg A (1998) Macromolecules 31:1144
38. Discher DE, Eisenberg A (2002) Science 297:967
39. Shen H, Eisenberg A (2000) Macromolecules 33:2561
40. Yu K, Bartels C, Eisenberg A (1999) Langmuir 15:7157
41. Zhang L, Yu K, Eisenberg A (1996) Science 272:1777
42. Nikova AT, Gordon VD, Cristobal G, Talingting MR, Bell DC, Evans C, Joanicot M, Zasadzinski JA, Weitz DA (2004) Macromolecules 37:2215
43. Kabanov AV, Bronich TK, Kabanov VA, Yu K, Eisenberg A (1998) J Am Chem Soc 120:9941
44. Santore MM, Discher DE, Won Y-Y, Bates FS, Hammer DA (2002) Langmuir 18:7299
45. Soo PL, Eisenberg A (2004) J Polym Sci B Polym Phys 42:923
46. Kickelbick G, Bauer J, Huesing N, Andersson M, Palmqvist A (2003) Langmuir 19:3198
47. Harris JK, Rose GD, Bruening ML (2002) Langmuir 18:5337
48. Terreau O, Bartels C, Eisenberg A (2004) Langmuir 20:637
49. Li X, Tang P, Qiu F, Zhang H, Yang Y (2006) J Phys Chem B 110:2024
50. Sachl R, Uchman M, Matejicek P, Prochazka K, Stepanek M, Spirkova M (2007) Langmuir 23:3395
51. Zupancich JA, Bates FS, Hillmyer MA (2006) Macromolecules 39:4286
52. Nolan D, Darcy R, Ravoo BJ (2003) Langmuir 19:4469
53. Bandyopadhyay P, Bharadwaj PK (1998) Langmuir 14:7537
54. Tanaka Y, Mayachi M, Kobuke Y (1999) Angew Chem Int Ed 38:504
55. Liu F, Wu Q, Eisenberg A (2003) Abstracts of Papers, 226th ACS National Meeting, New York, NY, United States, September 7–11, 2003
56. Cornelissen JJLM, Fischer M, Sommerdijk NAJM, Nolte RJM (1998) Science 280:1427
57. Sommerdijk NAJM, Holder SJ, Hiorns RC, Jones RG, Nolte RJM (1999) Polym Mater Sci Eng 80:29
58. Maskos M (2006) Polymer 47:1172
59. Zhang LF, Eisenberg A (1997) Macromol Symp 113:221
60. Yu Y, Eisenberg A (1997) J Am Chem Soc 119:8383
61. Yu K, Eisenberg A (1998) Macromolecules 31:3509
62. Schrage S, Sigel R, Schlaad H (2003) Macromolecules 36:1417
63. Weaver JVM, Armes SP, Liu S (2003) Macromolecules 36:9994

64. Chen D, Jiang M (2005) Acc Chem Res 38:494
65. Hu J, Liu G (2005) Macromolecules 38:8058
66. Yan X, Liu G, Hu J, Willson CG (2006) Macromolecules 39:1906
67. Zhang JX, Li XD, Yan MQ, Qiu LY, Jin Y, Zhu KJ (2007) Macromol Rapid Commun 28:710
68. Gohy J-F, Hofmeier H, Alexeev A, Schubert US (2003) Macromol Chem Phys 204:1524
69. Grubbs RB (2005) J Polym Sci A Polym Chem 43:4323
70. Kishimura A, Koide A, Osada K, Yamasaki Y, Kataoka K (2007) Angew Chem Int Ed 46:6085
71. Gao W-P, Bai Y, Chen E-Q, Li Z-C, Han B-Y, Yang W-T, Zhou Q-F (2006) Macromolecules 39:4894
72. Liu F, Eisenberg A (2003) J Am Chem Soc 125:15059
73. Zhang L, Eisenberg A (1996) Macromolecules 29:8805
74. Burke S, Shen H, Eisenberg A (2001) Macromol Symp 175:273
75. Schillen K, Bryskhe K, Mel'nikova YS (1999) Macromolecules 32:6885
76. Shen H, Eisenberg A (2000) Angew Chem Int Ed 39:3310
77. Reinecke AA, Doebereiner H-G (2003) Langmuir 19:605
78. Walther M, Faulhammer H, Finkelmann H (1998) Macromol Chem Phys 199:223
79. Haluska CK, Gozdz WT, Dobereiner H-G, Forster S, Gompper G (2002) Phys Rev Lett 89:238302
80. Chen Y, Du J, Xiong M, Guo H, Jinnai H, Kaneko T (2007) Macromolecules 40:4389
81. Riess G (2003) Prog Polym Sci 28:1107
82. Taton DG (2006) In: Lazzari ML, Liu G, Lecommandoux S (eds) Block copolymers in nanoscience. Wiley, Weinheim
83. Nardin C, Hirt T, Leukel J, Meier W (2000) Langmuir 16:1035
84. Stoenescu R, Meier W (2002) Chem Commun:3016
85. Brannan AK, Bates FS (2004) Macromolecules 37:8816
86. Gomez ED, Rappl TJ, Agarwal V, Bose A, Schmutz M, Marques CM, Balsara NP (2005) Macromolecules 38:3567
87. Holder SJ, Sommerdijk NAJM, Williams SJ, Nolte RJM, Hiorns RC, Sommerdijk NAJM, Jones RG (1998) Chem Commun:1445
88. Tian L, Nguyen P, Hammond PT (2006) Chem Commun:3489
89. Gao K-J, Li G, Lu X, Wu YG, Xu B-Q, Fuhrhop J-H (2008) Chem Commun:1449
90. Jenekhe SA, Chen XL (1998) Science 279:1903
91. Ilhan F, Galow TH, Gray M, Clavier G, Rotello VM (2000) J Am Chem Soc 122:5895
92. Drechsler U, Thibault RJ, Rotello VM (2002) Macromolecules 35:9621
93. Ding J, Liu G, Yang M (1997) Polymer 38:5497
94. Kesselman E, Talmon Y, Bang J, Abbas S, Li Z, Lodge TP (2005) Macromolecules 38:6779
95. Putauz J-L, Minatti E, Lefebvre C, Borsali R, Schappacher M, Deffieux A (2005) Faraday Discuss 128:163
96. Peng H, Chen D, Jiang M (2003) Langmuir 19:10989
97. Yao X, Chen D, Jiang M (2004) J Phys Chem B 108:5225
98. De Cuendias A, Le Hellaye M, Lecommandoux S, Cloutet E, Cramail H (2005) J Mater Chem 15:3264
99. Chan S-C, Kuo S-W, Lu C-H, Lee H-F, Chang F-C (2007) Polymer 48:5059
100. Edmonds WF, Hillmyer MA, Lodge TP (2007) Macromolecules 40:4917
101. Napoli A, Boerakker MJ, Tirelli N, Nolte RJM, Sommerdijk NAJM, Hubbell JA (2004) Langmuir 20:3487
102. Checot F, Lecommandoux S, Gnanou Y, Klok H-A (2002) Angew Chem Int Ed 41:1339
103. Kukula H, Schlaad H, Antonietti M, Foerster S (2002) J Am Chem Soc 124:1658
104. Sigel R, Losik M, Schlaad H (2007) Langmuir 23:7196
105. Zhang L, Eisenberg A (1995) Science 268:1728
106. Zhu J, Jiang Y, Liang H, Jiang W (2005) J Phys Chem B 109:8619
107. Vriezema Dennis M, Hoogboom J, Velonia K, Takazawa K, Christianen Peter CM, Maan Jan C, Rowan Alan E, Nolte Roeland JM (2003) Angew Chem Int Ed Engl 42:772
108. Li Z-C, Liang Y-Z, Li F-M (2002) New J Chem 26:1805

109. You L, Schlaad H (2006) J Am Chem Soc 128:13336
110. Borchert U, Lipprandt U, Bilang M, Kimpfler A, Rank A, Peschka-Suess R, Schubert R, Lindner P, Foerster S (2006) Langmuir 22:5843
111. Zhang Y, Zhang Z, Wang Q, Xu C, Xie Z (2006) Macromol Rapid Commun 27:1476
112. Napoli A, Valentini M, Tirelli N, Mueller M, Hubbell JA (2004) Nat Mater 3:183
113. Zipfel J, Lindner P, Tsianou M, Alexandridis P, Richtering W (1999) Langmuir 15:2599
114. Ahmed F, Discher DE (2004) J Control Release 96:37
115. Battaglia G, Ryan AJ (2005) J Am Chem Soc 127:8757
116. Wittemann A, Azzam T, Eisenberg A (2007) Langmuir 23:2224
117. Zhu H, Liu Q, Chen Y (2007) Langmuir 23:790
118. Du J, Chen Y, Zhang Y, Han CC, Fischer K, Schmidt M (2003) J Am Chem Soc 125:14710
119. Rakhmatullina E, Braun T, Chami M, Malinova V, Meier W (2007) Langmuir 23:12371
120. Yang J, Pinol R, Gubellini F, Levy D, Albouy P-A, Keller P, Li M-H (2006) Langmuir 22:7907
121. Li Y, Lokitz BS, McCormick CL (2006) Angew Chem Int Ed 45:5792
122. Du J, Tang Y, Lewis AL, Armes SP (2005) J Am Chem Soc 127:17982
123. Li X, Ji J, Wang X, Wang Y, Shen J (2007) Macromol Rapid Commun 28:660
124. Hordyjewicz-Baran Z, You L, Smarsly B, Sigel R, Schlaad H (2007) Macromolecules 40:3901
125. Maskos M, Harris JR (2001) Macromol Rapid Commun 22:271
126. Discher BM, Bermudez H, Hammer DA, Discher DE, Won Y-Y, Bates FS (2002) J Phys Chem B 106:2848
127. Jofre A, Hutchison JB, Kishore R, Locascio LE, Helmerson K (2007) J Phys Chem B 111:5162
128. Joralemon MJ, O'Reilly RK, Hawker CJ, Wooley KL (2005) J Am Chem Soc 127:16892
129. Li F, Ketelaar T, Marcelis ATM, Leermakers FAM, Cohen Stuart MA, Sudhoelter EJR (2007) Macromolecules 40:329
130. Ahmed F, Photos PJ, Discher DE (2006) Drug Dev Res 67:4
131. Lee JCM, Santore M, Bates FS, Discher DE (2002) Macromolecules 35:323
132. Pata V, Ahmed F, Discher DE, Dan N (2004) Langmuir 20:3888
133. Dimova R, Seifert U, Pouligny B, Forster S, Dobereiner HG (2002) Eur Phys J E Soft Matter 7:241
134. Dalhaimer P, Bates FS, Aranda-Espinoza H, Discher D (2003) Comptes Rendus Physique 4:251
135. Bermudez H, Hammer DA, Discher DE (2004) Langmuir 20:540
136. Aranda-Espinoza H, Bermudez H, Bates FS, Discher DE (2001) Phys Rev Lett 87:208301
137. Nardin C, Winterhalter M, Meier W (2000) Langmuir 16:7708
138. Kumar M, Grzelakowski M, Zilles J, Clark M, Meier W (2007) Proc Natl Acad Sci U S A 104:20719
139. Kimmich R (ed) (1997) NMR-tomography, diffusometry, relaxometry. Springer, Berlin Heidelberg New York
140. Leson A, Filiz V, Foerster S, Mayer C (2007) Chem Phys Lett 444:268
141. Battaglia G, Ryan AJ, Tomas S (2006) Langmuir 22:4910
142. Bauer A, Kopschuetz C, Stolzenburg M, Foerster S, Mayer C (2006) J Membr Sci 284:1
143. Yan Y, Hoffmann H, Leson A, Mayer C (2007) J Phys Chem B 111:6161
144. Choucair A, Soo PL, Eisenberg A (2005) Langmuir 21:9308
145. Wu J, Eisenberg A (2006) J Am Chem Soc 128:2880
146. Rigler P, Meier W (2006) J Am Chem Soc 128:367
147. Lin JJ, Silas JA, Bermudez H, Milam VT, Bates FS, Hammer DA (2004) Langmuir 20:5493
148. Lin John J, Bates Frank S, Hammer Daniel A, Silas James A (2005) Phys Rev Lett 95:026101
149. Lin JJ, Ghoroghchian PP, Zhang Y, Hammer DA (2006) Langmuir 22:3975
150. Nam J, Santore MM (2007) Langmuir 23:7216
151. Choucair AA, Kycia AH, Eisenberg A (2003) Langmuir 19:1001
152. Zhou Y, Yan D (2005) J Am Chem Soc 127:10468
153. Zhou Y, Yan D (2005) Angew Chem Int Ed 44:3223

154. Su W, Luo Y, Yan Q, Wu S, Han K, Zhang Q, Gu Y, Li Y (2007) Macromol Rapid Commun 28:1251
155. Meng F, Hiemstra C, Engbers GHM, Feijen J (2003) Macromolecules 36:3004
156. Zumbuehl O, Weder HG (1981) Biochim Biophys Acta Biomembr 640:252
157. Lee JC, Bermudez H, Discher BM, Sheehan MA, Won YY, Bates FS, Discher DE (2001) Biotechnol Bioeng 73:135
158. Photos Peter J, Bacakova L, Discher B, Bates Frank S, Discher Dennis E (2003) J Control Release 90:323
159. Dimitrov D, Angelova M (1987) Prog Colloid Polym Sci 73:48
160. Taylor P, Xu C, Fletcher PDI, Paunov VN (2003) Chem Commun:1732
161. Bucher P, Fischer A, Luisi PL, Oberholzer T, Walde P (1998) Langmuir 14:2712
162. Bagatolli LA, Gratton E (1999) Biophys J 77:2090
163. Sauer M, Haefele T, Graff A, Nardin C, Meier W (2001) Chem Commun:2452
164. Battaglia G, Ryan AJ (2006) J Phys Chem B 110:10272
165. Yildiz ME, Prud'homme RK, Robb I, Adamson DH (2007) Polym Adv Technol 18:427
166. Hauschild S, Lipprandt U, Rumplecker A, Borchert U, Rank A, Schubert R, Foerster S (2005) Small 1:1177
167. Napoli AS, Sebök D, Senti A, Meier W (2006) In: Lazzari ML, Liu G, Lecommandoux S (eds) Block copolymers in nanoscience. Wiley, Weinheim
168. Sauer M, Meier W (2001) Chem Commun 55
169. Bryskhe K, Jansson J, Topgaard D, Schillen K, Olsson U (2004) J Phys Chem B 108:9710
170. Murphy RM (1997) Curr Opin Biotechnol 8:25
171. Burchard W (1983) Adv Polym Sci 48:1
172. Norman AI, Cabral JT, Ho DL, Amis EJ, Karim A (2004) PMSE Preprints 90:339
173. Lindner P, Wignall G (1999) MRS Bull 24:34
174. Li Z-C, Shen Y, Liang Y-Z, Li F-M (2001) Chin J Polym Sci 19:297
175. Broz P, Driamov S, Ziegler J, Ben-Haim N, Marsch S, Meier W, Hunziker P (2006) Nano Lett 6:2349
176. Ahmed F, Pakunlu RI, Srinivas G, Brannan A, Bates F, Klein ML, Minko T, Discher DE (2006) Mol Pharm 3:340
177. Hinterdorfer P, Baber G, Tamm LK (1994) J Biol Chem 269:20360
178. Buijs J, Britt DW, Hlady V (1998) Langmuir 14:335
179. Oheim M, Loerke D, Stuhmer W, Chow RH (1998) Eur Biophys J 27:83
180. Pawley J (1997) Handbook of biological confocal microscopy. Kluwer, New York
181. Christian NA, Milone MC, Ranka SS, Li G, Frail PR, Davis KP, Bates FS, Therien MJ, Ghoroghchian PP, June CH, Hammer DA (2007) Bioconjugate Chem 18:31
182. Giessibl FJ (2003) Rev Modern Phys 75:949
183. Regenbrecht M, Akari S, Forster S, Mohwald H (1999) Surf Interf Anal 27:418
184. Ahmed F, Hategan A, Discher DE, Discher BM (2003) Langmuir 19:6505
185. Rakhmatullina E, Braun T, Kaufmann T, Spillmann H, Malinova V, Meier W (2007) Macromol Chem Phys 208:1283
186. Won Y-Y, Brannan AK, Davis HT, Bates FS (2002) J Phys Chem B 106:3354
187. Kita-Tokarczyk K, Grumelard J, Haefele T, Meier W (2005) Polymer 46:3540
188. Napoli A, Tirelli N, Wehrli E, Hubbell JA (2002) Langmuir 18:8324
189. Ding J, Liu G (1998) J Phys Chem B 102:6107
190. Ding J, Liu G (1998) Chem Mater 10:537
191. Luo L, Eisenberg A (2002) Angew Chem Int Ed 41:1001
192. Peng H, Chen D, Jiang M (2003) J Phys Chem B 107:12461
193. Valentini M, Napoli A, Tirelli N, Hubbell JA (2003) Langmuir 19:4852
194. Valentini M, Vaccaro A, Rehor A, Napoli A, Hubbell JA, Tirelli N (2004) J Am Chem Soc 126:2142
195. Rumplecker A, Forster S, Zahres M, Mayer C (2004) J Chem Phys 120:8740
196. Binder Wolfgang H (2008) Angew Chem Int Ed Engl 47:3092
197. Firestone Millicent A, Wolf Amanda C, Seifert S (2003) Biomacromolecules 4:1539

198. Frey Shelli L, Zhang D, Carignano Marcelo A, Szleifer I, Lee Ka Yee C (2007) J Chem Phys 127:114904
199. Maskarinec SA, Lee KYC (2003) Langmuir 19:1809
200. Yaroslavov AA, Melik-Nubarov NS, Menger FM (2006) Acc Chem Res 39:702
201. Maskarinec SA, Hannig J, Lee RC, Lee KYC (2002) Biophys J 82:1453
202. Johnsson M, Bergstrand N, Edwards K, Stlgren JJR (2001) Langmuir 17:3902
203. Kostarelos K, Tadros TF, Luckham PF (1999) Langmuir 15:369
204. Bhattacharya S, Moss RA, Ringsdorf H, Simon AJ (1997) Langmuir 13:1869
205. Krylova OO, Melik-Nubarov NS, Badun GA, Ksenofontov AL, Menger FM, Yaroslavov AA (2003) Chem Eur J 9:3930
206. Marks JD, Pan CY, Bushell T, Cromie W, Lee RC (2001) FASEB 15:1107
207. Moghimi SM, Hunter AC (2000) Trends Biotechnol 18:412
208. Lee RC, River LP, Pan FS, Ji L, Wollmann RL (1992) Proc Natl Acad Sci U S A 89:4524
209. Hussain H, Kerth A, Blume A, Kressler J (2004) J Phys Chem B 108:9962
210. Mudgil P, Dennis GR, Millar TJ (2006) Langmuir 22:7672
211. Peters K, Dennis Gary R, Anderton Philip J, Millar Thomas J (2003) Invest Ophthalmol Vis Sci 44:5089
212. Erukova VY, Krylova OO, Antonenko YN, Melik-Nubarov NS (2000) Biochim Biophys Acta Biomembr 1468:73
213. Firestone Millicent A, Seifert S (2005) Biomacromolecules 6:2678
214. Yaroslavov AA, Efimova AA, Lobyshev VI, Ermakov YA, Kabanov VA (1997) Membr Cell Biol 10:683
215. Demina T, Grozdova I, Krylova O, Zhirnov A, Istratov V, Frey H, Kautz H, Melik-Nubarov N (2005) Biochemistry 44:4042
216. Yaroslavov AA, Kuchenkova OE, Okuneva IB, Melik-Nubarov NS, Kozlova NO, Lobyshev VI, Menger FM, Kabanov VA (2003) Biochim Biophys Acta Biomembr 1611:44
217. Kozlova NO, Bruskovskaya IB, Okuneva IB, Melik-Nubarov NS, Yaroslavov AA, Kabanov VA, Menger FM (2001) Biochim Biophys Acta Biomembr 1514:139
218. Lomas H, Canton I, MacNeil S, Du J, Armes SP, Ryan AJ, Lewis AL, Battaglia G (2007) Adv Mater 19:4238
219. Bellomo EG, Wyrsta MD, Pakstis L, Pochan DJ, Deming TJ (2004) Nat Mater 3:244
220. Checot F, Brulet A, Oberdisse J, Gnanou Y, Mondain-Monval O, Lecommandoux S (2005) Langmuir 21:4308
221. Rodriguez-Hernandez J, Lecommandoux S (2005) J Am Chem Soc 127:2026
222. Checot F, Rodriguez-Hernandez J, Gnanou Y, Lecommandoux S (2007) Biomol Eng 24:81
223. Du JZ, Armes SP (2005) J Am Chem Soc 127:12800
224. Sauer M, Streich D, Meier W (2001) Adv Mater 13:1649
225. Dimitrov I, Trzebicka B, Mueller AHE, Dworak A, Tsvetanov CB (2007) Prog Polym Sci 32:1275
226. Rijcken CJF, Soga O, Hennink WE, van Nostrum CF (2007) J Control Release 120:131
227. Li Y, Smith AE, Lokitz BS, McCormick CL (2007) Macromolecules 40:8524
228. Chen X, Ding X, Zheng Z, Peng Y (2006) New J Chem 30:577
229. Qin S, Geng Y, Discher DE, Yang S (2006) Adv Mater 18:2905
230. Tong X, Wang G, Soldera A, Zhao Y (2005) J Phys Chem B 109:20281
231. Zhao Y (2007) Chem Rec 7:286
232. Su W, Han K, Luo Y, Wang Z, Li Y, Zhang Q (2007) Macromol Chem Phys 208:955
233. Cerritelli S, Velluto D, Hubbell JA (2007) Biomacromolecules 8:1966
234. Xiong XY, Li YP, Li ZL, Zhou CL, Tam KC, Liu ZY, Xie GX (2007) J Control Release 120:11
235. Li S, Byrne B, Welsh J, Palmer AF (2007) Biotechnol Progr 23:278
236. Ahmed F, Pakunlu RI, Brannan A, Bates F, Minko T, Discher DE (2006) J Control Release 116:150
237. Korobko AV, Jesse W, van der Maarel JRC (2005) Langmuir 21:34
238. Korobko AV, Backendorf C, van der Maarel JRC (2006) J Phys Chem B 110:14550

239. Brown MD, Schaetzlein A, Brownlie A, Jack V, Wang W, Tetley L, Gray AI, Uchegbu IF (2000) Bioconjugate Chem 11:880
240. Brown MD, Gray AI, Tetley L, Santovena A, Rene J, Schatzlein AG, Uchegbu IF (2003) J Control Release 93:193
241. Christian DA, Cai S, Bowen DM, Kim YH, Pajerowski JD, Discher DE (2008) Polym Preprints 49:1075
242. Axthelm F, Casse O, Koppenol WH, Nauser T, Meier W, Palivan CG (2008) J Phys Chem B 112:8211
243. Discher DE, Photos P, Ahmed F, Parthasarathy R, Bates FS (2002) Biomed Aspects Drug Target:459
244. Nam J, Santore MM (2007) Langmuir 23:10650
245. Meng F, Engbers GHM, Feijen J (2005) J Control Release 101:187
246. Gupta B, Levchenko TS, Torchilin VP (2005) Adv Drug Deliv Rev 57:637
247. Broz P, Benito SM, Saw C, Burger P, Heider H, Pfisterer M, Marsch S, Meier W, Hunziker P (2005) J Control Release 102:475
248. Broz P, Ben-Haim N, Grzelakowski M, Marsch S, Meier W, Hunziker P (2008) J Cardiovasc Pharmacol 51:246
249. Ben-Haim N, Broz P, Marsch S, Meier W, Hunziker P (2008) Nano Lett 8:1368
250. Meier W, Nardin C, Winterhalter M (2000) Angew Chem Int Ed 39:4599
251. Wong D, Jeon T-J, Schmidt J (2006) Nanotechnology 17:3710
252. Ho D, Chu B, Lee H, Montemagno CD (2004) Nanotechnology 15:1084
253. Onaca O, Nallani M, Ihle S, Schenk A, Schwaneberg U (2006) Biotechnol J 1:795
254. Nardin C, Widmer J, Winterhalter M, Meier W (2001) Eur Phys J 4:403
255. Ranquin A, Versees W, Meier W, Steyaert J, Van Gelder P (2005) Nano Lett 5:2220
256. Nardin C, Thoeni S, Widmer J, Winterhalter M, Meier W (2000) Chem Commun:1433
257. Nallani M, Benito S, Onaca O, Graff A, Lindemann M, Winterhalter M, Meier W, Schwaneberg U (2006) J Biotechnol 123:50
258. Graff A, Sauer M, Van Gelder P, Meier W (2002) Proc Natl Acad Sci U S A 99:5064
259. Mecke A, Dittrich C, Meier W (2006) Soft Matter 2:751
260. Choi H-J, Lee H, Montemagno CD (2005) Nanotechnology 16:1589
261. Choi H-J, Montemagno CD (2005) Nano Lett 5:2538
262. Arifin DR, Palmer AF (2005) Biomacromolecules 6:2172
263. Tiourina OP, Antipov AA, Sukhorukov GB, Larionova NI, Lvov Y, Mohwald H (2001) Macromol Biosci 1:209
264. Lvov Y, Antipov AA, Mamedov A, Moehwald H, Sukhorukov GB (2001) Nano Lett 1:125
265. Nallani M, de Hoog H-PM, Cornelissen JJLM, Palmans ARA, van Hest JCM, Nolte RJM (2007) Biomacromolecules 8:3723
266. Vriezema DM, Garcia PML, Oltra NS, Natzakis NS, Kuiper SM, Nolte RJM, Rowan AE, van Hest JCM (2007) Angew Chem Int Ed 46:7378
267. Casse O, Colombani O, Kita-Tokarczyk K, Mueller AHE, Meier W, Taubert A (2008) Faraday Discuss 139:179
268. Ghoroghchian PP, Frail PR, Susumu K, Blessington D, Brannan AK, Bates FS, Chance B, Hammer DA, Therien MJ (2005) Proc Natl Acad Sci U S A 102:2922
269. Ghoroghchian PP, Lin JJ, Brannan AK, Frail PR, Bates FS, Therien MJ, Hammer DA (2006) Soft Matter 2:973
270. Ghoroghchian PP, Frail PR, Li G, Zupancich JA, Bates FS, Hammer DA, Therien MJ (2007) Chem Mater 19:1309
271. Lu X, Gong S, Meng L, Li C, Liang F, Wu Z, Zhang L (2007) Eur Polym J 43:2891
272. Lecommandoux S, Sandre O, Checot F, Rodriguez-Hernandez J, Perzynski R (2005) Adv Mater 17:712
273. Sachsenhofer R, Binder WH, Farnik D, Zirbs R (2007) Macromol Symp 254:375
274. Metera KL, Sleiman H (2007) Macromolecules 40:3733
275. Haefele T, Kita-Tokarczyk K, Meier W (2006) Langmuir 22:1164
276. Rakhmatullina E, Meier W (2008) Langmuir 24:6254

Adv Polym Sci (2010) 224: 167–195
DOI:10.1007/12_2008_12

Published online: 5 March 2009

Biohybrid and Peptide-Based Polymer Vesicles

Annabelle Bertin, Florian Hermes, and Helmut Schlaad

Abstract This review covers the major processes and mechanisms involved in the production of biohybrid or peptide-based polymer vesicles by self-assembly. The formation of vesicles conventionally occurs based on geometric packing issues, and becomes predominant when the membrane-forming segment is stiffened due to hydrogen bonding and secondary structure interactions or supramolecular complexation. The vesicles are used for applications in life science, for the purpose of drug/gene delivery, cell surface recognition, and as bioreactors, and for the production of composite materials.

Keywords Aggregation, Biohybrid, Biomembrane, Block copolymer, Colloid, Glycopolymer, Polypeptide, Secondary structure, Self-assembly, Vesicle

Contents

A. Bertin, F. Hermes, and H. Schlaad (✉)
Max Planck Institute of Colloids and Interfaces, Colloid Department, Research Campus Golm, 14424 Potsdam, Germany
e-mail: schlaad@mpikg.mpg.de

List of Abbreviations

Ala, A	Alanine
Arg, R	Arginine
Asp, D	Aspartic acid
AspA	Aspartamide
Bzl, B	Benzyl
CD	Circular dichroism
Cys, C	Cysteine
DFM	Dark-field microscopy
DIC	Differential interference contrast
DLS	Dynamic light scattering
DMF	*N,N*-Dimethylformamide
DNA	Desoxyribonucleic acid
EYPG	Egg yolk phosphatidyl glycerol
FM	Fluorescence microscopy
FTIC	Fluoresceine isothiocyanate
Glc	Glucose
Gln, Q	Glutamine
Glu, E	Glutamic acid
IR	Infrared
Lac	Lactose
LCST	Lower critical solution temperature
Leu, L	Leucine
LSCM	Laser scanning confocal microscopy
Lys, K	Lysine
Mb	Myoglobin
Me, M	Methyl
MRI	Magnetic resonance imaging
NMR	Nuclear magnetic resonance
OM	Optical microscopy
PB	Polybutadiene
PDEGMA	Poly(diethyleneglycol methacrylate)
PEG, PEO	Poly(ethylene glycol), poly(ethylene oxide)
PELLys	Poly(N^{ε}-[2-(2-(methoxyethoxy)ethoxy)]acetyl-L-lysine)
PGEA	Poly(2-(β-D-glucopyranosyloxy)ethyl acrylate)
PGEMA	Poly(2-glucosyloxyethyl methacrylate)
Phe, F	Phenylalanine
PHPMA	Poly(*N*-(2-hydroxypropyl)methacrylamide)
PIAA	Polyisocyanodipeptide
PIC	Polyion complex
PMMA	Poly(methyl methacrylate)
PNIPAM	Poly(*N*-isopropylacrylamide)
PS	Polystyrene
R_g	Radius of gyration
R_h	Hydrodynamic radius

SANS Small-angle neutron scattering
SAXS Small-angle X-ray scattering
SEM Scanning electron microscopy
SFM Scanning force microscopy
SLS Static light scattering
TEM Transmission electron microscopy
THF Tetrahydrofuran
Z Benzyloxycarbonyl

1 Introduction

A vesicle (from the Latin "vesicula," small bubble) is a colloidal object, often spherical in shape and up to hundreds of micrometers in size, enclosing a volume with a thin membrane. The most prominent example of a biological vesicle is a living cell with a membrane built of phospholipid amphiphiles. Vesicles can also be formed from synthetic block copolymers, also referred to as "polymersomes," with better performance than phospholipid vesicles and adjustable properties including stability, fluidity, and dynamics [1–4]. Biohybrid polymer vesicles ("molecular chimeras" [5]) may inherit the advantageous features of both synthetic polymers (solubility, processability, and rubber elasticity) and biological polymers (secondary structure, chirality, functionality, and biocompatibility), making them interesting as mimetics for biomembranes [6] and particularly for biomedical applications [7, 8].

The scope of the present review is to summarize recent work, published up until June 2008, on this promising field of peptide- and sugar-based polymer vesicles (for reviews on the self-assembly of low-molecular weight amphiphiles, see [9, 10]). There was a particular concern to give a comprehensive description of the strategies and mechanisms involved in the production of vesicles by self-assembly. Yet the number of applications of bioinspired polymer vesicles is rather small, mainly focusing on drug delivery/release and the fabrication of primitive composite materials, which might be due to the restricted availability of biohybrid polymers (although peptide hybrid polymers are known for more than 30 years [11]). However, regarding the recent advances in synthetic polymer chemistry, especially in the synthesis of glycopolymers [12, 13], biohybrids will certainly gain greater importance not only for biomedical and pharmaceutical applications but also for materials science, biomineralization, and so on.

Besides the self-assembled polymer vesicles there are other types of membranes or capsules, which will not be mentioned here. Commercial membranes based on cellulose include dialysis bags or filter paper, to mention just the most common and widely spread examples [14]. Capsules made with sophistication through layer-by-layer assembly on sacrificial templates [15, 16] or using viruses as building blocks [17, 18] have recently been reviewed elsewhere.

2 Vesicle Formation

Conventionally, the self-assembly of block copolymers in aqueous environment is driven by the hydrophobic effect, which involves the dehydration (release of water molecules) and subsequently the aggregation of the hydrophobic chains in order to minimize contact with water. In terms of thermodynamics, the aggregation of amphiphiles occurs because of the entropic contributions to the free energy. Vesicles or bilayers arise when the value of the geometric packing parameter of the amphiphile is in the range of $0.5 \leq v/al \leq 1$ (v: volume of the hydrophobic part, a: interfacial area, l: chain length normal to the interface) or the spontaneous interfacial curvature of the amphiphile approaches zero [3], which is usually fulfilled when the weight fraction of hydrophobic moieties is larger than that of the hydrophilic moieties [1,2]. Those biohybrid polymers forming vesicles based on geometric packing issues are described in Sect. 2.1.

The formation of layered structures or vesicles becomes the predominant aggregation motif when the segment forming the membrane exhibits decreased flexibility or increased stiffness [3, 10]. Factors leading to a stiffening of the chain conformation include, among others, the occurrence of intramolecular and/or intermolecular hydrogen bonding and secondary structure interactions. Especially α-helical polypeptide chains assemble into layers with a high stiffness or bending modulus, due to the packing of into an ordered 2D (crystalline) array, as documented in Sect. 2.2.

A third approach towards the production of vesicles involves complementary supramolecular complexation, for instance by mixing oppositely charged block ionomers or by cofactor–enzyme interactions – two examples are presented in Sect. 2.3.

2.1 Packing Parameter and Interfacial Curvature

Linear polypeptide block copolymers, block copolymers with pendent sugar or peptide grafts, and modified linear or dendritic homopolymers have been used to produce vesicles based on hydrophobic interactions and packing issues. Usually, the peptides or sugars make the minority hydrophilic part of the copolymers and are thus incorporated in the corona and not in the membrane of the vesicles. For the inverse case, the hydrophobic peptides in the membrane are often too short to adopt a stable secondary structure.

2.1.1 Linear Block Copolymers

The linear polypeptide hybrid block copolymers and block copolypeptides reported to form vesicles in aqueous solution are listed in Fig. 1.

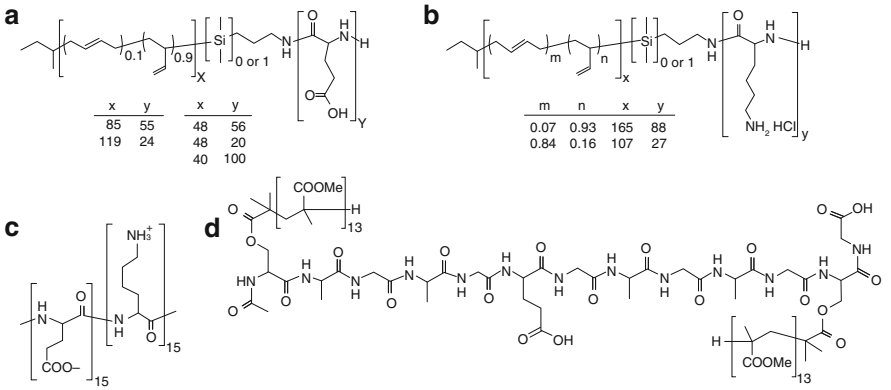

Fig. 1 a–d Chemical structures of linear peptide block copolymers **a** 1,2-Polybutadiene-*block*-poly(L-glutamate) (PB-*b*-PLGlu). **b** Polybutadiene-*block*-poly(L-lysine) (PB-*b*-PLLys). **c** Poly (L-glutamate)-*block*-poly(L-lysine) (PLGlu-*b*-PLLys). **d** Poly(methyl methacrylate)-*block*-peptide-*block*-poly(methyl methacrylate) (PMMA-*b*-peptide-*b*-PMMA)

The aggregation behavior of PB-*b*-PLGlu (Fig. 1a) in aqueous solution was investigated by Schlaad et al. [19] and Lecommandoux et al. [20] using DLS, SLS, SANS, and TEM. Samples containing 17–54 mol% glutamate were found to form unilamellar vesicles ("peptosomes") being 100–180 nm in diameter. Unexpectedly, however, vesicles were also observed for a PB-*b*-PLGlu with a very high hydrophilic content of 71 mol% [21].

Changing the pH of the solution affected not only the degree of ionization but also the secondary structure of the polypeptide coronal chains. The coil-to-helix transition was found to happen at about pH 6 (CD spectroscopy). DLS and SANS showed that neither the shape nor the morphology of aggregates were severely altered by pH. Vesicles were shrinking in size by 20% or less when switching from acidic to basic environment. Although brought into discussion [21], there is no evidence for a direct correlation between the hydrodynamic size of vesicles and the molecular dimension of polypeptide chains.

The pH-responsiveness of vesicles of $PB_{165}-PLLys_{88}$ (Fig. 1b) in dilute saline solution was studied in further detail by Sigel and Schlaad et al. using CD spectroscopy and a combined DLS/SLS analysis [22]. Vesicles were observed if the polypeptide segment was in a 100% coil conformation (pH 7.0) or in an 80% α-helical conformation (pH 10.3). Increasing pH and thus changing the conformation and degree of ionization of PLLys corona chains caused a large shrinkage of the aggregates by ∼40% (R_h : 364 → 215 nm). The change in size exceeds by far the contour length of the polypeptide chain in an all-*trans* conformation (∼30 nm); hence, the secondary structure can only be a minor factor determining vesicle size. Parallel to the decrease in size, the packing density of chains increased by 75% and the inter-chain distance at the core–corona interface decreases (b : 3.2 → 2.4 nm, assuming unilamellar bilayered membrane of vesicles). The size of aggregates is directly connected to the packing density of chains and is thus determined by the colloid stabilization properties of the PLLys chains (Fig. 2).

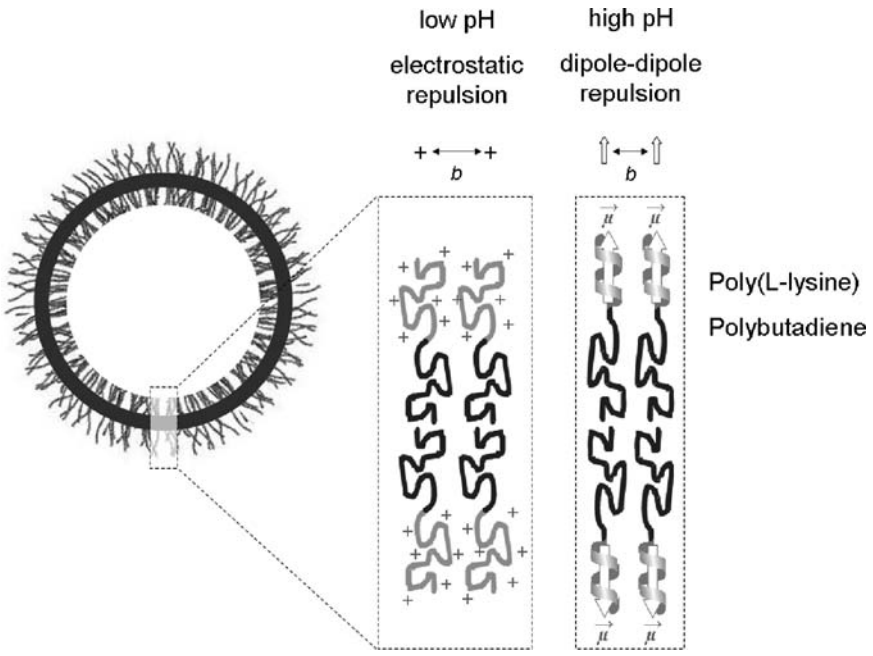

Fig. 2 Tentative structures of the bi-layered membrane of PB_{165}-*b*-$PLLys_{88}$ vesicles at different pH; *b* denotes the average distance of chains at the core–corona interface. Reprinted with permission from [22], copyright (2007) American Chemical Society

Very similar observations were made by Savin et al. [23] for vesicles of $PB_{107}-PLLys_{27}$ (Fig. 1b), which decreased in size from $R_h \sim 90$ nm (low pH) to 70 nm (high pH) sharply at pH 5. Also here, the change in size of vesicles exceeded the maximum possible difference in contour length of $PLLys_{27}$ all-*trans* and α-helical chains. Interestingly, stable vesicles were obtained at high pH (10.9) and high temperature (57 °C) when PLLys corona underwent a secondary structure transition from α-helices to β-sheets (CD). The size of vesicles increased from $R_h \sim 70$ nm (low T) to 140 nm (high T) owing to a relief of interfacial curvature. Another possible explanation could be a "flattening" of the interface due to the intermolecular hydrogen bonds in the polypeptide corona.

Zwitterionic $PLGlu_{15}$-*b*-$PLLys_{15}$ in water (Fig. 1c) can self-assemble into unilamellar vesicles with a hydrodynamic radius of greater than 100 nm (SANS), as shown by Rodríguez-Hernández and Lecommandoux [24]. A change of the pH from 3 to 12 induced an inversion of the structure of the membrane (NMR) and was accompanied by an increase of the size of vesicles from 110 to 175 nm (DLS). Whether the formation of vesicles was controlled by a secondary structure effect or simply by copolymer composition (geometry) remains an open question. Spectroscopic data supporting an α-helical conformation of the polypeptide in the hydrophobic part of the membrane, as speculated by the authors, were not provided. It appears that, however, the peptide segments could be too short to form a stable α-helix.

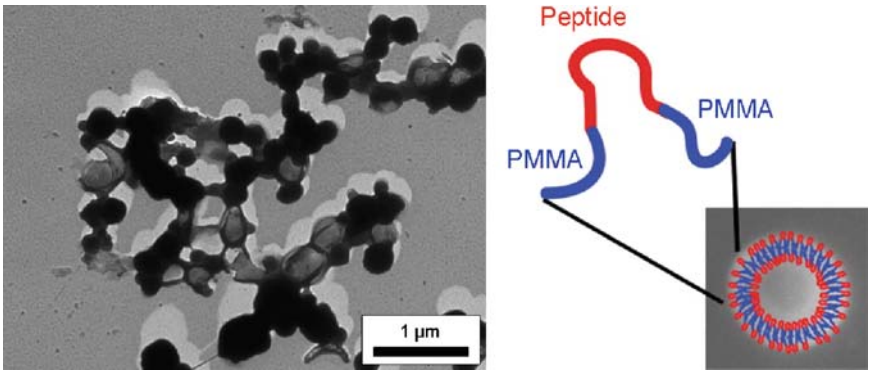

Fig. 3 *Left*: transmission electron micrograph of PMMA-*b*-peptide-*b*-PMMA vesicles (*platinum shadowed*) prepared by suspension of the triblock copolymer in THF, addition of water, and subsequent removal of THF. *Right*: illustration of the structure of vesicles. Reprinted with permission from [25], copyright (2005) Wiley Periodicals

A hybrid triblock copolymer (Fig. 1d) with a well-defined hydrophilic peptide sequence, known to form β-hairpins, flanked by two hydrophobic PMMA was prepared by van Hest et al. (by combination of solid phase synthesis and atom transfer radical polymerization) [25]. Upon suspension of the polymer in a mixture of THF and water, followed by the removal of THF, spherical aggregates (hollow or not) were formed. By different electron microscopy techniques (TEM, SEM, cryo-SEM), it was determined that these aggregates were polymer vesicles coexisting with large compound micelles (diameters ranging from 100 to 300 nm according to TEM and from 500 nm up to 10 µm according to cryo-SEM, Fig. 3) and were caused by phase separation of the hydrophilic peptide and the hydrophobic PMMA block. The expected β-hairpin formation was not observed for this peptide sequence when the polymer assembled into vesicular structures (IR spectroscopy). The authors suggested that PMMA tails aggregated within the vesicle wall thus preventing the creation of hydrogen bonds within the loop or that the aggregation occurred too rapidly, trapping the peptide in a random coil structure.

2.1.2 Graft Block Copolymers

Apart from block copolymers consisting of main-chain polypeptides (or polysaccharides), there are a couple of examples of vesicle-forming polymers carrying pendant bioorganic units. The functionalities attached as side-chains include dipeptides and sugars; see Fig. 4.

Polystyrene-*block*-poly(isocyanodipeptide)s PS_{40}-*b*-$PIAA_{10}$ (AA = L-alanine–L-alanine-$COO^{-}Na^{+}$) (Fig. 4a), introduced by Nolte et al. [26], were found to form bilayered vesicles in aqueous sodium acetate buffer solution at pH 5.6. The vesicles observed had diameters ranging from tens to hundreds of nanometers and a bilayer

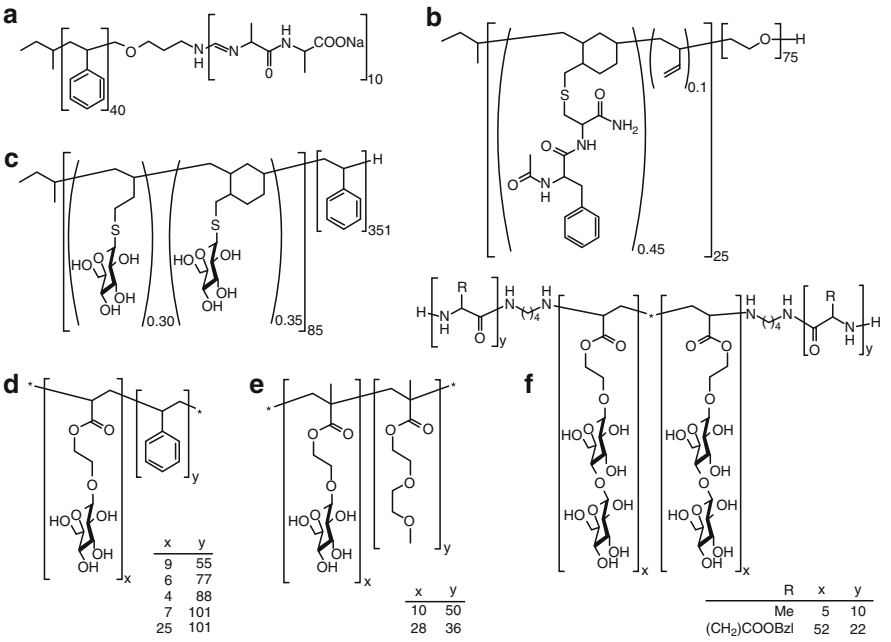

Fig. 4 a–f Chemical structures of graft block copolymers. **a** Polystyrene-*block*-polyisocyanodipeptide (PS-*b*-PIAA). **b** Dipeptide-grafted polybutadiene-*block*-poly(ethylene oxide). **c** Glycosylated polybutadiene-*block*-polystyrene. **d** Poly(2-(β-D-glucopyranosyloxy)ethyl acrylate)-*block*-polystyrene (PGEA-*b*-PS). **e** Poly(2-glucosyloxyethyl methacrylate)-*block*- poly(diethyleneglycol methacrylate) (PGEMA-*b*-PDEGMA). **f** Polypeptide-*block*-poly(2- acryloyloxyethyl lactoside)-*block*-polypeptide (PLAla-*b*-PAELA-*b*-PLAla, PBLGlu-*b*-PAELA-*b*-PBLGlu)

thickness of 16 nm. In addition, electrostatic interactions and a hydrogen bonding network between amino acids led to hierarchical superstructures such as bilayer filaments or superhelices, which could reach the length of several micrometers.

Geng and Schlaad et al. [27] (Fig. 4b) reported on the self-assembly of hybrid amphiphiles consisting of L-cysteine–L-phenylalanine dipeptide grafts attached to the PB block of PB_{25}-*b*-PEO_{75}. The precursor PB_{25}-*b*-PEO_{75} ($w_{EO} = 0.70$) at 0.1 wt% in water formed small spherical micelles with a hydrodynamic diameter of 45 nm (DLS and cryo-TEM), which with the attachment of the dipeptide ($w_{EO} = 0.43$) turned into giant vesicles of 2–5 µm in diameter (visualized by FM) (Fig. 5). The presence of the hydrophobic dipeptide decreased the weight fraction of hydrophilic EO units (w_{EO}) and thus shifted the morphology towards one with a lower curvature.

Glucose-grafted PB_{85}-*b*-PS_{351} (Fig. 4c) were found to self assemble into vesicles or "glycosomes" in organic and aqueous media [28]. In aqueous media, the vesicles measured about 240 nm in diameter (apparent value measured by DLS) and should be built of a polystyrene bilayered membrane and a glucose corona. However, the true structure of the vesicle membrane is not known yet.

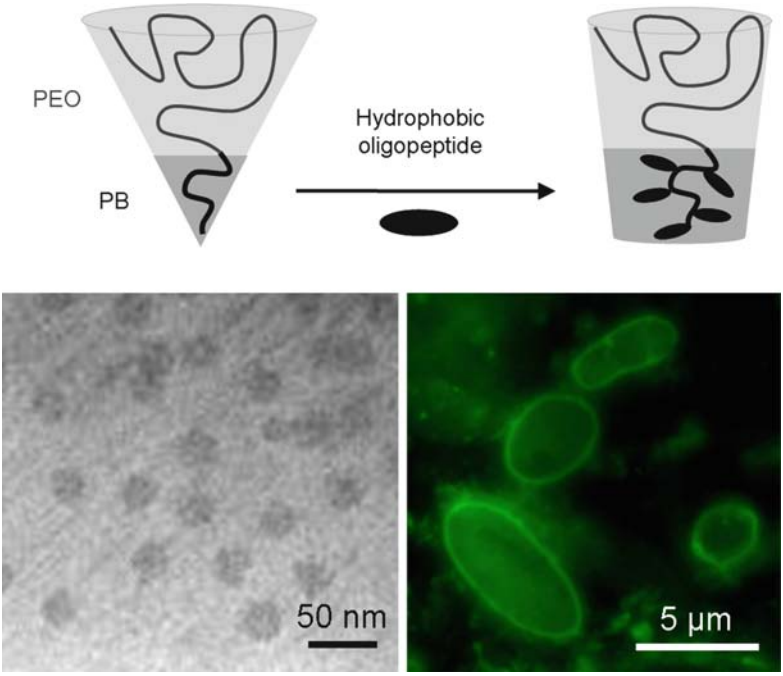

Fig. 5 Visualization of the self-assemblies of PB_{25}-*b*-PEO_{75} (*left*: cryogenic transmission electron micrograph) and of the corresponding dipeptide-grafted hybrid (*right*: fluorescence micrograph) in water [27]

Li et al. [29, 30] synthesized by ATRP a series of well-defined amphiphilic block copolymers consisting of hydrophobic PS and hydrophilic poly(2-(β-D-glucopyranosyloxy)ethyl acrylate) (PGEA) blocks (Fig. 4d). Molecular assemblies were prepared by first dissolving the copolymer in a common solvent (DMF, THF, dioxane, and their mixtures), followed by addition of water to "freeze" the PS block. Depending on the composition of the copolymer and of the solvent mixture, a variety of different morphologies could be observed including micelles, vesicles, hollow tubules, porous spheres, and large compound vesicles (clusters). The vesicular structures were usually polydisperse in size (diameter: 70–350 nm), and the membrane measured about 20–25 nm across.

Pasparakis and Alexander [31] applied controlled radical polymerization techniques (ATRP and RAFT) to synthesize two block copolymers based on the highly hydrophilic poly(2-glucosyloxyethyl methacrylate) (PGEMA) and the thermoresponsive poly(diethyleneglycol methacrylate) (PDEGMA; LCST at 28 °C) (Fig. 4e). As indicated by DLS and SEM, in dilute aqueous solution, the polymers assembled into vesicles with mean diameters of approximately 250 nm (polymer containing 15 wt% Glc) and 500 nm (34 wt% Glc) at 20 °C (Fig. 6). Actually, one would have expected that the less hydrophilic polymer formed the larger vesicles with lower curvature [27]. Above the LCST of PDEGMA, at 37 °C, the size of the vesicles

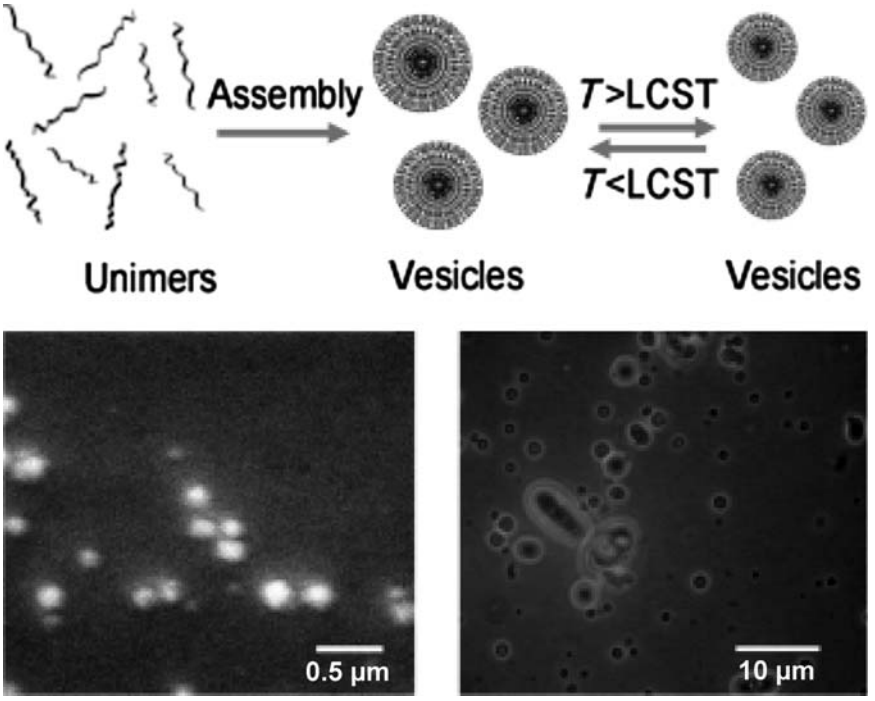

Fig. 6 *Top*: Self-assembly and thermal response of PGEMA-*b*-PDEGMA vesicles in aqueous solution. *Bottom, left*: Scanning electron micrograph of collapsed glycopolymer (15 wt% Glc) vesicles. *Bottom, right*: Optical micrograph of an 0.3 wt% aqueous solution of glycopolymer (34 wt% Glc) vesicles. Reprinted with permission from [31], copyright (2008) Wiley

decreased to 180 and 300 nm, respectively, which was attributed to the increased hydrophobicity and collapse of the PDEGMA blocks. More detailed information on the structure of vesicles is not provided (see illustration in Fig. 6).

In aqueous solution, symmetric triblock copolymers with a middle poly(2-acryloyloxyethyl lactoside) block and two outer polypeptide blocks (either poly(L-alanine) [32,33] or poly(γ-benzyl-L-glutamate) [32,33]) (Fig. 4f) formed aggregates being spherical in shape and 200–700 nm in diameter (TEM). TEM further revealed a compact structure of the aggregates like for multilamellar vesicles. The dimension of the particles, however, was decreasing with increasing concentration of the copolymer. Chaikof and Dong et al. discussed a combination of hydrophobic interactions and highly cooperative intramolecular and intermolecular hydrogen bonding as the driving force for the association of these glycopolymers in water.

2.1.3 Homopolymer Amphiphiles

A number of vesicle-forming biohybrid amphiphiles based on either hydrophilically or hydrophobically modified polymers have very recently been described – see the chemical structures in Fig. 7.

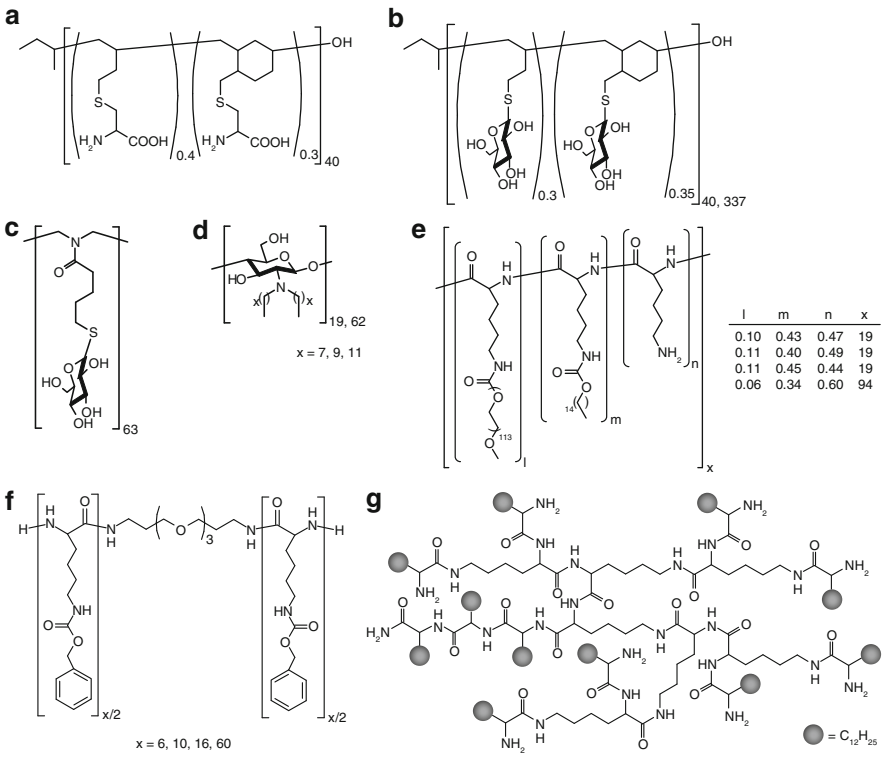

Fig. 7 a–g Chemical structures of biohybrid homopolymer amphiphiles. **a** L-Cysteine-grafted polybutadiene. **b** Glycosylated polybutadiene. **c** Glycosylated poly(2-oxazoline). **d** *N,N*-Dialkyl chitosan. **e** Amphiphilic poly(L-lysine). **f** PEGylated poly(*Z*-L-lysine). **g** Lipid-lysine dendron

Schlaad et al. [34] produced a biohybrid polymeric amphiphile by free-radical addition of an L-cysteine derivative onto a 1,2-PB with 40 repeat units (Fig. 7a). The zwitterionic polymer could be dispersed into very acidic $(\mathrm{pH} < 2.3)$ or basic $(\mathrm{pH} > 9)$ aqueous solutions under the formation of vesicles. As shown by DLS and SAXS in solution, the vesicles were about 250 nm in diameter and had a multilamellar structure with a lamellar spacing of about 7 nm.

PB_{40} and PB_{337} were glycosylated with thio-glucose (Fig. 7b) and used for the production of glucose-based vesicles or "glycosomes" [34, 35]. Both glycopolymers self-assembled in water into large unilamellar vesicles having a hydrodynamic radius of $R_\mathrm{h} \approx 260$–$280\,\mathrm{nm}$ and a less than 4 nm-thick (bilayered) membrane, as suggested by DLS/SLS, SAXS and TEM (Fig. 8). Due to the softness of the particles, neither the mass coverage of the vesicle shell nor the thickness of the membrane could be precisely determined. Interestingly, the two SAXS curves exhibited a vesicle form factor minimum at the same scattering vector, $s = 0.4\,\mathrm{nm}^{-1}$. The thickness of the membrane is thus not affected by the length of the PB chain, suggesting that the chains are oriented parallel to the interface. That is why a very thin polymer

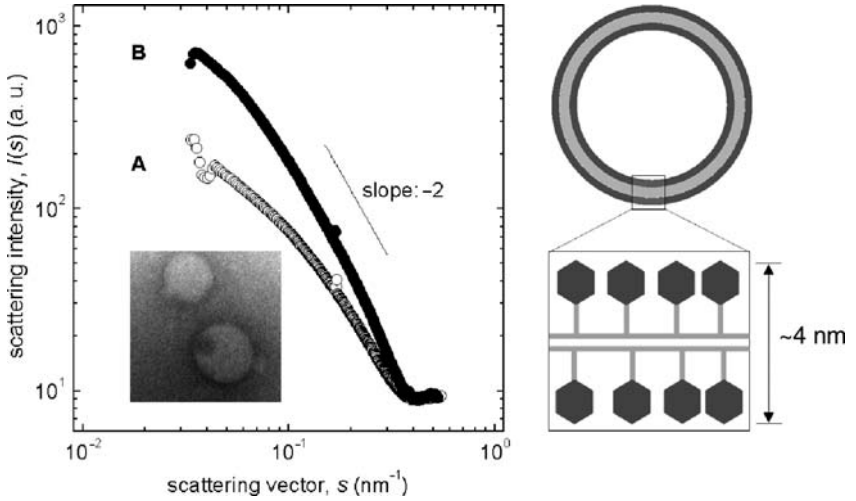

Fig. 8 *Left*: SAXS curves measured for 10 wt% aqueous solutions of glucose-grafted PB_{40} (*curve A*) and PB_{337} (*curve B*); *inset* shows cryo-TEM image of vesicles as formed in a 0.5 wt% solution of glucose-grafted PB_{40} (stained with OsO_4). *Right*: Schematic illustration of the structure of vesicles with a bilayered membrane (glucose units are represented as hexagons) [34, 35]

membrane of less than 4 nm can be formed, as thin as the membrane of a liposome. Another consequence of the "comb-shaped" structure of chains and the parallel orientation in the membrane is that vesicles are formed despite of the high weight fraction of hydrophilic glucose units ($w_{hydro} \sim 55\%$); phospholipids are usually much less hydrophilic, and block copolymers of such composition would have assembled into spherical or worm-like micelles [2].

Likewise, a glycosylated polyoxazoline or glycopolyamide homopolymer (Fig. 7c) formed spherical vesicles being about 60 nm in diameter (SEM). Further details concerning the structure membrane have not been provided. It is further noteworthy that the vesicle coexisted with hollow nanotubes [36].

Li et al. [37] described a series of *N*,*N*-dialkyl chitosans (alkyl = octyl, decyl, and dodecyl) (Fig. 7d), which in neutral water formed stable bilayered vesicles having hydrodynamic diameters in the range of 100–200 nm (DLS). It was found that the size of vesicles increased with increasing molecular weight of the hydrophilic chitosan backbone and/or increasing length of the hydrophobic alkyl side chains, which was attributed to a more compact structure of the membrane.

A new polymeric amphiphile based on cationic poly(L-lysine), which was partially modified with hydrophobic palmitoyl chains and hydrophilic neutral methoxy-poly(ethylene glycol) (Fig. 7e), was introduced by Uchegbu et al. [38, 39]. In water in the presence of cholesterol, these copolymers assembled into vesicles with diameters ranging from 200 to 600 nm (DLS, freeze-fracture TEM), depending on the chemical composition of the copolymer and the length of the polypeptide backbone. More detailed information about the secondary structure of chains and the structure of vesicle membranes were not given.

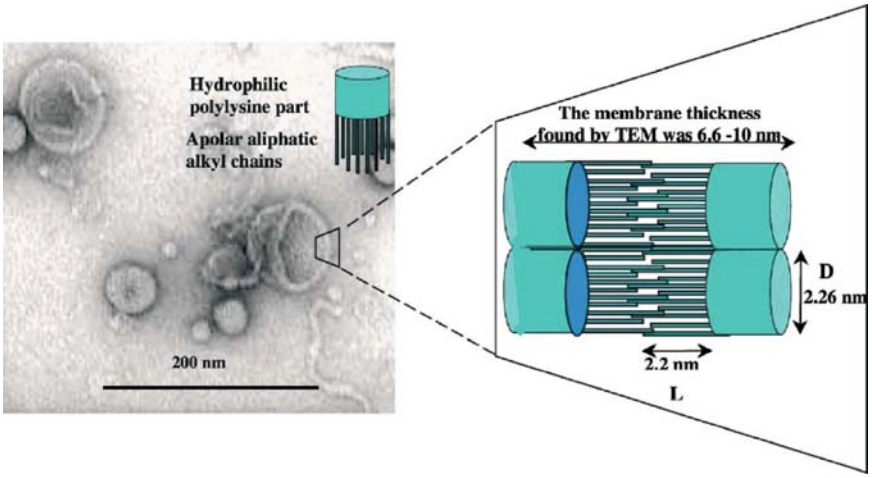

Fig. 9 *Left*: Transition electron micrograph of lipid-lysine dendron vesicles with a 6–10 nm thick membrane. *Right*: Illustration of the structure of the bilayered membrane. Reprinted with permission from [41], copyright (2003) Elsevier Science

Poly(*Z*-L-lysine)-based amphiphiles with 6–60 repeat units using diethylene glycol *bis*(3-amino propyl) ether as a bifunctional initiator (Fig. 7f) were synthesized by Jing et al. [40]. By dialysis from DMF into water, vesicles with hydrodynamic radii ranging from 40 to 160 nm (DLS), respectively 70 to 280 nm (TEM), were obtained. As expected, vesicle size increased with increasing molecular weight or hydrophobic fraction of PZLLys. The rather small size of the vesicle indicates that there is no major contribution from hydrogen bonding interactions or from the secondary structure.

Based on geometric considerations, amphiphiles consisting of a hyperbranched or dendritic hydrophilic part are not expected to assemble into vesicular aggregates in aqueous solution. However, Florence et al. [41, 42] reported that a lipid-lysine dendron (a lysine dendron made by solid-phase synthesis and subsequently hydrophobically modified by lipids) (Fig. 7g) can well produce small vesicles or "dendrisomes." These vesicles exhibited an average diameter of (311 ± 8) nm and a thickness of the membrane of 6–10 nm. Based on calculated dimensions, the authors postulate the formation of bilayer structures with the hydrophilic polylysine head groups directed towards the aqueous phase and the hydrophobic alkyl chains associating with the hydrophobic regions of neighboring dendrons (Fig. 9).

2.2 *Hydrogen Bonding and Secondary Structure Interactions*

Hydrogen bonding and secondary interactions may not be the origin of aggregation of block copolymers but can cause deviations from the "expected" phase behavior. An asymmetric block copolymer consisting of a minor polypeptide fraction may

assemble into vesicles, although the composition of the sample would suggest the formation of micelles. Evidently, vesicles are preferred for block copolymers with α-helical polypeptide chains whereas tape-like structures or fibrils are produced by β-sheet forming polypeptides [43, 44]. However, vesicles with other than polypeptide membranes have not been described yet (with one exception, see below). The polypeptide block copolymers reported to form vesicles through secondary structure interactions are shown in Fig. 10.

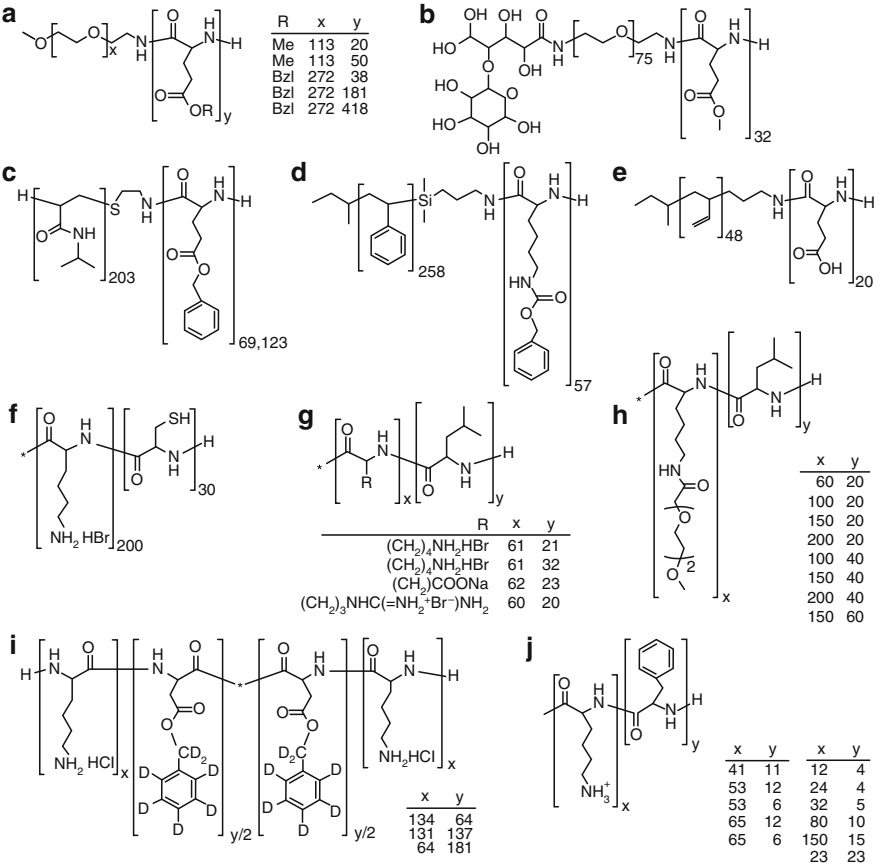

Fig. 10 a–j Chemical structures of hybrid and peptide-based block copolymers. **a** Poly(ethylene oxide)-*block*-poly(γ-methyl/benzyl-L-glutamate) (PEO-*b*-PMLGlu, PEO-*b*-PBLGlu). **b** Lactose-poly(ethylene oxide)-*block*-poly(γ-methyl-L-glutamate) (Lac-PEO-*b*-PMLGlu). **c** Poly(*N*-isopropylacrylamide)-*block*-poly(γ-benzyl-L-glutamate) (PNIPAM-*b*-PBLGlu). **d** Polystyrene-*block*-poly(Z-L-lysine) (PS-b-PZLLys). **e** 1,2-Polybutadiene-*block*-poly(L-glutamate) (PB-*b*-PLGlu). **f** Poly(L-lysine)-*block*-poly(L-cysteine) (PLLys-*b*-PLCys). **g** Poly(L-lysine)-*block*-poly(L-leucine) (PLLys-*b*-PLLeu), poly(L-glutamate)-*block*-poly(L-leucine) (PLGlu-*b*-PLLeu), poly(L-arginine)-*block*-poly(L-leucine) (PLArg-*b*-PLLeu). **h** Poly(N^{ε}-[2-(2-(methoxyethoxy)ethoxy)]acetyl-L-lysine)-*block*-poly(L-leucine) (PELLys-*b*-PLLeu). **i** Poly(L-lysine)-*block*-poly(γ-benzyl-d_7-L-glutamate)-*block*-poly(L-lysine) (PLyys-*b*-PBLGlu-*b*-PLLys). **j** Poly(L-lysine)-*block*-poly(L-phenylalanine) (PLLys-*b*-PLPhe)

2.2.1 Hybrid Block Copolymers

The aggregation behavior of PEO-*b*-PMLGlu (Fig. 10a) and Lac-PEO-*b*-PMLGlu in water (Lac = lactose, Fig. 10b) was studied by Yonese et al. [45]. As indicated by DLS, the block copolymers was formed of large aggregates with a hydrodynamic radius of about 250 nm, supposedly vesicles. Key in the aggregation behavior might be the association of α-helical poly(γ-methyl-L-glutamate) segments, as evidenced by CD spectroscopy, promoting the formation of plane bilayers which then close into vesicles. Further systematic study on this system and detailed analysis of structures are lacking. The lactose units were recognized by RCA_{120} lectin, indicating that they are located on the surface of the glycopolymer aggregate.

Closely related to this system are the PBLGlu-based block copolymers with a second PEO (Fig. 10a) or PNIPAM (Fig. 10c) block described by Cho et al. [46,47]. The aqueous polymer solutions, prepared by the dialysis of organic solutions against water, contained large spherical aggregates ($R_h > 200$ nm) with a broad size distribution (DLS). Although the size suggested a vesicular structure of the aggregate, the aggregation number was just about 100 (way of determination not specified); however, values of aggregation numbers of polymer vesicles are typically in the order of several thousands [1]. It is also noteworthy that the PNIPAM chains exhibit LCST behavior. Raising the temperature to the LCST (∼34 °C) had no serious impact on the size of aggregates, which, however, could be a matter of the "frozen" state of the PBLGlu core.

Schlaad et al. [48] demonstrated that PS_{258}-*b*-$PZLLys_{57}$ (Fig. 10d) with a rather low content of peptide (18 mol%) can assemble into vesicles and bilayers in dilute CCl_4 solution. The vesicles were about 300–600 nm in diameter (SEM). The preference for a lamellar structure was attributed to the stiffening of the PZLLys core by the 2D-arrangement of crystallizable α-helices.

Likewise, the dissolution of a glucose-grafted PB_{85}-*b*-PS_{351} (17 wt% glucose, Fig. 4c) into THF resulted in the formation of vesicles ($R_h \sim 250$ nm, DLS) with a membrane measuring about 15 nm across (TEM) [28]. The membrane is thought to be built of hydrogen-bridged glucose units.

Vesicles were also observed for PB_{48}-*b*-$PLGlu_{20}$ in THF and in CH_2Cl_2 organic solutions (R_h = 106–108 nm, DLS/SLS) [20]. The formation of vesicles rather than micelles was attributed to the α-helical secondary structure of the insoluble PLGlu. However, experimental proof for the presence of any α-helices in the membrane was not given.

2.2.2 Block Copolypeptides

Deming et al. [49, 50] synthesized a series of cysteine–lysine diblock copolypeptides (Fig. 10f) in order to direct the self assembly of silica and gold nanoparticles. Dynamic light scattering measurements of $PLCys_{30}$-*b*-$PLLys_{200}$ in aqueous solution (under nitrogen atmosphere) showed that this polymer self-assembled into large vesicular aggregates of about 600 nm in diameter. A feature of the cysteine residues is their ability to form covalent disulfide bonds as inter- and intrachain crosslinks

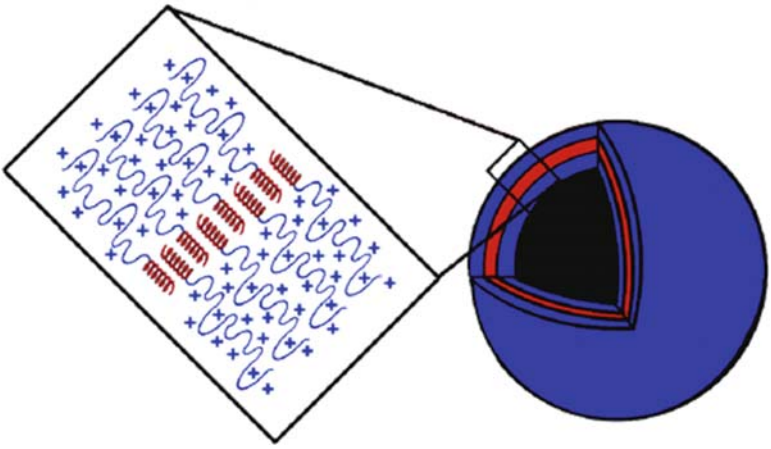

Fig. 11 Schematic drawing showing the self-assembly of $PLLys_{60}$-*b*-$PLLeu_{20}$ into vesicles. Reprinted with permission from [51], copyright (2005) American Chemical Society

upon oxidation of the thiol groups for instance in air. The formation of such disulfide crosslinks was evident from the high viscosity exhibited by this sample upon exposure to water. Dynamic light scattering measurements showed that upon oxidation the block copolymer vesicles increased in size by a factor of two (diameter: 1.3 µm).

Further studies involved the aqueous self-assembly of a series of poly(L-lysine)-*block*-poly(L-leucine) copolymers (PLLys-*b*-PLLeu, Fig. 10g) [51]. The PLLys segments are highly charged cationic polyelectrolytes at neutral pH and dissolve readily in water; the hydrophobic PLLeu segments can adopt α-helical conformations if the length of the block is sufficiently long. $PLLys_{60}$-*b*-$PLLeu_{20}$ formed giant unilamellar vesicles (Fig. 11) being 1–3 µm in diameter (as observed by TEM, DIC, and LSCM), which can be explained with the intermembrane repulsion between highly charged chains. Importantly, only those samples with predominantly helical hydrophobes were forming vesicles. The vesicular self-assembly shows dynamic properties, indicating a high degree of membrane fluidity (TEM). This characteristic provides stimuli-responsive properties to the vesicles and allows fine adjustment of vesicle size using liposomes-based extrusion techniques.

Nonionic block copolypeptides made of PEGylated L-lysine and L-leucine residues, PELLys-*b*-PLLeu (Fig. 10h) have also been described [52]. The copolymers adopted a rod-like conformation, due to the strong tendency of both segments to form α-helices (CD spectroscopy), and produced a variety of self-assembled structures in aqueous solution. Micrometer vesicles and sheet-like membranes could be obtained for copolymers with fractions of the hydrophobic leucine ranging from 10 to 30 mol%. Conventional uncharged block copolymers of this composition would be expected to form spherical or cylindrical micelles. The assembly into bilayers was related to a secondary structure effect, as illustrated in Fig. 12. Accordingly, samples with the same composition but nonhelical chain conformation (CD),

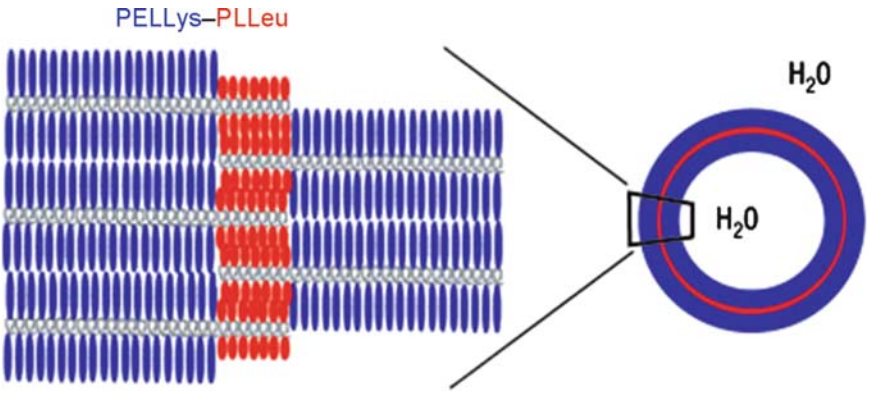

Fig. 12 Illustration of the packing of α-helical PELLys-*b*-PLLeu copolymer chains in the vesicle wall. Reprinted with permission from [52], copyright (2004) Macmillan

prepared by polymerization of racemic monomers, were not found to form giant vesicles. It is further noteworthy that the vesicles gained pH-responsiveness when L-leucine residues in the hydrophobic part were statistically substituted by L-lysine. Acidification of the solution resulted in a protonation of the amine functionalities and the near-instantaneous disruption of the vesicle membrane.

Poly(L-arginine)$_{60}$-*block*-poly(L-leucine)$_{20}$ (PLArg-*b*-PLLeu, Fig. 10g) showed similar physical properties as PLLys$_{60}$-*b*-PLLeu$_{20}$ and also formed micrometer-sized vesicles in aqueous solution. These vesicles were able to entrap water-soluble species, such as dextran, and could be extruded through polycarbonate filters to yield stable, low-polydispersity vesicles of controllable diameter down to 50 nm [53].

Iatrou and Hadjichristidis et al. [54] reported on amphiphilic triblock copolypeptides based on two poly(L-lysine hydrochloride) outer blocks and an (once broken) α-helical poly(γ-benzyl-d$_7$-L-glutamate) middle block (Fig. 10i). All samples, which had similar molecular weights with varying contents of PBLGlu (19–74%), formed vesicles with $R_g \approx R_h$ = 130–145 nm (SLS/DLS) in water at neutral pH at 25 °C. Further evidence for the existence of vesicles was provided by SANS, cryo-TEM, SEM, and SFM. Owing to the architecture of the copolypeptide, it was proposed that the membrane had a monolayered structure. The robustness and compactness of the membrane increased with increasing fraction of PBLGlu, as supported by SANS and SFM. Interestingly, the size of vesicles could be triggered by changing pH and/or temperature. Samples initially measured at pH 7.4 were brought to pH 11.7 (PLLys: random coil → α-helix, CD spectroscopy), resulting in a shrinkage of the vesicles ($R_h \sim 140 \rightarrow 100$ nm) without noticeable change in the aggregation numbers (DLS/SLS). Since the PBLGlu block is not sensitive to any change of pH or temperature (CD), the changes in size of vesicles were attributed to the reduced molecular dimensions of the PLLys block (extended coil vs α-helix, see Fig. 13). Annealing of the solution at 37 °C for 4 h resulted in the formation of larger vesicles ($R_h \sim 100 \rightarrow 140$ nm), similar or slightly larger than the vesicles detected at pH 7.4 at 25 °C. The dimension of the vesicles was rationalized by the transition of the PLLys chains from α-helix to β-sheet (CD), as illustrated in Fig. 13.

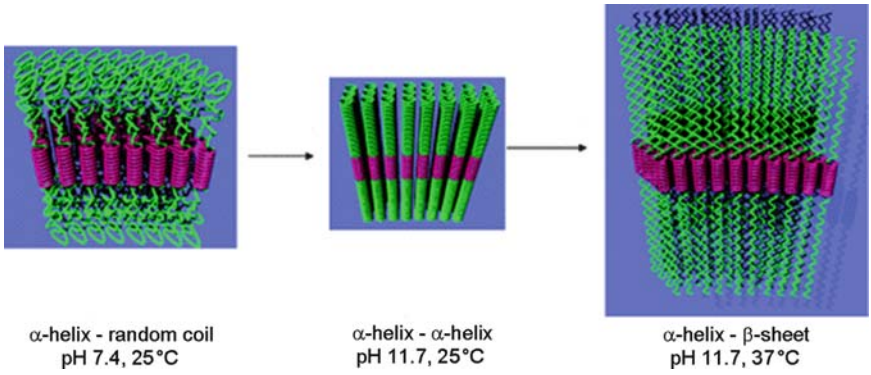

Fig. 13 Schematic representation of PLLys-*b*-PBLGlu-*b*-PLLys vesicles and the influence of the pH and temperature on the dimensions of the PBLGlu monolayer and vesicle size. Reprinted with permission from [54], copyright (2007) American Chemical Society

Jing et al. [55] and Shantz et al. [56] studied the aggregation behavior of cationic poly(L-lysine)-*block*-poly(L-phenylalanine) copolypeptides (PLLys-*b*-PLPhe, Fig. 10j) in aqueous solution. The polymers consisted of 4–15 phenylalanine repeat units with a hydrophobic mole fraction ranging from 8 to 25% (one sample contained 50 mol% PPhe with 23 units) and were found to assemble into large vesicles with diameters of 1–6 μm (SFM) [55] or 100–400 nm (DLS) [56]. Evidence for the existence of vesicles came from SFM (samples spin-coated on silicon wafers) or from TEM (silica replica), respectively. The formation of vesicles from these nonsymmetric copolymers is surprising (see above) and has been explained by hydrogen bonding interactions between the PPhe chains and by the secondary structure, but without providing any experimental evidence [55]. Speaking against a secondary structure effect is, however, that copolymer samples with a racemic poly(DL-phenylalanine) block also assembled into vesicles [56]. Another unexpected observation was that the vesicles increased in size with increasing length of the block copolymer chains and increasing Lys/Phe ratio. After all, the mechanism of PLLys-*b*-PLPhe vesicle formation needs to be clarified.

2.3 Supramolecular Complexation

Two supramolecular biohybrid block copolymer systems forming vesicles in aqueous solution have been described in the literature (Fig. 14).

Kataoka et al. [57, 58] investigated the formation of polyion complexes (PIC) from a pair of oppositely charged polypeptide block copolymers, namely of anionic poly(ethylene oxide)-*block*-poly(α,β-aspartate) and cationic poly(ethylene oxide)-*block*-poly([2-aminoalkyl]-α,β-aspartamide) (see structure in Fig. 14a), in an aqueous milieu. Mixing of the double-hydrophilic copolymers at an equimolar

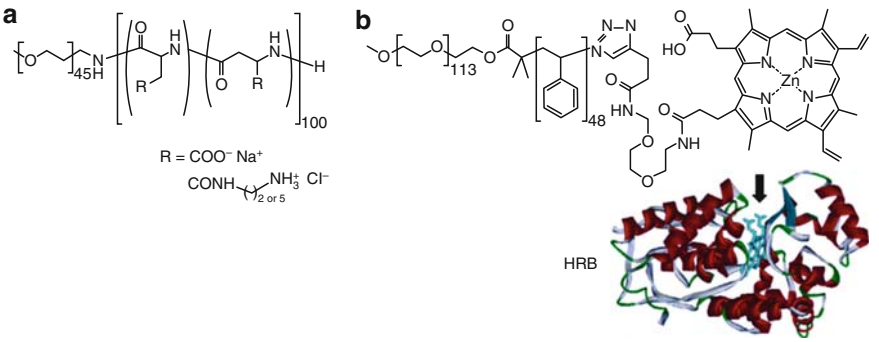

Fig. 14 a,b Chemical structures of **a** poly(ethylene glycol)-*block*-poly(α,β-aspartate) (PEG-*b*-PAsp) and poly(ethylene glycol)-*block*-poly(α,β-aspartamide) (PEG-*b*-PAspA), **b** poly(ethylene oxide)-*block*-polystyrene–protoporphyrin IX (PEO-*b*-PS-PPIXZn) and crystal structure of horse radish peroxidase (HRP); the *arrow marks* the positioning of the cofactor

ratio of charged units at pH 7.4 resulted in the formation of hollow spherical particles or vesicles being up to 10 µm in diameter, as indicated by dark-field microscopy (DFM). The optimized ratio of charged segments relative to the PEO segments led to the formation of the vesicles (referred to as "PICsomes") rather than micelles [59]. Interestingly, the size of the vesicles decreased significantly to <1 µm when the alkyl spacer in the cationic segment consisted of two instead of five methylene units, which was attributed to the flexibility of the PIC membrane. The hydrophobic PIC membrane was not only flexible but also exhibited semipermeable character, which is amazing considering that a polyion complex should be a highly cross-linked physical network.

Nolte et al. [60, 61] introduced a route towards giant amphiphiles by cofactor reconstitution. A synthetic polymer, polystyrene or poly(ethylene oxide)-*block*-polystyrene, was first functionalized with a heme cofactor, protoporphyrin IX (PPIXZn), and subsequently reconstituted with an apo protein, myoglobin or horse radish peroxidase (HRP) (see Fig. 14b and Fig. 15). The PEO_{133}-*b*-PS_{48} precursor formed small spherical micelles in water (Fig. 15); the solution was prepared by injection of the polymer in THF into water. After the reconstitution with the hydrophilic apo-HRP, the triblock biohybrid sample PEO_{113}-*b*-PS_{48}-*b*-HRP assembled into submicron vesicles with broad size distribution. The hydrophobic membrane is built by the polystyrene middle block and is stabilized by poly(ethylene oxide) chains and protein. Whether the membrane has a mono- or a bilayered structure and whether the PEO and HRP are segregated or mixed in the corona is not know yet. Also, the opposite of what would be expected, increasing the hydrophilic fraction in a block copolymer (by attachment of protein) led to the formation of aggregates with a lower curvature.

It is further noteworthy that a large variety of other aggregate structures (micellar rods, toroids, etc.) could be produced depending on the protein and the composition of the precursor block copolymer.

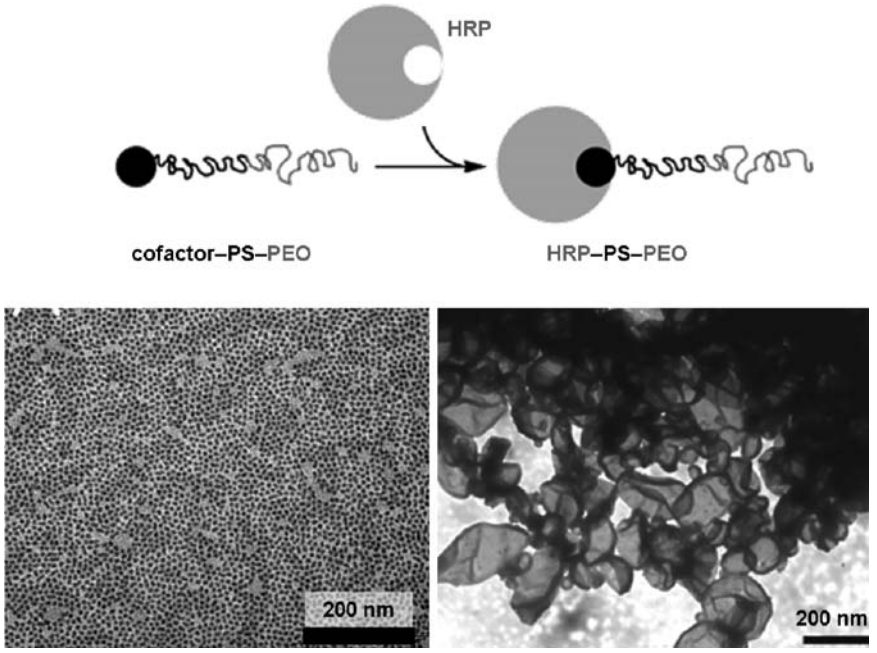

Fig. 15 *Top*: formation of a giant amphiphile from a synthetic polymer reconstituted with a heme cofactor and horse radish peroxididase (HRB). *Bottom*: transmission electron micrographs of PEO_{113}-*b*-PS_{48} micelles (*left*) and PEO_{113}-*b*-PS_{48}-HRP vesicles (*right*) formed in water. Reprinted with permission from [60], copyright (2007) American Chemical Society

3 Applications

Some of the sugar- and peptide-based vesicles described in the previous chapter have been used for very few applications in the field of life science (as carriers for drug, genes, etc. or as bioreactors) and for the fabrication of organic/inorganic composite materials (encapsulation of inorganic nanoparticles).

3.1 Life Science

Low-molar mass lipids have been known for more than 30 years for their ability to self-assemble into vesicles or liposomes, however, with limited overall stability. Polymer membranes, on the other hand, are almost one order of magnitude tougher and at least 10 times less permeable to water than common phospholipids bilayers, due to the increased length and conformational freedom of polymer chains compared to lipids [1]. Biohybrid polymer vesicles combine the toughness of polymers and the biocompatibility of peptides or sugars, making them promising candidates

for biomembrane formation with improved drug delivery properties. The use of polymer vesicles for drug delivery and gene therapy was pioneered by Ringsdorf et al. [62]. Other potential applications of polymer vesicles include the use as bioreactors, artificial cells, etc.

3.1.1 Drug and Gene Carriers

The multilamellar vesicles based on zwitterionic L-cysteine modified PB (Fig. 7a) were considered by Koňák and Štěpánek et al. [63] as gene delivery vectors mimicking the surface of viruses. The surface could effectively be coated with a positively charged hydrophilic poly(*N*-(2-hydroxypropyl)methacrylamide) copolymer (PHPMA) carrying reactive thiazolidine-2-thione groups, rendering the vesicles stable against changes in pH. It is supposed that the covalent coating with PHPMA may protect the delivery vector from interactions with proteins and cells, thus avoiding degradation, and prolong the circulation time in blood. Biological tests are pending.

The polymer vesicles based on cationic poly(L-lysine) modified with palmitoyl and PEG chains (Fig. 7e) strongly interacted with anionic plasmid DNA (polymer:DNA $\geq$ 5:1 w/w) under the formation of polyion complexes ("polyplexes") [38]. The interaction was strong despite the decreased number of binding sites and the absence of receptor specific ligands, and the gene transfer to human tumor cell lines was improved in comparison to the PLLys. In vitro biological testing revealed that the modified poly(L-lysine) vesicle–DNA complexes are more hemolytic but about one to two orders of magnitude less cytotoxic than the parent PLLys–DNA.

The micron-sized vesicles based on poly(L-lysine)-*block*-poly(L-phenylalanine) (Fig. 10j) were investigated for a potential use in drug and gene delivery [55]. Jing et al. suggested a very strong binding of DNA to these copolypeptides because of electrostatic interactions with lysine units and hydrophobic interactions between nucleobases and phenyl groups [64]. Accordingly, the addition of the copolymer to calf-thymus DNA solution resulted in the formation of irregular particles of $<2\,\mu m$ in size rather than vesicles. Further studies remain to be carried out.

Iatrou and Hadjichristidis et al. [54] showed that plasmid DNA (pDNA) could be condensed onto the large vesicles of poly(L-lysine hydrochloride)-*block*-poly(γ-benzyl-d_7-L-glutamate)-*block*-poly(L-lysine hydrochloride) (Fig. 10i). The fact that the copolypeptide vesicles remained intact could be attributed to the rigidity of the hydrophobic membrane built of helical PBLGlu chains. The molecular characterization of the vectors (UV spectroscopy, DLS, and SFM) indicated that the pDNA was partially condensed on the PLLys phase and partially encapsulated inside the vesicle. The synthesized vectors thus combine the advantages of the polylysine–DNA systems to condense large amounts of genes, as well as those of the liposome–DNA systems to better protect the encapsulated DNA. These vectors are expected to present better gene transfection efficiency to the cell nucleus.

Deming et al. [53] used large vesicles based on poly(L-arginine)$_{60}$-*block*-poly(L-leucine)$_{20}$ (Fig. 10g) (labeled with fluoresceine for LSCM imaging) for

intercellular delivery. The rational for using poly(L-arginine) goes back to protein-transduction domains (PTD) to enhance the intracellular delivery of cargoes. A well-studied example is the arginine-rich segment (residues 49–57: RKKRRQRRR) of the transactivator of transcription for HIV-1 (HIV-1 Tat), which could even be replaced by a simple nonamer of arginine (references in [53]).

In order to see if the PLArg segments enhance a transport across membrane interfaces, the authors studied the partitioning of the polypeptide vesicles at water/chloroform interfaces. Similar to PTD conjugates, the copolypeptide vesicles remained in the aqueous phase when the chloroform phase contained a neutral zwitterionic lipid and was transferred into the organic phase when an anionic lipid (egg yolk phosphatidyl glycerol, EYPG) was used. This attests to the importance of counterion binding to the arginine residues for transport. Furthermore, when the chloroform–EYPG solution was layered with a fresh aqueous phase containing sulfate ions, which bind to guanidine residues stronger than to phospholipid headgroups, the vesicles were found to migrate back from the organic to the aqueous phase, demonstrating the capability for transport in and out of a hydrophobic environment, analogous to membrane transport.

The testing of the potential use of $PLArg_{60}$-*b*-$PLLeu_{20}$ for intracellular delivery in vitro was done with 100 nm-sized vesicles containing the model cargo Texas-Red-labeled dextran. Examination of the nonfixed cells using LSCM showed that the vesicles and their contents were rapidly taken up by two representative cell lines (epithelial and endothelial relevant in oral and intravenous drug delivery, respectively), similar to the uptake observed for smaller oligoarginine PTDs. However in this system the polyarginine segments are tethered together in the vesicular assembly and thus not free to diffuse in solution, which can mask some of the guanidine groups by allowing only the chain ends to interact with the cell surfaces. Furthermore, as the oligoleucine hydrophobic interactions are stronger than the polyarginine–cell interactions, the vesicles do not disrupt cell binding, showing the robust nature of these vesicles and their potential to carry large cargoes across interfaces without leakage. Thus, self-assembly of the PLArg-*b*-PLLeu copolypeptides into vesicles helps them to function as effective intracellular delivery vehicles, despite the presence of large polycationic segments.

3.1.2 Cell Surface Recognition

Pasparakis and Alexander [31] studied the polyvalent binding activity of glycopolymer vesicles bearing glucose recognition elements on the surface (PGEMA-*b*-PDEGMA, Fig. 4e) by assays with FTIC-concanavalin A (con A), a lectin with high affinity to glucose (and extensively used to study carbohydrate interactions). It could be demonstrated that the glycopolymer vesicles were able to accommodate the lecitin at their surfaces, more efficiently than the model PGEMA homopolymer. Further studies involved carbohydrate interaction of the vesicles with a mutant *Escherichia coli* strain (MG1655pGFP) that is both green fluorescent and expresses the *fim*H protein having binding specificity for glucose and mannose. The smaller

vesicles of $PGEMA_{10}$-*b*-$PDEGMA_{50}$ (250 nm in diameter) formed large aggregates with the bacteria, each cluster containing approximately 60–90 vesicles and 100–150 bacteria, whereas the larger vesicles of $PGEMA_{28}$-*b*-$PDEGMA_{36}$ (500 nm, comparable to the size of *E. coli*) did bind to the bacteria but did not form clusters (as observed by FM). The induction of bacterial cluster formation followed the same trend as with con A interactions, which the authors attributed to the different size, mass, surface–volume ratios, and momentum in suspension of the two vesicles. Addition of glucose into the preformed bacteria–vesicle aggregates resulted in a dose-dependent breakdown of the cell–polymer clusters. This effect was most noticeable for the smaller vesicles, but was also apparent in the mixture of the larger vesicles with *E. coli*. Furthermore, it was demonstrated that the disruption of vesicles and the delivery of a molecular cargo could be triggered by the contact with bacteria. Vesicles of $PGEMA_{28}$-*b*-$PDEGMA_{36}$ were loaded with an orange–red fluorescent dye, ethidium bromide, and exposed to *E. coli*. The bacteria associated with vesicles initially showed green fluorescence, which over time (30 min) changed into orange–red through the transfer of ethidium bromide from the vesicle to the bacterial cytoplasm (Fig. 16). This process of molecular transfer is specific as it only occurs for those vesicles that are bound to a cell. The glycopolymer vesicles are therefore considered as mimics of natural cells with potential applications in cell sensing, therapeutics, and synthetic biology.

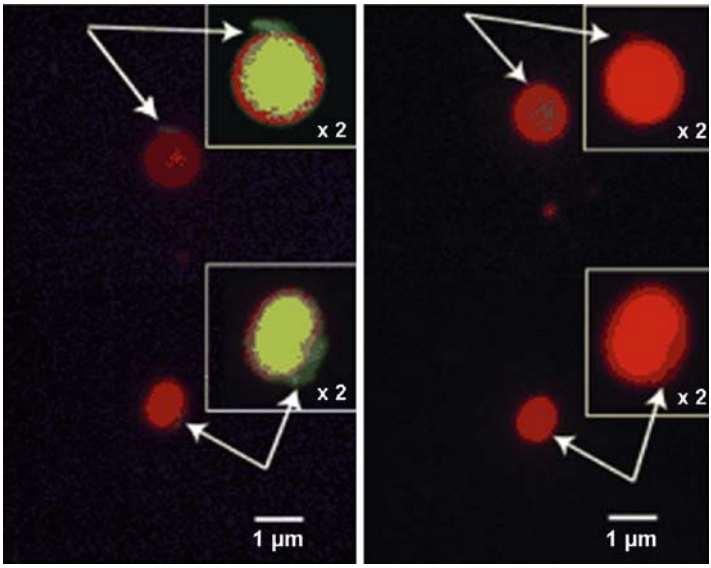

Fig. 16 Optical micrographs (fluorescence mode) of aggregates of glycopolymer vesicles (loaded with ethidium bromide, *orange–red*) and *E. coli* bacteria cells (*green*, marked with arrows) at $t = 0$ min (*left*) and $t = 30$ min (*right*). *Insets* show vesicles at higher image contrast and $\times 2$ magnification. Reprinted with permission from [31], copyright (2008) Wiley

3.1.3 Bioreactors

Polyion complex vesicles ("PICsomes") made from PEG-*b*-PAsp and PEG-*b*-PAspA (Fig. 14a), as described by Kataoka et al. [57, 58], are stable in proteinous medium and have a semipermeable membrane with a three layered structure. Vesicles loaded with Mb were prepared by simply mixing aqueous solutions of PEG-*b*-PAsp containing Mb and PEG-*b*-PAspAP at equimolar ratio of charges. The encapsulation of Mb into the PICsomes, being 0.5–5 µm in size, could be directly observed by LSCM and was also confirmed by UV spectroscopy. The practical feasibility of this system as an oxygen carrier could be demonstrated by the alternating introduction of oxygen and argon gas to the solution. The oxygenation/deoxygenation cycle of Mb in the PICsome was found to be fully reversible (Fig. 17).

Enzyme–polymer hybrid vesicles, which consisted of horse radish peroxidase (HRP) or myoglobin (Mb) reconstituted with PS coupled to ferriprotoporphyrin XI (cf. Fig. 14b), were investigated according to their enzymatic activity, Nolte et al. [61,65]. Although both proteins retained their original functionality, the reconstitution had an appreciable effect on their activity. In the case of HRP, the enzymatic activity decreased and for Mb the stability of the oxy complex was reduced. This could be explained by the introduction of a PS chain which seems to result in a somewhat modified binding of the heme in the reconstituted protein (evidenced by UV spectroscopy). Several factors could be responsible for this behavior, like an unfavorable interaction of the protein with the PS chain or a disturbance of the 3D-structure of the protein due to the aggregation of the hybrid molecules. In addition, both proteins have their substrate access channels located near the site of attachment of the PS chains, which means that these channels might be partly shielded from the aqueous solution. However, the residual activity also might have arisen from smaller (micellar) aggregates having a more dynamic structure than the larger vesicles.

3.2 Composite Materials

Polymers are versatile building blocks for the synthesis of structured organic/inorganic composite materials [66]. Biohybrid or polypeptide-based vesicles, however, have scarcely been used for this purpose, only for the production or encapsulation of nanoparticles.

Lecommandoux et al. [67] obtained stable dispersions of super-paramagnetic vesicles by combining aqueous solution of PB_{48}-*b*-$PLGlu_{56}$ (Fig. 1a) with a ferrofluid consisting of maghemite (γ-Fe_2O_3) nanoparticles in CH_2Cl_2. Incorporation of one mass equivalent of ferrofluid into the hydrophobic core of aggregates did not alter their morphology, as deducted from SLS and SANS data, but caused a substantial increase of the outer diameter by a factor of 6 (DLS). Interestingly, the hybrid vesicles underwent deformation under a magnetic field, as shown by 2D-SANS experiments. These hybrid nanoparticles could for instance be used in biomedicine as a probe for magnetic resonance imaging (MRI).

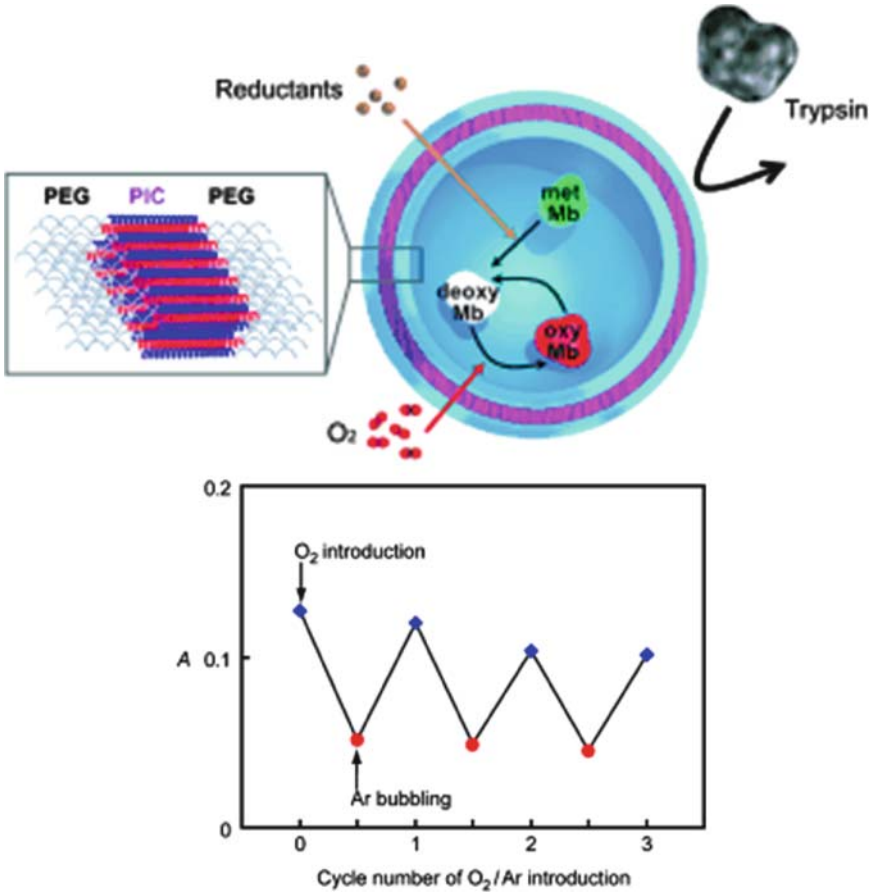

Fig. 17 *Top*: illustration of the reversible Mb oxygenation inside the PICsome self-assembled from a pair of oppositely charged block copolymers. *Bottom*: change in the absorbance at 434 nm of the Mb–PICsome by the alternating introduction of O_2/Ar gas to the solution. Reprinted with permission from [58], copyright (2007) Wiley

Shantz et al. [56] obtained a series of inorganic nanospheres (silica, silver bromide, and silica/silver bromide) with sizes in the range of 20–250 nm using vesicles of PLys-*b*-PPhe (Fig. 10j) as templates. Freshly prepared 1 M solution of orthosilicilic acid was mixed with a solution of copolypeptide $(0.2\,\text{mg mL}^{-1})$ buffered to pH 7. Hollow silica spheres were obtained with symmetric copolypeptides $(\text{Lys}:\text{Phe} = 1{:}1)$, whereas compact silica spheres were formed at higher comonomer ratios (TEM). The reason for the formation of compact spheres was seen in the destabilization of vesicles due to the highly extended conformation of the lysine at neutral pH. AgBr particles were prepared using $AgNO_3$ solution and PLys(HBr)-*b*-PPhe in water. The sizes of vesicles (DLS), dependent on the

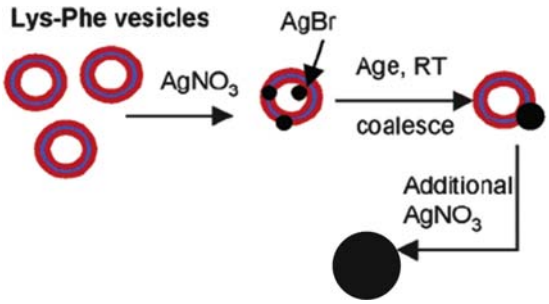

Fig. 18 Proposed mechanism of the growth of silver bromide nanoparticles in the presence of PLys-*b*-PPhe vesicles. Reprinted with permission from [56], copyright (2005) American Chemical Society

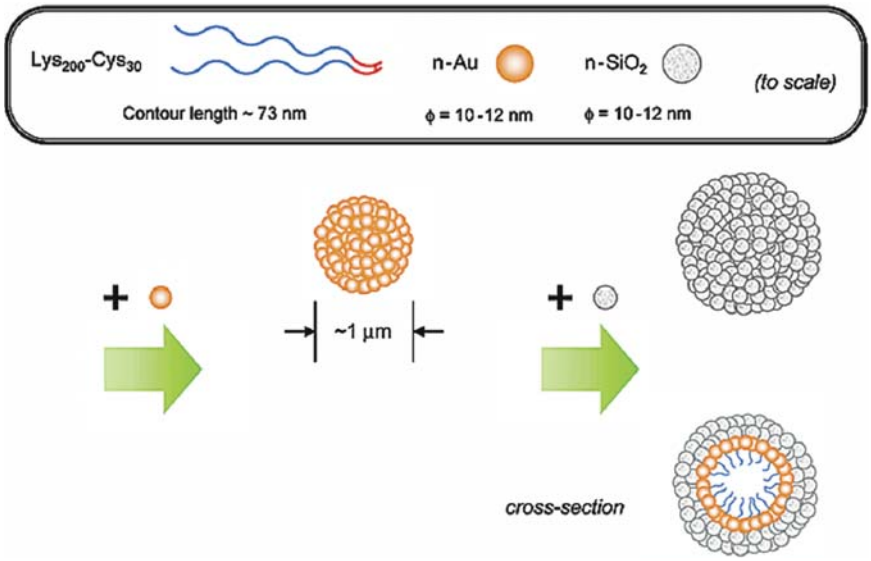

Fig. 19 Schematic diagram showing the self-assembly of gold and silica nanoparticles into hollow spheres with a two-layer shell structure. Reprinted with permission from [49], copyright (2002) American Chemical Society

copolypeptide used, were comparable to those of the corresponding AgBr spheres (SEM), indicating that the vesicles served as templates. The size of particles could also be adjusted by the amount of silver nitrate added, as illustrated in Fig. 18.

Deming et al. [49] described a "one pot" coassembly of silica and gold nanoparticles into micron-sized hollow spheres using $PLCys_{30}$-*b*-$PLLys_{200}$ (Fig. 10f), as illustrated in Fig. 19. The function of the PLCys block was to bind to gold (or silver) nanoparticles via sulfide and disulfide (formed during the deprotection of the polymer in the air) and that of the PLLys to promote adhesion to the silica nanoparticles via electrostatic interactions. Reacting first the copolypeptide with the

gold nanoparticles prior to silica nanoparticles produced hollow spheres (0.8–4 μm) consisting of a distinct layer of gold nanoparticles surrounded by an outer 250 nm–thick layer silica nanoparticles, as confirmed by TEM and SEM. The dimension of the spheres could be controlled by the lengths of the polypeptide blocks, initial copolypeptide concentrations, and nanoparticles/copolypeptide ratios. The walls were found to be porous (TEM) and thermally robust (stable up to 1,100 °C), making the spheres interesting materials for a containment and transport of molecules.

4 Summary

Advanced synthetic polymer chemistry provides a variety of sophisticated biohybrid polymers consisting of synthetic polymers and biologically relevant peptides and sugars. Biohybrid polymers can combine the advantageous features of being processable and robust as well as being biocompatible, functional, and selective. Biohybrid vesicles or membranes are considered as mimetics of biomembranes but with a better performance than liposomes.

Biohybrid polymers can be assembled into vesicles by appropriately adjusting the composition (geometrical packing of chains) or by making use of hydrogen bonding and secondary structure interactions as well as supramolecular complexation. Hydrogen bonding and secondary structure are predominant when the peptide or sugar is the membrane-forming segment. However, the mechanisms involved in the formation of vesicles may not always be understood, and the characterization of structures is often fragmentary. Also, information on the mechanical properties of membranes is lacking.

The era of biomimetic peptide- and sugar-based polymer vesicles has just begun and seems very promising. Bioinspired vesicles are mainly applied for drug delivery/release and the fabrication of composite materials, but could readily be used for biomimetic materials science, biomineralization, and so on. Especially interesting are “smart” vesicles changing properties in response to an external stimulus (temperature, pH, ions).

Acknowledgements H.S. thanks all former and present coworkers working in the field of biohybrid polymers and Erich C. (beerandfunandloudmusic). Financial support was given by the *Max Planck Society* and the *German Research Foundation* (within the Eurocores Programme BIOSONS).

References

1. Discher DE, Eisenberg A (2002) Science 297:967
2. Jain S, Bates FS (2003) Science 300:460
3. Antonietti M, Förster S (2003) Adv Mater 15:1323
4. Ringsdorf H, Schlarb B, Venzmer J (1988) Angew Chem Int Ed Engl 27:113

5. Schlaad H, Antonietti M (2003) Eur Phys J E 10:17
6. Kita-Tokarczyk K, Grumelard J, Haefele T, Meier W (2005) Polymer 46:3540
7. Deming TJ (2007) Prog Polym Sci 32:858
8. Freiberg S, Zhu XX (2004) Int J Pharm 282:1
9. Löwik DWPM, van Hest JCM (2004) Chem Soc Rev 33:234
10. Lim Y-B, Moon K-S, Lee M (2008) J Mater Chem 18:2909
11. Gallot B (1996) Prog Polym Sci 21:1035
12. Ladmiral V, Melia E, Haddleton DM (2004) Eur Polym J 40:431
13. Lutz J-F, Schlaad H (2008) Polymer 49:817
14. Edgar KJ, Buchanan CM, Debenham JS, Rundquist PA, Seiler BD, Shelton MC, Tindall D (2001) Prog Polym Sci 26:1605
15. Sukhorukov GB, Möhwald H (2007) Trends Biotechnol 25:93
16. Wang Y, Angelatos AS, Caruso F (2008) Chem Mater 20:848
17. Vriezema DM, Comellas Aragonès M, Elemans JAAW, Cornelissen JJLM, Rowan AE, Nolte RJM (2005) Chem Rev 105:1445
18. Fischlechner M, Donath E (2007) Angew Chem Int Ed Engl 46:3184
19. Kukula H, Schlaad H, Antonietti M, Förster S (2002) J Am Chem Soc 124:1658
20. Chécot F, Brûlet A, Oberdisse J, Gnanou Y, Mondain-Monval O, Lecommandoux S (2005) Langmuir 21:4308
21. Chécot F, Lecommandoux S, Klok H-A, Gnanou Y (2003) Eur Phys J E 10:25
22. Sigel R, Losik M, Schlaad H (2007) Langmuir 23:7196
23. Gebhardt KE, Ahn S, Venkatachalam G, Savin DA (2008) J Colloid Interf Sci 317:70
24. Rodríguez-Hernández J, Lecommandoux S (2005) J Am Chem Soc 127:2026
25. Ayres L, Hans P, Adams J, Lowik DWPM, vanHest JCMJ (2005) J Polym Sci A Polym Chem 43:6355
26. Cornelissen JJLM, Fischer M, Sommerdijk NAJM, Nolte RJM (1998) Science 280:1427
27. Geng Y, Discher DE, Justynska J, Schlaad H (2006) Angew Chem Int Ed 45:7578
28. You L, Schlaad H (2006) J Am Chem Soc 128:13336
29. Li Z-C, Liang Y-Z, Li F-M (1999) Chem Commun:1557
30. Liang Y-Z, Li Z-C, Li F-M (2000) New J Chem 24:323
31. Pasparakis G, Alexander C (2008) Angew Chem Int Ed 47:4847
32. Dong C-M, Sun X-L, Faucher KM, Apkarian RP, Chaikof EL (2004) Biomacromolecules 5:224
33. Dong C-M, Faucher KM, Chaikof EL (2004) J Polym Sci A Polym Chem 42:5754
34. Hordyjewicz-Baran Z, You L, Smarsly B, Sigel R, Schlaad H (2007) Macromolecules 40:3901
35. You L (2007) Dissertation, University of Potsdam, Germany
36. Gress A, Smarsly B, Schlaad H (2008) Macromol Rapid Commun 29:304
37. Li M, Su S, Xin M, Liao Y (2007) J Colloid Interf Sci 311:285
38. Brown MD, Schätzlein A, Brownlie A, Jack V, Wang W, Tetley L, Gray AI, Uchegbu IF (2000) Bioconj Chem 11:880
39. Wang W, Tetley L, Uchegbu IF (2001) J Colloid Interf Sci 237:200
40. Sun J, Shi Q, Chen X, Guo J, Jing X (2008) Macromol Chem Phys 209:1129
41. Al-Jamal KT, Sakthievel T, Florence AT (2003) Int J Pharm 254:33
42. Al-Jamal KT, Sakthievel T, Florence AT (2005) J Pharm Sci 94:102
43. Börner HG, Schlaad H (2007) Soft Matter 3:394
44. Hamley IW (2007) Angew Chem Int Ed 46:8128
45. Toyotama A, Kugimiya S-I, Yamanaka J, Yonese M (2001) Chem Pharm Bull 49:169
46. Cheon J-B, Jeong Y-I, Cho C-S (1998) Korea Polym J 6:34
47. Cheon J-B, Jeong Y-I, Cho C-S (1999) Polymer 40:2041
48. Schlaad H (2006) Adv Polym Sci 202:53
49. Wong MS, Cha JN, Choi KS, Deming TJ, Stucky GD (2002) Nano Lett 2:583
50. Cha JN, Stucky GD, Morse DE, Deming TJ (2000) Nature 403:289
51. Holowka EP, Pochan DJ, Deming TJ (2005) J Am Chem Soc 127:12423
52. Bellomo EG, Wyrsta MD, Pakstis L, Pochan DJ, Deming TJ (2004) Nat Mater 3:244
53. Holowka EP, Sun VZ, Kamei DT, Deming TJ (2007) Nat Mater 6:52

54. Iatrou H, Frielinghaus H, Hanski S, Ferderigos N, Ruokolainen J, Ikkala O, Richter D, Mays J, Hadjichristidis N (2007) Biomacromolecules 8:2173
55. Sun J, Chen X, Deng C, Yu H, Xie Z, Jing X (2007) Langmuir 23:8308
56. Jan J-S, Lee S, Carr CS, Shantz DF (2005) Chem Mater 17:4310
57. Koide A, Kishimura A, Osada K, Jang W-D, Yamasaki Y, Kataoka K (2006) J Am Chem Soc 128:5988
58. Kishimura A, Koide A, Osada K, Yamasaki Y, Kataoka K (2007) Angew Chem Int Ed 46:6085
59. Kataoka K, Harada A, Nagasaki Y (2001) Adv Drug Deliv Rev 47:113
60. Reynhout IC, Cornelissen JJLM, Nolte RJM (2007) J Am Chem Soc 129:2327
61. Boerakker MJ, Botterhuis NE, Bomans PHH, Frederik PM, Meijer EM, Nolte RJM, Sommerdijk NAJM (2006) Chem Eur J 12:6071
62. Pratten MK, Lloyd JB, Hörpel G, Ringsdorf H (1985) Makromol Chem 186:725
63. Koňák C, Šubr V, Kostka L, Štěpánek P, Ulbrich K, Schlaad H (2008) Langmuir 24:7092
64. Regina M, Santella, Li HJ (1975) Biochemistry 14:3604
65. Boerakker MJ, Hannink JM, Bomans PHH, Frederik PM, Nolte RJM, Meijer EM, Sommerdijk NAJM (2002) Angew Chem Int Ed 41:4239
66. Smarsly B, Antonietti M (2006) Eur J Inorg Chem:1111
67. Lecommandoux S, Sandre O, Chécot F, Rodríguez-Hernández J, Perzynski R (2005) Adv Mater 17:712

Adv Polym Sci (2010) 224: 197–233
DOI:10.1007/12_2008_7

Published online: 5 March 2009

Comparison of Simulations of Lipid Membranes with Membranes of Block Copolymers

Kostas Ch. Daoulas and Marcus Müller

Abstract An overview of molecular models and computer simulation techniques for amphiphilic vesicles formed either by lipid or block copolymer molecules is presented. First, system-specific, atomistic or coarse-grained representations of amphiphilic vesicles, which account for the detailed, chemical structure of the system, are briefly considered. The common features of collective phenomena on the mesoscale (e.g., the self-assembly into vesicles, their rupture or fusion), observed in a broad class of amphiphilic systems, suggest a universal underlying mechanism. This observation forms the basis for modeling large-scale properties of amphiphilic vesicles by minimal models. These coarse-grained models describe the underlying atomistic structure through a few relevant interactions, whose strength is characterized by coarse-grained parameters. The discussion of these coarse-grained models particularly focuses on how their parameterization can be related to the material properties of specific systems. In this context, the concept of combining density functional representations of amphiphilic systems with particle-based simulation techniques is introduced. As an illustration, a solvent-free model based on a virial expansion functional is elaborated and applied to investigate the behavior of polymersomes loaded with long homopolymers. Although the interactions are cast in a density functional language, the model is a particle-based one and its equilibrium properties are obtained from a straightforward Monte-Carlo scheme. The mechanical properties of the vesicles are established and compared to the properties of a planar bilayer. Selected results concerning the effect of loading on vesicle stability and mechanical properties of its bilayer shell are presented.

Keywords Block copolymers, Coarse-grained models, Collective phenomena, Computer simulation, Fusion, Lipid membranes, Monte Carlo techniques, Polymersome, Pore formation, Self-assembly, Self consistent field theory, Vesicle

K. Ch. Daoulas and M. Müller
Institut für Theoretische Physik, Georg-August Universität, 37077 Göttingen, Germany
e-mail: {daoulas, mmueller}@theorie.physik.uni-goettingen.de

Contents

1 Introduction

1.1 Liposomes and Polymersomes

Biological membranes constitute structures of high complexity, comprising a diversity of lipid and protein molecules. Lipids are a representative example of amphiphilic molecules containing a hydrophilic, polar headgroup connected to one or more hydrophobic tails, which are typically short hydrocarbons (comprised of 12–20 carbon atoms). In aqueous solutions they aggregate into structures where the hydrophilic headgroups are exposed to water, shielding the hydrophobic tails. A qualitative insight into how the shape of these structures is determined can be obtained using the molecular packing concept [1]. It assigns to lipid molecules a mean shape determined by factors like lipid architecture/chemical composition, solution conditions (e.g., salt concentration or pH), and external parameters such as temperature. If the average molecular shape is close to a cylinder, the lipids organize into bilayers and it is exactly this arrangement that characterizes biological membranes. Historically, a significant step towards understanding the organization of membranes was the formulation of the "fluid mosaic model" by Singer and Nicholson [2] representing it as a lipid bilayer engulfing isolated proteins, dispersed at low concentrations. Within this model, the lipids and the proteins can diffuse freely in the bilayer plane. Currently, it is acknowledged [3–6] that this simple picture has to be enriched to account for protein aggregation into functional complexes, lipid–protein association, bilayer-cytoskeleton and bilayer-glycocalyx coupling, presence of adhesion sites, etc., leading to more complicated, non-Brownian dynamics [3, 7, 8] of the lipids inside the bilayer. Nevertheless, despite the synergy of the components of the biological membranes, the understanding of their properties can significantly benefit from the experimental and theoretical consideration of simplified analogs. Thus, lipid bilayers composed of a single type of lipids or a mixture of different species, with various kinds of inclusions have been the subject of intense research.

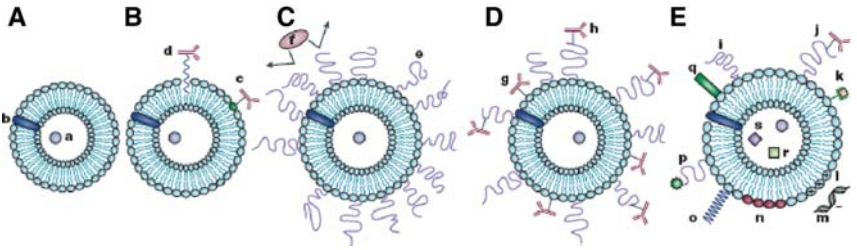

Fig. 1 Liposome evolution. **A**: Early "plain" liposomes with hydrophilic or hydrophobic drug entrapped (**a**) in the interior and (**b**) in the bilayer, respectively. **B**: Antibody-targeted immunoliposome with antibody covalently coupled (**c**) to the reactive membrane phospholipids, or anchored (**d**) with a hydrophilic moiety **C**: Long-circulating liposome decorated with protective polymer (**e**) acting as a shield against opsonizing proteins (**f**). **D**: Long-circulating liposome with protective polymer and antibody attached to surface (**g**) or, preferably, to the free end of a grafted chain (**h**) **E**: New generation liposome with different surface modifications (separate or combined) such as: attached protective polymer (**i**), protective polymer with targeting ligand (**j**), diagnostic label (**k**), incorporated positively charged lipids (**l**) for complexation with DNA (**m**), incorporated stimuli sensitive lipids (**n**) and polymers (**o**), cell-penetrating peptides (**p**), virial components (**q**). Apart from drugs, examples of vesicle's load include: magnetic targeting (**r**) particles, colloidal gold or silver particles (**s**) for electron microscopy. Reprinted by permission from Macmillan Publishers Ltd: Nature Reviews: Drug discovery (Ref. 9), copyright (2005)

Apart from being simplified models of biological membranes, these systems are related to medical applications such as drug delivery and diagnostic imaging by virtue of their implementation in the form of liposomes. Liposomes in their topology resemble cells. They are closed bilayer vesicles, serving as a container of hydrophilic or hydrophobic loads (e.g., drugs, biomolecules, nanoparticles) in their cavity or shell, respectively. An overview of the current progress in liposomology can be found, for example, in [9], from which we reproduce in Fig. 1 an instructive chart. The advancements have been so significant that several liposome-based drugs have been approved [9, 10] and clinically implemented. The research interest, however, remains high in view of the various issues that still need to be resolved. For instance, one of the important questions is the improvement of the control over liposome size which is crucial for their ability to penetrate into diseased tissues [11] and their storage stability [12]. Typically liposomes would be rapidly eliminated from the blood stream by the reticuloendothelial (RES) system. "Stealth"-liposomes with prolonged circulation times can be created by incorporating lipids conjugated to polyethylene glycol (PEO) chains [13] into the shell, which sterically repel the blood plasma proteins mediating the clearance by the immune system [14]; hence the "stealth" properties. Targeting of liposomes to diseased tissues can be achieved by attaching to their shell proper ligands [9, 15] (e.g., antibodies, folate, transferrin). Liposome decoration with biomolecular components, like the proteins of a viral envelope [16], can be used to control the delivery of the load into targeted cells as well. The delivery mechanism can be also tuned by properly selecting the lipid composition of the shell. pH-responsive liposomes are a characteristic example [17, 18].

In analogy to lipids, amphiphilic block copolymers, i.e., macromolecules composed of at least one hydrophilic and one hydrophobic, covalently linked, polymer chains can form in aqueous solutions vesicles; the so-called "polymersomes." Generally, in self-assembling copolymer solutions, a rich diversity of morphologies is possible. An overview of the various factors important for vesicle formation, including copolymer architecture, presence of additives, solvent composition, and temperature, is given in [19]. To illustrate polymersome structures we reproduce from [21] on the top row of Fig. 2 cryo-TEM images of vesicles formed by 1.0 wt % aqueous solution of PEO–*b*–PBD (PEO, polyethylene oxide; PBD, polybutadiene) diblock copolymer for three different sizes of the PEO and PBD blocks.

The potential of polymersomes in biomedical applications have been extensively discussed in several reviews [19, 22–26], so they are mentioned here only briefly. Mainly due to the high molecular weight of their amphiphiles they differ from liposomes in several aspects, which makes them beneficial for certain purposes. (1) Typically, they have a much thicker shell. For the vesicles shown in Fig. 2c the hydrophobic core thickness is $d = 21$ nm, while for lipid membranes typically $d \approx 3$ nm. (2) Due to the larger thickness, polymeric membranes are much less susceptible to fluctuations and defects, and they can withstand larger deformations than lipid systems. It is remarkable that, while lipid bilayers can be stretched only 5%

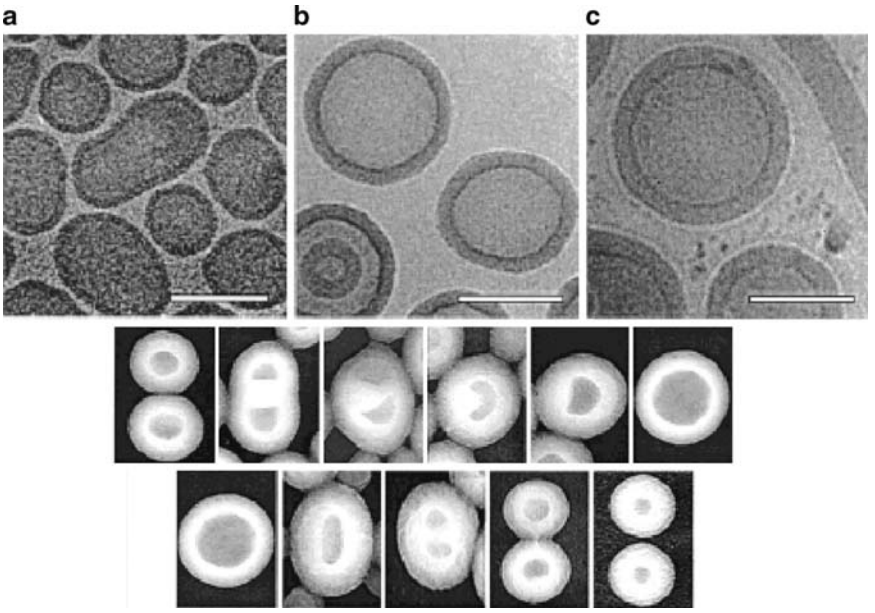

Fig. 2 *Top row*: Cryo-TEM images of 1.0 wt % aqueous solution of PEO–*b*–PBD diblock copolymer, for three different block sizes **a** EO_{26}–BD_{46}, **b** EO_{80}–BD_{125}, and **c** EO_{150}–BD_{250}. The *darker areas* denote the BD-rich area, forming the hydrophobic part of the bilayer. *Scale bars* correspond to 100 nm. Reprinted with permission from Ref. [21]. Copyright 2002 American Chemical Society. Reprinted with permission from Ref. [20]. Copyright 2001 American Chemical Society

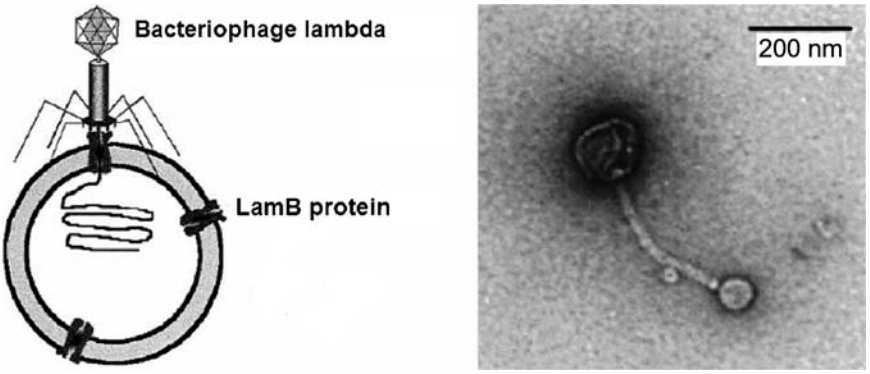

Fig. 3 *Left*: Schematic representation of a DNA-loaded triblock-based polymersome. The virus, a λ phage, binds a LamB protein and the DNA is transferred across the block copolymer membrane. *Right*: An electron micrograph of negatively stained complexes formed between λ phage and vesicles bearing LamB proteins at 37^o C. The λ phage (*large structure on the top left corner*) is attached to one vesicle via its tail. Ref. [27]. Copyright (2002) National Academy of Sciences, U.S.A

prior to rupturing, the critical area strain for polymer membranes typically [21] lies between 20 and 50%. Thus, polymersomes outperform the liposomes with respect to robustness and stability. (3) Due to the increased thickness the permeability of the polymersome shell is reduced and longer load retention times can be achieved [22]. The robustness of polymersomes can be further increased by cross-linking the amphiphiles [28–30]. (4) Proper selection of block size and chemistry of the synthetic copolymers offers significant opportunities for application-oriented tailoring of polymer vesicles properties. For example, PEO–*b*–PBD polymersomes demonstrate prolonged circulation in *vivo*, outperforming the PEO-decorated, stealth, liposomes due to the denser structure of the PEO brush [31]. Targeted delivery of therapeutic loads can be achieved by creating polymeric vesicles responsive to environmental stimuli, such as pH change (see [32] for more details) or biodegradable polymersomes [33, 34]. Further functional diversity and interfacing with biological systems can be achieved by incorporating proteins into the polymersome membrane. A nice example, reproduced in Fig. 3, is presented in [27], where viruses (λ phages) were able to bind to LamB proteins incorporated into polymersomes and inject their DNA into the artificial container.

1.2 Modeling Lipid and Polymer Vesicles: General Considerations

Computer simulations allow for a systematic exploration of the relationships between the structure of the individual molecular components, external control parameters that influence self-assembly, and the properties of the bio-mimetic vesicles. Therefore they can provide important guidance for their engineering in view of the applications highlighted in the previous section. The computer modeling offers an

unambiguous control of the numerous system parameters and characteristics, while as an output, it can provide information on properties that are not directly accessible in experiments, such as details of local molecular structure, system organization, or evolution pathways. Generally, in each case the modeling approach is determined by the specifics of the question under study. To this end, the mesoscale behavior of lipid and polymeric amphiphiles demonstrates that, despite the rich chemical and structural diversity, they present similar self organization patterns. This universal behavior should be attributed to their generic feature: the connectivity of the hydrophobic and hydrophilic parts. Essentially, it plays the role of an effective, attractive, long range interaction counterbalancing the more local hydrophilic–hydrophobic repulsion [35–37]. Self-assembly driven by competing interactions has been proposed [35], within a phenomenological Landau-Ginzburg description, as the underlying mechanism for the formation of spatially modulated phases in a variety of different systems, such as copolymers, lipids, superconductor films, magnetic materials. In some cases, universality is not only observed in the structural properties of the self-assembled amphiphile morphologies but also in the dynamics of various processes. An instructive example is presented on the two last rows of Fig. 2 taken from [20] showing vesicle fusion (middle row) and vesicle fission (bottom row), reminiscent of similar events in lipid membranes. The observed universality motivates [5,38–40] an attempt to obtain a qualitative understanding of the basic principles underlying the collective behavior of these systems in the framework of simple, minimal, coarse-grained models. These representations incorporate only the relevant interactions/features that are necessary to reproduce the phenomena of interest, and the parameters, which describe the strength of the interactions, are expressed [41] through "invariant quantities," encoding the characteristic time, energy, and length scales. Typically, these are treated as input parameters, established by comparison to experimental data or atomistic simulations. On the other hand, the examples of modern bio-mimetic vesicles shown in Fig. 1 suggest that, for understanding certain phenomena and designing specific applications, fine details of the molecular components maybe important. Depending on the desired resolution, these can be incorporated either via detailed atomistic representations or coarse-grained models obtained through "systematic" coarse-graining approaches, a well established technique in polymer physics [42]. The latter schemes integrate out some atomistic degrees of freedom, and the smaller number of remaining degrees of freedom or effective, coarse-grained beads, are interacting via soft potentials. However, in contrast to minimal models, these interactions are more detailed and are tuned to reproduce certain structural, thermodynamic and dynamic properties. It is well-known that [39,43] the decimation of the degrees of freedom can only be performed approximately. Generally, the coarse-grained degrees of freedom interact via a multibody free-energy functional. In practice, these multibody interactions among the coarse-grained beads are approximated by pair-wise potentials and the form of the interactions depends on the choice of quantities that are to be reproduced on larger scales. Moreover, unlike the microscopic interaction energies, the coarse-grained interactions have the status of free energies and depend on the specific

thermodynamic state defined by temperature, density, and pressure. Inhomogeneous systems may additionally require a composition-dependent parameterization.

Both of the above statements are reflected in the subdivision of the current computer simulation approaches to lipid and polymeric vesicles. Ample investigations have been aimed at acquiring a generic, qualitative understanding of the mechanisms behind the structural properties of bio-mimetic vesicles like shape, elastic constants, amphiphile partitioning, spatial distribution of hydrophobic or hydrophilic loads, and the dynamics of various processes such as fusion, rupture, budding, and coupling to external flows. These works employ simplified amphiphile representations and rely on the concept of universality. On the other hand, numerous studies focus on describing the liposome/polymersome behavior in context of models, representing specific systems and providing an insight into how the vesicle properties are affected by the fine details of the molecular structure. This review will highlight both approaches. We discuss simulation studies considering the particle-based models within standard techniques such as Monte-Carlo (MC), Molecular, Brownian or Dissipative Particle Dynamics (MD, BD or DPD), and field-theoretic approaches like Self-Consistent Field (SCF) theory or Dynamic Density Functional Theory (DDFT). Studies addressing vesicle properties within analytical or numerical solutions of phenomenological theories will not be covered in detail, although some of their predictions will be recalled in context of simulation results. Representative works of this kind can be found in [44–53].

The paper is organized as follows: Sect. 2 is dedicated to models considering specific lipid and polymer vesicle systems. We will start from high-resolution representations, gradually proceeding to coarser ones. Basic simulation and data analysis techniques will be presented, and results will be discussed in the context of system-specific properties and from the viewpoint of universality. Minimal models and pertinent simulation techniques will be described in Sect. 3. A working example of a minimal model approach to polymersomes will be elaborated, illustrating how the coarse-grained parameters that quantify the strength of relevant interactions can be obtained by the concept of "invariant quantities." Finally, the last section contains the main conclusions and discusses some open problems and directions of future simulation studies of bio-mimetic vesicles.

2 Component-Specific Modeling of Liposomes and Polymersomes

2.1 Atomistic Modeling and Systematic Coarse-Graining

In principle, detailed atomistic simulations could offer a straightforward approach for describing bio-mimetic membranes with chemical accuracy. Commonly, they employ Molecular Dynamics (MD) methods built around "force-fields" representing the interactions of chemically bonded and non-bonded atoms, to obtain

information on structural and dynamical properties. Currently, several force-fields are available to serve as a platform for interaction representation. AMBER [54], CHARMM [55], GROMOS96 [56], OPLS-AA [57,58], and Encad [59] are typical examples. Often, however, a fully atomistic approach to practically relevant liposome or polymersome systems, is currently not feasible. This can be anticipated considering that [9,25,26] the sizes of liposomes and polymersomes typically range from 50 to 1,000 nm. In polymer vesicles the need to consider systems with large dimensions is further perplexed by the large relaxation times of the amphiphiles. Their diffusion coefficient, D, is smaller than $0.1\mu m^2 s^{-1}$. For these reasons, only very few atomistic simulations of lipid vesicles have been performed, while, to the best of our knowledge, no atomistic polymersome study has been reported. Reference [60] illustrates the dimensions and length scales of lipid vesicles that can be currently addressed within an atomistic approach. The authors report a MD study of spontaneous vesicle formation in an aqueous solution of dipalmitoylphosphatidylcholine (DPPC) lipids. They have employed a variant [61,62] of the GROMOS force-field, considering 1,017 DPPC lipids (each comprised of 50 interaction centers) embedded in 106563 water molecules. The evolution of self-assembly has been monitored up to 90 ns leading to the formation of a vesicle with dimensions on the order of 15 nm. After a simulation run of 90 ns, the vesicle was still imperfect, exhibiting several pores in the shell.

Atomistic simulations can be much more beneficial when used as an integral part of systematic, coarse-graining approaches. In this scope, they focus on smaller systems in order to provide the information necessary for gauging the mesoscopic interactions. For example, a description of a systematic development of a coarse-grained model for lipids and the study of vesicles in aqueous solutions by MD simulations is presented in [63,64], where the authors developed coarse-grained representations of dipalmitoylphosphatidylethanolamine (DPPE), DPPC, lysoPS lipids, and water in spirit of earlier approaches [65–67]. The parameters of the non-bonded (Lennard-Jones and screened electrostatic) and bonded (soft spring and bond angle dependent) interactions were optimized to reproduce various properties such as densities of the pure liquids (e.g., water), mutual solubilities, area per lipid, and spatial electron density distributions, available from experiments or atomistic simulations. The vesicle formation process was monitored starting from a random initial configuration (biased in the sense that the lipids were placed near the center of the simulation cell to avoid the formation of bilayer connected via periodic boundary conditions) and is reproduced in the top panel of Fig. 4. It can be observed that in the initially random phospholipid solution, a rapid clustering to micelles takes place which, almost immediately, coalesce into interconnected worms. These structures transform into a single bilayer, the bicelle, with curved ends of a high line tension, gradually minimized by encapsulating water. Thus, a cup-like vesicle with a small pore is formed, which eventually seals so that a stable vesicle is created. The calculation of Minkowski functionals of the assembled structures suggests that the tendency to minimize the lipid/water interfacial area and the mean curvature of the aggregate surface are the driving forces for the process.

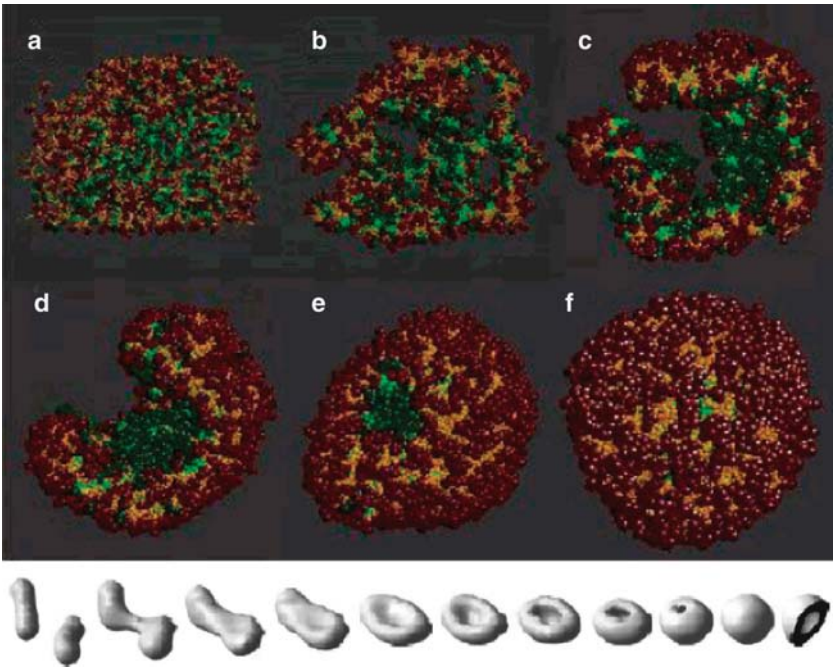

Fig. 4 *Top*: Formation process of DPPC lipid vesicles obtained from coarse-grained molecular dynamics (CGMD) simulations starting from a random aqueous solution configuration. *Red/orange colors* show the lipid head/tail groups of the outer monolayer, while *dark green/light green* show those of the inner one. Water is omitted for clarity. The snapshots are shown at **a** 0 ns, **b** 4 ns, **c** 20 ns, **d** 80 ns, **e** 200 ns and **f** 240 ns. Reprinted with permission from Ref. [63]. Copyright 2003 American Chemical Society. *Bottom*: A similar pathway of a single vesicle formation, observed in DDFT simulations of a generic amphiphile model. The last image of the sequence shows a cut through the final intact vesicle. Reprinted from Ref. [68]. Copyright 2005 American Chemical Society

The pathway of vesicle assembly observed within the systematically obtained coarse-grained lipid representation has been identified in numerous systems described with different generic models and simulation techniques, such as MC [69], BD [70], DPD [71], DDFT [68] and, thus, can be considered universal for a broad class of amphiphiles. To illustrate this we reproduce on the bottom of Fig. 4 a sequence of snapshots showing vesicle formation, obtained by DDFT [68]. One should, however, be cautious in extrapolating this pathway to the formation of polymersomes in solutions of polymeric amphiphiles. It has been suggested [72] that, due to the large length of the copolymer molecules and the relative weakness of interactions, the aggregation dynamics may be different. In this study, spinodal decomposition triggers nucleation of amphiphilic droplets and the copolymers aggregate to these nuclei. As their size grows, they restructure into micelles, then into semi-vesicles, and finally into vesicles. Coalescence events are absent from this pathway. This point deserves attention because understanding the assembly dynamics potentially offers means for controlling vesicle dimensions and achieving size-uniformity.

The high curvature of the small liposomes that were studied (diameters about $15-20$ nm) causes the inner and outer monolayers of the shell to differ in structure and drives lipid partitioning between the two leaflets in mixed vesicle systems. The asymmetry between the monolayers manifests itself, for instance, through the different dynamics of the lipids. The self-diffusion coefficient for the amphiphiles of the outer layer is $D = 4.8 \times 10^{-7}\text{cm}^2\,\text{s}^{-1}$ as opposed to the $D = 2.5 \times 10^{-7}\text{cm}^2\,\text{s}^{-1}$ of the inner ones, i.e., they move almost twice as fast. An interesting result of the simulations is the continuous exchange of water through the shell, between the interior of the stable liposome and the external solution. The permeability coefficient, P, has been estimated to be on the order of $10^{-3}\,\text{cm}\,\text{s}^{-1}$.

Systematically derived, coarse-grained lipid models have also been used to study the interaction between vesicles, in particular their fusion. This is a key event in numerous biological processes, including virial infection, endo- and exocytosis, synaptic release, and cell trafficking [73–76]. Thus, it has attracted abiding interest [40]. Its initial stage in biological systems is regulated by proteins, which bring, for instance, the membranes into proximity. Nevertheless there is evidence [77–79] that the mechanism of fusion itself is driven by the amphiphiles. Reference [64] addressed the fusion of small vesicles with various DPPE, DPPC, lysoPS lipid compositions. Once the vesicles were brought into close proximity (a few nm), the observed fusion events were triggered by a fluctuation in one of the monolayers due to which some head groups merged into the apposing monolayer. The fusion then proceeded along two pathways. Pathway I reproduced the classical assumption [80,81] encompassing the sequence of stalk, hemifusion diaphragm (HD), expanded HD, and finally fusion pore. This pathway, with its intermediate structures is depicted in Fig. 5. Pathway II, however, exhibited leakage and proceeded along

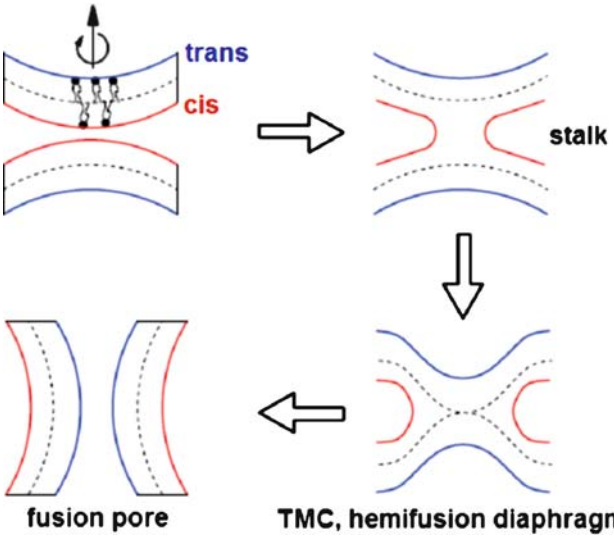

Fig. 5 Illustration of the classical fusion pathway. Reprinted from Ref. [40]. Copyright (2006), with permission from Elsevier

the stalk-hole mechanism [82]: after the appearance of a stalk, a pore in one of the two vesicles was formed in its vicinity remaining open for a certain period of time. After that, the stalk encircled the pore forming an HD-like structure which subsequently evolved as in pathway I. Vesicle fusion pathways and issues regarding the stalk evolution and the metastability of the HD have been also considered in [83], by combining atomistic and coarse-grained models within a "reverse" approach. Coarse-grained simulations of mixed vesicles of DPPC and palmitic acid (PA) have been conducted to provide template configurations. Subsequently these have been used to create atomistic configurations of a vesicle connected with its periodic image via a stalk, through reverse mapping and a multistep equilibration procedure. The detailed atomistic simulations started from these initial configurations also confirmed the existence of the stalk-hole fusion pathway. As in the case of the kinetics of vesicle assembly, fusion pathways with leakage similar to those of [64, 83] have been observed in other works using very different models [70, 84], providing strong evidence of their universality. Interestingly, they are first observed in the case of a different local membrane geometry, namely the fusion of planar membranes, which correspond to a vesicle with an infinite curvature radius. In [39, 82] a Monte-Carlo study of the fusion of planar polymeric membranes has been conducted using a lattice representation of amphiphiles – the Bond Fluctuation Model (BFM). The surrounding solvent has been described by homopolymers representing a group of solvent molecules. These simulations have revealed two leaking fusion pathways, the first one being similar to the pathway II of [64], i.e., involving a single hole formation near the stalk. The second pathway of [39, 82] is another variant of stalk-hole mechanism where holes are formed in each of the two bilayer membranes in the vicinity of the stalk which subsequently elongates to encircle them and thereby creates the fusion pore.

The study of closed polymeric vesicles, combining systematically derived coarse-grained models with MD (in the following denoted by CGMD [85]) is still limited by the large number of particles that has to be considered [86]. For this reason, CGMD studies of the assembly of polymersomes from a random solution have not been reported, although aspects of the dynamics of spontaneous copolymer aggregation into planar bilayers and micelles have been addressed [87]. Typically, the structural and the mechanical properties of polymersomes are derived from modeling planar bilayer patches. In this context, as well as in lipid membranes, an important methodological issue is the determination of the tensionless state of the membrane [88], i.e., the equilibrium area per amphiphile, A_o. The mechanical tension acting on planar bilayer spanning the x and y dimensions of an orthorhombic box with fixed lengths h_x,h_y, and h_z can be expressed as

$$\Sigma = h_z \left\langle P_{zz} - \frac{1}{2}(P_{xx} + P_{yy}) \right\rangle, \tag{1}$$

where P_{xx},P_{yy}, and P_{zz} are the diagonal components of the pressure tensor. To control the mechanical stress of the modeled membranes, various statistical ensembles have been proposed [89, 90]. Typical examples include the $nP_{zz}AT$, where h_z fluctuates

and the conjugated normal pressure P_{zz} is controlled ($A = h_x h_y$ denotes the lateral box area, n is the number of amphiphiles, and T is the temperature) or the $nP_{zz}\Sigma T$ ensemble. Some discussions focused on the accuracy with which the membrane stress can be controlled within constant tension ensembles [88, 91, 92]. It has been argued that [91] the tension, Σ, does not corresponds to the "macroscopic" membrane stress, because the finite size of the simulation cell eliminates long wavelength membrane undulations. Thus, it is not clear if $\Sigma = 0$ indeed corresponds to a "macroscopically" stress-free membrane. This important point has been questioned in [92] presenting simulation data which exhibit only a weak dependence of A_o on system size. In fact, the influence of interface fluctuations has been studied in the context of wetting phenomena. Long-wavelength capillary waves give rise to a size-dependent correction to the tension of the form $\ln(A)/A$.

It should be further mentioned that the choice of the ensemble also depends on whether or not the solvent is explicitly modeled. In particular, care has to be exerted concerning the number of intensive variables of the ensemble. This can be understood considering the Gibbs phase rule for interfaces [93]: $f = 2 + c - p$, with f being the number of independent intensive variables needed to describe the interface, p the number of different phases in the interface, and c denoting the number of different components. A lipid bilayer comprising one sort of lipid embedded into an implicit solvent corresponds to a one-component system [1], $c = 1$, *in one-phase state* so that $p = 1$; hence $f = 2$. On the other hand, a model with explicit solvent yields $c = 2$, $p = 1$, and $f = 3$. Thus, implicit solvent models can be simulated within $n\Sigma T$ ensemble while for explicit-solvent models an additional intensive quantity has to be controlled, e.g., the $nP_{zz}\Sigma T$ ensemble is appropriate.

Polymeric membrane patches have been modeled in [85, 87] using an $nP_{zz}AT$ ensemble. In these works the CGMD strategy has been utilized to investigate the properties of polymeric membranes formed by PEO–*b*–PEE amphiphiles (PEE, polyethylene ethylene) closely related to experimentally studied systems [94]. Among the questions addressed is the dependence of the thickness of the hydrophobic part, d, of the membrane on the molecular weight of the hydrophobic block, MW_{phob}. Experimental data [94] suggest a power-law dependence, $d \propto (MW)^{\varsigma}$ with ς being characteristic of the chain conformations in the hydrophobic layer: $\varsigma = 1$ for fully stretched chains, $\varsigma = 2/3$ in the strong segregation case, or $\varsigma = 1/2$ for random coil configurations. Interestingly, it is the value $\varsigma = 1/2$ that the experiments [21] report, suggesting that the chains in the hydrophobic core are rather unperturbed from their ideal state. CGMD simulations can relate this observation with the microscopic, internal structure of the bilayer. For high MW_{phob}, the chains of the two bilayer leaflets are highly interdigitated and the experimental power law, $\varsigma = 1/2$, is recovered. However, for short blocks, the interdigitation of the opposing monolayers is significantly reduced, becoming lipid-like, which is demonstrated by the prominent dip in the hydrophobic core density profile. In this case $\varsigma \sim 0.82$, reminiscent of strongly stretched molecular conformations.

[1] The amphiphile constitutes a single component despite its internal hydrophilic/hydrophobic block structure.

An important material property of membranes, that can be used as a reference point for comparing simulation results with experiments is the area elastic modulus, k_α, defined as

$$\Sigma = k_\alpha \frac{\Delta A}{A_o}, \tag{2}$$

where ΔA is the magnitude of change of membrane area from its equilibrium value A_o induced by the stress Σ. An interesting experimental observation of several polymersome PEO–*b*–PBD and PEO–*b*–PEE systems [21, 22, 94] is that the value k_α apparently does not depend on the molecular weight of the amphiphiles. k_α is constant within 10% over a fivefold change in molecular weight. This is illustrated in Fig. 6 reproduced from [85]. Moreover, simple arguments balancing molecular compression and interfacial energy [1] suggest that k_α is related to the water/hydrophobic core surface tension, γ as $k_\alpha = 4\gamma$ (ignoring the possibility of screening by the hydrophilic moieties), which seems to be confirmed by experiments. This rather nontrivial result has been confirmed by CGMD simulations (which are also shown in Fig. 6), and has been used to argue that the surface elasticity in membranes will depend only on the chemical nature of the amphiphile components around the interface.

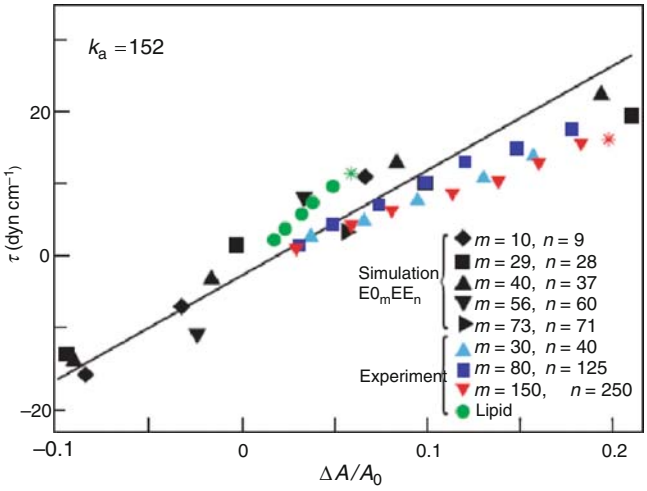

Fig. 6 Plot of membrane tension τ as a function of dilation for a wide range of copolymer amphiphiles as extracted from MD simulations. The computational models, derived from systematic coarse-graining (*black symbols*), show nearly the same dilational behavior marked by the *solid line*. The slope of the line, k_α, is very close to experimental measurements performed on giant vesicles (*colored symbols*). Experimental data for a dimyristoyl phosphatidylcholine lipid membrane are also shown. The point of membrane lysis as observed experimentally for selected lipid and polymersome systems is also shown in the plot with *green* and *red stars*, respectively. Reprinted by permission from Macmillan Publishers Ltd: Nature Materials, Ref. [85], copyright (2004)

2.2 Dissipative Particle Dynamics models

Since the modeling of entire amphiphilic vesicles requires the consideration of larger length and time scales, higher-level coarse-graining techniques have to be employed. In this context, DPD methods have been particularly powerful allowing for the simulation of large amphiphilic systems. Generally, DPD approaches have been covered extensively in the literature, the interested reader is referred to the publications [95–97] for example. Here, the basics of the DPD method will be described briefly, mostly to highlight the concepts invoked for obtaining realistic representations of lipid or polymer membrane systems. Owing to the fact that DPD initially aimed at simulating fluid flow, one bead in the DPD representation of water or amphiphile components, corresponds to the volume occupied by a group of several water molecules or amphiphilic monomers. Due to this representation, the non-bonded interactions between two DPD particles are "soft" and are typically described by a force of the form

$$F_{ij} = -a_{ij}\left(1 - \frac{|\mathbf{r}|}{r_c}\right)\frac{\mathbf{r}}{|\mathbf{r}|} \quad \text{for } r \le r_c \text{ and } F_{ij} = 0 \text{ for } r > r_c, \tag{3}$$

where $\mathbf{r}$ is the vector between the two particles of species i and j, r_c is the cut-off distance defining the unit of length, and the coefficients a_{ij} encode the interaction strength. The amphiphilic architecture is captured by bonded interaction potentials, $V_{\text{bond}}(|\mathbf{r}|)$, which in the most simple case are Hookean springs:

$$V_{(1)\text{bond}}(|\mathbf{r}|) = k_{\text{bond}}\mathbf{r}^2 \text{ or } V_{(2)\text{bond}}(|\mathbf{r}|) = \frac{k_{\text{bond}}}{2}(|\mathbf{r}| - l_o)^2, \tag{4}$$

where $\mathbf{r}$ is the vector connecting consecutive beads along the amphiphile's backbone, k_{bond} is the spring stiffness, and l_o characterizes the mean bond length. These interactions can be further combined with bending potentials [98, 99] of the form

$$V_{(1)\text{bend}} = \frac{k_{\text{bend}}}{2}(\vartheta - \vartheta_o)^2 \text{ or } V_{(2)\text{bend}} = k_{\text{bend}}(1 - \cos(\vartheta - \vartheta_o)). \tag{5}$$

In the equation above, k_{bend} is the stiffness parameter, while ϑ and ϑ_o stand for the instantaneous and the average angles between consecutive bonds, respectively. Apart from the two conservative interactions, DPD particles experience pairwise dissipative forces, depending on the relative speed of the particles, and pairwise random forces that depend on their relative distances. The properties of the dissipative and the stochastic forces are chosen to ensure local momentum conservation and that the equilibrium states of the system comply with the Boltzmann distribution of the ensemble [96].

When representing an aqueous solution of amphiphiles within soft DPD models, the first conceptual point consists in determining how many elementary chemical building blocks correspond to one DPD particle. To this end, a significant amount

of DPD representations of amphiphilic membranes followed the original works of Groot et al. [96, 100], where one DPD water bead corresponds to three atomistic water molecules. Typically, the DPD representation introduces only a few different bead species to represent an amphiphilic molecule. For instance, in [100] only three different bead species have been used to represent a phosphatidylethanolamine (PE) lipid – two h beads for the hydrophilic head, one e bead for the ester linkage, and five t beads for each of the two hydrophobic tails. In most cases, it is postulated that the amount of matter contained in each t or h DPD bead is the same and equal to the one of a water particle. The coefficients, a_{ij}, can be chosen so as to reproduce the compressibility and the mutual solubility of the species i and j [96]. However, in view of the general complexity of the amphiphilic systems, a more promising strategy is to tune them so as to reproduce certain structural and dynamical properties of the considered membranes. To this end, a large diversity of DPD models with different bead species and sets of a_{ij} parameters have been devised for numerous amphiphilic systems. For instance, tuning the a_{hh} parameter, one controls the lipid phase behavior [101], while using different parameters for intermolecular and intramolecular interactions between hydrophobic beads one reproduces realistic rupture behavior [102]. More recently [86], an alternative to the traditional "equal mass" mapping has been explored for DPD modeling of PEO–*b*–PEE based polymersomes in order to obtain realistic values for hydrophobic layer thicknesses and membrane elasticity parameters. In particular, each bead species was assigned its own mass, so that the bulk density of pure the substances would match the experimental data. Additional means for controlling the bilayer structure and properties are provided by the bonded potentials of equations (4) and (5).

The amphiphilic models obtained following the above concepts have been extensively used to address various phenomena in lipid and polymer vesicles. It should be mentioned, however, that by virtue of the high degree of coarse-graining invoked in DPD models, the borderline between lipid and polymeric amphiphiles within this description becomes less distinct.

Due to the rather small number of segments of the hydrocarbon tails and the rather rigid structure of the hydrophilic head, lipids have a limited amount of conformational degrees of freedom compared to polymers. Thus, details of the interactions and of the molecular architecture become much more important than in the case of polymers. One expects that the range of properties that can be addressed through a DPD mapping in polymeric amphiphilic systems is broader than in lipids so that in the last case using the terms "system-specific" or "generic" becomes a rather subtle issue. To this end, we choose to consider the lipid vesicle DPD simulations to have a more "generic" character and they will be discussed at the beginning of Sect. 3. On the other hand, the DPD simulations of copolymer amphiphiles combined with the previously described mapping reproducing the *individual* component bulk densities, have been successful in systematically reproducing various membrane properties. For example, in [86] the area elastic modulus of PEO–*b*–PEE membranes has been computed to be $k_\alpha = 137\,\mathrm{mN\,m^{-1}}$, which is very close to the experimentally reported value [22] $k_\alpha = 120 \pm 20\,\mathrm{mN\,m^{-1}}$. The same work presents evidence that in the DPD model, in agreement with the previously described experimental data and

CGMD simulations, the k_α is independent of the copolymer molecular weight, as well. Concerning the structural properties of the polymersome shell, the DPD results show a clear power law $d \propto (MW)^{\varsigma}$, with $\varsigma = 0.48$, i.e., in accordance with the unperturbed, almost ideal chain, structure of the hydrophobic layer suggested by the experiments and the CGMD simulations. Apart from the equilibrium vesicle properties, a preliminary study of the kinetics of polymersome rupturing under an osmotic pressure gradient was performed [86]. The gradient was generated by artificially increasing the amount of the water in the polymersome cavity. The DPD simulations then suggest that a possible poration mechanism involves disruption and micellization of the internal monolayer, which exposes the hydrophobic core to water. This triggers the micellization of the outer monolayer so that multiple pores are formed in the shell, allowing the contents of the cavity to escape.

3 Generic Vesicle Simulations

3.1 Universality vs Specificity in Dissipative Particle Dynamics Models

Following the last part of the previous section, the DPD models of lipid vesicles can be considered as being, essentially, in-between the more detailed, coarse-grained, system-specific representations of these systems and the highly coarsened, minimal models. In this context, quite elaborated DPD models can be used to reproduce several membrane properties that are expected to be important for the phenomena of interest. Recently the kinetics of vesicle fusion has been addressed [103, 104] using an optimized a_{ij} parameter set, combined with properly tuned $V_{(2)\text{bond}}$ and $V_{(2)\text{bend}}$ potentials, capable of mimicking geometric and elastic properties (area per lipid, bilayer thickness, area elastic modulus, volume compressibility) of dimyristoylphosphatidylcholine (DMPC) lipids. In addition, the membranes described with the models of [102–104] exhibit a realistic resistance to rupture; they can sustain only a $10-30\%$ relative area stretch prior to lysis. An important dynamical property of the DPD mappings in discussion is that they result in a relatively high ($\sim 10 k_B T$) energy barrier for intermembrane lipid exchange in case of adhering bilayers. Both factors have a significant impact on the observed fusion pathways and on the dependence of the free energy barrier for fusion on the membrane tension. These simulations reveal how fine mapping details can have qualitative effects, particularly in addressing dynamical phenomena. An earlier work [105], allowing for a 60% membrane stretchability and fast flips between adhering bilayers, showed different fusion pathways and did not indicated any tension-dependent free energy barriers, contrary to experimental observations [106]. More generic DPD representations of amphiphiles with 4–7 beads connected with Hookean springs have been used to address kinetics of vesicle assembly [71], phase separation and shape evolution in multicomponent vesicles[107, 108]. In [107] the simulations were started

from a single, A_1 amphiphile-component, planar bilayer which was allowed to deform, encapsulating water, and create a closed vesicle. A part of the A_1 molecules was then exchanged to A_2 molecules and the evolution of the system was monitored. A similar strategy was followed in [108]. In both works, the DPD parameterization was such that the flip-flop events were negligible (in agreement with the CGMD simulations [63]), while in [108] the shell was in addition made practically impermeable to the water, enforcing a constant area-to-volume ratio. In [107] the vesicle shape evolution, e.g., budding and pinching-off, was investigated as a function of the distribution of the A_2 amphiphiles among the inner/outer monolayer leaflets, and of the strength of segregation. The two reported prevailing pathways are shown in the main panel of Fig. 7. In particular, an A_2 amphiphile distribution favoring rather strongly the outer monolayer, promotes a "classical budding" scheme (see left of top row in Fig. 7), presumably due to the area-difference effect [109]. On the other hand, a strong A_1-A_2 incompatibility promotes membrane cleavage along the A_1-A_2 interface with subsequent fission (see right panel of top row of Fig. 7). The effect of area-to-volume ratio on the shape of multicomponent vesicles was addressed in [108] considering the evolution of two types of systems: (1) vesicles with an equilibrium area-to-volume ratio and (2) artificially deflated vesicles. In both cases, the distribution of the A_2 amphiphiles was selected with no preference to inner or outer leaflets (i.e., the ratio of A_2 molecules in the two bilayers was equal to the one of the single component system). Characteristic snapshots are reproduced on the left and right panels of the bottom row of Fig. 7, respectively. It can be seen that for the first case no budding is observed, although the A_2-rich domains have a somewhat cup-like shape. In the second case, however, the excess area allows a part of the caps to evolve into buds which vesiculate and pinch off.

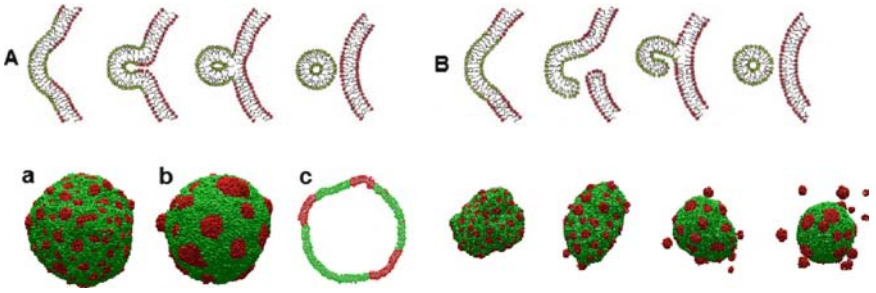

Fig. 7 *Top row*: Two budding and fission pathways observed in the DPD simulations. Reprinted with permission from Ref. [107]. Copyright 2003, American Institute of Physics. **A** For local asymmetry in the composition between the two bilayer leaflets. **B** For strong interfacial energy at the domain boundary or strong thermally induced undulation of the domain. Fission is initiated by cleavage along the interface. *Bottom row*: Snapshots of phase separating vesicles observed in the DPD simulation. Reprinted with permission from Ref. [108]. Copyright (2004) by the American Physical Society. A vesicle with an equilibrium area-to-volume ratio is shown on the left at the initial, (**a**), and a later stage, (**b**), of phase separation. Snapshot (**c**) shows a slice taken at the last stages demonstrating that the domains in both monolayers are in registration. The evolution of a deflated vesicle is shown on the *right*. At the last stage, the pinching-off of vesicles is observed

3.2 Solvent-Free Models

In the DPD modeling of amphiphilic vesicles a significant amount of computation time is spent on simulating the water molecules. For example, in the systems of [108] 1,472,000 particles of the total 1,536,000 were water. To this end, a frequent approach in minimal amphiphilic models is to eliminate the water molecules, taking them into account by proper, effective interactions between the amphiphilic components. Formally, the elimination of solvent degrees of freedom can be rationalized by considering the system as incompressible on the mesoscale, so that they can be integrated out. This, leads to a "solvent free" amphiphilic system, which is compressible, with the local amphiphile density, $\rho(\mathbf{r})$, to be allowed to fluctuate so that $0 \leq \rho(\mathbf{r}) \leq \rho_o$, where ρ_o is the density of the original incompressible system. For practical implementations, however, it should be taken into account, that because $\rho(\mathbf{r})$ is bounded from above, the effective interactions might not be well represented [40] by *density-independent pair potentials*. Also, all solvent hydrodynamic effects are lost, which might affect the description of membrane dynamics and the ability to model various processes.

Drouffe et al. [110] studied the assembly of amphiphilic vesicles by representing the amphiphiles with spheres interacting with a combination of hard core repulsions, orientation-dependent potentials, and multibody interactions. The multibody character of the interactions had to be introduced to mimic the "hydrophobic effect" so that a stable, fluid "membrane" in the form of a single monolayer of spheres forms at high temperatures. A more realistic solvent-free minimal model of amphiphilic bilayers was introduced by Noguchi and Takasu [70], representing the amphiphilic molecules by rigid rods with three interaction centers: two for the hydrophobic tail and one for the hydrophilic head. These centers interact through a repulsive soft core potential and a multibody, density-dependent, attractive potential mimicking the hydrophobic effect. It is instructive to reproduce these functional forms. The soft core repulsion is given by

$$U_{\text{rep}}(r) = \epsilon \exp\left[-20\,(r/\sigma - 1)\right], \tag{6}$$

where r is the distance between the two particles, ϵ defines the energy scale and σ the monomer size. The potential in equation (6) is truncated and shifted at 1.3σ. The multibody interaction experienced by a hydrophobic particle at point $\mathbf{r}$ of space is given as

$$U_{\text{multi}}(\rho(\mathbf{r})) = \begin{cases} -0.5\rho(\mathbf{r}) & \rho(\mathbf{r}) < \rho^* - 1 \\ 0.25\,(\rho(\mathbf{r}) - \rho^*)^2 - c & \rho^* - 1 \leq \rho(\mathbf{r}) < \rho^*, \\ -c & \rho^* \leq \rho(\mathbf{r}) \end{cases} \tag{7}$$

where $\rho^* = 10$ and $c = 4.75$ for the first tail bead (counting from the head) and $\rho^* = 14$ and $c = 6.75$ for the second one. $\rho(\mathbf{r})$ stands for the local density around the reference particle, calculated by defining a small sphere around it, such that

$$\rho(\mathbf{r}) = \sum_{\mathbf{r}'} h\left(|\mathbf{r}-\mathbf{r}'|\right), \quad h(r) = \begin{cases} 1 & r < 1.6\sigma \\ \frac{1}{\exp[20(r/\sigma - 1.9)]+1} & 1.6\sigma \le r < 2.2\sigma \\ 0 & 2.2\sigma \le r \end{cases}, \tag{8}$$

The summation over $\mathbf{r}'$ is performed over the coordinates of all intermolecular hydrophobic segments. It can be seen that at low density, $\rho < \rho^* - 1$, $U_{\text{multi}}(\rho)$ is a pairwise potential. At high densities $\rho^* \le \rho$ the model assumes that the hydrophobic particle is shielded by the beads that already interact with it so that $U_{\text{multi}}(\rho)$ becomes constant. It is exactly this feature that prevents the tails from locally collapsing to high densities and crystallizing. This model has the advantage of yielding membranes with a normal bilayer structure, composed of two monolayers of the rod-like amphiphilic particles and it has been used to address the kinetics of vesicle formation [70], vesicle fusion [111], and the change of vesicle structure in response to mechanical forces [112]. Like many similar models invoking complex multibody interactions to obtain stable amphiphilic membranes, its parameterization lacks a transparent connection with material properties. In combination with the rather simplistic description of amphiphile architecture this makes the calibration of these representations for describing realistic amphiphilic systems rather questionable. Nevertheless, it is exactly from the point of elucidating the universal features of amphiphile behavior that these models are beneficial. For instance, when considering the kinetics of vesicle fusion the Noguchi and Takasu model yields two pathways that are similar to those observed in vesicle simulations conducted with systematically coarse-grained lipid models [64] and generic simulations of planar bilayer fusion [39,82]. In particular, the first one resembles the classical hemifusion mechanism (see Fig. 5) while the second, invokes the stalk-hole mechanism; i.e., reproduces the leaking fusion pathway of [39,82].

A first solvent-free model invoking only pairwise, Lennard-Jones-type, interactions for studying amphiphilic membranes was reported in [113]. Subsequent models [114–116] used improved two-body interaction schemes obtaining the crucial property of unassisted bilayer self-assembly. Particularly [114] put forward the importance of the interactions range. In this work, the amphiphiles where described by a chain of three beads: one for the hydrophilic head and two for the hydrophobic tail. The beads were linked via FENE bonds, and an additional control over the molecular conformations was obtained by utilizing a harmonic spring potential acting between the head and the *last* tail bead. The excluded volume interactions between all the particles have been captured by a Weeks–Chandler–Andersen (WCA) potential. The hydrophobic beads were considered to experience an additional, two-body, longer range interaction of the form

$$U_{\text{att}}(r) = \begin{cases} -\varepsilon & r < r_c \\ -\varepsilon \cos^2\left(\frac{\pi(r-r_c)}{2w_c}\right) & r_c \le r \le r_c + w_c \\ 0 & r > r_c + w_c \end{cases}. \tag{9}$$

In the above expression, ε and σ (with σ being the tail–tail collision diameter) are the energy and the length units respectively, r_c is the cut-off length, while the decay range is determined by the parameter w_c. The later was shown to be of key importance for the model and can be used to tune the amphiphile phase diagram and the material properties such as area per amphiphile, bilayer structure, elastic constants, and diffusivity. The functional form of the pair potential between the lipid tails given by the combination of the WCA potential with the attractive interaction of (9) is reproduced by the solid line in the inset on the left of Fig. 8, while the main panel shows the phase behavior of the amphiphiles.

In connection with amphiphilic vesicles this model has been applied to study cylindrical vesicles [117], evolution of multicomponent systems [114] and the vesiculation of planar membranes driven by curvature inducing proteins or nanoparticles [118]. The time evolution of a vesicle, composed of a 50:50 mixture of immiscible A_1, A_2 amphiphiles, is shown in the right main panel of Fig. 8. As in the case of the DPD simulations of [108] (see left bottom of Fig. 7) the domains in the inner and outer leaflets match each other. The budding and the subsequent vesicle pinching-off is induced by the available domain size and the line tension between the A_1-rich and A_2-rich domains. It should be mentioned that in the studies of vesicle shape evolution with solvent-free models the constraint of constant area-to-volume ratio, present in simulations with explicit solvent, is relaxed such that the kinetics might be quite different. This absence of explicit solvent might become a drawback for studying vesicle behavior in external flow fields or confinement; the case of vesicle extrusion is a good example.

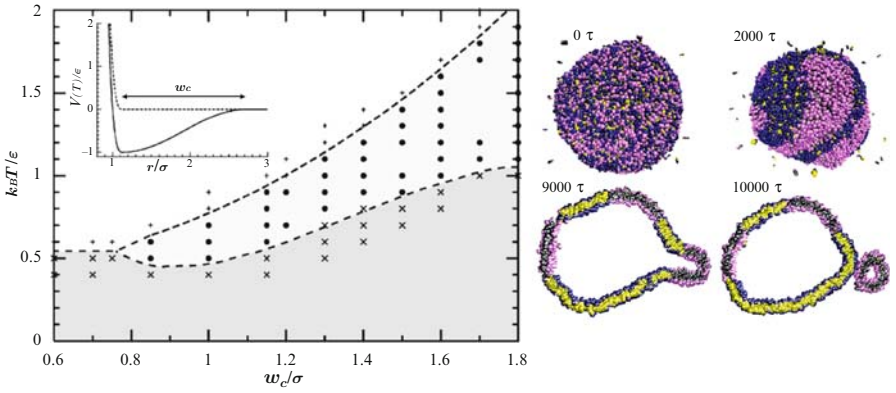

Fig. 8 *Left*: The phase behavior of amphiphiles as observed with the model of [114,115], is shown in the *main panel*, plotted as a function of rescaled temperature k_BT/ε and attraction width w_c/σ at zero lateral tension. Each symbol corresponds to one simulation and identifies different bilayer phases. *Crosses* denote the gel phase, *solid circles* mark fluid bilayers, and *vertical crosses* indicate the region where bilayers are unstable. The *dashed lines* are merely guides to the eye. The *inset* shows the pair potential between tail beads (*solid line*) and the purely repulsive head–head and head–tail interaction (*dashed line*). Reprinted with permission from Ref. 114. Copyright (2005) by the American Physical Society. *Right*: Phase separation and budding sequence for a vesicle containing a 50:50 mixture of two lipids. The vesicle is in equilibrium with a very dilute "vapor of amphiphiles" (i.e., the lipids seen floating in the exterior volume). From [114]

The study of protein mediated vesiculation [118] is a nice illustration of the power of generic models to describe processes in bio-mimetic membranes on large time and length scales. In that work the above model was combined with a generic representation of curvature inducing proteins, i.e., particles curving locally the membrane by attracting preferentially the hydrophilic lipid heads. Although the direct interaction potential between the particles is only a short-ranged WCA repulsion, the local membrane deformation gives rise to an effective attractive force, leading to protein clustering. The membrane induces an effective interaction among the inclusions, but the inclusions, in turn, also have a dramatic impact on the membrane: The cooperative deformation generated by the protein clusters leads to membrane vesiculation as is shown in the last stages of the pathway in Fig. 9.

Reconsidering the model of Noguchi and Takasu, it is noted that (7) and (8) define the interactions of hydrophobic particle with its surroundings as a function of the local density of the hydrophobic beads. This can be considered as a special case of the more general idea of expressing the complicated interactions in an amphiphilic solution within a density functional theory. Some advantages of such an approach are: (1) easy parameter calibration, starting from "initial guess" values obtained through a transparent connection with some characteristic membrane material properties, (2) using the model as a base for efficient particle-based techniques, including Monte-Carlo methods [119–123] and the Single-Chain-in-Mean-Field (SCMF) simulations scheme [122, 124], and (3) possibility to interface with SCF techniques [125–129], which are extremely efficient computationally and have the significant advantage to offer an easy estimate of the free energy of the morphology (within the mean-field approximation) [130–132]. The last point can be particularly important when understanding pathways of structure evolution. In what follows, we will present an illustration of such an approach, developed for the study of polymersomes loaded with long polymeric molecules. Modeling these

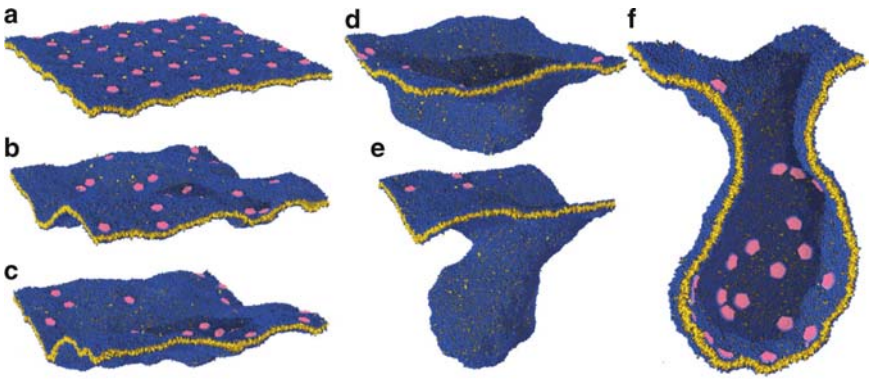

Fig. 9 Successive stages of a vesiculation event driven by 36 cap-shaped proteins on a membrane containing 46,080 lipids. The side length of the initial membrane corresponds to ~ 160 nm, while the times of the simulation snapshots are **a** 0 τ, **b** 20,000 τ, **c** 40,000 τ, **d** 50,000 τ, **e** 60,000 τ, and **f** 70,000 τ; the last corresponding roughly to 1 ms. Reprinted by permission from Macmillan Publishers Ltd: Nature, (Ref. 118), copyright (2007)

systems was motivated by the experimental study of virus-assisted loading of polymersomes presented in [27], already highlighted in the introduction. In that work, bacterial channel forming proteins LamB were reconstituted in the shell of an *ABA*-triblock polymersome. In a normal bacterial cell membrane these proteins are a specific transporter for maltodextrins; however they can also be targeted by λ phage viruses, which bind to them and inject their DNA into the cell. It was demonstrated that, after being incorporated into the vesicle shell, the protein functionality was preserved: the λ phage viruses were still able to bind to them and inject their DNA into the artificial container. These experiments, presenting a perspective concept for gene therapy, are illustrated in Fig. 3.

3.3 Bridging Between Particle-Based and Field-Theoretic Models

The development of a density functional description of an amphiphilic system comprises two stages: (1) the representation of the molecular architecture and (2) the construction of the density functional for the non-bonded interactions. For the example described above, the molecular architecture will be considered within a bead-spring model, which takes into account the polymeric nature of the amphiphiles and the load. In the following, we only consider linear, flexible molecules but generalizations to more complex molecular architectures, including chain stiffness (see 5)) or branching, are straightforward in a particle-based description. We assume the amphiphilic molecules to be *AB*-diblock copolymers and the loading homopolymer, *h*, to be comprised of segments of type *C*. The *A*-type beads will be considered as hydrophobic, while *B*- and *C*-type beads are hydrophilic. Then, the connectivity Hamiltonian, H_b, will be

$$\frac{\mathcal{H}_{b(m)}[\mathbf{r}(s)]}{k_B T} = \sum_{s=1}^{N_{(m)}-1} \frac{3(N_{(m)}-1)}{2{R_{e(m)}}^2} \left[\mathbf{r}_i(s) - \mathbf{r}_i(s+1)\right]^2, \tag{10}$$

where $\mathbf{r}_i(s)$ is the coordinate of s^{th} bead of molecule *i*. The index *m* stands for the chemical species of the molecule (i.e., $m = AB$ or *h*). $R^2_{e(m)}$ is the corresponding mean squared end-to-end distance of the unperturbed molecule, while k_B and T are the Boltzmann constant and temperature, respectively. $N_{(m)}$ denote the number of beads used to discretize the molecular species and, although they explicitly appear in (10), they do not have a specific physical meaning, i.e., a different contour descritization yields an equivalent model.

Lengths in the coarse-grained model can be identified with a real system by matching the characteristic molecular extension, $R_{e(m)}$ of one species with the experimental value. This quantity is conserved by the representation and is an example of an *invariant* quantity [41] mentioned in the introduction. In a generic model, these quantities are the only parameters that convey a specific physical information, establishing relevance with the energy, length and time scales of the real systems.

In principle, it is the invariant quantities that can be expressed through certain material properties. Their number, required for each generic model parameterization, depends on the complexity of the chosen representation.

In the following, all lengths will be expressed in units of the end-to-end distance, $R_{e(AB)}$, of the amphiphile. The loading polymer is much larger than the amphiphile, $R_{e(h)} \approx 8R_{e(AB)}$. We will use $N_{AB} = 32$ beads for the amphiphiles. Ten of them are hydrophilic; the remaining 22 are hydrophobic. The homopolymer h will be represented by $N_{\mathrm{h}} = 2,048$ coarse-grained beads.

The choice of the density functional for describing the non-bonded interactions is dictated by the specifics of the problem. In polymer physics, the most widely used approach for modeling multicomponent melts employs a Flory–Huggins description of the incompatibility of different species. The polymeric liquid is assumed to be either incompressible or to have a limited compressibility. In case of AB amphiphilic copolymer membranes a similar description has been used within studies [38, 82, 130, 132] representing large groups of water molecules with B-type homopolymers. In those models, the non-bonded energy for a given configuration of the amphiphilic system, as determined from the coordinates of all beads, is given by the interaction Hamiltonian:

$$\frac{\mathcal{H}_I}{k_B T} = \chi \rho_o \int \mathrm{d}\mathbf{r} \hat{\phi}_A(\mathbf{r}) \hat{\phi}_B(\mathbf{r}), \quad \hat{\phi}_\alpha(\mathbf{r}) = \frac{1}{\rho_o} \sum_{i=1}^{n} \sum_{s=1}^{N(i)} \delta(\mathbf{r} - \mathbf{r}_{\mathrm{i}}(s)) \gamma_\alpha(s), \tag{11}$$

where n is the total number of molecules in the system (AB copolymers and B homopolymers), χ the Flory–Huggins parameter, ρ_o the bead number density in the bulk, and $\hat{\phi}_\alpha(\mathbf{r})$ denotes the volume fraction of species α at point $\mathbf{r}$ of space. In addition, $\gamma_\alpha(s) = 1$ if the s^{th} segment of the i^{th} molecule is of type α (with $\alpha = A$, or B) and $\gamma_\alpha(s) = 0$ otherwise. When the system is assumed to be incompressible, the molecular configurations are subjected to the constraint $\hat{\phi}_A(\mathbf{r}) + \hat{\phi}_B(\mathbf{r}) = 1$, which can be taken into account in the statistical mechanical formalism [125]. In case of limited assumption, a simple density-dependent quadratic term [133] $\frac{\kappa\rho_o}{2} \int \mathrm{d}\mathbf{r} (\hat{\phi}_A(\mathbf{r}) + \hat{\phi}_{\mathrm{B}}(\mathbf{r}) - 1)^2$ is added to (11), where $\kappa\rho_o$ controls the magnitude of density fluctuations, being proportional to the inverse compressibility. More realistic representations of local fluid structure can be used, as was demonstrated in the density functional studies of lipid bilayers [134, 135]. Equation (11) augmented with the quadratic compressibility term, is essentially a second-order virial expansion of the interaction energy with respect to the component densities.

We note that higher order terms in the virial expansion naturally arise during the systematic coarse-graining procedure, where some degrees of freedom are integrated out. In this spirit, higher order expansions can be exploited to represent amphiphilic system without explicitly describing solvent molecules. For the solvent-free model of AB-amphiphilic vesicle loaded with a C homopolymer used in the following, the interaction Hamiltonian takes the form

$$\frac{\mathcal{H}_I}{k_BT} = \int \frac{\mathrm{d}\mathbf{r}}{R^3_{e(AB)}} \left\{ \frac{1}{2} \sum_{\alpha=A,B,C} \sum_{\beta=A,B,C} v_{\alpha\beta} \hat{\rho}_\alpha(\mathbf{r}) \hat{\rho}_\beta(\mathbf{r}) \right.$$
$$\left. + \frac{1}{3} \sum_{\alpha=A,B,C} \sum_{\beta=A,B,C} \sum_{\gamma=A,B,C} w_{\alpha\beta\gamma} \hat{\rho}_\alpha(\mathbf{r}) \hat{\rho}_\beta(\mathbf{r}) \hat{\rho}_\gamma(\mathbf{r}) \right\}, \tag{12}$$

where $v_{\alpha\beta}$ are $w_{\alpha\beta\gamma}$ are symmetric with respect to index permutations, standing for the second- and the third-order virial coefficients, respectively. In (12) all lengths are expressed in units of the end-to-end distance, $R_{e(AB)}$, of the amphiphile. Thus, the dimensionless second order virial coefficients play the role of a Fixmann parameter in the theory of polymer solutions. The dimensionless densities, $\hat{\rho}_\alpha(\mathbf{r})$, are defined as

$$\hat{\rho}_\alpha(\mathbf{r}) = \frac{R^3_{e(AB)}}{N_{AB}} \sum_{i=1}^{n} \sum_{s=1}^{N(i)} \delta(\mathbf{r} - \mathbf{r}_\mathrm{i}(s)) \gamma_\alpha(s) \tag{13}$$

with N_{AB} being the number of beads used for amphiphile discretization and in this case the definition of $\gamma_\alpha(s)$ is modified to take into account the additional segment species C. In this scope, the $\hat{\rho}_\alpha(\mathbf{r})$ express the segmental densities at point $\mathbf{r}$ of space, as the number of equivalent AB strands at $\mathbf{r}$. The virial coefficients $v_{\alpha\beta}$ and $w_{\alpha\beta\gamma}$ are related to the *segmental* virial coefficients $\tilde{v}_{\alpha\beta}$ and $\tilde{w}_{\alpha\beta\gamma}$

$$v_{\alpha\beta} = \frac{\tilde{v}_{\alpha\beta} N^2_{AB}}{R^3_{e(AB)}}, \quad w_{\alpha\beta} = \frac{\tilde{w}_{\alpha\beta\gamma} N^3_{AB}}{R^6_{e(AB)}}. \tag{14}$$

Therefore all quantities appearing in the definition of the functional $\mathcal{H}_I$, are invariants, i.e., independent of the number of beads used to discretize the polymer chains.

Equations (10), (11), and (12) in combination with a proper parameter choice, constitute a complete representation of the amphiphilic system. It should be noted that, although the interactions are cast in a density functional language, the model is still particle-based: the densities, in terms of which the functionals are expressed, are determined from the particle coordinates in each system configuration. At this point, the particle-based description can be converted to a field theoretical one by reformulating the multi-particle problem in terms of independent amphiphilic molecules in fluctuating external fields through a Hubbard–Stratonovich transformation. This shifts the difficulty of describing the statistical mechanics of mutually interacting molecules to the equally challenging problem of functional integration over fluctuating external fields. Commonly, the functional integrals over the fluctuating fields are approximated by their saddle-point values. The mean-field approximation, which underlies the SCF theory, inherently ignores all fluctuation effects. It has been employed to identify possible fusion pathways in planar membranes [130] and vesicles [132]. In these studies, the average density fields of the intermediates along different fusion pathways, which have previously been observed in simulations [38,82], have been generated by identifying an appropriate reaction coordinate that parameterizes the fusion pathway, and the relevant free energy barriers have

been calculated within mean-field theory. Despite the computational efficiency of SCF calculations and the direct accessibility of free energies that it offers, more accurate, alternative techniques may be required in some circumstances [136]. For instance, in bio-mimetic assembling systems, the energy scale of the interactions between the different components is frequently comparable to k_BT while the free energy barriers along the fusion pathway are only of the order of tens of k_BT. Under these conditions, thermal fluctuations cannot be ignored and the concept of a free energy barrier that is extracted from a constraint equilibrium calculation may become inaccurate in describing the kinetics of collective phenomena.

Modeling the kinetics of self-assembly and morphology evolution by field-theoretic methods is also a formidable task. Typically, it is performed within a Landau–Ginzburg expansion of the free energy, relating the local evolution of the order parameter (i.e., the component density field) to the chemical potential gradient through an Onsager coefficient. Due to the spatially extended molecular architecture of the amphiphiles, this relation is nonlocal. Because of numerical implications, however, simplified local forms are commonly used. In this context, it is highly desirable to retain the particle-based description as defined by (10), (11), (12), and use them as a basis for simulation. In simulations, the interplay between the dynamics of individual molecules and the kinetics of collective fields is transparent, the dynamic algorithm of the simulation can be chosen as to realistically mimic the single-molecule dynamics [137], and it is not assumed that the molecular conformations are in instantaneous equilibrium with the collective variables, as it is implicitly done in the field-theoretic framework by integrating out the molecular degrees of freedom.

To parameterize the polymersome model, the identification of the virial coefficients, $v_{\alpha\beta}$ and $w_{\alpha\beta\gamma}$, is driven by the requirement that the amphiphiles described by (10) and (12) should create a stable bilayer with given material properties. Assuming that the hydrophobic interior should be in a melt state, the coefficients v_{AA} and w_{AAA} are determined such that (12) enforces the A-blocks to create a melt in equilibrium with its "vapor" which, in a solvent free model, represents the surrounding water. It can be shown, from (12), that the equation of state of such a homogeneous melt, within mean-field approximation, is [138]

$$\frac{PR^3_{e(AB)}}{k_BT} = \rho_A + \frac{v_{\mathrm{AA}}}{2}(\rho_A)^2 + \frac{2w_{\mathrm{AAA}}}{3}(\rho_A)^3, \tag{15}$$

where ρ_A is the average density of the hydrophobic region, expressed in terms of equivalent AB strands (i.e., an invariant). A representative graph of (15) in the ρ_A–$PR^3_{e(AB)}/k_BT$ plane, is shown on the left of Fig. 10. The intersection of this curve with the ρ_A axis at $PR^3_{e(AB)}/k_BT = 0$ (marked by the green line) determines the melt density at coexistence (since the amphiphile concentration in the vapor is negligible). The slope of the P/k_BT curve at the intersection (marked with the red line) expresses the compressibility, $\frac{1}{\kappa_\tau} = \rho_A \frac{\partial P}{\partial \rho_A}$, of the A melt at the coexistence point.

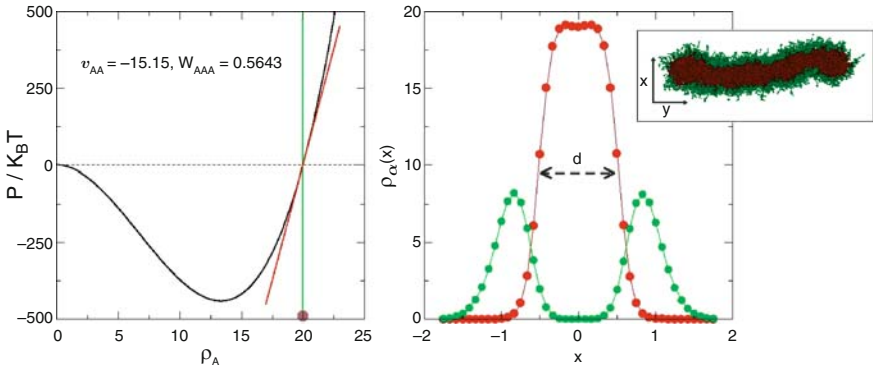

Fig. 10 *Left*: Mean-field equation of state for the hydrophobic A strand melt, for $v_{AA} = -15.15$ and $w_{AAA} = 0.564375$ (see (15)). The vertical *green line* marks, at $P/k_BT = 0$, the coexistence density of the melt with its vapor, $\rho_A = 20$. The *red line* marks the tangent to the P/k_BT curve at $P/k_BT = 0, \rho_A = 20$. Its slope is inversely proportional to the melt compressibility. *Right*: The density distribution of the A and B bilayer components is shown across a free edge, membrane patch (see *inset*) which is thin in the z direction (i.e., vertically to the graph plane). The *red* and the *green symbols* correspond to the densities of the hydrophobic and the hydrophilic segments, respectively

Thus, the v_{AA} and w_{AAA}, for given values of ρ_A and compressibility are obtained from the equations

$$\begin{aligned} \rho_A + \frac{v_{AA}}{2}(\rho_A)^2 + \frac{2w_{AAA}}{3}(\rho_A)^3 &= 0 \\ \rho_A + v_{AA}(\rho_A)^2 + 2w_{AAA}(\rho_A)^3 &= \frac{\rho_A}{12(\xi/R_{e(AB)})^2} \end{aligned} \tag{16}$$

where we have exploited the relationship between the Edwards correlation length, ξ and the compressibility: $\frac{1}{k_BT\kappa_\tau} = \frac{\rho_A R^2_{e(AB)}}{12\xi^2}$. In experimental systems [21, 94], typical values of ρ_A will be between 10 and 100. Therefore, we choose to set $\rho_A = 20$ in the following example. Generally the magnitude of total density fluctuations in a polymer liquid is negligible on the mesoscopic scale. The length scale threshold, after which the polymer melt can be considered as incompressible, is set by the correlation length ξ, which is microscopic ($\sim$1 nm). In this example we choose a larger value, $\xi \sim 0.02R_{e(AB)}$. This choice facilitates the simulations by making the polymer liquid "softer", while still restricting the role of density fluctuations below the characteristic bilayer mesoscopic scales. The above requirements yield $v_{AA} = -15.15$ and $w_{AAA} = 0.564375$. The determination of the v_{AB} is related to the desired degree of incompatibility between the hydrophobic and the hydrophilic monomers, typically expressed through χN_{AB}. It can be shown to be connected to the virial coefficients as

$$\chi N_{AB} \approx \rho_A \frac{2v_{AB} - v_{AA} - v_{BB}}{2}. \tag{17}$$

For the example application of a loaded polymersome, we require $\chi N_{AB} \approx 30.5$. The determination of the coefficients of the hydrophilic moieties is motivated by reproducing for them good solvent conditions. In the following, we set all the third order virial coefficients between the hydrophilic units to zero. The second order coefficients should have a positive value, which in the case of the B monomers determines the size of the hydrophilic head of the amphiphile. The coefficient v_{BB} has to be empirically determined to comply with the bilayer stability (e.g., large values of v_{BB} gives rise to micelle formation instead of bilayers). In this work, we use $v_{BB} = v_{\mathrm{CC}} = 0.1$. Substitution of v_{BB} and v_{AA} into (17) yields $v_{AB} = -6$. Table 1 summarizes the values of the virial coefficients used to study the loaded polymersomes.

The model defined by (10) and (12) is studied in the following using a Monte-Carlo approach. The implementation of this scheme requires the assignment of a spatial density distribution to a given configuration of amphiphiles. To achieve this [119,122,124] a cubic lattice $\{\mathbf{c}\}$ with a grid spacing ΔL is defined in the simulation box. Then, the densities are assigned to each grid point, $\mathbf{c}$, from the positions of the beads as

$$\hat{\rho}_\alpha(\mathbf{c}) = \frac{1}{N_{AB}} \sum_{i=1}^{n} \sum_{s=1}^{N(i)} \Pi(\mathbf{r}_i(s), \mathbf{c}) \gamma_\alpha(s). \tag{18}$$

The function $\Pi(\mathbf{r}, \mathbf{c})$ performs the particle assignment to the grid points of the lattice. In this work we use a linear extrapolation:

$$\Pi(\mathbf{r}, \mathbf{c}) = \frac{1}{\Delta L^3} \Pi_{\alpha=\mathrm{x,y,z}} \left(1 - \frac{|r_\alpha - c_\alpha|}{\Delta L}\right), \tag{19}$$

if the distance between the grid point and the bead along each Cartesian direction is less than ΔL, and $\Pi(\mathbf{r}, \mathbf{c}) = 0$ otherwise. A similar approach is used in particle to mesh methods in electrostatics [139, 140]. The grid size ΔL should be considered as an additional model parameter, setting the range of the interactions, and in this example we use $\Delta L = 0.166 R_{e(AB)}$. After defining the assignment of particle coordinates to lattice densities, the Monte-Carlo sampling is straightforward. In particular, various moves such as random local segment displacement, slithering-snake, chain translation, identity exchange can be used to create new system configurations. Using the proposed particle coordinates the new density distribution, $\rho_\alpha^{new}(\mathbf{c})$, is obtained via (18) and the energy of the non-bonded interactions can be calculated from (12) in the proposed configuration. The Monte-Carlo moves are then accepted

Table 1 Values of the virial coefficients used in (12) to study loaded vesicles

$v_{AA} = -15.15,\ v_{BB} = v_{CC} = v_{BC} = 0.1,\ v_{AB} = v_{AC} = -6$
$w_{AAA} = w_{AAB} = w_{ABB} = w_{AAC} = w_{ACC} = 0.564375$
$w_{BBB} = w_{CCC} = w_{BBC} = w_{BCC} = w_{ABC} = 0$

according to a Metropolis criterion, $p_{acc} = \min\left[1, e^{-(\Delta\mathcal{H}_b+\Delta\mathcal{H}_I)/k_BT}\right]$, where $\Delta\mathcal{H}_b$ is the difference in bonded interactions and $\Delta\mathcal{H}_I$ is the change in the non-bonded interactions between the proposed and the old system configurations, respectively. Here, only random local displacement moves have been used in order to mimic a realistic bead dynamics [137].

Before modeling loaded polymersomes, simulations of planar bilayers comprised of *AB*-amphiphiles, with the parameters of Table 1 have been performed to establish various material properties. The information concerning the area per amphiphile, A_o, in the tensionless state will be particularly important for creating the initial configurations of the loaded vesicles. The grid utilized in the current Monte-Carlo scheme for calculating the density distribution creates certain difficulties for obtaining A_o using statistical ensembles that invoke changes in box dimensions (e.g., the $n\Sigma T$ ensemble). In principle, gridless methods could be used [119], however, at the expense of computational efficiency. Therefore, to obtain A_o we follow here an approach similar to the one of [39,82], where polymeric membranes have been studied within a coarse-grained lattice model. An nVT simulation of an isolated bilayer patch was performed, with a setup as shown in the inset on the right of Fig. 10. The patch, with its normal oriented roughly along the x axis, spanned the system in the short z direction but not in the long one, the y-direction. In this direction the membrane patch can freely adjust its extension, until it neither grows nor shrinks. In this case, the mechanical tension, Σ, vanishes. The average profile of the densities $\rho_A(x)$ and $\rho_B(x)$ was then calculated from the middle of the bilayer (to omit the bulging at the free bilayer edges), which is shown in the main panel on the right of Fig. 10. Almost no dip is observed in the midplane of the hydrophobic core density profile, similarly to what has been reported [85, 86] for CGMD simulations of polymeric membranes with high molecular weight. The density in the inner part of the bilayer is slightly below the value, $\rho_A = 20$ predicted by the mean-field equation of state, (15). The hydrophobic thickness, d, of the bilayer can be estimated from the $\rho_A(x)$ profile half-width to $d = 1.1R_{e(AB)}$, while the area per amphiphile is obtained after integrating the $\rho_A(x)$ and $\rho_B(x)$ profiles, yielding $A_o = 0.066R^2_{e(AB)}$.

The calculation of materials properties such as bending rigidity, κ, or area elastic modulus, k_α, requires the simulation of large systems. The inset of Fig. 11 shows a representative snapshot of the large bilayer membranes that have been studied for the purpose of this work, in the nVT ensemble. The bilayer was preassembled to span the box in the y- and z-directions with $L_y = L_z = 15R_{e(AB)}$. To obtain a tensionless membrane, the number of *AB* molecules was calculated from the previously described simulations of free edge patches; thus the snapshot of the graph contains 6,800 amphiphiles. To study membranes under tension, bilayers with larger areas per amphiphile (i.e., a smaller number of *AB* molecules) have been also simulated. We observed that the bilayers parameterized according to Table 1 were able to sustain a $10-15\%$ area dilation for an extended Monte-Carlo simulation with local monomer displacements.

Commonly the bending rigidity of the membrane can be calculated by comparing the simulation results to the prediction of the Helfrich–Hamiltonian [44, 141].

Within this continuum description, the membrane is conceived as a thin elastic sheet. If one assumes that the membrane fluctuations are small, its surface can be parameterized within a Monge representation via a height function, $h(y,z)$, describing its position over some reference plane. Then, the Helfrich–Hamiltonian takes the form

$$\mathcal{H} = \int dydz \left[\frac{\Sigma}{2} (\nabla h)^2 + \frac{\kappa}{2} (\triangle h)^2 \right]. \tag{20}$$

Expanding $h(y,z)$ in Fourier space and using the equipartition theorem allows to calculate the power spectrum of membrane fluctuations [40, 48]:

$$\sigma^2 \equiv \langle |h_{\mathrm{q}}^2| \rangle = \frac{k_B T}{\Sigma q^2 + \kappa q^4}. \tag{21}$$

To employ this approach in the considered example, the membrane was described in a continuum limit through a surface, $h(y,z)$, identified as the position of the bilayer midplane. The results of such an analysis for the cases of a tensionless and a $\sim$10% stretched membrane are shown in the main panel of Fig. 11 with red and black solid symbols, respectively. The solid lines are fits of the power spectrum h_{q}^2 with (21). It can be seen that, indeed, $A_o = 0.066 R^2_{e(AB)}$ (predicted by the free edge simulations) corresponds to the membrane tensionless state. The bending rigidity of the bilayer is $4.5 k_B T$ and seems to decrease with tension, presumably due to membrane thinning.

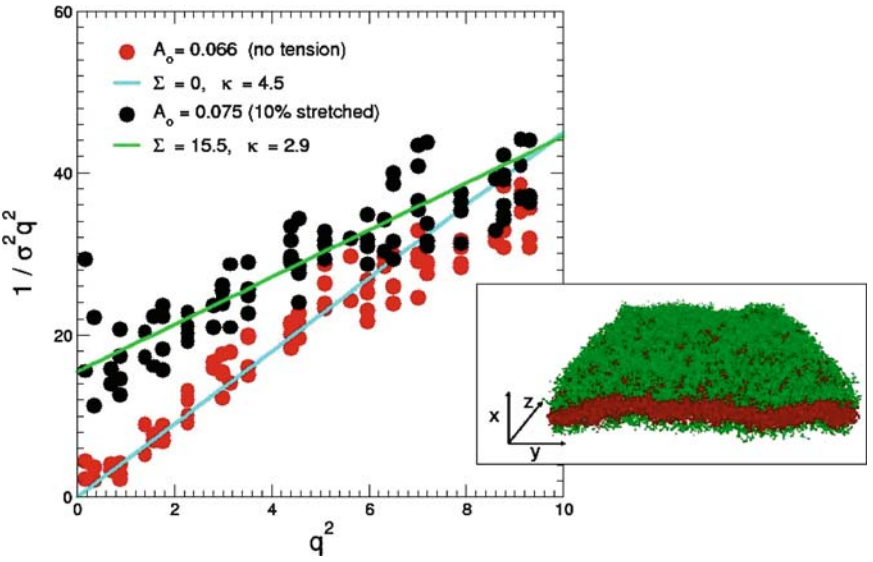

Fig. 11 Shown in the *main panel* is the power spectrum of the fluctuations of large bilayer patches (the *inset* shows a representative snapshot). The simulations where conducted in nVT ensemble and the number of molecules in the bilayer was chosen to reproduce a tensionless (*red circles*) and a 10% stretched (*black circles*) membrane. The *solid lines* are fits according to equation (21)

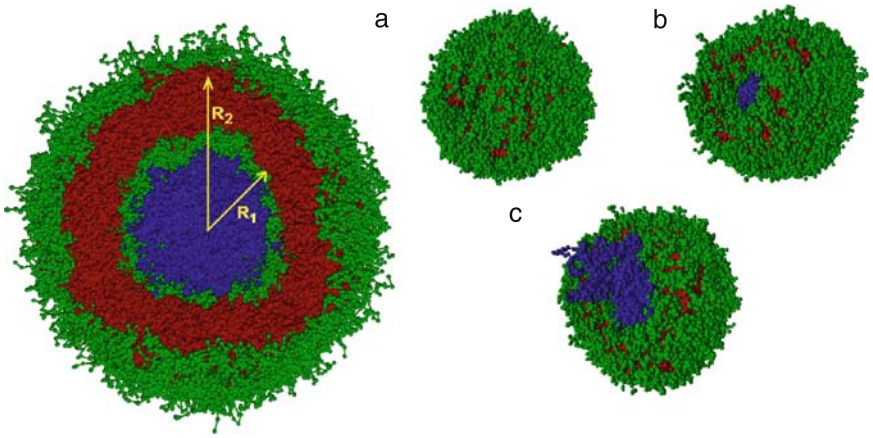

Fig. 12 Shown on the *left* is a cut through an initial configuration of a vesicle loaded with polymer chains. The hydrophobic and hydrophilic segments of the amphiphile and the hydrophilic beads of the polymer load are shown in *red, green,* and *blue*, respectively. Three characteristic snapshots of a rupturing polymersome, loaded with $n_h = 10$ long hydrophilic polymers are shown on the *right*

It can be seen that implementing the power spectrum of fluctuations for the calculation of bending rigidity requires an efficient sampling on large spatial scales of the membrane (low q values). In this scope, casting the recently reported [142] Mode Excitation MC approach in context of the presented model could be very promising.

The data regarding A_o were subsequently utilized to create initial configurations of polymersomes. A representative cut-through is shown in the left of Fig. 12, where the amphiphilic A, B and the loading polymer C segments are shown in red, green, and blue, respectively. The radius of the sphere corresponding to the AB interface of the outer and the inner monolayer is denoted as R_1 and R_2, respectively. In the initial configurations it was set $R_1 = 3R_{e(AB)}$ and $R_2 = 4R_{e(AB)}$, i.e., the diameter of the cavity is smaller than the size of the loading polymer, $R_{e(h)} \sim 8R_{e(AB)}$, which was placed in it in a random configuration. The number of the amphiphiles in the outer, n_{AB}^{out}, and in the inner, n_{AB}^{in}, shell was selected according to $n_{AB}^{\text{out}} = 4\pi R_2^2/A_o$ and $n_{AB}^{\text{in}} = 4\pi R_1^2/A_o$ so that the whole vesicle contained 4,696 amphiphiles. In this way polymersomes containing different numbers, n_h, of loading polymer chains have been prepared, ranging from $n_h = 0$ (empty vesicles) to $n_h = 30$. The initial configurations were subjected to long Monte-Carlo simulations, in order to create well equilibrated series of system snapshots. The long hydrophilic polymer confined in the polymersome will swell and, due to the small dimensions of the vesicle cavity, will create a pressure on the amphiphilic shell. It is observed that the polymersomes could sustain only a limited amount of loading polymers, up to $n_h = 15$. For higher loading amounts, the polymeric containers ruptured during the initial stages of the simulation. On the other hand, for moderate loads $n_h \leq 10$, the polymersomes remained mostly stable through the runs, exceeding several times the longest relaxation time of the high molecular weight polymer.

The configurations of the equilibrated, stable polymersomes were then analyzed, to extract the bending rigidity κ following an approach similar to the one that was

used in the early vesicle simulations of Drouffe et al. [110]. In particular, the position of the shell midplane is calculated from the vesicle configurations, so that they are described through a single surface, $R(\theta,\phi)$, in spherical coordinates. This can be expanded in spherical harmonics around a sphere of radius R_V, which has the same volume as the vesicle, so that

$$R(\theta,\phi) = R_V \left[1 + \sum_{l,m} u_{\mathrm{lm}} Y_{l,m}(\theta,\phi) \right]. \tag{22}$$

As in the case of the planar bilayer, the energy of this elastic surface can be assigned a Hamiltonian [46, 48]:

$$\mathcal{H} = \sum_{l\geq 2} \sum_{m=-l}^{l} \frac{|u_{\mathrm{lm}}|^2}{2} (l+2)(l-1) \left[\Sigma R_V^2 + l(l+1)\kappa \right], \tag{23}$$

where, as in the case of the planar bilayer, Σ and κ denote the mechanical tension and the bending rigidity. The corresponding power spectrum is [48]

$$\sigma^2 \equiv \langle |u_{\mathrm{lm}}|^2 \rangle = \frac{k_B T}{(l-1)(l+2)[\Sigma R_V^2 + \kappa l(l+1)]}. \tag{24}$$

The main panel of Fig. 13 presents the power spectrum calculated for empty and loaded ($n_h = 5$ and $n_h = 10$) vesicles, while the inset shows the fitting of this

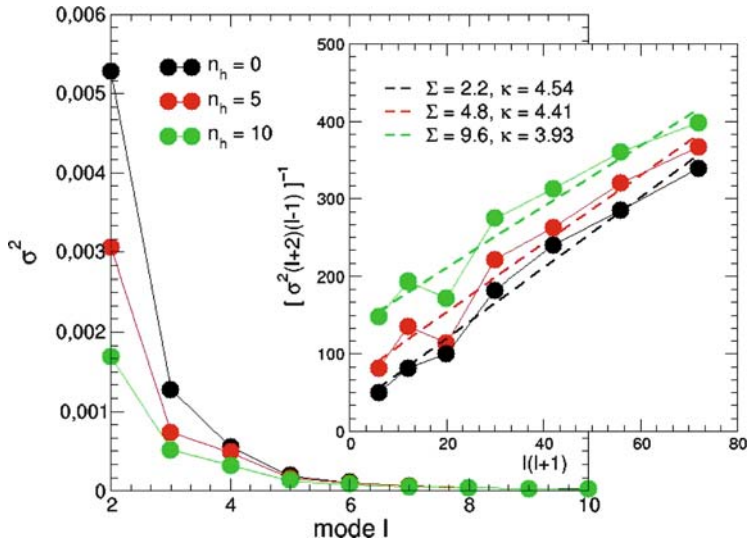

Fig. 13 Shown in the *main panel* is the power spectrum of the fluctuations of vesicles at various amounts of loading polymers: empty vesicle ($n_h = 0$, *black symbols*), five ($n_h = 5$, *red symbols*) and ten ($n_h = 10$, *green symbols*) chains. The *inset* shows the same data fitted with equation (24)

spectrum with (24). The main graph shows that with higher load the shell fluctuations decrease (i.e., σ^2 goes down) due to the increase of the tension, while the fits demonstrate that the shell of the empty vesicles has almost the same rigidity as the planar membrane. This bending rigidity decreases as more polymers are added into the cavity and the polymersome shell becomes more stretched.

4 Conclusions and Outlook

Over the last few years, computer modeling has demonstrated an increasing potential for describing biology-related molecular systems. Among these, bio-mimetic amphiphilic vesicles have attracted abiding attention due to numerous applications in therapeutics and medical imaging. Because they exhibit a diversity of characteristic length and time scales, they constitute a challenge for modeling, so different techniques have to be applied depending on the information to be gained. Atomistic and systematically derived coarse-grained models can account in detail for the chemical architecture, being on the high resolution edge of the spectrum of simulation models. Therefore, they are powerful [40, 88, 143] in realistically representing the local structural and dynamic properties, such as spatial organization of molecular components/chemical groups, molecular conformations, motion of individual particles. This information is important for understanding phenomena depending significantly on the specifics of molecular structure (e.g., drug transport through a membrane). At this point, however, the simulation of amphiphilic vesicles faces the difficulty that focusing on small scale properties does not always imply that the entire vesicle structure can be ignored. In particular, in small systems they will be significantly affected by the vesicle size manifesting itself by the high curvature of the bilayer shell. Therefore, for example, the inner and the outer monolayer leaflets will differ in molecular organization and component dynamics. On the other hand, in larger vesicles the curvature effects are expected to become less important and the local bilayer shell properties can be decoupled from the vesicle's geometry. Thus they can be extracted from smaller systems of planar membrane patches described with the atomistic or detailed coarse-grained models. In this case, the quality of the predictions will depend on the fine details of the interaction force field.

Besides issues related to the accuracy of force fields in spatially inhomogeneous systems comprising many chemically distinct components, the basic restriction related to the chemically detailed models is the rather small length and time scales that they can access. This limitation imposes severe restrictions for considering collective phenomena in amphiphilic vesicles, i.e., processes that involve large particle numbers. Typical examples include vesicle assembly, vesicle fusion, phase separation and shape transformations of multicomponent amphiphilic vesicles. For many of these processes, it is expected that the underlying atomistic details of the molecular constituents can be captured by a small number of relevant characteristics and universality classes, comprised of systems with a rather different atomistic structure, can be identified. These phenomena can be successfully investigated via minimal

models incorporating the universal characteristics and invoking a large degree of coarse-graining. The advantages of generic approaches are both, computational and conceptual. Apart from allowing the modeling of large length ($\sim$100 nm) and time ($\sim$ms) scales due to the significant reduction of degrees of freedom and the softer interactions on the mesosocpic scale, they can promote understanding and identifying of the physical mechanisms driving collective phenomena. Since the underlying atomistic complexity is reduced to a rather restricted set of parameters, generic models allow the systematic investigation of the way by which these coarse-grained parameters influence collective processes; thus they can provide guidelines concerning the direction to which the atomistic structure of the system should be tailored in order to achieve a desired mesoscopic behavior.

As was illustrated in this work, certain aspects of mesoscopic behavior are universal for liposomes and polymersomes, and they arise mainly due to the amphiphilic nature of the molecules they are comprised of. However, it should be mentioned that generic models are expected to perform much better quantitatively for the latter case than for the former. Due to the large number of building units, polymers exhibit a self-similar structure [144, 145]; thus the possibility to systematically reduce the degrees of freedom, i.e. to perform a coarse-graining procedure, is inherently present in these systems. On the other hand, lipid molecules are composed of a few, often different, structural units. In this restricted conformational space the concept of scale invariance is not applicable and the details of the chemical structure become more important. Therefore, to reproduce certain membrane characteristics, generic coarse-grained models of lipids frequently invoke interactions and parameterizations which only have a rather phenomenological, qualitative justification.

The development of generic models for bio-mimetic membranes remains an area of active research, particularly regarding the elaboration of approaches allowing for a physically transparent justification of interactions and a clear connection of model parameters with the material properties of the studied systems. Models, capable of addressing large amphiphilic systems have been available for less than one decade, therefore most issues related to the large scale behavior of vesicles have not received sufficient coverage; vesicle/vesicle and vesicle/substrate interactions being characteristic examples. For instance, while modeling efforts have been focused on fusion between vesicles, systematic simulations of alternative phenomena such as vesicle/vesicle adhesion and engulfment [146] are still lacking. Understanding how the later processes depend on the amphiphile molecular characteristics is important in view of their close relevance to endocytosis and mechanisms of uptake of certain drug delivery systems by cells. The adhesion of vesicles is related to the more general study of the processes taking place during interactions of vesicles with various substrates. One of the interesting questions associated with these systems is the understanding of how the stability of the vesicles can be affected by the presence of a surface. Modeling these systems, requires the ability to capture significant rearrangements in the vesicle topology like, pore formation or shell disintegration, which can be fully described only through particle-based models as opposed to representations based on continuum descriptions (like the Helfrich–Hamiltonian). Vesicles with various types of inclusions and molecules attached to

the bilayer constitute important objects for future studies. For instance, a recent work on membrane vesiculation driven by curvature inducing proteins [118] illustrates that approaches considering decorated membranes have to account for their "softness," the ability to rearrange significantly in response to both *individual* and *collective* action of the bilayer attachments/incapsulants. Therefore, for example, modeling the protein shielding effects of long polymers attached to amphiphilic bilayers by representing them as a polymeric brush grafted to a solid substrate might be too oversimplifying.

The study of nonequilibrium dynamical phenomena in vesicles is of special interest. For medical applications this is important for tailoring the coupling of artificial vesicles to their environment, so that the therapeutic loads could be delivered to the targeted areas. Membrane destabilization by changing the amphiphile architecture through hydrolytic degradation, is an illustrative example. Modeling vesicles out of equilibrium is also significant for considering cases when the conditions in their internal, loading cavity are modified. A simple example of a polymersome response to internal pressure generated by a long loading polymer was demonstrated in this work; however more complicated systems can be envisioned, particularly in cases when the amphiphilic vesicles are used as nanoreactors.

Acknowledgement It is a great pleasure to thank M. Deserno, M. Schick, and V.P. Torchilin for their valuable comments on the manuscript and discussions. Financial support was provided by the Volkswagen foundation and the SFB 803. JSC Jülich and HLRN Hannover are acknowledged for ample computing time.

References

1. Israelachvili J (1991) Intermolecular and surface forces. Academic, New York
2. Singer SJ, Nicolson GL (1972) Science 175:720
3. Engelman DM (2005) Nature 438:578
4. Sackmann E (1995) Biological membranes architecture and function. In: Handbook of biological physics, vol. 1. Elsevier, Amsterdam
5. Venturoli M, Sperotto MM, Kranenburg M, Smit B (2006) Phys Rep 437:1
6. Takamori S, Holt M, Stenius K, Lemke EA, Gronborg M, Riedel D, Urlaub H, Schenck S, Brügger B, Ringler P, Müller SA, Rammner B, Gräter F, Hub JS, De Groot BL, Mieskes G, Moriyama Y, Klingauf J, Grubmüller H, Heuser J, Wieland F, Jahn R (2006) Cell 127:831
7. Kusumi A, Nakada C, Ritchie K, Murase K, Suzuki K, Murakoshi H, Kasai RS, Kondo J, Fujiwara T (2005) Annu Rev Biophys Biomol Struct 34:351
8. Murtola T, Rog T, Falck E, Karttunen M, Vattulainen I (2006) Phys Rev Lett 97:238102
9. Torchilin VP (2005) Nat Rev Drug Disc 4:145
10. Allen TM, Cullis PR (2004) Science 303:1818
11. Allen TM, Moase EH (1996) Adv Drug Deliv Rev 21:117
12. Malmsten M (2006) Soft Matter 2:760
13. Mori A, Klibanov AL, Torchilin VP, Huang L (1991) FEBS Lett 284:263
14. Semple SC, Chonn A, Cullis PR (1998) Adv Drug Deliv Rev 32:3
15. Allen TM (2002) Nat Rev Cancer 2:750
16. Kaneda Y (2000) Adv Drug Deliv Rev 43:197
17. Straubinger RM, Duzgunes N, Papahadjopoulos D (1985) FEBS Lett 179:148

18. Simoes S, Moreira JN, Fonseca C, Duzgunes N, de Lima MC (2004) Adv Drug Deliv Rev 56:947
19. Lim-Soo P, Eisenberg A (2004) J Polym Sci B Polym Phys 42:923
20. Luo L, Eisenberg A (2001) Langmuir 17:6804
21. Bermudez H, Brannan AK, Hammer DA, Bates FS, Discher DE (2002) Macromolecules 35:8203
22. Discher BM, Won Y, Ege DS, Lee JC-M, Bates FS, Discher DE, Hammer DA (1999) Science 284:1143
23. Discher DE, Eisenberg A (2002) Science 297:967
24. Hamley IW (2005) Soft Matter 1:36
25. Mecke A, Dittrich, Meier W (2006) Soft Matter 2:751
26. Discher D, Ahmed F (2006) Annu Rev Biomed Eng 8:323
27. Graff A, Sauer M, Gelder PV, Meier W (2002) PNAS 99:5064
28. Ding J, Liu G (1998) J Phys Chem B 102:6107
29. Nardin C, Hirt T, Leukel J, Meier W (2000) Langmuir 16:1035
30. Maskos M, Harris JR (2001) Macromol Rapid Commun 22:271
31. Photos PJ, Bacakova L, Discher B, Bates FS, Discher DE (2003) J Control Release 90:323
32. Taubert A, Napoli A, Meier W (2004) Curr Opin Chem Biol 8:598
33. Ahmed F, Discher DE (2004) J Control Release 96:37
34. Nardin C, Bolikal D, Kohn J (2004) Langmuir 20:11721
35. Seul M, Andelman D (1995) Science 267:476
36. Ohta T, Kawasaki K (1986) Macromolecules 19:2621
37. Glotzer SC, Solomon MJ (2006) Nat Mater 6:557
38. Müller M, Katsov K, Schick M (2002) J Chem Phys 116:2342
39. Müller M, Katsov K, Schick M (2003) J Polym Sci B Polym Phys B41:1441
40. Müller M, Katsov K, Schick M (2006) Phys Rep 434:113
41. Müller M (2006) Comparison of self-consistent field theory and Monte Carlo simulations. In: Gompper G, Schick M (eds) Soft matter, vol. 1. Wiley, Weinheim
42. Kremer K, Müller-Plathe F (2002) Mol Sim 28:729
43. Müller-Plathe F (2002) ChemPhysChem 3:754
44. Helfrich W (1973) Z Naturforsch 28:693
45. Zhong-can O, Helfrich W (1987) Phys Rev Lett 59:2486
46. Milner ST, Safran SA (1987) Phys Rev A 36:4371
47. Morse DC, Milner ST (1995) Phys Rev E 52:5918
48. Seifert U (1997) Adv Phys 46:13
49. Safran SA, Gov N, Nicolas A, Schwarz US, Tlusty T (2005) Physica A 352:171
50. Döbereiner HG, Evans E, Kraus M, Seifert U, Wortis M (1997) Phys Rev E 55:4456
51. Döbereiner HG, Gompper G, Haluska CK, Kroll DM, Petrov PG, Riske KA (2003) Phys Rev Lett 91:048301
52. Lebedev VV, Turitsyn KS, Vergeles SS (2007) Phys Rev Lett 99:218101
53. Atilgan E, Sun SX (2007) J Chem Phys 126:095102
54. Weiner SJ, Kollman PA, Case DA, Singh UC, Ghio C, Alagona G, Profeta S, Weiner P (1984) J Am Chem Soc 106:765
55. Brooks BR, Bruccoleri RE, Olafson BD, States DJ, Swaminathan S, Karplus M (1983) J Comp Chem 4:187
56. van Gunsteren WF, Berendsen HJC (1987) Groningen molecular simulation (GROMOS) library manual. Biomos, Groningen
57. Jorgensen WL, Maxwell SD, Tirado-Rives J (1996) J Am Chem Soc 118:11225
58. Kaminski GA, Friesner RA, Tirado-Rives J, Jorgensen WL (2001) J Phys Chem B 105:6474
59. Levitt M (1990) Energy calculations and dynamics program. Molecular Applications Group, Standford and Yeda, Behovot, Israel
60. de Vries AH, Mark AE, Marrink JS (2004) JACS 126:4488
61. Anezo C, de Vries AH, Höltje HD, Tieleman DP, Marrink SJ (2003) J Phys Chem B 107:9424
62. Berger O, Edholm O, Jähnig (1997) Biophys J 72:2002
63. Marrink SJ, Mark AE (2003) J Am Chem Soc 125:15233

64. Marrink SJ, Mark AE (2003) J Am Chem Soc 125:11144
65. Smit B, Hilbers PAJ, Esselink K, Rupert LAM, Van Os NM, Schlijper AG (1991) J Phys Chem 95:6361
66. Götz R, Gompper G, Lipowsky R (1999) Phys Rev Lett 82:221
67. Shelley JC, Shelley M, Reeder R, Bandyopadhyay S, Klein ML (2001) J Phys Chem B 105:4464
68. Sevink GJA, Zvelindovsky AV (2005) Macromolecules 38:7502
69. Bernardes AT (1996) Langmuir 12:5763
70. Noguchi H, Takasu MP (2001) Phys Rev E 64:041913
71. Yamamoto S, Maruyama A, Hyodo S (2002) J Chem Phys 116:5842
72. Xe X, Schmid F (2006) Macromolecules 39:2654
73. Chernomordik L, Kozlov MM, Zimmerberg J (1995) J Membr Biol 146:1
74. Mayer A (2002) Ann Rev Cell Dev Biol 18:289
75. Tamm LK, Crane J, Kiessling V (2003) Curr Opin Struct Biol 13:453
76. Blumenthal R, Clague MJ, Durell SR, Epand RM (2003) Chem Rev 103:53
77. Zimmerberg J, Chernomordik L (1999) Adv Drug Deliv Rev 38:197
78. Lee J, Lentz BR (1997) Biochemistry 36:6251
79. Lentz BR, Malinin V, Haque MdE, Evans K (2000) Struct Biol 10:607
80. Kozlov MM, Markin VS (1983) Biofizika 28:255
81. Chernomordik LV, Melikyan GB, Chizmadzhev YA (1987) Biochim Biophys Acta 906:309
82. Müller M, Katsov K, Schick M (2003) Biophys J 85:1611
83. Knecht V, Marrink SJ (2007) Biophys J 92:4254
84. Smeijers AF, Markvoort AJ, Pieterse K, Hilbers PAJ (2006) J Phys Chem B 110:13212
85. Srinivas G, Discher DE, Klein ML (2004) Nat Mater 3:638
86. Ortiz V, Nielsen SO, Discher DE, Klein ML, Lipowsky R, Shillcock J (2005) J Phys Chem B 109:17708
87. Srinivas G, Shelley JC, Nielsen SO, Discher DE, Klein ML (2004) J Phys Chem B 108:8153
88. Scott LH (2002) Curr Opin Struct Biol 12:495
89. Zhang Y, Feller SE, Brooks BR, Pastor RW (1995) J Chem Phys 103:10252
90. Feller SE, Zhang Y, Pastor RW (1995) J Chem Phys 103:10267
91. Feller SE, Pastor RW (1996) Biophys J 71:1996
92. Marrink SJ, Mark AE (2001) J Phys Chem B 105:6122
93. Pugnaloni LA, Ettelaie R, Dickinson E (2004) J Chem Phys 121:3775
94. Bermudez H, Hammer DA, Discher DE (2004) Langmuir 20:540
95. Espanol P, Warren PB (1995) Europhys Lett 30:191
96. Groot RD, Warren PB (1997) J Chem Phys 107:4423
97. Warren PB (1998) Curr Opin Colloid Interface Sci 3:620
98. Kranenburg M, Venturoli M, Smit B (2003) J Phys Chem B 107:11491
99. Shillock JC, Lipowsky R (2002) J Chem Phys 117:5048
100. Groot RD, Rabone KL (2001) Biophys J 81:725
101. Kranenburg M, Smit B (2005) J Phys Chem B 109:6553
102. Gao L, Shillcock JC, Lipowsky R (2007) J Chem Phys 126:015101
103. Grafmüller A, Shillcock JC, Lipowsky R (2007) Phys Rev Lett 98:218101
104. Gao L, Lipowsky R, Shillcock JC (2008) Soft Matter 4:1208
105. Shillcock JC, Lipowsky R (2005) Nat Mater 4:225
106. Monck JR, de Toledo GA, Fernandez JM (1990) PNAS 87:7804
107. Yamamoto S, Hyodo S (2003) J Chem Phys 118:7937
108. Laradji M, Kumar PBS (2004) Phys Rev Lett 93:198105
109. Miao L, Seifert U, Wortis M, Döbereiner HG (1994) Phys Rev E 49:5389
110. Drouffe JM, Maggs AC, Leibler S (1991) Science 254:1353
111. Noguchi H, Takasu MP (2001) J Chem Phys 115:9547
112. Noguchi H, Takasu MP (2002) Phys Rev E 65:051907
113. Farago O (2003) J Chem Phys 119:596
114. Cooke IR, Kremer K, Deserno M (2005) Phys Rev E 72:011506
115. Cooke IR, Deserno M (2005) J Chem Phys 123:224710

116. Brannigan G, Philips PE, Brown FLH (2005) Phys Rev E 72:011915
117. Harmandaris VA, Deserno M (2006) J Chem Phys 125:204905
118. Reynwar BJ, Illya G, Harmandaris VA, Müller MM, Kremer K, Deserno M (2007) Nature 447:461
119. Laradji M, Guo H, Zuckermann MJ (1994) J Phys Rev E 49:3199
120. Soga KG, Zuckermann MJ, Guo H (1996) Macromolecules 29:2289
121. Miao L, Guo H, Zuckermann MJ (1996) Macromolecules 29:2289
122. Daoulas KCh, Müller M (2006) J Chem Phys 125:184904
123. Kang H, Detcheverry FA, Mangham AN, Stoykovich MP, Daoulas KCh, Hamers RJ, Müller M, de Pablo JJ, Nealey PF (2008) Phys Rev Lett 100:148303
124. Müller M, Smith GD (2005) J Polym Sci B Polym Phys 43:934
125. Hong KM, Noolandi J (1981) Macromolecules 14:727
126. Matsen MW, Schick M (1994) Phys Rev Lett 72:2660
127. Fredrickson GH, Ganesan V, Drolet F (2002) Macromolecules 35:16
128. Müller M, Schmid F (2005) Adv Polym Sci 185:1
129. Fredrickson GH (2005) The equilibrium theory of inhomogeneous polymers. Oxford University Press, Oxford
130. Katsov K, Müller M, Schick M (2004) Biophys J 87:3277
131. Katsov K, Müller M, Schick M (2006) Biophys J 90:915
132. Lee JY, Schick M (2008) Biophys J 94:1699
133. Helfand E, Tagami Y (1971) J Chem Phys 56:3592
134. Frink LJD, Frischknecht A (2005) Phys Rev E 72:041923
135. Frischknecht A, Frink LJD (2006) Biophys J 91:4081
136. Müller M, Daoulas KCh (2008) J Chem Phys 128:024903
137. Müller M, Daoulas KCh (2008) J Chem Phys 129:164906
138. Müller M, MacDowell LG, Virnau P, Binder K (2002) J Chem Phys 117:5480
139. Eastwood JW, Hockney RW, Lawrence DN (1980) Comput Phys Commun 19: 215
140. Deserno M, Holm C (1998) J Chem Phys 109:7678
141. Canham PB (1970) J Theor Biol 26:61
142. Farago O (2008) J Chem Phys 128:184105
143. Karplus M, McCammon JA (2002) Nat Struct Biol 9:646
144. de Gennes PG (1979) Scaling concepts in polymer physics. Cornell University Press, New York
145. Rubinstein M, Colby RH (2003) Polymer physics. Oxford University Press, New York
146. Nam J, Santore M (2007) Langmuir 23:10650

Index